

Nanostructuring of Fe(II) spin crossover complexes using block copolymer micelles

DISSERTATION

Zur Erlangung des akademischen Grades eines
Doktors der Naturwissenschaften (Dr. rer. nat.) in der Bayreuther
Graduiertenschule für Mathematik und Naturwissenschaften
(BayNAT)
der Universität Bayreuth

vorgelegt von

Dipl. Chem. Ottokar Klimm
aus Zwickau

Bayreuth, 2019

Die vorliegende Arbeit wurde in der Zeit von November 2013 bis April 2017 in Bayreuth an der Professur für Anorganische Chemie IV unter Betreuung von Frau Prof. Dr. Birgit Weber angefertigt.

Vollständiger Abdruck der von der Bayreuther Graduiertenschule für Mathematik und Naturwissenschaften (BayNAT) der Universität Bayreuth genehmigten Dissertation zur Erlangung des akademischen Grades eines Doktors der Naturwissenschaften (Dr. rer. nat.).

Dissertation eingereicht am: 08.04.2019

Zulassung durch das Leistungsgremium: 10.04.2019

Wissenschaftliches Kolloquium: 08.10.2019

Amtierender Direktor: Prof. Dr. Markus Lippitz

Prüfungsausschuss:

Prof. Dr. Birgit Weber (Gutachterin)

Prof. Dr. Mukundan Thelakkat (Gutachter)

Prof. Dr. Frank Hahn (Vorsitz)

Prof. Dr. Markus Retsch



GEWIDMET MEINER FAMILIE

Man muss das Unmögliche versuchen, um das Mögliche zu erreichen

HERMANN HESSE

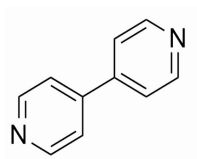


Abbreviations

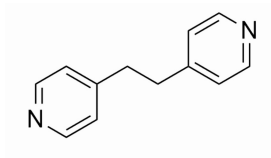
BCP	block copolymer
bipy	4,4'-bipyridine
bpea	1,2-di(pyridine-4-yl)ethane
bpee	<i>trans</i> -1,2-di(pyridine-4-yl)ethene
bpey	1,2-di(pyridine-4-yl)ethyne
CI	cooperative interactions
cmc	critical micellar concentration
CP	coordination polymer
DLS	dynamic light scattering
Δ_o	octahedral ligand field strength
EDX	energy dispersive X-ray
EPR	electron paramagnetic resonance
HS	high spin
$h\nu$	Planck's constant
IR	infra-red
LS	low spin
MeOH	methanol
M-L	metal to ligand distance
NMR	nuclear magnetic resonance
NP	nanoparticle
P	spin pairing energy
P4VP	poly-(4-vinylpyridine)
PS	polystyrene
PXRD	powder X-ray diffraction
REM	Rasterelektronenmikroskop
SCO	spin crossover
SEM	scanning electron microscopy
ST	spin transition
SQUID	superconducting quantum interference device

<i>T</i>	temperature
TEM	transmission electron microscopy
tBCP	triblock copolymer
VP	vinylpyridine

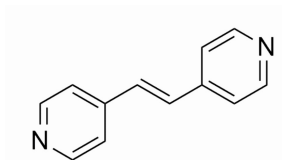
Register of illustrations



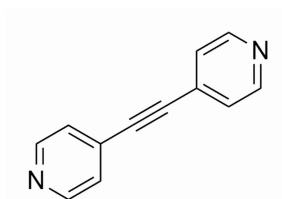
4,4' - bipyridine



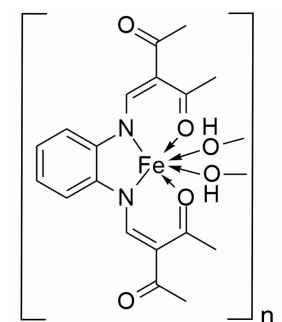
1,2-di(pyridine-4-yl)ethane



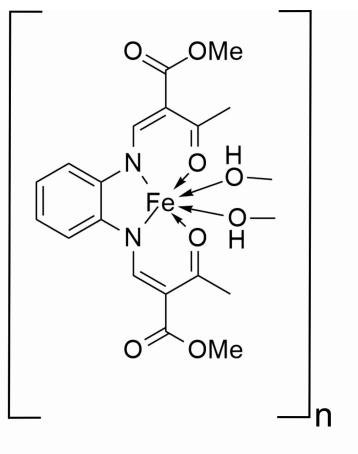
trans-1,2-di(pyridine-4-yl)ethene



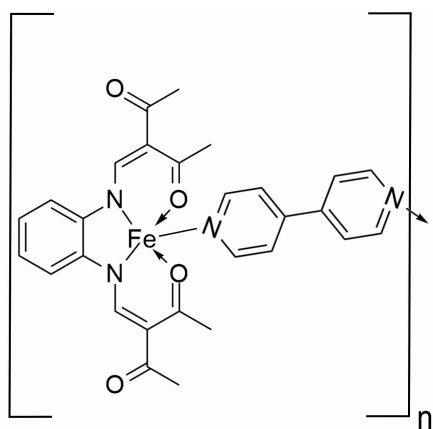
1,2-di(pyridine-4-yl)ethyne



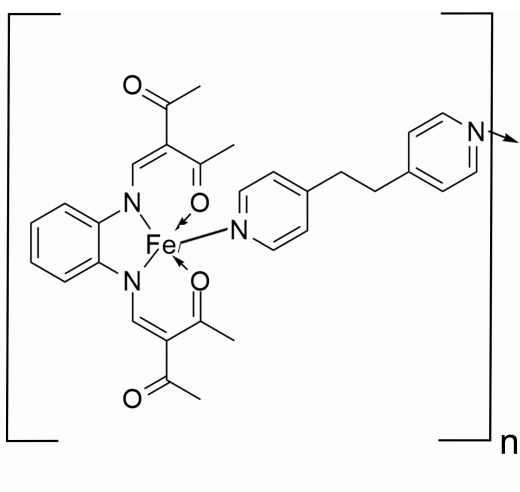
[Fe(Lb)(MeOH)₂]



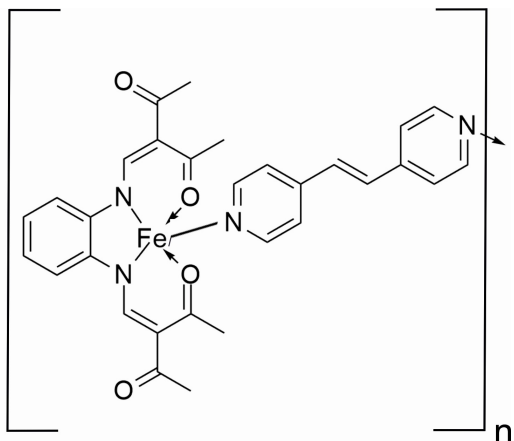
[Fe(Lc)(MeOH)₂]_n



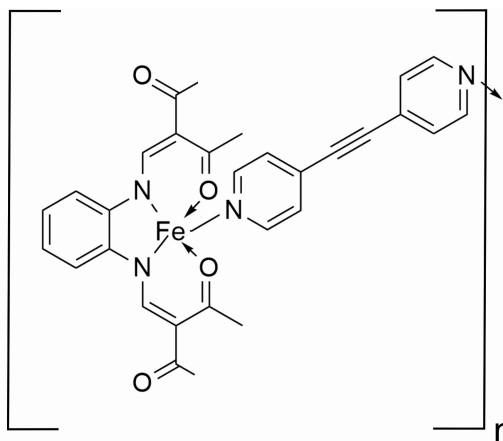
[Fe(Lb)(bipy)]_n



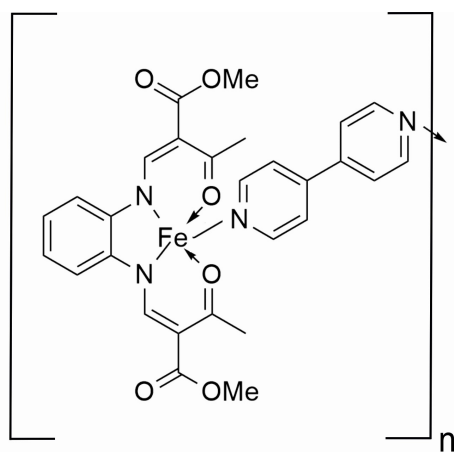
[Fe(Lb)(bpea)]_n



$[\text{Fe}(\text{Lb})(\text{bpec})]_n$



$[\text{Fe}(\text{Lb})(\text{bpey})]_n$



$[\text{Fe}(\text{Lc})(\text{bipy})]_n$



Table of contents

1. Summary/Zusammenfassung	1
1.1 Summary.....	1
1.2 Zusammenfassung	2
2. Introduction	4
2.1. The spin crossover phenomenon	4
2.1.1 Thermal SCO	6
2.1.2 Cooperativity in solution and solid state.....	8
2.2 Schiff base-like ligand systems	9
2.3 Nanostructuring of functional materials	11
2.3.1 Spin crossover nanoparticles.....	13
2.3.2 Block copolymers	16
2.3.3 Block Copolymers – Coordination Polymer Nanocomposites	17
2.4 References	19
3. Overview	27
3.1 Synopsis.....	27
3.2 Individual contributions to joint publications.....	41
4. Synthesis of $[\text{Fe}(\text{L})(\text{bipy})]_n$ Spin Crossover Nanoparticles using Blockcopolymer Micelles	46
Introduction	47
Results and discussion	48
Conclusions	57
Experimental.....	57
References	60
Supporting Information	65
5. Synthesis of $[\text{Fe}(\text{Leq})(\text{Lax})]_n$ Coordination Polymer Nanoparticles using Blockcopolymer Micelles	83
Introduction	84
Results and Discussion	86
Conclusion.....	93
Experimental.....	95
References	98
Supporting Information	104
6. The influence of the block copolymer composition on particle size and shape of Fe(II) SCO nanoparticles in block copolymer micelles	120
Introduction	121

Results and Discussion	122
Conclusion	128
Experimental.....	129
References	132
Supporting Information	135
7. Synthesis of different Fe(II) SCO nanoparticles with SCO over and below room temperature using BCP micelles	142
Introduction	143
Results and Discussion	144
Conclusion.....	153
Experimental.....	154
References	158
Supporting Information	161
8 List of Publications.....	169
“Probing Interactions of N-Donor Molecules with Open Metal Sites within Paramagnetic Cr-MIL-101: A Solid-State NMR Spectroscopic and Density Functional Theory Study”	169
Contributions to national and international conferences	170
9 Acknowledgment	171
10 Declaration	172

1. Summary/Zusammenfassung

1.1 Summary

The aim of this thesis, was to synthesize and characterize nanostructures of Fe(II) spin crossover (SCO) complexes. The nanoscaling of known SCO bulk materials is important for potential applications of SCO in devices or as switches. Possible approaches are to transfer such functional complexes into a matrix such as block copolymers (BCP) or to porous materials or to produce SCO films. In this thesis, BCPs were used as nanoreactors to synthesise SCO nanoparticles. A combination of the repeating units polystyrene (PS) and poly-(4-vinylpyridine) (P4VP) leads to a self-assembly of the BCPs (PS-*b*-P4VP). The size and shape of a BCP nanoparticle is influenced by the molecular mass, the nature of the monomers, the relative block-ratio and the solubility of the single chains (units). Styrene has a better solubility than 4-vinylpyridine in solvents as toluene or tetrahydrofuran which consequently leads to a micellar structure with PS as a shell and P4VP as core. After coordination of a starting iron complex [Fe(Lx)] to the P4VP units of the BCP micelles, a bridging ligand (Lax) was added and a coordination polymer (CP) [Fe(Lx)(Lax)]_n was obtained (first reaction cycle). In each additional synthesis step, [FeLx(MeOH)₂] and bridging ligand was added to enable a growth of the CP. Different numbers of reaction cycles (RC) were used to investigate the influence on the particle growth and on the SCO properties. Furthermore, reaction time, temperature, the solvent used for the synthesis and the BCB were varied. For [Fe(Lb)(bipy)]_n@BCP, after the first RC, no spin crossover occurred. Two or three RC led to a gradual SCO, four and five to a SCO with small hysteresis. With higher number of RC, a higher crystallinity of the nanoparticles was obtained, confirmed by powder x-ray diffraction (PXRD). Nanoparticles of various SCO systems were synthesised to yield different SCO properties (i.e. gradual, with hysteresis, above and below room temperature). The influence of the particle size and the interaction with the BCP matrix to the SCO properties was investigated. Nanoparticles with different sizes and shapes could be realised by varying the molecular masses (block lengths) of the BCP and the amount of P4VP. Due to the increase of P4VP from 15% to 25% and 33%, different structures of the nanoparticles appeared from spherical nanoparticles towards nanorods or vesicles. Dynamic light scattering (DLS), transmission electron microscopy (TEM) and scanning electron microscopy (SEM) were used to characterize the obtained nanocomposites and verified the nanostructures of the synthesised particles with a narrow size distribution.

1.2 Zusammenfassung

Ziel der vorliegenden Dissertation war die Synthese von Fe(II) Spin Crossover (SCO) Nanopartikeln. Für die Anwendung von SCO, ist es wichtig, vorhandene SCO Materialien in Nanometermaßstab zu überführen und in eine Matrix wie z. B. Blockcopolymer oder poröse Materialien einzubauen. Als Nanooreaktoren für die Nanopartikelsynthese in dieser Arbeit dienten dabei Blockcopolymer mit zwei unterschiedlichen Blöcken (Repetiereinheiten): Polystyrol (PS) und Poly-(4-Vinylpyridin) (P4VP) (PS-*b*-P4VP). Die Struktur und die damit verbunden Größe und Form der Nanopartikel wird maßgeblich durch die Molmasse des BCP, die Monomere, das Verhältnisses zwischen den beiden Blöcken und der Löslichkeit der einzelnen Ketten bestimmt. Durch die höhere Löslichkeit des PS Blocks gegenüber P4VP in Toluol oder Tetrahydrofuran, kommt es zur Selbstorganisation (self-assembly) und Ausbildung mizellarer Strukturen mit P4VP als Kern und PS als Schale. Nach Koordination eines Vorläufer-Eisenkomplexes [Fe(Lx)] an die 4-Vinylpyridineinheiten des Blockcopolymer erfolgte die Zugabe des jeweiligen Brückenliganden (Lax) und es bildete sich das Koordinationspolymer (CP) [FeLx(Lax)]_n in der Blockcopolymermatrix (1 Reaktionszyklus). In jedem weiteren Reaktionszyklus (RZ) wurden erneut [Fe(Lx)(MeOH)₂] und Brückenligand zugegeben. Es wurden verschiedene RZ verwendet, um den Einfluss auf das Partikelwachstum, die SCO Eigenschaften und die Wechselwirkungen mit der Blockcopolymermatrix zu untersuchen. Zusätzlich wurden der Einfluss von Reaktionszeit und -temperatur, Lösemittel und BCP auf die Partikelgröße und die SCO Eigenschaften untersucht. Zudem wurden unterschiedliche SCO Komplexe eingesetzt um SCO Nanopartikel mit verschiedenen Eigenschaften zu erhalten (z.B. graduell, mit Hysterese, oberhalb und unterhalb von Raumtempertatur). Es zeigte sich, dass SCO Systeme des Typs [Fe(Lb)(bipy)]_n nach einem RZ keine SCO Eigenschaften aufwiesen. Bereits nach 2 RZ konnten für die meisten SCO Systeme graduelle Spin Übergänge erreicht werden bis hin zu schmalen Hysteresen nach 4 oder mehr RZ. Eine erhöhte Kristallinität der erhaltenen Nanopartikel mit zunehmender Anzahl an RZ wurde mittels Pulverdiffraktometrie (PXRD) Messungen nachgewiesen. Durch den Einsatz von Blockcopolymeren verschiedener Blocklängen, Gesamtmassen und verschiedenen prozentualen P4VP-Anteilen wurden Nanopartikel unterschiedlicher Größenordnungen und Formen erhalten. Durch Änderung von 15% auf 25% und 33% P4VP und damit einer Erhöhung der möglichen Koordinationsmöglichkeiten im BCP wurden Strukturunterschiede festgestellt von sphärischen Nanopartikel bis hin zu Stäbchen und Vesikeln. Dynamische Licht Streuung (DLS), Transmissions

Elektronen Mikroskopie (TEM) und Raster Elektronen Mikroskopie (REM) Aufnahmen bestätigten die Nanostrukturierung der erhaltenen Partikel und deren Größenverteilung.

2. Introduction

2.1. The spin crossover phenomenon

In the 1930s *Cambi et al.* firstly reported the observation of a spin crossover (SCO) phenomenon.^[1,2] With the help of the *crystal field theory* by Hans Bethe^[3] and John H. Van Vleck^[4] the underlying SCO phenomenon was understood. Transition metals in an octahedral coordination geometry split their *d*-orbitals into two states: t_{2g} and e_g^* . Due to this splitting, $3d^4$ - $3d^7$ transition metal complexes (TMC) can occur either in a high spin (HS) state, following the Hund's rule to maximise S , or a low spin (LS) state. TMC mostly have a well-defined state, either HS if the spin pairing energy P is larger than the octahedral ligand field strength Δ_o ($P \gg \Delta_o$, i.e. $[\text{Fe}(\text{H}_2\text{O})_6]^{2+}$) or LS if P is much smaller than Δ_o ($\Delta_o \gg P$, i.e. $[\text{Fe}(\text{CN})_6]^{4-}$) as shown in Figure 2.1 for Fe(II). If Δ_o and P are of the same dimension, a SCO between those two states, induced by physical or chemical stimuli such as light, pressure or temperature is possible.

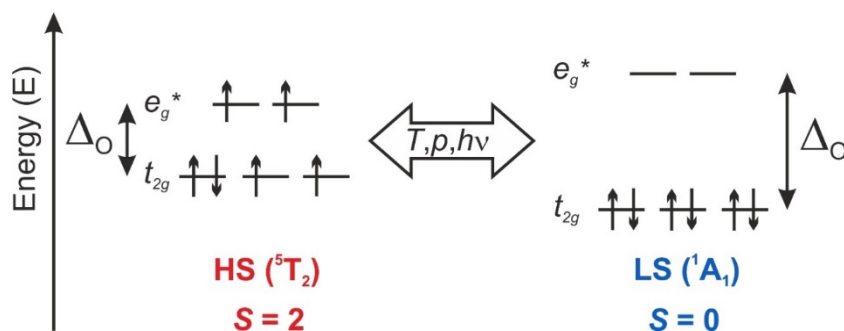


Figure 2.1: Schematic presentation of the energetic splitting of the d-orbitals and electron distribution in an octahedral coordinated $3d^6$ transition metal in HS state (left) and LS state (right) i.e. Fe(II). The SCO can be triggered by external stimuli such as temperature, pressure or light.

The ligand field splitting depends on the chosen ligands and the metal ion. The strength of a ligand to split the ligand field is given by its place in the spectrochemical row.^[5] The most attractive SCO compounds possess an Fe(II) metal center, because it is possible to switch magnetic properties between a diamagnetic LS ($S=0$) and a paramagnetic HS ($S=2$) state. Also, there is a change in the physical properties of the complex, for example the color. The relative energy of the two different

molecular states, the LS and HS (respectively 1A_1 and 5T_2 for a Fe(II) complex) is given in Figure 2.2.

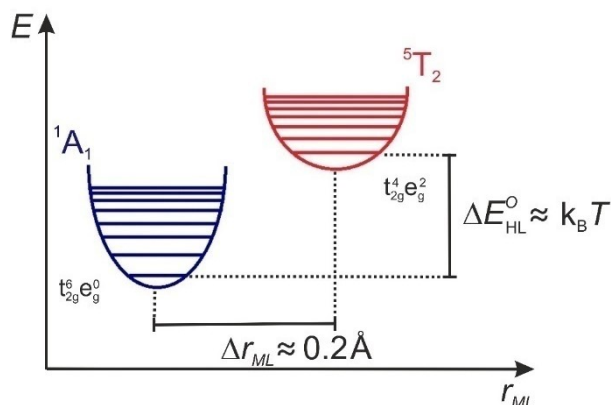


Figure 2.2: Jablonski diagram of the $3d^6$ transition metal Fe(II) in the LS state (blue) and the HS state (red).

In the LS state, the antibonding e_g^* orbitals are empty and all six electrons are in the t_{2g} orbital. For an $3d^6$ transition metal in the HS state, four electrons are in the t_{2g} orbital and two electrons are in the antibonding e_g^* .^[6] Due to the two electrons in the antibonding orbitals, the metal to ligand distance (M-L) in the HS is larger than in the LS. The M-L increase for Fe(II) is about 0.2 \AA .^[7]

This increase leads to a change in the vibrational modes of the molecule. The energies of 1A_1 and 5T_2 are presented as function of Δ_O in a Tanabe-Sugano diagram.^[8-9] As shown in Figure 2.3 the $3d^6$ transition metal Fe(II) has an electronic ground state 5T_2 until a specific ligand field strength Δ_{crit} .^[10,11] Above Δ_{crit} , the ground state changes towards 1A_1 .

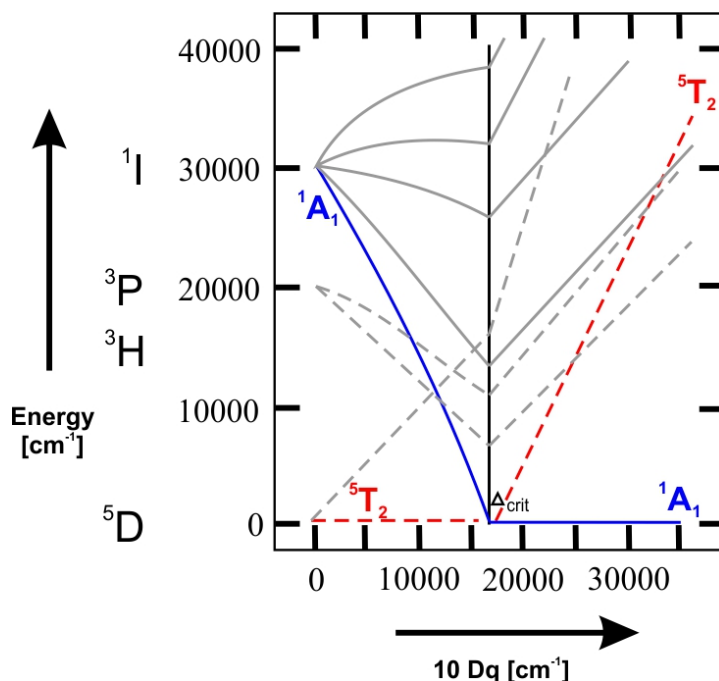


Figure 2.3: Tanabe-Sugano diagram to show the electronic ground states 1A_1 (LS, blue) and 5T_2 (HS, red) for an octahedral Fe(II) complex.^[12]

Several other transition metals can undergo SCO like Cr(II),^[13-17] Mn(II),^[18] Mn(III),^[19,20] Fe(III),^[1,2,21,22] Co(II),^[21,23,24] and Co(III) complexes^[25,26]. The SCO can be followed using magnetic measurements (e.g. with a SQUID magnetometer) or NMR or EPR spectroscopy. Structural changes can be detected via single crystal or powder X-ray diffraction (PXRD), vibrational changes can be detected via IR- and Raman-spectroscopy.

2.1.1 Thermal SCO

The transition from LS to HS takes place, when the free enthalpy ΔG (Gibbs-Helmholtz equation, Δ corresponds to the difference between HS and LS) is negative:

$$\Delta G = \Delta H - T\Delta S \quad (2.1)$$

$$\text{if } \Delta G < 0 \quad (2.2)$$

$$\text{then } \Delta H < T\Delta S \quad (2.3)$$

In the HS state there are lower vibrational frequencies (weaker M-L bonding) resulting a higher density of vibrational states, thus ΔS is always positive. The product $T\Delta S$ can exceed ΔH if T is high enough. The critical temperature T_C or $T_{1/2}$ shows the equilibrium of HS and LS molecules, here $\Delta G = 0$ [12].

$$T_{1/2} = \frac{\Delta H}{\Delta S} \quad (2.4)$$

The free energy ΔG is given with:

$$\Delta G = -k_B T \ln(K) \quad (2.5)$$

K is the equilibrium constant between HS and LS.

$$K = \frac{\gamma_{HS}}{\gamma_{LS}} = \frac{\gamma_{HS}}{1-\gamma_{HS}} \quad (2.6)$$

γ_{HS} and γ_{LS} show the amount of molecules in HS and LS state with possible values from 0 to 1. To illustrate the temperature dependence of γ_{HS} , ΔG has to be equated:

$$\Delta H - T\Delta S = -k_B T \ln\left(\frac{\gamma_{HS}}{1-\gamma_{HS}}\right) \quad (2.7)$$

$$\gamma_{HS} = \frac{1}{1 + e^{\frac{\Delta H}{k_B T} - \frac{\Delta S}{k_B}}} \quad (2.8)$$

For a Fe(II) spin crossover complex the value of ΔH is about 6-15 kJ/mol and ΔS about 40-65 J/Kmol with a spin transition temperature around 130 K. [12]

2.1.2 Cooperativity in solution and solid state

There are different types of SCO in solid state and solution: gradual, stepwise, abrupt, abrupt with hysteresis and incomplete. The three most important are gradual, stepwise and abrupt with hysteresis (Figure 2.4). Usually, the temperature dependent magnetic properties of SCO complexes are plotted as a function of the HS fraction (γ_{HS}) against the temperature or the molar susceptibility temperature product ($\chi_{\text{M}}T$) against the temperature T (Figure 2.4).

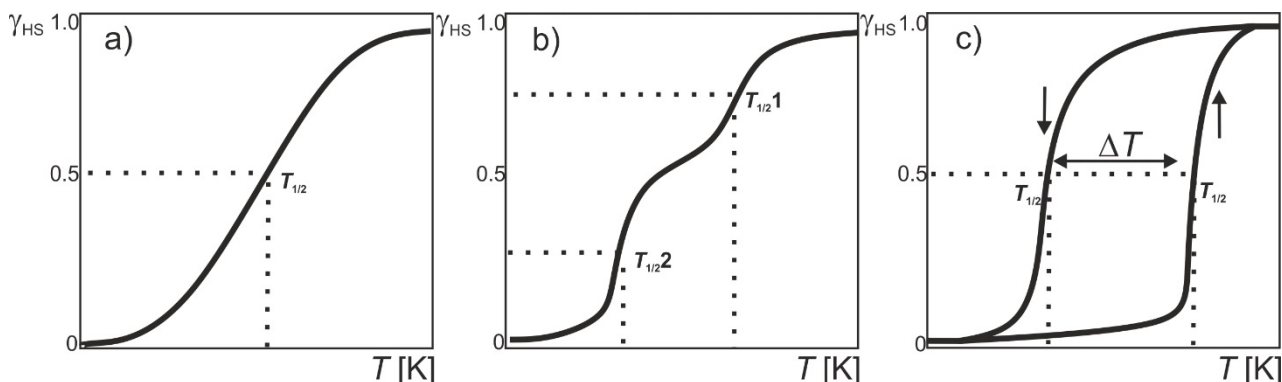


Figure 2.4: HS fraction γ_{HS} plotted vs. temperature T for different SCO a) gradual, b) stepwise, c) abrupt with hysteresis.

The reasons for different types of SCO are cooperative interactions (CI). Van der Waals- and π - π -interactions or hydrogen bonding are intermolecular interactions which lead to CIs.^[27,28,29] Those CIs are forwarding the spin transition information from one molecule to another through the crystal lattice due to a shortening or elongation of the metal-ligand distances to the neighbored molecules.^[27,28] In solution there is nearly no interaction between molecules so the SCO is gradual.^[30] Different lattice sites of one molecule can lead to stepwise spin crossover. The bistability of molecules at defined temperatures leads to the most interesting SCO with hysteresis. For a SCO with hysteresis, there is a $T_{1/2\downarrow}$ where 50% of HS and LS exist during cooling mode and a $T_{1/2\uparrow}$ where 50% of HS and LS exist during heating mode. First the CIs hinder the ST on several metal centres so the difference of $T_{1/2\downarrow}$ and $T_{1/2\uparrow}$ is due to the stepwise transition (Figure 2.5, b, c) of the lattice metal centres from pure HS (Figure 2.5, a) to LS (Figure 2.5, d) and $T_{1/2\downarrow}$ is at lower temperatures than $T_{1/2\uparrow}$.^[31,32] Due to very high cooperativity the system has an internal pressure able to inhibit ST partially or completely. Halcrow proposed in 2009, that any general change in

structure (i.e. ligand rotation) can lead to SCO with hysteresis, not only the volume change during SCO itself.^[33]

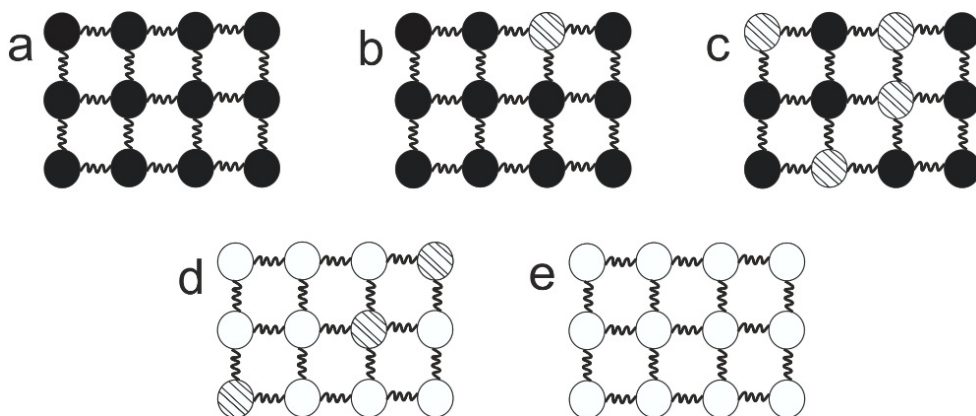
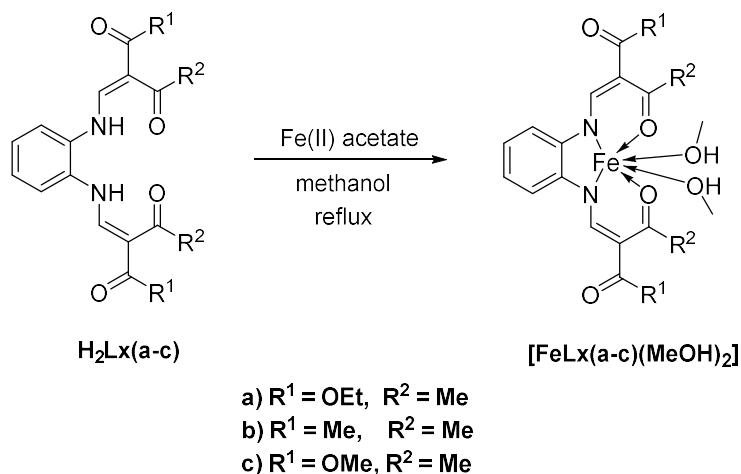


Figure 2.5: Schematic representation of a SCO system with internal pressure. The springs represent the intermolecular interactions, the black spheres represent Fe(II) centres in HS state, white spheres Fe(II) centres in LS state and the black lined spheres represent Fe(II) centres that are not defined due to intermolecular interactions which adapt the spin state of the whole system.^[12]

2.2 Schiff base-like ligand systems

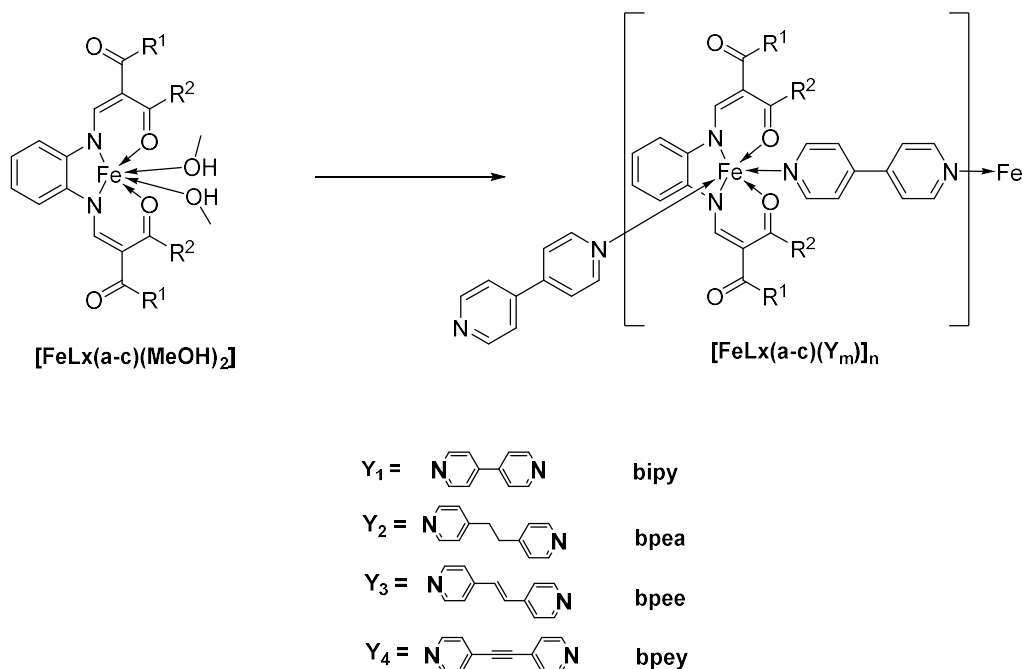
The ligand systems used in this work are Schiff base-like ligands, which show a good ability to form SCO complexes. Due to their $[N_2O_2]$ coordination sphere (square planar) and the possibility to change the substituents R^1 and R^2 , the ligand field strength can be adjusted quite sensitively. First synthesised by Jäger *et al.*,^[34] this ligand system is used for the synthesis of a wide variety of different complexes and continuously develop further.^[35] The SCO properties and cooperative interactions of the corresponding iron(II) complexes can be influenced by changing R^1 and R^2 or by using different bridging ligands (Scheme 2.3 and Figure 2.6). For the complexes used in this work, illustrated in Scheme 2.2, in the bulk material, $[Fe(Lc)(bipy)]_n$ shows two types of SCO due to two different polymorphs. Slow precipitation leads to SCO above RT whereas fast precipitation with reflux favors a gradual ST at lower temperatures.^[36]

2. Introduction



Scheme 2.2: Different Schiff base-like ligands (left) and Fe(II) complexes with two methanol molecules in axial position (right).

The bridging ligands **bpey** and **bipy** are rigid ligands leading to cooperative SCO in the bulk material with hysteresis, as illustrated in Fig. 2.6. Bridging ligands like **bpea** or **bpee**^[36,37] with an ethylene or ethene bridge between the two pyridine rings show the possibility to rotate or give *cis*-, *trans*- isomerism. Due to this rising flexibility, more gradual SCO are observed.



Scheme 2.3: Formation of 1D Fe(II) SCO coordination polymer with different pyridine-like bridging ligands (i.e. **bipy**, **bpea**, **bpee**, **bpey**).

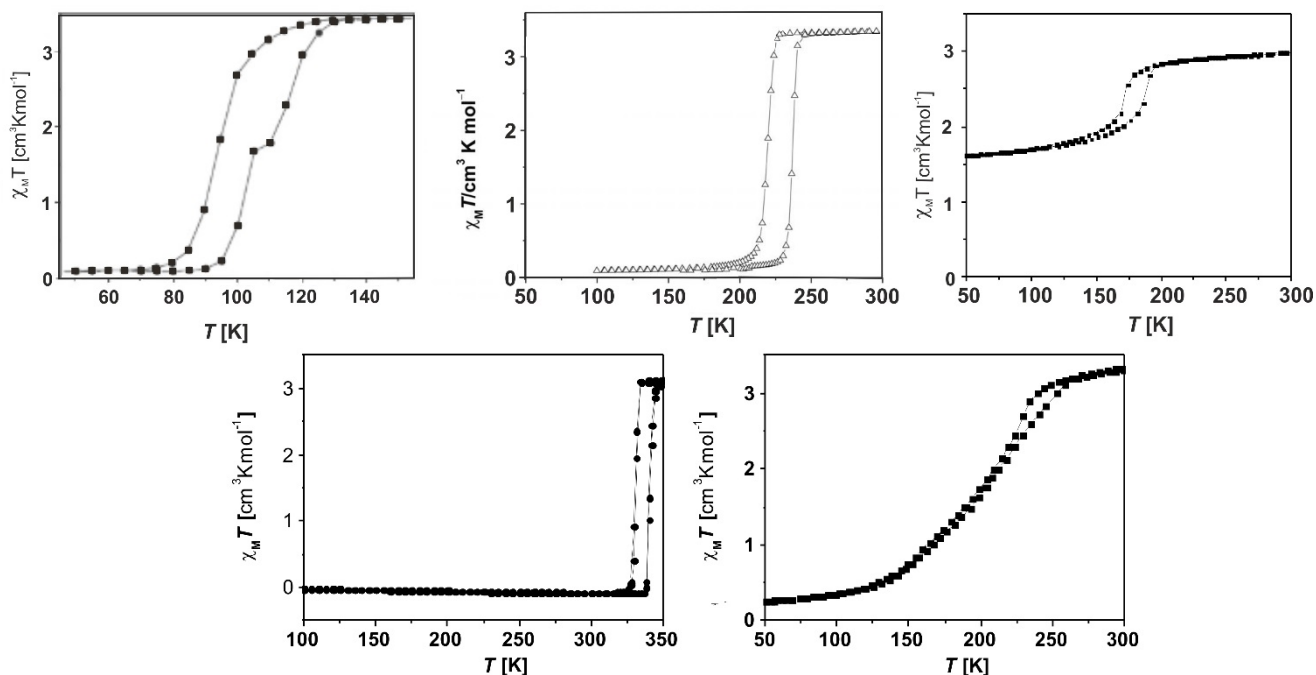


Figure 2.6: magnetic measurements of the bulk complexes of $[\text{Fe}(\text{Lb})(\text{bpea})]_n$ (top left), $[\text{Fe}(\text{Lb})(\text{bipy})]_n$ (top, middle), $[\text{Fe}(\text{Lb})(\text{bpey})]_n$ (top right) and the two different polymorphs of $[\text{Fe}(\text{Lc})(\text{bipy})]_n$ with SCO above RT (down left) and below RT (down right).^[36,37,38]

2.3 Nanostructuring of functional materials

The miniaturisation of functional and/or composite materials has a high impact for applications in modern technologies. Coordination polymers and (porous) coordination networks (e.g. metal organic frameworks (MOFs), spin crossover coordination polymers/networks) are of special interest because of their discussed high potential in drug delivery,^[39] chemical sensing, as well as contrast agents, in catalysis, battery electrodes or solid electrolytes.^[40–42]

The chief difficulty is the step from a bulk material to the nano-size and the incorporation into a functional device or composite material to gain advantages in processing or device constructions. Via self-assembly, colloidal suspensions of MOF NPs were already deposited on substrate surfaces, but it is difficult to realise a large-area ordering.^[40,41] In general, nanoparticles can be synthesised via top-down and bottom-up approach (Figure 2.7).^[43,44] In a top-down approach, a bulk material is physically (i.e. by a laser beam or ultra-sonic bath) or mechanically (i.e. by a ball mill) crushed until it reaches nanoscale. This method leads to an irregular size distribution and

thus, no exact size control is possible. The bottom-up approach is a much more sensitive way to prepare nanoparticles with narrow size distribution. This method is used to control the growth of the nanoparticles and regulate the particle size. Small building units such as precursor molecules or single atoms are used as starting materials to be transformed into clusters and nanoparticles afterwards.

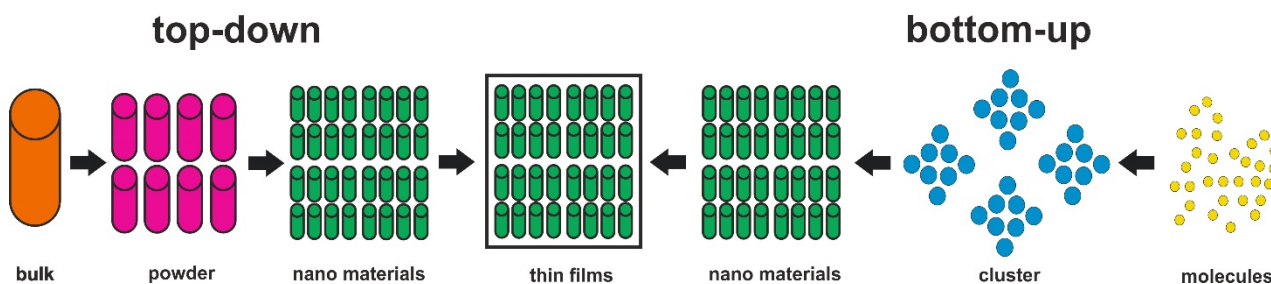


Figure 2.7: Top-down (left) and bottom-up approach (right) to yield nanoparticles in well-defined sizes.

Various methods are known for the synthesis of NPs of inorganic solids as the controlled decomposition of complexes, the reduction of metal salts or the micro-emulsion technique.^[45] Compared to this, there is a limited number of methods to synthesise nanostructured coordination polymers or coordination networks (2D/3D).^[40,41,46] They can be classified into six approaches: a) controlled precipitation (solvent-induced precipitation, microwave, ultrasonic, control seed formation and growth of crystals, modulators, capping ligands, ect.)^[40,41,47,48,49], b) micro-emulsion as micro-reactors for size control^[40,41,50], c) solvothermal synthesis^[46], d) spray techniques^[51], e) synthesis on patterned templates as polymer^[52] or f) electrostatic stabilisation.^[53]

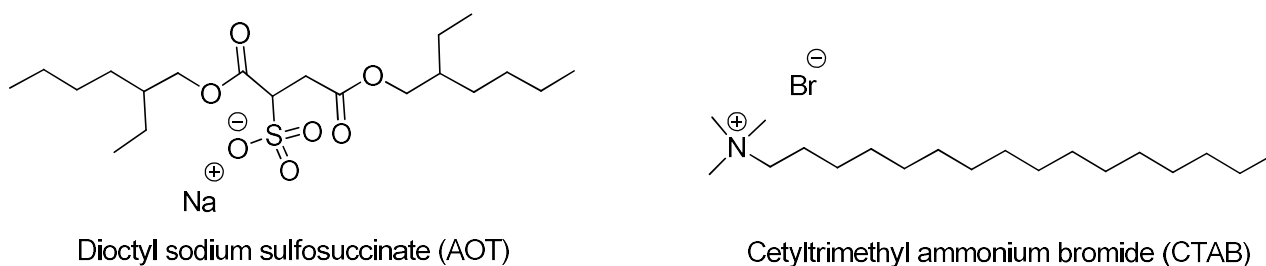
In 2005, Mirkin^[48] and Wang^[49] independently reported firstly successful methods to synthesise coordination polymer (CP) NPs by the use of solvent-induced precipitation. Previously, the starting materials had to be soluble in the same solvent as the reaction product. After the synthesis, an “antisolvent” induced the precipitation of the CP. An ingenious change in the reaction conditions, allowed the control of size and morphology of them. Only a small indication was given about how and why one particle size or morphology preferred another. By varying reaction conditions as changes in solvent, counter ion or ancillary ligand, it was even possible to gain reversible morphology changes.^[46] In a further method, micro-emulsion (surfactants) was used to synthesise nanostructured CPs.^[40,41,50] Mallah and co-workers produced nanoparticles of Prussian blue analogue $Cs_xNi[Cr(CN)_6]_y$ (interesting due to its application potential for coatings, photomagnetic switches, electrocatalysts or sensors)^[54] from spontaneous electrostatic stabilisation

as dispersion in aqueous solution.^[11] Using various coating agents, 6.5 nm bimetallic NPs can be achieved. Subsequently, the coating agent influenced the magnetic properties, obtaining a superparamagnetic or a spin glass like behaviour. Due to electrostatic stabilisation of surfactant free particles, core-multishell nanocrystals could be obtained by epitaxial growth of variant shells on different charged cores. A nanometer scale controlled shell was acquired and could be repeated for different metal ions.^[55] Interface-induced interactions effected the (photo-) magnetic properties of multi-layer composites.^[56] Another synthetic route towards Prussian blue mesostructures was the use of amphiphilic ligands, similar to the aqueous liquid-crystal-templating trail for the synthesis of chalkogenides and oxides.^[57] By varying the chain length and/or the chain end, the mesostructure can be modified. A large range of ligands and metal centers enable a wide flexibility in designing coordination networks or CPs with special properties. A further “fine-tuning” of the properties, depends on chain length, chain end, the packing (crystallinity vs. amorphous) and monodispersity.^[46] Not every nanoscaled CP or coordination network can be synthesised, there are limitations in the control of size, morphology or shape with the afore-remarked approaches. Thus the development of new synthetic routes for nano-structured materials is needed.

2.3.1 Spin crossover nanoparticles

As described before, there is a high interest in the development of materials with sensing properties and nanoscale resolution for application in biological systems or microcircuits.^[50,58] SCO complexes show properties like the memory effect (bistability) or the possibility to fine-tune a transition temperature. An special advantage of SCO materials is the possibility to combine the SCO with additional properties, e.g. fluorescence properties.^[59,60] Due to the promising properties of SCO materials, the investigation of the influence of decreasing particle size^[61-63], crystallinity and matrix effects^[64-66] on the SCO behaviour of the nano-material is highly interesting. The rigidity of matrices can have large effects on SCO properties, e.g. the width of the hysteresis in Hoffman Clathrates^[64] or triazole based systems^[66]. Hysteresis close to room temperature was observed for particles with a rigid SiO₂ shell, down to very small particle sizes. A study on the size dependence of thermal hysteresis loops by Bouseksou et al. presented, that below a critical diameter the cooperativity is restored.^[62] As described before, requirement for a hysteresis (bistability) are cooperative interactions between single spin centres, that are shared through intermolecular contacts. This communication strongly depends on the crystallinity and the

crystal packing of the (nano-) material. Plenty of applications demand abrupt spin transition or spin transition with hysteresis around room temperature, so the synthesis conditions have to be considered well to develop new strategies for NP preparation. Some strategies for the synthesis of nano-structured SCO coordination polymers and networks are used already.^[42,67] Good results were achieved by inverse micelle technique which is used quite frequently. Pioneer for the synthesis of SCO NPs by this method was Corronado et al.^[68], followed by Letard et al.^[69], Real et al.^[70a], Mallah et al.^[70b] and many others.^[61,65,71] In a polar solvent (water or methanol/ethanol) micro-emulsions of the starting materials are prepared by the use of surfactants as NaAOT (sodium bis(2-ethylhexyl)sulfosuccinate) or CTAB (cetyltri-methyl ammonium bromide) (scheme 2.4) and an unpolar phase (e.g. n-heptan or n-octane).



Scheme 2.4: Representation of two common surfactants CTAB (right) and AOT (left).

In the following step, the micellar exchange starts by mixing the micro emulsions which leads to the formation of the coordination network or polymer (figure 2.8).

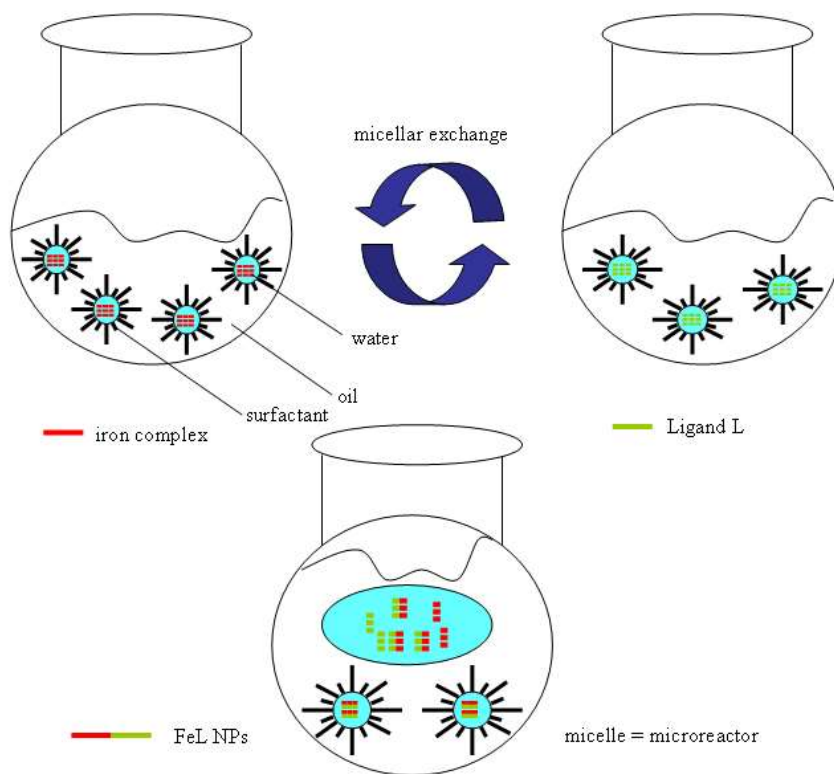


Figure 2.8: Schematic representation of NP growth by micro-emulsion with micelles techniques.

The control of the particle size can be achieved through an alteration of the solvent:surfactant ratio and variation of the concentration of the starting materials.^[61] A well suited material for using this method are triazole-based 1D coordination polymers^[63,65,68,72], as shown by spin transition with hysteresis maintained down to nanoscaled particle sizes, which allows, for example, examination on the conductivity as function of the spin state of the NPs.^[73] An indirect read out of the spin state is possible, by deposition of those NPs on graphene, which influences the conductivity from the graphene.^[74] 2D and 3D networks of Hofmann clathrates showed a loss of hysteresis due to size reduction^[70] (micro-emulsion). However, as described before, it can reappear below a critical size^[62] or after coating the NPs in a rigid matrix^[64]. A layer by layer technique is a different way to nanostructure Hofmann clathrates based systems^[75], where the hysteresis is preserved. Matrix effects, different polymorphs or changes in the crystalline quality of various sized nanoparticles are possible reasons, which are discussed for this phenomenon.

2.3.2 Block copolymers

The incorporation of metals in polymers leads to functional soft materials with new and attractive properties which keep the ability to shape polymers with the common progressing routes.^[78] Such composite materials are for example out of shape, low density, magnetic ceramic from metal-containing organosilicon polymer networks^[76] or the synthesis of a high surfaced area mesoporous etheneslica.^[77] Block copolymers (BCPs) are of great interest for the synthesis of nanoparticles, reasoned to the nanostructuring through self-assembly,^[79] as e.g. in some MOF-polymer composites^[80] with some advanced properties as proton conductivity^[85a], gas separation^[81b-d] or even a benefit in processing. Intracellular diagnostics and drug delivery^[82] are possible applications due to the combination of NPs with biopolymers, e.g. through the synthesis of spherical conjugated nucleic acids. Mirkin et al. synthesised nucleid acid-MOF NP conjugates through functional design on the UiO-66-N₃ surface via click-reaction.^[83] As shown by the authors, the pores are empty while the surface of the particles became functionalised. Compared to the pure MOF NPs, the coverage of the surface leads to a rise of stability and a better cellular uptake. The Mirkin group presented that those particles infiltrate cells and alter protein expression, which adepts them for an adequate gene knock-down.^[84] Functionalising the surface of nanoscales CPs with interfering RNA to create an efficient drug delivery for e.g. *cis*-platinum^[85] to tumor cells which prohibits a drug resistance of ovarian cancer cells. In the polymer chain included tellurium is one example for the combination of block copolymers with coordination compounds, to create stimuli-responsive delivery systems. Nanocarriers loaded with *cis*-platinum and indocyanine green were used, which produce reactive oxygen species (ROS) upon light irradiation. The tellurium gets oxidised and the drug release takes place.^[86] Further applications for the use of CP NPs in combination with BCPs were photocatalysts for water cleaning^[87], water-processed hybrid solar cells through the combination of water soluble conjugated polymer (poly[(3,4-dibromo-2,5-thienylene vinylene)-co-(p-phenylene-vinylene)]) with CdTe nanocrystals.^[88] Using one of the synthesis mechanisms explained in the passage below, materials are normally prepared in a two-step progress. First, the CP nanoparticles are synthesised and afterwards those NPs are linked to or dispersed in the polymer matrices. A great simplification in the process of CP NPs is the combination of both steps via direct synthesis in a polymer matrix, to e.g. avoid the usage of toxic surfactants or solvents, reduce the amount of solvent needed and to increase the yield. Also, there will be the opportunity of controlled deposition on different surfaces, e.g. formation of single-layered films through self-assembly^[89] of block copolymer based micelles (PS-*b*-P4VP).

Those micelles were already used for the deposition of e.g. Au^[90] or iron oxides^[91] NPs on large areas. The crystallinity of unprotected CPs or MOFs may be destroyed through contact with air or water^[41], so another positive effect for the use of BCPs is a kind of protective lamination. To achieve a precise control of size and composition, the polymer operates as nanoreactor for a formation of single NPs during heating.^[92]

2.3.3 Block Copolymers – Coordination Polymer Nanocomposites

Tang et al. presented one example for the use of block copolymers (BCPs) to realize coordination network or polymer nanostructures. He synthesized NPs of iron(III) with tannic acid through flash nanoprecipitation by the use of amphiphilic BCPs for polymer-directed self assembly.^[93] MacLachlan et al. formed soluble Prussian blue nanoworms through assembly of metal-organic block ionomers using a diblock copolymer (PS-*b*-PHEMA). The hydroxyethyl-methylacrylate (HEMA) group were functionalised to achieve monoquaternised 4,4'-bipyridine. Due to a self-assembly with the ionic block in the inflexible core, the block ionomer forms reverse micelles in less polar solvents. A NH₃ group of the iron(II) precursor Na₃[Fe(CN)₅NH₃] gets replaced through the coordination in the ionomer proved by UV-Vis spectroscopy. Through the addition of a second metal salt (e.g. iron(III), zinc(I) or cobalt(II) nitrate), a crosslinking of the received metal-organic block ionomer to a Prussian blue-type network was possible and led to worm-like nanostructures with an inner diameter of around 20 nm which are monodisperse and reproducible. The characterisation of the nanoparticles was done via TEM and EDX. Furthermore the synthesis of hollow nanocontainers becomes possible through the alteration of block lengths and reaction conditions. Those nanocontainers were used for encapsulation through emulsion-induced assembly of the metal-containing block ionomers.^[94] Also those capsules can be modified towards the encapsulation (selectively permeable) of methylene blue by a fine tune of the size through alteration of the reaction conditions. Schiff base-like ligand system of the Weber group, presented in 2.2, is highly qualified for the synthesis of spin crossover complexes with thermal hysteresis loops.^[95] The spin state switch can be modified towards properties such as switchable luminescence^[64] or amphiphilic properties.^[96] Experiments to synthesise SCO NPs by the use of the inverse micelles technique were not successful and resulted in a mixture of nano-sized particles and microcrystals. In 2014, the SCO coordination polymer (CP) [Fe(L)(bipy)]_n (L = Schiff base-like ligand, bipy = 4,4'-bipyridine) was incorporated in the polymer matrix poly(4-vinylpyridine).

A 20 K thermal hysteresis loop was observed around 225 K for the bulk material^[97]. The Fe(II) complex ($[\text{Fe}(\text{L})]$), can coordinate at the 4-vinylpyridine unit of the polymer with the axial coordination site, whereas the second axial coordination site is free for a coordination of a 4,4'-bipyridine. The free nitrogen at the 4,4'-bipyridine can coordinate the next Fe(II) complex again (Figure 2.9).

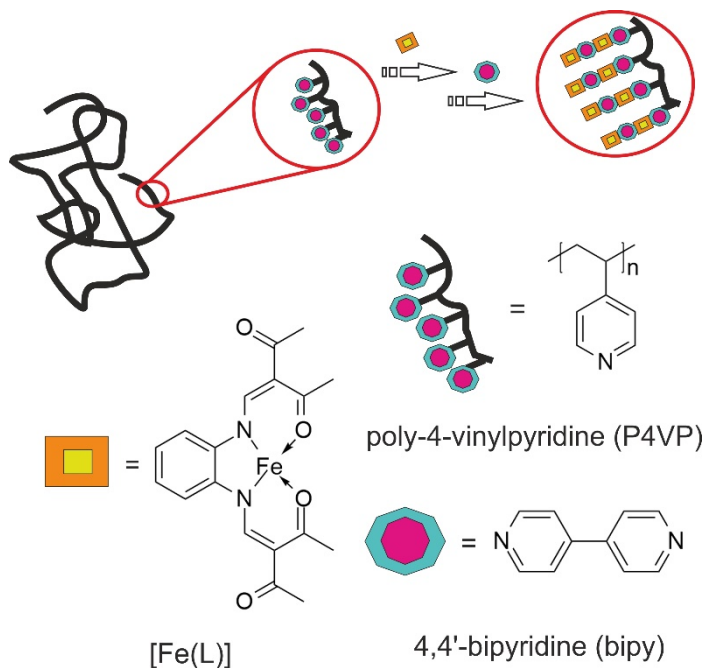


Figure 2.9: Schematic representation of the general approach for the synthesis of micro- and nanoparticles of Fe(II) coordination polymers in a polymer matrix (poly(4-vinylpyridine)).^[63]

A controlled growth of the microcrystals in the polymer matrix was observed by the subsequent addition of iron complex and 4,4'-bipyridine. Below a critical size, the spin transition is quenched and no gradual SCO appears, but above this critical size of the particles, the same cooperative spin transition with hysteresis as for the bulk material occurs.^[98] Based on those results, block copolymers with poly(4-vinylpyridine) as one block (e.g. PS-*b*-P4VP), were used to synthesise SCO NPs in this thesis. Future projects can be envisioned by varying the blocks of the BCP, to allow a specific change towards special properties as water solubility or conductivity. Possible systems are polystyrene-*b*-polyethylene glycol (PS-*b*-PEO)^[99,100,101] for water soluble or polystyrene-*b*-polythiophene (PS-*b*-H3PT)^[102,103] for conductive BCPs.

2.4 References

- [1] L. Cambi, L. Szegö, *Ber. dtsh. Chem. Ges. A/B*, **1931**, 64, 2591–2598.
- [2] L. Cambi, L. Malatesta, *Ber. dtsh. Chem. Ges. A/B*, **1937**, 70, 2067–2078.
- [3] H. Bethe, *Ann. Phys.*, **1929**, 3, 135–206.
- [4] J. H. Van Vleck, *J. Chem. Phys.*, **1935**, 3, 803–813.
- [5] Hollemann, Wiberg, *Lehrbuch der anorg. Chemie*, de Gruyter, Berlin New York, DE, **2007**.
- [6] P. Guionneau, M. Marchivie, G. Bravic, J.-F. Létard, D. Chasseau, *Spin Crossover in Transition Metal Compounds I-III*, Springer, Berlin, DE, **2004**.
- [7] Y. Bodenthing, D. G. Kurth, G. Schwarz, *Chem. Unserer Zeit*, **2008**, 42, 256–263.
- [8] Y. Tanabe, S. Sugano, *J. Phys. Soc. Jpn.* **1954**, 9(5), 753–766.
- [9] S. Sugano, Y. Tanabe, H. Kamimura, *Pure and Applied Physics, Vol. 33*, Academic Press, New York, **1970**, 82.
- [10] G. Racah, *Phys. Rev.* **1943**, 63, 367–382.
- [11] G. Racah, *Phys. Rev.* **1949**, 76, 1352–1365.
- [12] B. Weber, *Koordinationschemie*, Springer, Berlin Heidelberg, DE, **2014**.
- [13] D. M. Halepoto, D. G. L. Holt, L. F. Larkworthy, G. J. Leigh, D. C. Povey, G. W. Smith, *J. Chem. Soc., Chem. Commun.*, **1989**, 1322–1323.
- [14] P. Gütllich, A. B. Gaspar, V. Ksenofontov, Y. Garcia, *J. Phys. Condens. Matter*, **2004**, 16, S1087–S1108.
- [15] M. Sorai, Y. Yumoto, D. M. Halepoto, L. F. Larkworthy, *J. Phys. Chem. Solids*, **1993**, 54, 421–430.
- [16] H. Sitzmann, M. Schär, E. Dormann, M. Kelemen, *Z. Anorg. Allg. Chem.*, **1997**, 623, 1850–1852.
- [17] A. K. Hughes, V. J. Murphy, D. O'Hare, *J. Chem. Soc., Chem. Commun.*, **1994**, 163–164.
- [18] F. Franseschi, J. Hesschenbrouck, E. Solari, C. Floriani, N. Re, C. Rizzoli, A. Chiesi-Villa, *J. Chem. Soc., Dalton Trans.*, **2000**, 593–604.
- [19] P. G. Sim, E. Sinn, *J. Am. Chem. Soc.*, **1981**, 103, 241–243.
-

- [20] L. Kaustov, M. E. Tal, A. I. Shames, Z. Gross, *Inorg. Chem.*, **1997**, *36*, 3503–3511.
- [21] M. Halcrow, *Spin-Crossover Materials*, John Wiley & Sons Ltd., Chichester, UK, **2013**.
- [22] P. J. van Koningbruggen, Y. Maeda, H. Oshio, *Spin Crossover in Transition Metal Compounds I-III*, Berlin, DE, **2004**.
- [23] H. A. Goodwin, *Spin Crossover in Transition Metal Compounds I-III*, Springer, Berlin, DE, **2004**.
- [24] S. Hayami, Y. Komatsu, T. Shimizu, H. Kamihata, Y. H. Lee, *Coord. Chem. Rev.*, **2011**, *255*, 1981–1990.
- [25] W. Eberspach, N. El Murr, W. Kläui, *Ang. Chem. Int. Ed.*, **2003**, *21*, 915–916.
- [26] P. Gütllich, B. R. McGarvey, Kläui, *Inorg. Chem.*, **1980**, *19*, 3704–3706.
- [27] O. Kahn, C. J. Martinez, *Science* **1998**, *279*, 44–48.
- [28] O. Sato, J. Tao, Y.-Z. Zhang, *Angew. Chem.* **2007**, *119*, 2200.
- [29] P. Gütllich, H. A. Goodwin, *Topics in Current Chemistry, Vol. 233* (Eds.: P. Gütllich, H. A. Goodwin), Springer, Wien, New York, **2004**, 1–39.
- [30] P. Gütllich, Y. Garcia, H. A. Goodwin, *Chem. Soc. Rev.*, **2000**, *29*, 419–427.
- [31] B. Weber, W. Bauer, T. Pfaffeneder, M. M. Dîrtu, A. D. Naik, A. Rotaru, Y. Garcia, *Eur. J. Inorg. Chem.*, **2011**, 3193–3206.
- [32] J. A. Real, A. B. Gaspar, V. Niel, M. C. Muñoz, *Coord. Chem. Rev.*, **2003**, *236*, 121–141.
- [33] M. A. Halcrow, *Coord. Chem. Rev.*, **2009**, *253*, 2493–2514.

- [34] E.-G. Jäger, E. Häussler, M. Rudolph, A. Schneider, *Z. anorg. allg. Chem.*, **1985**, 525, 67–85.
- [35] W. Bauer, T. Ossiander, B. Weber, *Z. Naturforsch. B*, **2010**, 65, 323–328.
- [36] W. Bauer, W. Scherer, S. Altmannshofer, B. Weber, *Eur. J. Inorg. Chem.*, **2011**, 2803–2818.
- [37] B. Weber, *Coord. Chem. Rev.*, **2009**, 253, 2432–2449.
- [38] R. Nowak, W. Bauer, T. Ossiander, B. Weber, *Eur. J. Inorg. Chem.*, **2013**, 5-6, 975–983.
- [39] P. Horcajada, T. Chalati, C. Serre, B. Gillet, C. Sebrie, T. Baati, J. F. Eubank, D. Heurtaux, P. Clayette, C. Kreuz, J.-S. Chang, Y. K. Hwang, V. Marsaud, P.-N. Bories, L. Cynober, S. Gil, G. Férey, P. Couvreur, R. Gref, *Nat Mater* **2010**, 9(2), 172–178.
- [40] E. A. Flügel, A. Ranft, F. Haase, B. V. Lotsch, *J. Mater. Chem.* **2012**, 22(20), 10119–10133.
- [41] M. Sindoro, N. Yanai, A.-Y. Jee, S. Granick, *Acc. Chem. Res.* **2014**, 47(2), 459–469.
- [42] K. Otsubo, T. Haraguchi, H. Kitagawa, *Coord. Chem. Rev.* **2017**, 346, 123–138.
- [43] R. Dittmeyer, W. Keim, G. Kreysa, A. Oberholz, *Chemische Technik. Prozesse und Produkte*, Wiley, Weinheim, **2004**.
- [44] Y. Liu, S. Mai, N. Li, C. K.Y. Yiu, J. Mao, D. H. Pashley, F. R. Tay, *Acta Biomater. Author manuscript*, **2012**, 1–19.
- [45] a) H. You, S. Yang, B. Ding, H. Yang, *Chem. Soc. Rev.* **2013**, 42(7), 2880–2904; b) C. Altavilla, E. Ciliberto, Eds, *Inorganic nanoparticles: Synthesis, applications, and perspectives*; CRC Press, Boca Raton, FL, **2011**.
- [46] A. M. Spokoyny, D. Kim, A. Sumrein, C. A. Mirkin, *Chem. Soc. Rev* **2009**, 38(5), 1218–1227.
- [47] a) P. Chakraborty, M.-L. Boillot, A. Tissot, A. Hauser, *Angew. Chem. Int. Ed.* **2013**, 52(28), 7139–7142; b) A. Tissot, J.-F. Bardeau, E. Rivière, F. Brisset, M.-L. Boillot, *Dalton Trans* **2010**, 39(33), 7806.
- [48] M. Oh, C. A. Mirkin, *Nature* **2005**, 438(7068), 651–654.
- [49] X. Sun, S. Dong, E. Wang, *J. Am. Chem. Soc.* **2005**, 127(38), 13102–13103.

- [50] L. Catala, T. Mallah, *Coord. Chem. Rev.* **2017**, *346*, 32–61.
- [51] a) H. J. Lee, W. Cho, M. Oh, *Chem. Commun.* **2012**, *48*(2), 221–223; b) P. N. Martinho, T. Lemma, B. Gildea, G. Picardi, H. Müller-Bunz, R. J. Forster, T. E. Keyes, G. Redmond, G. G. Morgan, *Angew. Chem. Int. Ed.* **2012**, *51*(48), 11995–11999.
- [52] D. Brnzei, L. Catala, N. Louvain, G. Rogez, O. Stéphan, A. Gloter, T. Mallah, *J. Mater. Chem.* **2006**, *16*(26), 2593–2599.
- [53] A. Carné-Sánchez, I. Imaz, M. Cano-Sarabia, D. Maspoch, *Nat. Chem.* **2013**, *5*(3), 203–211.
- [54] a) S.-i. Ohkoshi, H. Tokoro, *Acc. Chem. Res.* **2012**, *45*(10), 1749–1758, b) S. Vaucher, M. Li, S. Mann, *Angew. Chem. Int. Ed.* **2000**, *39*, 1793–1796; c) T. Uemura, S. Kitagawa, *J. Am. Chem. Soc.*, **2003**, *125*, 7814–7815.
- [55] L. Catala, D. Brnzei, Y. Prado, A. Gloter, O. Stéphan, G. Rogez, T. Mallah, *Angew. Chem. Int. Ed.* **2009**, *48*(1), 183–187.
- [56] a) M. F. Dumont, E. S. Knowles, A. Guet, D. M. Pajeroski, A. Gomez, S. W. Kycia, M. W. Meisel, D. R. Talham, *Inorg. Chem.* **2011**, *50*(10), 4295–4300; b) A. C. Felts, M. J. Andrus, E. S. Knowles, P. A. Quintero, A. R. Ahir, O. N. Risset, C. H. Li, I. Maurin, G. J. Halder, K. A. Abboud, M. W. Meisel, D. R. Talham, *J. Phys. Chem. C* **2016**, *120*(10), 5420–5429.
- [57] X. Roy, L. K. Thompson, N. Coombs, M. J. MacLachlan, *Angew. Chem. Int. Ed.* **2008**, *47*(3), 511–514.
- [58] a) C. D. S. Brites, P. P. Lima, N. J. O. Silva, A. Millan, V. S. Amaral, F. Palacio, L. D. Carlos, *Nanoscale* **2012**, *4*(16), 4799–4829; b) O. Kraieva, C. M. Quintero, I. Suleimanov, E. M. Hernandez, D. Lagrange, L. Salmon, W. Nicolazzi, G. Molnar, C. Bergaud, A. Bousseksou, *Small* **2016**, *12*(46), 6325–6331.
- [59] a) Y. Garcia, F. Robert, A. D. Naik, G. Zhou, B. Tinant, K. Robeyns, S. Michotte, L. Piraux, *J. Am. Chem. Soc.* **2011**, *133*(40), 15850–15853; b) C.-F. Wang, R.-F. Li, X.-Y. Chen, R.-J. Wei, L.-S. Zheng, J. Tao, *Angew. Chem. Int. Ed.* **2015**, *54*(5), 1574–1577.
- [60] C. Lochenie, K. G. Wagner, M. Karg, B. Weber, *J. Mater. Chem. C* **2015**, *3*(30), 7925–7935.

- [61] M. Giménez-Marqués, García-Sanz de Larrea, M. Luisa, E. Coronado, *J. Mater. Chem. C* **2015**, 3(30), 7946–7953.
- [62] G. Félix, W. Nicolazzi, L. Salmon, G. Molnár, M. Perrier, G. Maurin, J. Larionova, J. Long, Y. Guari, A. Bousseksou, *Phys. Rev. Lett* **2013**, 110(23), 235701.
- [63] J. R. Galán-Mascarós, E. Coronado, A. Forment-Aliaga, M. Monrabal-Capilla, E. Pinilla-Cienfuegos, M. Ceolin, *Inorg. Chem* **2010**, 49(12), 5706–5714.
- [64] Y. Raza, F. Volatron, S. Moldovan, O. Ersen, V. Huc, C. Martini, F. Brisset, A. Gloter, O. Stephan, A. Bousseksou, L. Catala, T. Mallah, *Chem. Commun* **2011**, 47(41), 11501–11503.
- [65] C. Bartual-Murgui, E. Natividad, O. Roubeau, *J. Mater. Chem. C* **2015**, 3(30), 7916–7924.
- [66] J. M. Herrera, S. Titos-Padilla, Pope, Simon J. A, I. Berlanga, F. Zamora, J. J. Delgado, K. V. Kamenev, X. Wang, A. Prescimone, E. K. Brechin, E. Colacio, *J. Mater. Chem. C* **2015**, 3(30), 7819–7829.
- [67] a) K. Senthil Kumar, M. Ruben, *Coord. Chem. Rev.* **2017**, 346, 176–205; b) P. N. Martinho, C. Rajnak, M. Ruben in *Spin-Crossover Materials*; (Ed. M. A. Halcrow), John Wiley & Sons Ltd, Chichester, **2013**, 375–404.
- [68] E. Coronado, J. R. Galán-Mascarós, M. Monrabal-Capilla, J. García-Martínez, P. Pardo-Ibañez, *Adv. Mater* **2007**, 19(10), 1359–1361.
- [69] T. Forestier, S. Mornet, N. Daro, T. Nishihara, S.-I. Mouri, K. Tanaka, O. Fouche, E. Freysz, J.-F. Letard, *Chem. Commun.* **2008**(36), 4327–4329.
- [70] a) I. Boldog, A. B. Gaspar, V. Martínez, P. Pardo-Ibañez, V. Ksenofontov, A. Bhattacharjee, P. Gütllich, J. A. Real, *Angew. Chem. Int. Ed* **2008**, 47(34), 6433–6437; b) F. Volatron, L. Catala, E. Rivière, A. Gloter, O. Stéphan, T. Mallah, *Inorg. Chem* **2008**, 47(15), 6584–6586.
- [71] a) T. Forestier, A. Kaiba, S. Pechev, D. Denux, P. Guionneau, C. Etrillard, N. Daro, E. Freysz, J.-F. Letard, *Chem. Eur. J.* **2009**, 15(25), 6122–6130; b) V. Martínez, I. Boldog, A. B. Gaspar, V. Ksenofontov, A. Bhattacharjee, P. Gütllich, J. A. Real, *Chem. Mater* **2010**, 22(14), 4271–4281; c) A.

Tissot, *New J. Chem.* **2014**, 38(5), 1840; d) S. M. Neville, C. Etrillard, S. Asthana, J.-F. Létard, *Eur. J. Inorg. Chem.* **2010**, (2), 282–288.

[72] A. Tokarev, L. Salmon, Y. Guari, W. Nicolazzi, G. Molnár, A. Bousseksou, *Chem. Commun.* **2010**, 46(42), 8011.

[73] F. Prins, M. Monrabal-Capilla, E. A. Osorio, E. Coronado, H. S. J. van der Zant, *Adv. Mater.* **2011**, 23(13), 1545–1549.

[74] J. Dugay, M. Aarts, M. Giménez-Marqués, T. Kozlova, H. W. Zandbergen, E. Coronado, H. S. J. van der Zant, *Nano Letters* **2017**, 17(1), 186–193.

[75] a) S. Cobo, G. Molnár, J. A. Real, A. Bousseksou, *Angew. Chem. Int. Ed* **2006**, 45(35), 5786–5789; b) G. Molnár, S. Cobo, J. A. Real, F. Carcenac, E. Daran, C. Vieu, A. Bousseksou, *Adv. Mater* **2007**, 19(16), 2163–2167; c) C. Thibault, G. Molnár, L. Salmon, A. Bousseksou, C. Vieu, *Langmuir* **2010**, 26(3), 1557–1560; d) J. Larionova, L. Salmon, Y. Guari, A. Tokarev, K. Molvinger, G. Molnár, A. Bousseksou, *Angew. Chem. Int. Ed.* **2008**, 47(43), 8236–8240.

[76] M. J. MacLachlan, M. Ginzburg, N. Coombs, T. W. Coyle, N. P. Raju, J. E. Greedan, G. A. Ozin, I. Manners, *Science* **2000**, 287(5457), 1460–1463.

[77] G. A. Ozin, T. Asefa, M. J. MacLachlan, N. Coombs, *Nature* **1999**, 402(6764), 867–871.

[78] G. R. Whittell, M. D. Hager, U. S. Schubert, I. Manners, *Nat Mater* **2011**, 10(3), 176–188.

[79] G. Liu, M. Lazzari, S. Lecommandoux, Eds, *Block Copolymers in Nanoscience*; Wiley, Weinheim, Chichester, **2006**.

[80] a) T. Kitao, Y. Zhang, S. Kitagawa, B. Wang, T. Uemura, *Chem. Soc. Rev.* **2017**, 46, 3108–3133; b) Q.-L. Zhu, Q. Xu, *Chem. Soc. Rev.*, **2014**, 43, 5468–5512.

[81] a) B. Wu, J. Pan, L. Ge, L. Wu, H. Wang, T. Xu, *Scientific Reports* **2014**, 4, 4334; b) T. Rodenas, I. Luz, G. Prieto, B. Seoane, H. Miro, A. Corma, F. Kapteijn, Llabrés i Xamena, Francesc X, J. Gascon, *Nat. Mater.* **2015**, 14(1), 48–55; c) T.-S. Chung, L. Y. Jiang, Y. Li, S. Kulprathipanja, *Prog. Polymer Sci.* **2007**, 32(4), 483–507; d) M. A. Aroon, A. F. Ismail, T. Matsuura, M. M. Montazer-Rahmati, *Separation and Purification Technology* **2010**, 75(3), 229–242.

- [82] a) S. Dhar, W. L. Daniel, D. A. Giljohann, C. A. Mirkin, S. J. Lippard, *J. Am. Chem. Soc.* **2009**, *131*(41), 14652–14653; b) X.-Q. Zhang, X. Xu, R. Lam, D. Giljohann, D. Ho, C. A. Mirkin, *ACS nano* **2011**, *5*(9), 6962–6970.
- [83] W. Morris, W. E. Briley, E. Auyeung, M. D. Cabezas, C. A. Mirkin, *J. Am. Chem. Soc.* **2014**, *136*(20), 7261–7264.
- [84] C. M. Calabrese, T. J. Merkel, W. E. Briley, P. S. Randeria, S. P. Narayan, J. L. Rouge, D. A. Walker, A. W. Scott, C. A. Mirkin, *Angew. Chem. Int. Ed.* **2015**, *54*(2), 476–480.
- [85] C. He, D. Liu, W. Lin, *Biomaterials* **2015**, *36*, 124–133.
- [86] F. Li, T. Li, W. Cao, L. Wang, H. Xu, *Biomaterials* **2017**, *133*, 208–218.
- [87] X. Xu, T. Lu, X. Liu, X. Wang, *Chem. Eur. J* **2015**, *21*(48), 17430–17436.
- [88] H. Wei, H. Zhang, G. Jin, T. Na, G. Zhang, X. Zhang, Y. Wang, H. Sun, W. Tian, B. Yang, *Adv. Funct. Mater* **2013**, *23*(32), 4035–4042.
- [89] S. Förster, M. Antonietti, *Adv. Mater.* **1998**, *10*(3), 195–217.
- [90] a) S.-H. Yun, S. I. Yoo, J. C. Jung, W.-C. Zin, B.-H. Sohn, *Chem. Mater.* **2006**, *18*(24), 5646–5648; b) W. Lee, S. Y. Lee, X. Zhang, O. Rabin, R. M. Briber, *Nanotechnology* **2013**, *24*(4), 45305.
- [91] R. D. Bennett, G. Y. Xiong, Z. F. Ren, R. E. Cohen, *Chem. Mater.* **2004**, *16*(26), 5589–5595.
- [92] C. Tang, D. Amin, P. B. Messersmith, J. E. Anthony, R. K. Prud'homme, *Langmuir* **2015**, *31*(12), 3612–3620.
- [93] X. Roy, J. K.-H. Hui, M. Rabnawaz, G. Liu, M. J. MacLachlan, *Angew. Chem. Int. Ed.* **2011**, *50*(7), 1597–1602.
- [94] X. Roy, J. K.-H. Hui, M. Rabnawaz, G. Liu, M. J. MacLachlan, *J. Am. Chem. Soc.* **2011**, *133*(22), 8420–8423.

- [95] a) B. Weber, W. Bauer, J. Obel, *Angew. Chem. Int. Ed.* **2008**, *47*(52), 10098–10101; b) B. Weber, W. Bauer, T. Pfaffeneder, M. M. Dîrtu, A. D. Naik, A. Rotaru, Y. Garcia, *Eur. J. Inorg. Chem.* **2011**, (21), 3193–3206; c) C. Lochenie, W. Bauer, A. P. Railliet, S. Schlamp, Y. Garcia, B. Weber, *Inorg. Chem.* **2014**, *53*(21), 11563–11572; d) K. Dankhoff, C. Lochenie, F. Puchtler, B. Weber, *Eur. J. Inorg. Chem.* **2016**, (13-14), 2136–2143; e) C. Lochenie, A. Gebauer, O. Klimm, F. Puchtler, B. Weber, *New J. Chem.* **2016**, *40*(5), 4687–4695.
- [96] a) S. Schlamp, K. Dankhoff, B. Weber, *New J. Chem.* **2014**, *38*(5), 1965–1972; b) S. Schlamp, P. Thoma, B. Weber, *Chem. Eur. J.* **2014**, *20*(21), 6462–6473; c) S. Schlamp, B. Weber, A. D. Naik, Y. Garcia, *Chem. Commun* **2011**, *47*(25), 7152–7154.
- [97] a) B. Weber, R. Tandon, D. Himsl, *Z. Anorg. Allg. Chem.* **2007**, *633*(8), 1159–1162; b) B. Weber, E. S. Kaps, C. Desplanches, J.-F. Létard, *Eur. J. Inorg. Chem.* **2008**, (19), 2963–2966.
- [98] C. Göbel, T. Palamarciuc, C. Lochenie, B. Weber, *Chem. Asian J.* **2014**, *9*(8), 2232–2238.
- [99] K. Wu, L. Shi, W. Zhang, Y. An, X. Zhang, Zhanyong Li, X. X. Zhu, *Langmuir*, *Vol. 22*, **2006**, 1474–1477.
- [100] R. Ma, B. Wang, X. Liu, Y. An, Y. Li, Z. He, and L. Shi, *Langmuir*, **2007**, 7498–7504.
- [101] X. Jiang and B. Zhao, *Macromolecules*, **2008**, *41* (23), 9366–9375.
- [102] Reichstein, P., Gödrich, S., Papastavrou, G., Thelakkat, M., *Macromolecules*, **2016**, *49*(15), 5484–5493.
- [103] C.D. Heinrich; M. Thelakkat, *Journal of Materials Chemistry C*, **2016**, *4*, 5370–5378.

3. Overview

This thesis comprises four chapters (4-7), of those are two accepted publications and two to be submitted. The individual contributions to joint publications are pointed out in Chapter 3.2.

3.1 Synopsis

As explicated in 2.3.3, this work covers the synthesis and characterisation of spin crossover (SCO) nanoparticles with the aim to build miniaturised functional materials in a matrix, to produce SCO-based devices like sensors or smart contrast agents. The main goal is to synthesise stable SCO nanoparticle systems by using polystyrene-*b*-poly-(4-vinylpyridine) (PS-*b*-P4VP) block copolymers, to characterise them and to study the SCO properties of the nanoparticles in comparison to the SCO bulk material. Additionally, the size control of the nanoparticles by the use of block copolymers with various block lengths and different amounts of poly-(4-vinylpyridine) (P4VP) should be investigated. The control of the particle size should lead to tailored SCO properties.

In the first part of this work, the growth of the coordination polymer in a BCP matrix was studied. The used BCP has a molecular weight of about $150000 \text{ g}\cdot\text{mol}^{-1}$ with 15% wt of P4VP (≈ 204 units) and 85% wt of PS (≈ 1234 units). A combination of the repeating units polystyrene (PS) and poly-(4-vinylpyridine) (P4VP) leads to a self-assembly of the BCPs (PS-*b*-P4VP). Styrene has a better solubility than 4-vinylpyridine in solvents as toluene or tetrahydro-furan which in consequence leads to a micellar structure with PS as a shell and P4VP as core. To control the size and shape of the nanoparticles TEM images were taken. The obtained samples showed no micro crystal impurities that would significantly influence the magnetic properties. The shape of the NPs was spherical with a core-shell structure and a narrow size distribution (Figure 3.1).

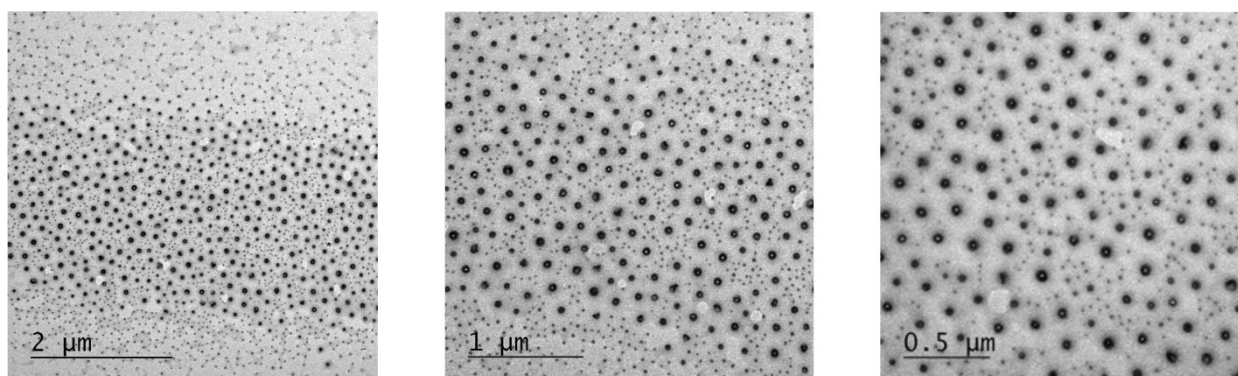


Figure 3.1: TEM images of NPs synthesised by refluxing PS-*b*-P4VP and [Fe(Lb)(MeOH)₂] in THF at three different magnifications.

To optimize the reaction conditions, the optimal ratio [Fe(Lb)(MeOH)₂] : 4,4'-bipyridine (**bipy**) was determined. A concentration row from 1:1-1:5 was done. TEM images were taken to find the best distribution of the nanoparticles in the polymer matrix and the ratio 2.5:1 was chosen for the first synthesis step. After two hours of reflux, the bridging ligand **bipy** was added and the synthesis was refluxed for one more hour. This synthesis step should lead to a growth of a coordination polymer (CP) [Fe(Lb)(bipy)]_n in the BCP matrix (Figure 3.2). After adding the bridging ligand, one reaction cycle (RC) was completed. To yield a slow and controlled particle growth, further reaction cycles were done with five RC as maximum, with subsequently addition of **bipy** and [Fe(Lb)(MeOH)₂]. At the end, the solvent was removed via cold distillation and all samples were dried via lyophilisation (freeze drying) with liquid nitrogen.

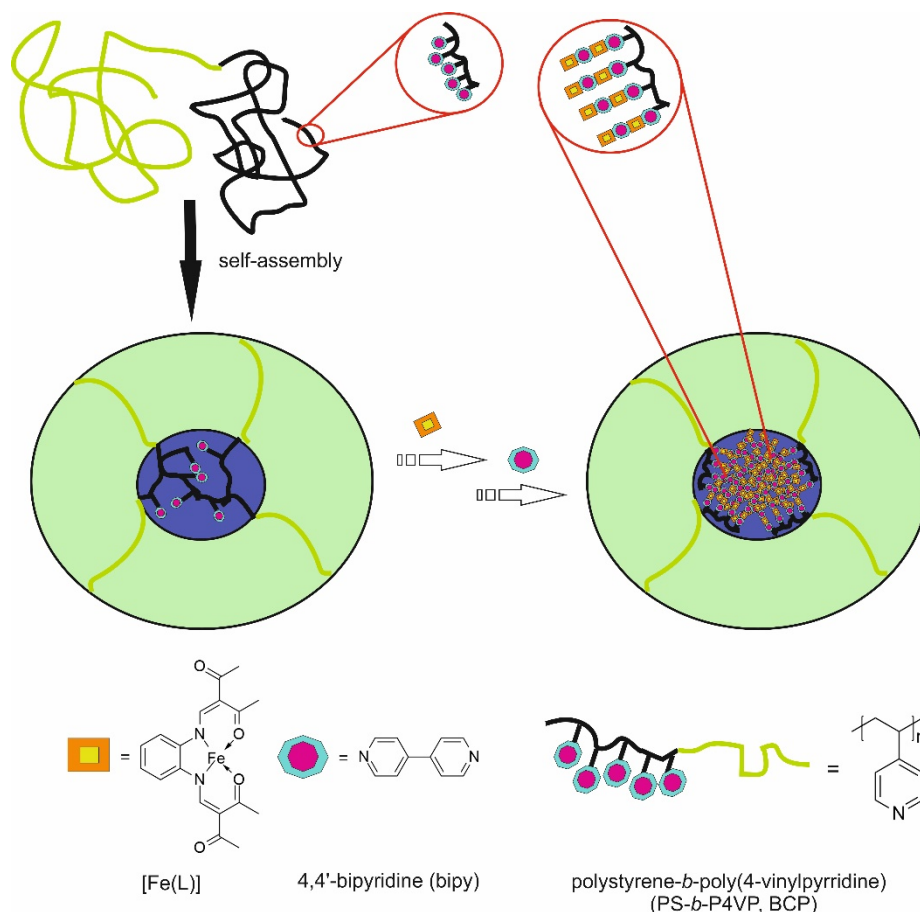


Figure 3.2: Schematic presentation of the formation of CPs in a BCP matrix using inverse micelles as nanoreactors and different RC to increase the crystallinity of the nanoparticles.

TEM and SEM images of all synthesised products showed no micro or sub-micro crystals and an average core size of about 40-60 nm. Dynamic light scattering (DLS) was done to examine the hydrodynamic radius of the particles in solution. An energy dispersive X-ray spectroscopy (EDX) measurement of the product after five RC was done, to show the presence of iron inside the core of the nanoparticles. EDX showed Fe, O and N in the core of the nanoparticles, a proof of the SCO CP in the polymer matrix. Powder X-ray diffraction measurements of 1-5 RC showed an increase in the crystallinity of the nanoparticles. IR spectra of 1-5 RC showed an increase of the characteristic C=O bond in the Fe(II) complex at about 1600 cm^{-1} (Figure 3.3).

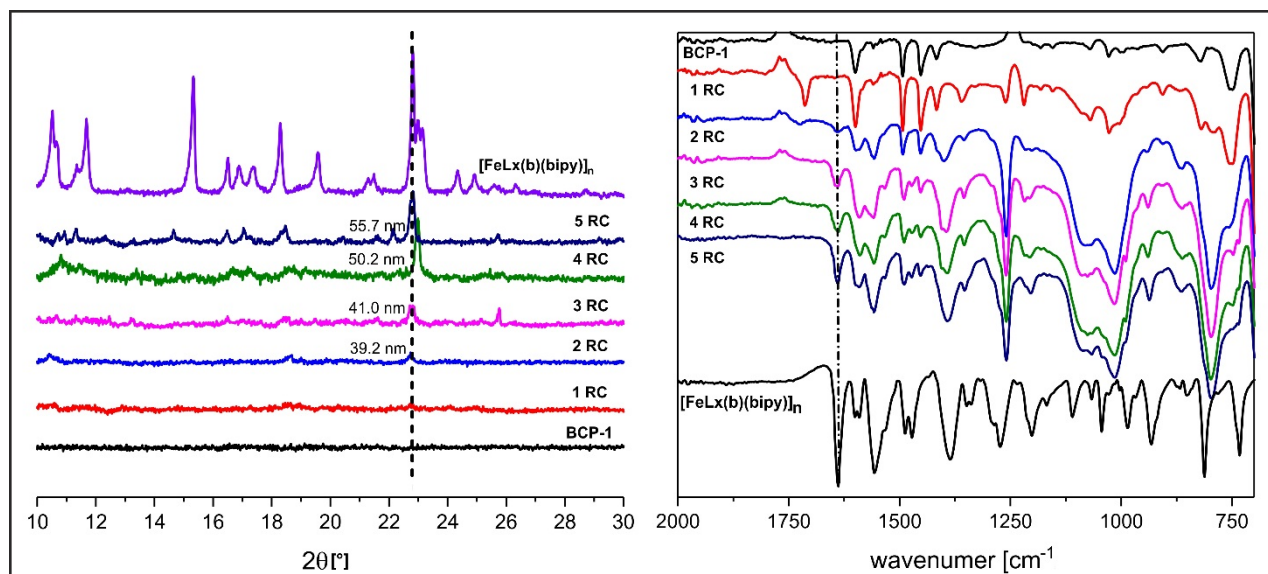


Figure 3.3: Increase of crystallinity of the nanoparticles in powder XRD (left) and particle growth showed by an increase of the characteristic C=O bond about 1600 cm^{-1} in IR (right).

Temperature dependent magnetic measurements were done to investigate the SCO properties of the nanoparticles. Those measurements showed no SCO behaviour for one RC, a rising gradual SCO up from two to four RC and a small hysteresis of about 3 K after five reaction cycles. The oxidation state and the ratio of Fe(II) in the high spin- (HS) and low spin (LS) state at room temperature (RT) were measured by Mössbauer spectroscopy.

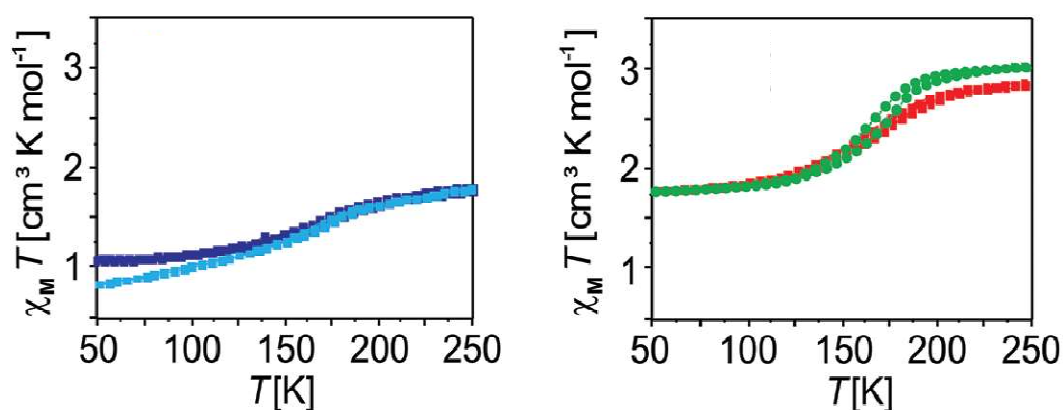


Figure 3.4 SQUID measurements of 2,3 (left, blue and purple) and 4 (right, red) RC with rising gradual SCO. After 5 RC, a 3 K wide hysteresis appeared (right, green).

Mössbauer spectroscopy measurements showed a HS vs. LS ratio of about 50:50 for two RC rising up to about 100% HS at five RC. The Fe(II)-LS fraction results from Fe(II) centers coordinated by two 4VP units of the BCP.

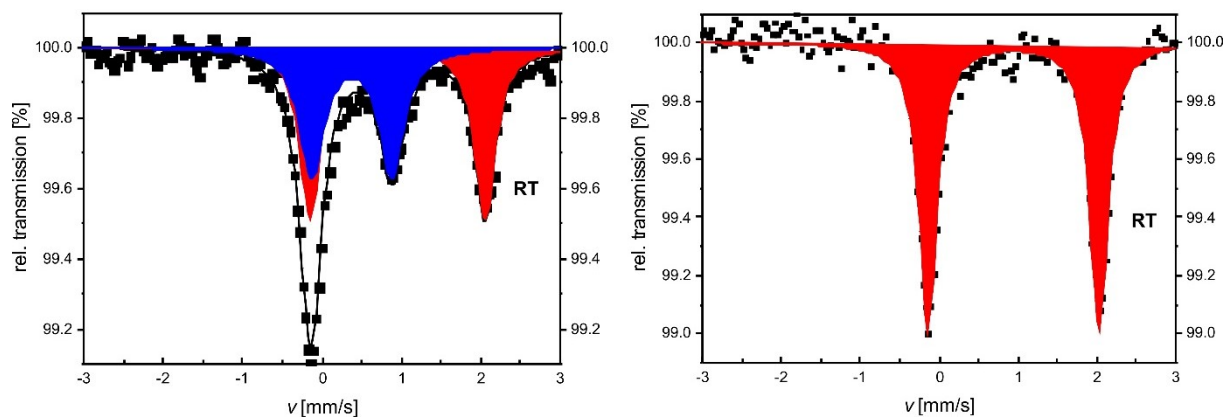


Figure 3.5: Mössbauer spectroscopy measurements of $[\text{Fe}(\text{Lb})(\text{bipy})]_n$ nanoparticles after 2 (left) and 5 (right) RC at room temperature. The HS : LS ratio after two RC is about 50% and rises up to 100% HS at five RC.

After the successful synthesis of Fe(II) SCO nanoparticles, the aim of chapter 5 was to synthesise nanoparticles of other known SCO systems. There are different possibilities to change the SCO behaviour, either by a change of R^1 and R^2 from the Schiff base-like ligands (see chapter 2.2) or a change of the bridging ligand 4,4'-bipyridine towards other bipyridine-like ligands i.e. 1,2-bis(pyrid-4-yl)ethane (**bpea**), 1,2-bis-(pyrid-4-yl)ethylene (**bpee**) or 4,4'-dipyridylethyne (**bpey**). In chapter 5 the relation between the flexibility of the bridging ligand and the formation of nanoparticles vs. small crystals was investigated. The critical complex concentration in the BCP before the formation of micro-crystals is observed, was determined as function of the used bridging ligand. The ligands **bpea**, **bpee** and **bpey** show different flexibility (**bpea** > **bpee** > **bpey**) leading to significant differences in the solubility of the corresponding coordination polymer. A higher flexibility leads to a higher solubility of the CP that could support the formation of micro-crystals as unwanted side product.

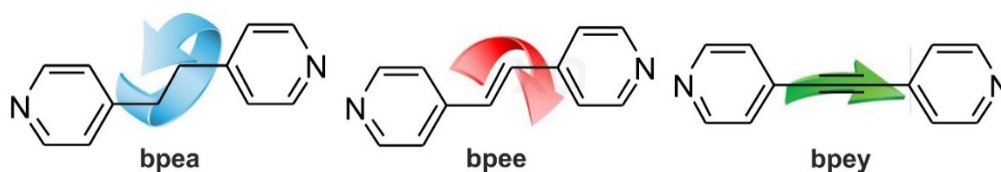


Figure 3.6 Schematic representation of the different flexibilities of the bridging ligands **bpea** (left), **bpee** (middle) and **bpey** (right).

The syntheses of the CPs@BCP composite were the same as described in chapter 4. Samples with different numbers of RC (1-5) were prepared with either THF or toluene as solvent and in the end, the solvent was removed via cold distillation and the sample was dried via lyophilisation. All synthesised samples were analysed with TEM images and x-ray diffraction. The average size of the nanoparticles did not depend on the number of RC or the used solvent. The nanoparticles showed an average size of about 40-50 nm. For toluene as solvent micro crystals were observed for all samples after two or three RC. From THF, CPs with **bpea** showed sub-micro crystals after five RC, with **bpee** already after four RC. Similar to the CP with **bipy** from chapter 4, the CPs with **bpey** did not show sub-micro crystals at all. Obviously, the flexibility of the bridging ligand influences the crystal growth (Figure 3.7), but it is not the only important factor.

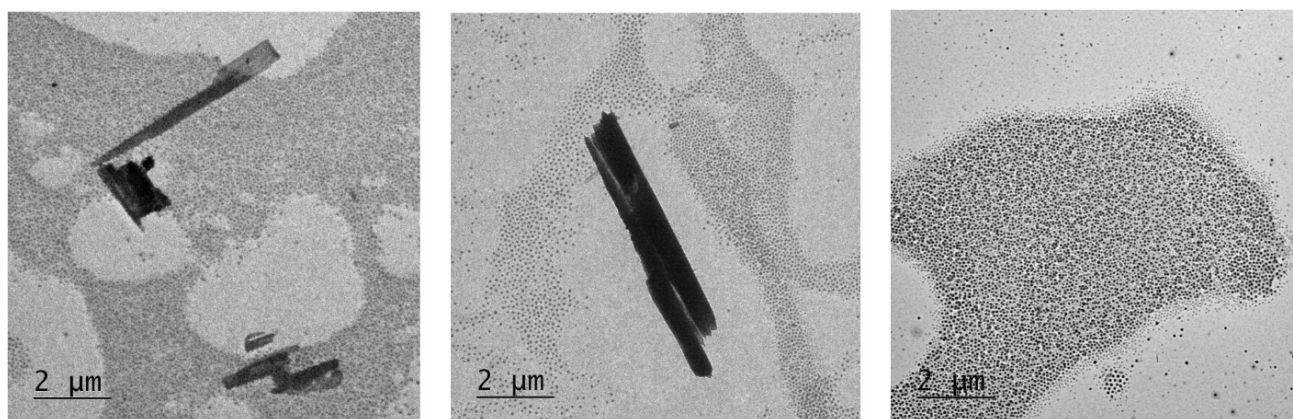


Figure 3.7: TEM images of Fe(II) complexes with five RC with **bpea** (left), four RC with **bpee** (middle) and five RC with **bpey** (right) in BCP-1.

IR measurements were done for all samples to show the growth of the CP by the increase of the characteristic C=O bond at about 1600 cm^{-1} . SQUID measurements of Fe(II) complexes with one RC showed no SCO behaviour. For samples with two to four RC with **bpea** and **bpey** a gradual SCO occurred. All samples with **bpee** showed pure HS. $[\text{Fe}(\text{Lb})(\text{bpea})]_n@BCP-1$ with five RC showed a small hysteresis due to the formation of sub-micro crystals. $[\text{Fe}(\text{Lb})(\text{bpey})]_n@BCP-1$ with five RC looks a gradual SCO. To determine the spin transition of $[\text{Fe}(\text{Lb})(\text{bpey})]_n@BCP-1$ exactly, the first derivation of the graph, $d(\chi_M T)/d(T)$ vs. T was done and illustrated. A two stepped SCO appeared with a maximum at 185 K and 115 K (Figure 3.9).

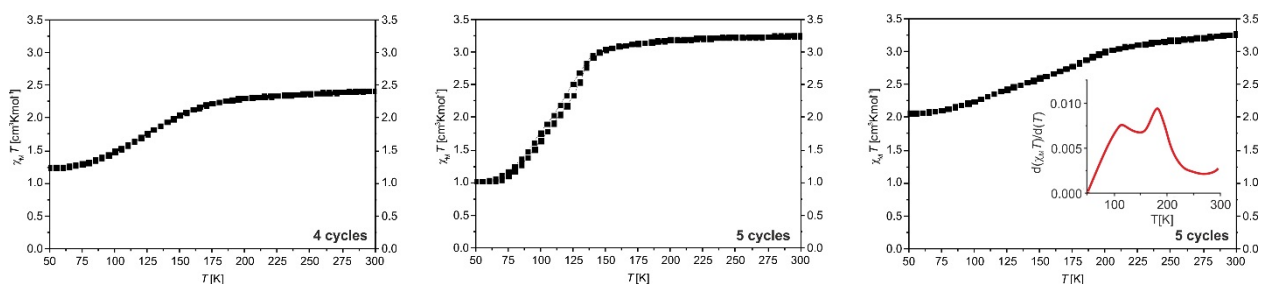


Figure 3.8: SQUID measurements for four and five RC with bpea (left and middle) and five RC with bpey (right). The first derivation $d(\chi_M T)/d(T)$ vs. T of the gradual SCO (right) was done to illustrate a stepwise SCO behaviour of $[\text{Fe}(\text{Lb})(\text{bpey})]_n$ with two different maxima (ST) at 185 K and 115 K.

In chapter 5 we could show, that **bpee** leads to the fastest formation of sub-micro crystals. This illustrates, that not only the flexibility of the ligand, but also the spin state of the complex is of importance for the formation. TEM images showed the expected order for the formation of sub-micro crystals (**bpee** > **bpea** > **bpey**).

For complexes with an octahedral geometry, a weak ligand field splitting leads to a HS compound and antibonding orbitals are occupied. This configuration supports ligand exchange and a fast exchange increases the possibility to form sub-micro crystals outside the polymer matrix. In agreement with this consideration, the complex $[\text{Fe}(\text{Lb})(\text{bpee})]_n$ as a pure HS compound shows the weakest ligand field splitting. This leads to the fastest crystallisation outside of the polymer matrix. The SCO compounds $[\text{Fe}(\text{Lb})(\text{bpea})]_n$, $[\text{Fe}(\text{Lb})(\text{bpey})]_n$ follow the order of rigidity. With an increasing flexibility of the bridging ligand, the probability to form sub-micro crystals increases.

Chapter 4 showed the possibility to create SCO nanoparticles by using BCP nanoreactors. Chapter 5 showed the influence of the flexibility of the bridging ligand to the formation of sub-micro crystals in Fe(II) SCO complexes. In Chapter 6, the influence of the molar mass and the amount of P4VP of the BCPs was investigated. First tests with different block copolymers led to different particles sizes and shapes. In chapter 4 and 5 PS-*b*-P4VP (BCP-1) with a molecular mass of about 150000 g·mol⁻¹ and 15% of P4VP was used. In this chapter two other BCPs (BCP-2 and BCP-3) were used to synthesise nanoparticles. The molar masses and amounts of P4VP are given in Table 3.1.

Table 3.1: Molecular mass and amount of P4VP of the used BCPs.

block copolymer	molecular mass [g·mol ⁻¹]	amount of P4VP [%]
BCP-1	150000	15
BCP-2	100000	25
BCP-3	250000	33

[Fe(Lb)(bipy)]_n was used in chapter 6 and the ratio polymer : Fe complex had to be calculated due to the different molecular masses of the BCP. It is shown, that higher molecular masses of the BCP lead to an increase in particle sizes, whereas a rising amount of P4VP leads to a change in the shape of the nanoparticles. For the pure BCPs it is reported that an amount of more than ≈19% of P4VP leads to nanorods and/or vesicles. BCP-1 and BCP-2 showed spherical nanoparticles, whereas BCP-3 formed spherical nanoparticles, nanorods or vesicles. The results for BCP-1 are reported in chapter 4 and are in the following compared with the samples with BCP-2 and BCP-3 that were synthesised here. All samples with different RC (1-5) were synthesised similar to those in chapter 4 and 5. TEM images were taken to characterise size and shape of the nanoparticles and to control the presence of micro- or sub-micro crystals. Samples with 1-3 RC showed no sub-micro crystals. In RC four, BCP-2 as well as BCP-3 showed sub-micro crystals. However, the samples with five RC as well BCP-2 as BCP-3 showed pure nanoparticles without coexistence of sub-micro crystals. An explanation of the sub-micro crystals was given by powder XRD measurements (Figure 3.9), namely a partial oxidation of the sample

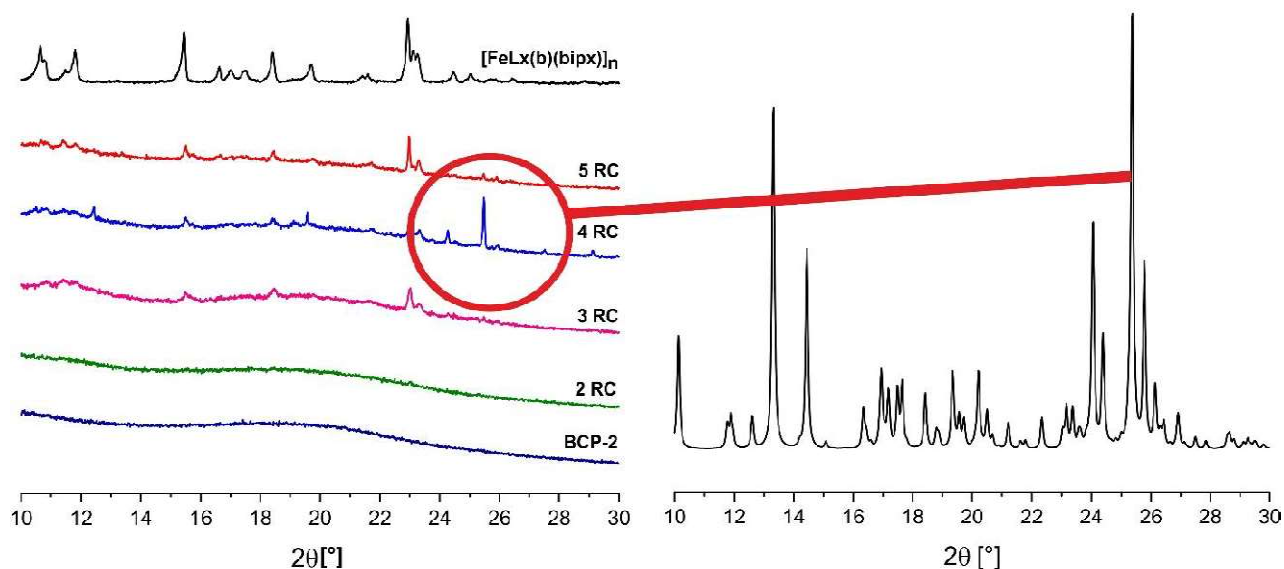


Figure 3.9: Powder XRD measurement of 1-5 RC of $[\text{Fe}(\text{Lb})(\text{bipy})]_n@ \text{BCP-2}$ with a 2θ peak at about 26° , characteristic for an oxidised Fe(III) complex (right) after four RC.

Both, the samples synthesised in BCP-2 and BCP-3 with four RCs showed a partially oxidised signal at 2θ of about 26° . The oxidised μ -oxido complex of the Fe showed a high affinity to crystallise. Thus the oxidation of the Fe complex could be responsible for the formation of sub-micro crystals at four RCs. The average particle sizes of the three different CP@BCPs are given in Table 3.2.

Table 3.2: Average particle sizes of the SCO nanoparticles in different polymers.

block copolymer	TEM average size [nm]	molecular mass [$\text{g}\cdot\text{mol}^{-1}$]
BCP-2	44	100000
BCP-1	53	150000
BCP-3	75	250000

The increase in the particle size with a higher molecular mass of the BCPs is observed (Table 3.2). BCP-3 with the highest molecular weight led to nanoparticles with the highest average size of 75 nm. TEM images also showed different particle shapes from BCP-1 to BCP-3 (Figure 3.10).

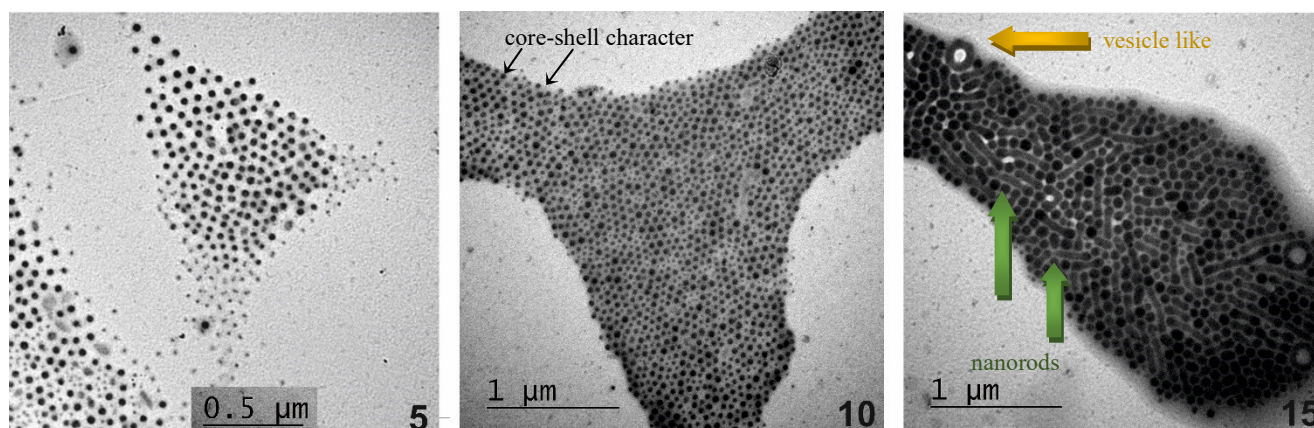


Figure 3.10: TEM images from nanoparticles with five RCs in BCP-1 (left), BCP-2 (middle) and BCP-3 (right) to show the different shapes of the nanoparticles and the change in their typical core-shell character from BCP-1 towards BCP-3.

In the pure BCP an amount of more than 19% P4VP led to rods. By the use of BCP-3 as nanoreactor, a mixture of spherical nanoparticles, nanorods and vesicles occurred, whereas BCP-2 showed monodisperse, spherical nanoparticles similar to BCP-1. The expected change in shape occurred somewhere between 25% and 33% of P4VP (Figure 3.11). Please note that in contrast to the pure BCP, that is treated as melt, the NPs are synthesized in a solution leading to different boundary conditions.

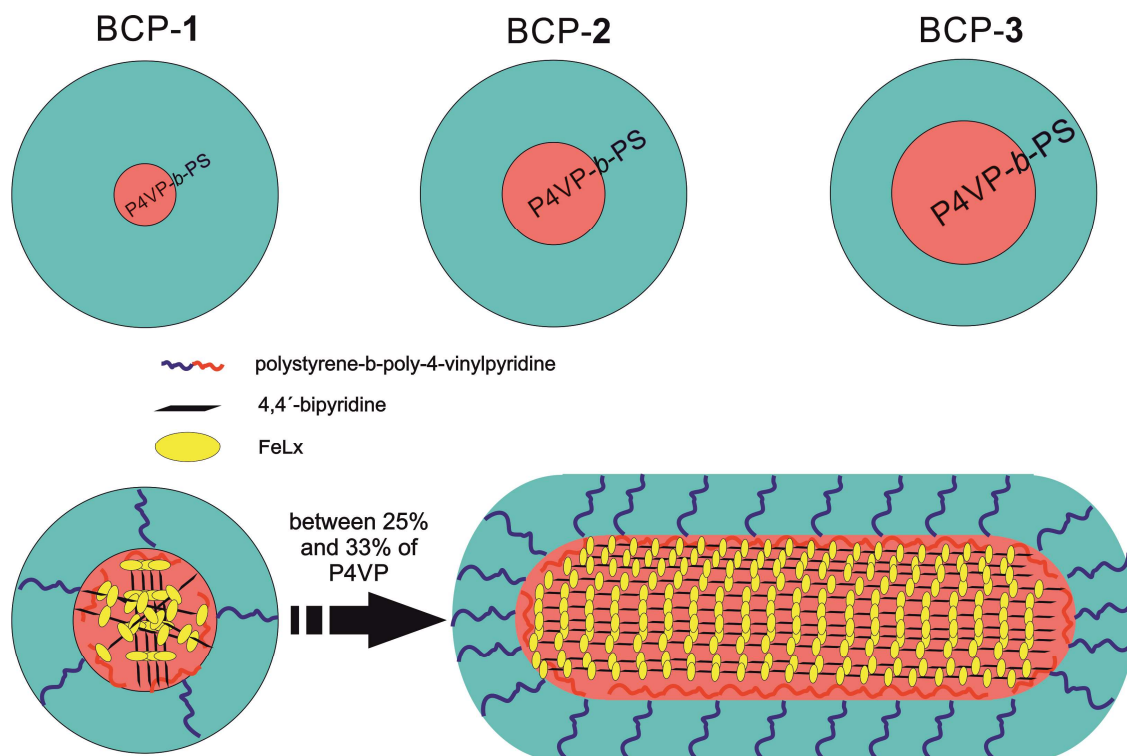


Figure 3.11: Schematic representation of the trend towards rods (idealised) or vesicles with higher amounts of P4VP in the BCP.

SQUID measurements of the Fe(II) complexes showed no SCO behaviour for one RC. After two RC as well in BCP-2 as in BCP-3 a gradual SCO appeared. After the third RC, a transition from a gradual SCO towards hysteresis started. Four and five RC showed an incomplete SCO with a 25 K wide hysteresis with a $T_{1/2\downarrow}$ of 200 K and a $T_{1/2\uparrow}$ of 225 K. The nanoparticles@BCP-3 matrix shows a wide hysteresis at five RC (Figure 3.14). Five RC with BCP-3 showed no sub-micro crystals.

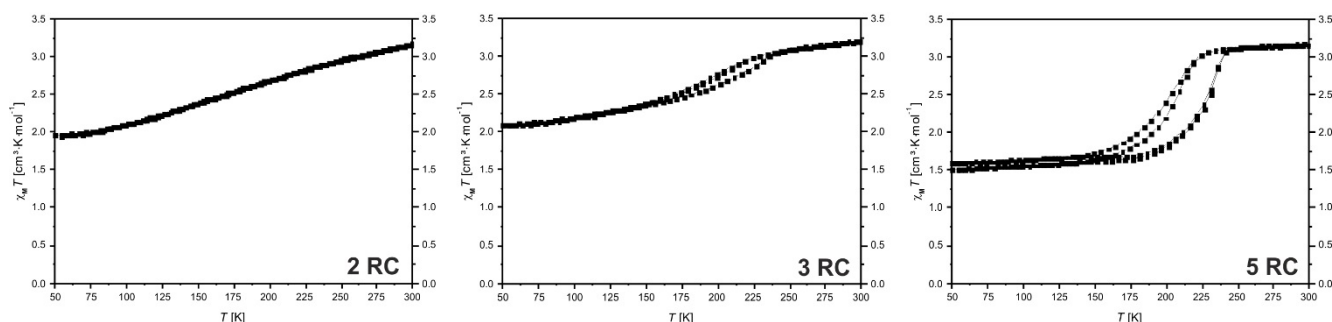


Figure 3.12: Magnetic measurements of two (left), three (middle) and five (right) RC of $[\text{Fe}(\text{Lb})(\text{bipy})]_n@BCP-3$ to show the rising SCO with higher crystallinity of the synthesised nanoparticles.

In Chapter 6 it was shown the nanoparticle size is controlled by the molar mass of the used BCP. The amount of P4VP is responsible for the nanoparticle shape. Between 25% and 33% of P4VP the shape changed from pure spherical particles towards a mixture of spherical nanoparticles, nanorods and vesicle-like structures, differentiated by TEM pictures.

In Chapter 7 the SCO compound $[\text{Fe}(\text{Lc})(\text{bipy})]_n$ was used to synthesise SCO nanoparticles. For the bulk material of this complex two different species are known with a gradual SCO between 280 K and 110 K and an abrupt SCO with a 6 K wide hysteresis with $T_{1/2\downarrow}$ of 330 K and $T_{1/2\uparrow}$ of 336 K, as shown in chapter 2.2. In this chapter, the targeted synthesis of both SCO systems was carried out. To gain nanoparticles with different sizes and shapes, BCP-1 and BCP-2 were used. Synthesis with fast diffusion under reflux should lead to SCO below RT, synthesis with slow diffusion without reflux should lead to SCO above RT. Two percent of methanol were added to the toluene solution to help the micelles formation. All synthesis were done as described in chapter 4-6. Different RC (1-5) were used to grow the CP in the BCP matrix and increase the crystallinity of the particles. TEM images were made to investigate the particle sizes and shapes. Table 3.3 gives an overview of all samples prepared in chapter 7.

Table 3.3: Overview of all samples with $[\text{Fe}(\text{Lc})(\text{bipy})]_n$ in BCP-1 and BCP-2.

sample	BCP	RC	solvent
1	1	2	toluene
2	1	3	toluene
3	1	4	toluene
4	1	5	toluene
5	1	2	THF
6	1	3	THF
7	1	4	THF
8	1	5	THF
9	2	2	toluene
10	2	3	toluene
11	2	4	toluene
12	2	5	toluene

3. Overview

13	2	2	THF
14	2	3	THF

In BCP-1 without reflux, after five RC sub-micro crystals appeared. In BCP-2 without reflux, after three RC sub-micro crystals appeared. Longer reaction time without reflux led to a higher affinity to crystallise. Likewise, without refluxing, nanorods and vesicles appeared in BCP-1, too. Synthesis with reflux led to sub-micro crystals with BCP-1 after five RC, whereas the synthesis with BCP-2 with reflux led to no sub-micro crystals at all (Figure 3.13). DLS measurements of all samples with five RC showed no monodisperse signals due to the formation of sub-micro crystals and due to the formation of nanorods in BCP-2.

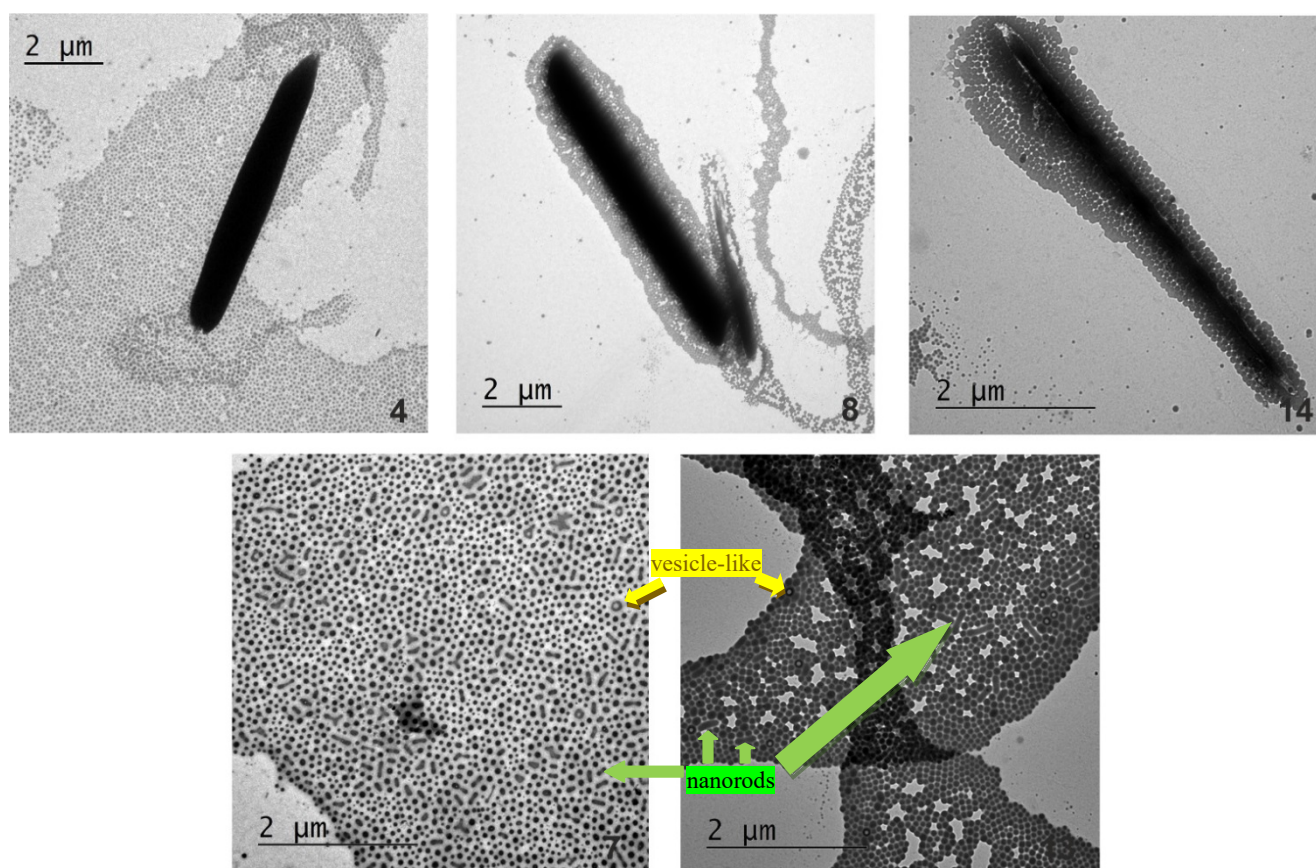


Figure 3.13: TEM images of $[\text{Fe}(\text{Lc})(\text{bipy})]_n$ in BCP-1 with reflux after five RC (top left), BCP-1 without reflux after four RC (top middle) and BCP-2 without reflux after three cycles (top right). As well TEM images of BCP-1 without reflux at three RC (bottom left) and BCP-2 without reflux at two RC (bottom right) are showed to illustrate the growth of nanorods and vesicle-like structures without refluxing.

SQUID measurements of all samples with more than two RC without reflux showed SCO above RT. Slow diffusion of the reaction led to a mixture of both SCO species with three or more RC (**6-8**). There is a rise of the 6 K wide hysteresis from the bulk material to a 28 K wide hysteresis with $T_{1/2\uparrow}$ of 338 K and $T_{1/2\downarrow}$ of 310 K. The $\chi_M T$ values for the full HS compound at 350 K is $3.2 \text{ cm}^3 \text{ K mol}^{-1}$, expected for an $\text{Fe}^{(\text{II})}$ HS. The hysteresis is followed by an incomplete gradual SCO between 300 K and 100 K with a $\chi_M T$ of about $1.0 \text{ cm}^3 \text{ K mol}^{-1}$ (Figure 3.14). All samples with reflux showed SCO below RT. Three and four RC (**10, 11**) led to an incomplete gradual SCO between 270 K and 70 K, comparable with the SCO of the bulk material (280 K – 110 K). Five RC (**12**) led to a gradual SCO with beginning hysteresis of about 8 K with $T_{1/2\downarrow}$ of 200 K and $T_{1/2\uparrow}$ of 208 K.

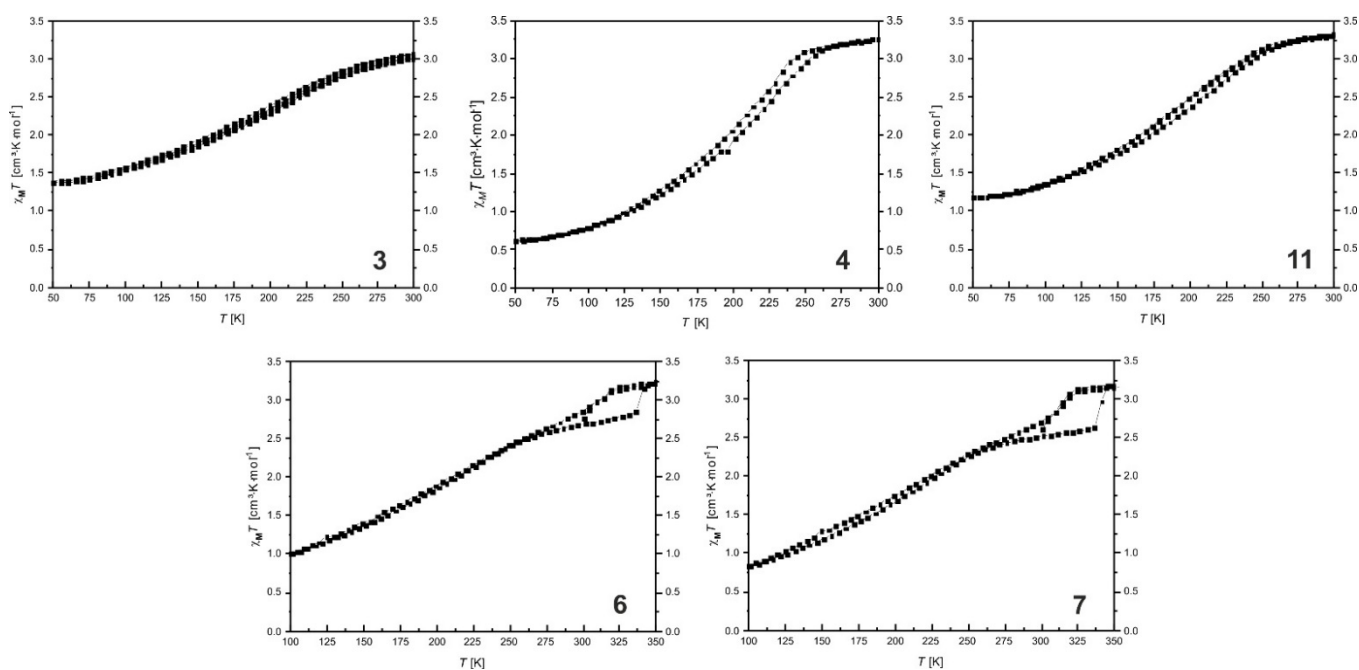


Figure 3.14: SQUID measurements of four RC (**3**) with reflux in BCP-1 (top left), five RC (**4**) with reflux in BCP-1 (top middle), four RC (**11**) with reflux in BCP-2 (top right), three RC (**6**) without reflux in BCP-1 (bottom left) and four RC (**7**) without reflux in BCP-1 (bottom right).

3.2 Individual contributions to joint publications

The results presented in this thesis were obtained in collaboration with others and are published, accepted, or are to be submitted as indicated below. In the following, the contributions of all co-authors to the publications are specified. The asterisk denotes the corresponding authors.

Chapter 4

This work was published in *Nanoscale* (*Nanoscale*, **2016**, *8*, 19058–19065) with the title

“Synthesis of [Fe(L)(bipy)]_n spin crossover nanoparticles using blockcopolymer micelles”.

Ottokar Klimm,^a Christoph Göbel,^a Sabine Rosenfeldt,^b Florian Puchtler,^c

Nobuyoshi Miyajima,^d Katharina Marquardt,^d Markus Drechsler,^e Josef Breu,^c

Stephan Förster,^b and Birgit Weber*^a

I synthesised and characterised all samples presented in this work, carried out the magnetic measurements, TEM measurements, DLS measurements, IR measurements, elemental analysis and wrote the experimental section, the conclusion and parts of the result section (TEM imaging, magnetic measurements, IR measurements, Powder XRD measurements). Christoph Göbel carried out parts of the TEM measurements. Katharina Marquardt and Nobuyoshi Miyajima carried out the EDX measurements at the BGI of the University of Bayreuth, interpreted the EDX data and I wrote this part in the manuscript. Florian Puchtler carried out the PXRD measurements and I interpreted the PXRD measurements and wrote this part in the manuscript. Sabine Rosenfeldt helped interpreting DLS measurements. Prof. Dr. Birgit Weber supervised this work, helped interpreting the magnetic (SQUID and Mössbauer) and imaging (TEM, DLS) data, wrote the introduction and was involved in scientific discussions and correction of the manuscript.

Chapter 5

This work was published in Beilstein Journal of Nanotechnology (*Beilstein J. Nanotech.*, **2017**, *8*, 1318–1327) with the title

“Synthesis of [Fe(Leg)(Lax)]_n Coordination Polymer Nanoparticles using Blockcopolymer Micelles”.

Christoph Göbel^a, Ottokar Klimm^a, Florian Puchtler^b, Sabine Rosenfeldt^c, Stephan Förster^c and Birgit Weber^{a*}

I synthesised and characterised the samples presented in this work, carried out the magnetic measurements, TEM images, DLS measurements, IR measurements and elemental analysis. Christoph Göbel reproduced all samples and their characterization and wrote the manuscript with experimental section, the conclusion and the result section (TEM imaging, magnetic measurements, IR measurements, Powder XRD measurements). Florian Puchtler carried out the PXRD measurements and I interpreted the PXRD measurements. Christoph Göbel repeated the data treatment and wrote this part in the manuscript. Prof. Dr. Birgit Weber supervised this work, helped interpreting the magnetic (SQUID and Mössbauer) and imaging (TEM, DLS) data, wrote the introduction and was involved in scientific discussions and correction of the manuscript.

Chapter 6

This work is to be submitted.

“The influence of block copolymer tuning to particle size and shape of Fe(II) SCO nanoparticles in block copolymer micelles”.

Ottokar Klimm^a, Florian Puchtler^b, Sabine Rosenfeldt^c, Stephan Förster^c and Birgit Weber^{a*}

I synthesised and characterised all samples presented in this work, carried out the magnetic measurements, TEM images, DLS measurements, elemental analysis and wrote the experimental section, the conclusion and parts of the result section (TEM imaging, magnetic measurements, Powder XRD measurements). Florian Puchtler carried out the PXRD measurements and I interpreted the PXRD measurements and wrote this part in the manuscript. Prof. Dr. Birgit Weber supervised this work, helped interpreting the magnetic (SQUID and Mössbauer) and imaging (TEM, DLS) data and was involved in scientific discussions and correction of the manuscript.

Chapter 7

This work is to be submitted.

“Synthesis of different Fe^(II) SCO nanoparticles with SCO over and below room temperature using BCP nanoreactors”.

Ottokar Klimm^a, Florian Puchtler^b, Sabine Rosenfeldt^c, Stephan Förster^c and Birgit Weber^{a*}

I synthesised and characterised all samples presented in this work, carried out the magnetic measurements, TEM images, DLS measurements, elemental analysis and wrote the experimental section, the conclusion and parts of the result section (TEM imaging, magnetic measurements, Powder XRD measurements). Florian Puchtler carried out the PXRD measurements and I interpreted the PXRD measurements and wrote this part in the manuscript. Prof. Dr. Birgit Weber supervised this work, helped interpreting the magnetic (SQUID and Mössbauer) and imaging (TEM, DLS) data and was involved in scientific discussions and correction of the manuscript

4. Synthesis of [Fe(L)(bipy)]_n Spin Crossover Nanoparticles using Blockcopolymer Micelles

Ottokar Klimm,^a Christoph Göbel,^a Sabine Rosenfeldt,^b Florian Puchtler,^c Nobuyoshi Miyajima,^d Katharina Marquardt,^d Markus Drechsler,^e Josef Breu,^c Stephan Förster,^b Birgit Weber^{a*}

[a] Anorganische Chemie II, Universität Bayreuth, Universitätsstraße 30, NW I, 95440 Bayreuth, Germany, E-mail: weber@uni-bayreuth.de, <http://www.ac2-weber.uni-bayreuth.de>.

[b] Physikalische Chemie I, Universität Bayreuth, Universitätsstraße 30, NW I, 95440 Bayreuth, Germany.

[c] Anorganische Chemie I, Universität Bayreuth, Universitätsstraße 30, NW I, 95440 Bayreuth, Germany.

[d] Bayerisches Geoinstitut, Universität Bayreuth, Universitätsstr. 30, 95440 Bayreuth, Germany.

[e] Soft Matter Electron Microscopy, BIMF, Universität Bayreuth, Universitätsstraße 30, NW I, 95440 Bayreuth, Germany.

Published in *Nanoscale*, **2016**, *8*, 19058–19065.

Reproduced by permission of The Royal Society of Chemistry

Abstract: Nowadays there is a high demand for specialized functional materials for specific applications in sensors or biomedicine (e.g. fMRI). For the implementation in devices, nanostructuring and the integration in a composite matrix are indispensable. Spin crossover complexes are a highly promising family of switchable materials where the switching process can be triggered by various external stimuli. In this work, the synthesis of nanoparticles of the spin crossover iron(II) coordination polymer [Fe(L)(bipy)]_n (with L = 1,2-phenylene-bis(iminomethylidene)bis(2,4-pentanedionato)(2-) and bipy = 4,4'-bipyridine) is described using

polystyrene-poly-4-vinylpyridine blockcopolymer micelles as template defining the final size of the nanoparticle core. A control of the spin crossover properties can be achieved by precise tuning of the crystallinity of the coordination polymer via successive addition of the starting material Fe(L) and bipy. By this we were able to synthesize nanoparticles with a core size of 49 nm and a thermal hysteresis loop width of 8 K. This is, to the best of our knowledge, a completely new approach for the synthesis of nanoparticles of coordination polymers and should be easily transferable to other coordination polymers and networks. Furthermore, the use of blockcopolymers allows a further functionalization of the obtained nanoparticles by variation of the polymer blocks and an easy deposition of the composite material on surfaces via spin coating.

Introduction

The synthesis of nanostructured and composite materials is of growing importance for coordination polymers and (porous) coordination networks (e.g. MOFs) that are discussed for their high potential in drug delivery, sensing, catalysis, or as contrast agents.^[1,2] Such applications require the incorporation into composite materials or mesoscopic systems. Additionally, there is a great interest in tailoring size-dependent physical properties such as light absorption. A well-known example are the different colours of colloidal gold nanoparticles.^[3] Nowadays many methods for the synthesis of metal- or metalchalcogenate nanoparticles are available, e.g. decomposition of complexes, reduction of metal salts, fast precipitation, or inverse micelle techniques.^[4] Whereas for the synthesis of nanostructured coordination polymers or coordination networks (including MOFs), the number of methods is restricted and further depends strongly on the used system.^[1,2] The potential of block copolymers for the synthesis of coordination network nanoparticles is almost unexplored.^[5]

Spin crossover (SCO) coordination polymers and networks are well established model systems to develop new synthesis strategies for nanostructured coordination compounds and further to investigate size and matrix effects.^[6] Those materials can be switched by external stimuli between a low-spin (LS) and a high-spin (HS) state.^[7] This switching ability is associated with changes in the chemical and physical properties, explaining the high interest for applications in sensors,^[8] display devices^[9] or as functional contrast agents.^[10] For potential applications it is essential to understand the interplay between the particle size and/or matrix effects and the SCO properties. In bulk material, cooperative spin transitions with hysteresis (bistability)^[11] are possible due to

intermolecular interactions. There are only a few systems, where 1D coordination polymers nanoparticles or 3D coordination network nanoparticles were prepared, generally accompanied by loss of the spin crossover behaviour of the bulk material.^[12,13–16] For most of those systems the inverse micelle technique was used^{13–17} and few attempts were made to entrap nanoparticles in a matrix^[16,18,19] Nearly no examples preserving the hysteresis in a nanostructured system are known.^[18,20] Nanospheres of mononuclear spin crossover complexes can be obtained through self-assembly of amphiphilic complexes.^[21] In this work we investigate the size and crystallinity of nanoparticles and show how it is possible to preserve the spin crossover properties of the bulk material down to particles sizes below 50 nm.

We use our extensive library of mononuclear and poly-nuclear spin crossover complexes to investigate systematically the origin of cooperative effects (e.g. thermal hysteresis loops or steps) during the spin transition.^[22] Recently, we reported a strong influence of a poly-4-vinylpyridine (P4VP) matrix on the spin transition properties of sub-microcrystals of the SCO coordination polymer [Fe(L)(bipy)]_n.^[23] Inspired by the results we used P4VP based block copolymers (BCP) as template for the nanoparticle synthesis. Polystyrene-poly-4-vinylpyridine BCPs are known for their ability to build micellar structures via self-assembly.^[24] The direct synthesis of nanoparticles (NPs) in the polymer micelles is expected to bring large yields while omitting toxic surfactants and using less-toxic solvents compared to the inverse micelle technique. In addition, the block morphology of the polymer offers the possibility of controlled deposition on various surfaces.^[24] PS-P4VP based BCPs are used for large area deposition of inorganic nanoparticles such as gold^[25] or iron oxide.^[26] The incorporation of SCO NPs in such a polymer matrix may lead to an increased stability against degradation in aerobic conditions. Consequently we decided to use PS-P4VP based micelles as nanoreactors for the synthesis of nanoparticles of the Fe(II) complex [Fe(L)(bipy)]_n. A Schematic representation of the general approach using a self-assembly strategy is given in Scheme 1.

Results and discussion

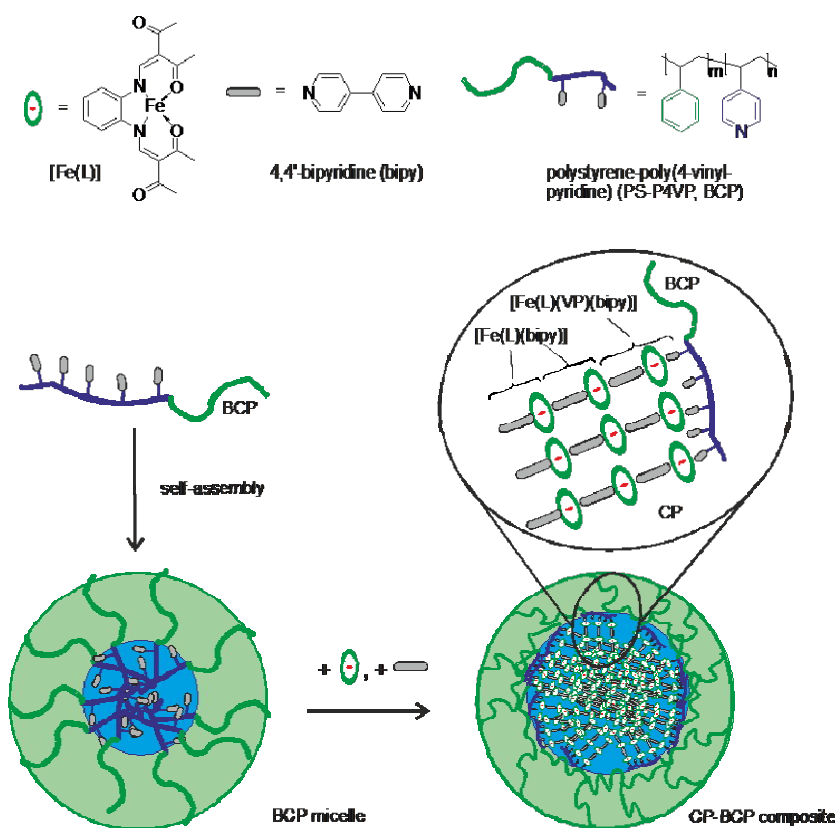
Synthesis of the nanoparticles

For the synthesis of the coordination polymer (CP) – blockcopolymer (BCP) composite materials, the self-assembly approach recently reported for sub-microcrystals in a poly(4-vinylpyridine)

4. Synthesis of $[\text{Fe}(\text{L})(\text{bipy})]_n$ Spin Crossover Nanoparticles using Blockcopolymer Micelles

matrix was used.²³ The polystyrene-poly-4-vinylpyridine BCP (PS-P4VP, $M = 150\,000$ g/mol, 1250 PS units, 200 P4VP units, 14% P4VP) was dissolved in THF and stirred for 15 min to allow self-assembly. The resulting empty BCP micelles have a hydrodynamic radius of 63 nm (SI, Figure S1). For the CP-BCP composite materials, a solution of the BCP with the precursor Fe(II) complex $[\text{Fe}(\text{L})]$ was used as starting material. In the solid state $[\text{Fe}(\text{L})]$ is stabilized by two additional methanol molecules as axial ligands that are easily replaced by pyridine derivatives. Based on the size of $[\text{Fe}(\text{L})]$ of 12×9 Å, approximately one iron complex can coordinate per 3 – 4 vinylpyridine (VP) units. Thus a ratio of 1:4.5 of $[\text{Fe}(\text{L})]$:VP-units is chosen to avoid uncoordinated iron complex in the reaction mixture. It results in two Fe(II) species, namely the penta-coordinated $[\text{Fe}(\text{L})(\text{VP})]$ (20%, high-spin, HS) and the octahedral $[\text{Fe}(\text{L})(\text{VP})_2]$ (80 %, low-spin, LS; see Mössbauer spectrum of compound **1**, Figure S2).

After 2h of reflux (66°C) the bridging ligand 4,4'-bipyridine (bipy) was added to the solution. Due to the LS state of the majority species $[\text{Fe}(\text{L})(\text{VP})_2]$, ligand exchange is expected to be slowed down. To allow crystalline growth of the CP in the BCP micelles, further successive additions of $[\text{Fe}(\text{L})]$ and bipy were used (= number of cycles; each with the same ratio of $[\text{Fe}(\text{L})]$:bipy).



Scheme 1: Top: formula of the compounds with the used abbreviations. Bottom: Schematic representation of a self-assembled block copolymer micelle for the use as nanoreactor. Successive

4. Synthesis of [Fe(L)(bipy)]_n Spin Crossover Nanoparticles using Blockcopolymer Micelles

addition of the complex [Fe(L)] and the bridging ligand bipy to the block copolymer (BCP) micelle will lead to a growth of the coordination polymer (CP) in the core of the micelle.

Table 1: Sample overview.

sample	cycles	[Fe(L)]:bipy [mol:mol]	total time [h]	temperature [°C]
1	0	1:0	2	66
2	1	1:2.5	3	66
3	2	1:2.5	4	66
4	3	1:2.5	5	66
5	4	1:2.5	6	66
6	5	1:2.5	7	66
7	1	1:1	3	66
8	1	1:3	3	66
9	1	1:4	3	66
10	1	1:5	3	66
11	3	1:6	5	66
12	3	1:7	5	66
13	3	1:8	5	66
14	3	1:9	5	66
15	3	1:10	5	66
16	1	1:2.5	2.25	66
17	2	1:2.5	2.50	66
18	3	1:2.5	2.75	66
19	4	1:2.5	3.00	66

4. Synthesis of [Fe(L)(bipy)]_n Spin Crossover Nanoparticles using Blockcopolymer Micelles

20	5	1:2.5	3.25	66
21	1	1:2.5	3	RT
22	2	1:2.5	4	RT
23	3	1:2.5	5	RT
24	5	1:2.5	7	RT

To optimize the reaction conditions for the formation of the CP, the [Fe(L)]:bipy ratio, reaction time, and reaction temperature were varied. An overview of the used reaction conditions is given in Table 1. Tables S1 and S2 summarise the results of this screening.

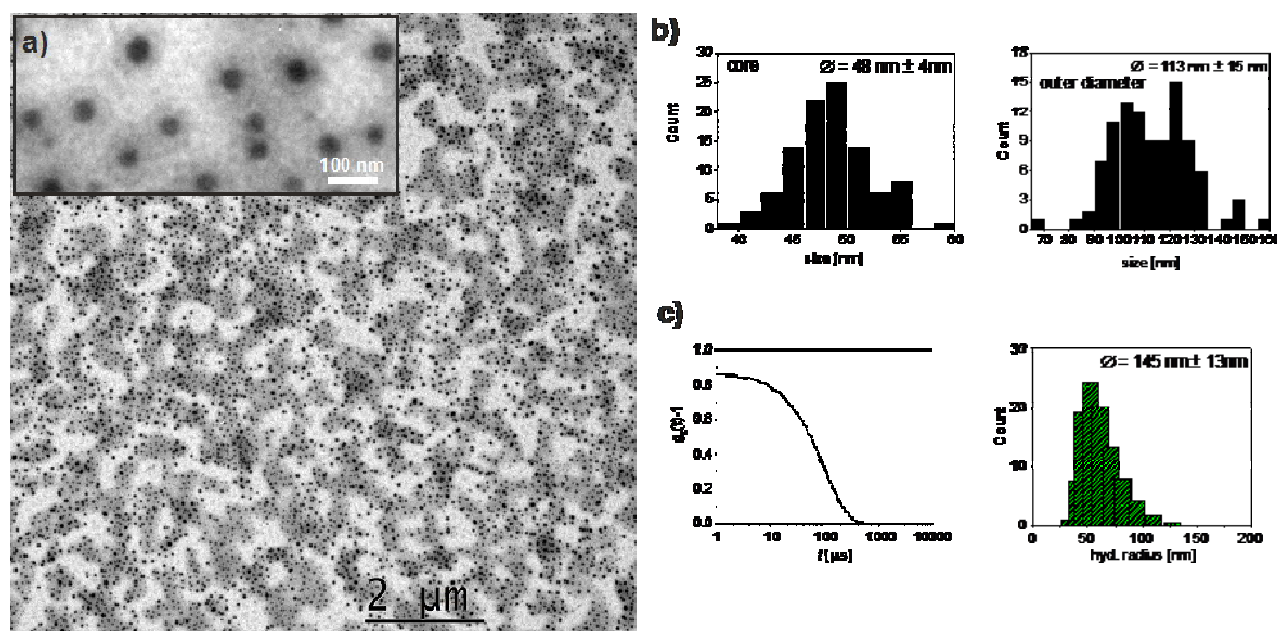


Figure 1: Characterization of CP-BCP composite micelles. a) TEM pictures of **6** (5 cycles) at two different magnifications illustrating the core shell nature of the particles. b) Size histogram from the TEM picture given in Figure 1a. c) Autocorrelation function (left) of the CP-BCP particles in THF (43 wt%) and resulting distribution of the hydrodynamic radius (right).

Independent of the [Fe(L)]:bipy ratio, well defined spherical particles are obtained for the samples **7 – 15**. For too high amounts of 4,4'-bipyridine (samples **13 – 15**), gradual spin transitions and an increasing LS fraction were observed (see Table S2). This hints to the formation of the mononuclear complex [Fe(L)(bipy)₂] or very short detached CP chains. Consequently the

4. Synthesis of [Fe(L)(bipy)]_n Spin Crossover Nanoparticles using Blockcopolymer Micelles

[Fe(L)]:bipy ratio was fixed to 1:2.5 for the following screening to prevent the formation of [Fe(L)(bipy)₂] species. For the samples stirred at room temperature (**21** – **24**), larger aggregates and less well defined spherical particles were observed in the TEM pictures (Table S2), thus a higher reaction temperature (66°C is the boiling point of the solvent THF) supports the formation of uniform composite nanoparticles. The increase of the reaction time from 15 min (samples **16** – **20**) to 1 hour (samples **2** – **6**) for each cycle, improves the SCO properties of the composite materials. This can be related to the time available for crystallite growth, as will be shown in the following.

Each additional cycle leads to an increasing amount of CP in the BCP micelles. This is reflected in an increase of the $\nu(\text{C}=\text{O})$ stretching vibrations (1640 cm^{-1} and 1560 cm^{-1}) of [Fe(L)] in the composite material, followed by IR spectroscopy, see Figure S3. Transmission electron microscopy (TEM) was used to study the size, shape and uniformity of the obtained material and Mössbauer spectra to determine the conversion of the octahedral [Fe(L)(VP)₂] LS fraction. In agreement with an increasing amount of the desired [Fe(L)(bipy)] units of the CP (see Scheme 1), the LS fraction decreases from 47% for sample **3** to 45%, 16%, and finally 0% for the samples **4**, **5**, and **6**, respectively. The results are summarized in Table S3. Further, magnetic measurements were performed to get information about the spin crossover properties.

Control of the crystallite size of the coordination polymer

The investigated CP-BCP composite material consists of a BCP micelle in which the CP was incorporated. As a representative example of the morphology of the CP-BCP composite micelles, in Figure 1 transmission electron microscopy (TEM) pictures of sample **6** (5 cycles) are given. TEM images of further samples are provided in Table S1. In all cases spherical core-shell morphology was obtained. Based on the differences in contrast, the iron complexes in the P4VP part form the core while the PS part is the shell. An energy dispersive X-ray spectroscopy analysis (EDX) of **6** was done to confirm the regio-selectivity of the [Fe(L)(bipy)] complex to the VP units of the BCP micelles (SI, Figure S4).

Dynamic light scattering (DLS) was used to determine the total size of the CP-BCP composite micelles in solution. There is a slight increase in the hydrodynamic size upon loading the BCP micelle with the CP. After the first addition of the CP, the outer diameter of the CP-BCP

composite micelle increases from 126 nm for the empty micelle to 147 nm for the loaded one. For the following additions of CP, the outer diameter stays more or less constant. TEM was used to determine the size of the core and the outer diameter in the dried state. Independent of the amount of added CP, for loaded CP-BCP micelles the same core and total diameter was obtained in the range of the error. This indicates that the BCP micelle is an ideal template for the synthesis of spherical particles, in our case of the CPs. This opens up a new route to obtain CP nanoparticles with a spherical morphology instead of the usually obtained needle-like structures.

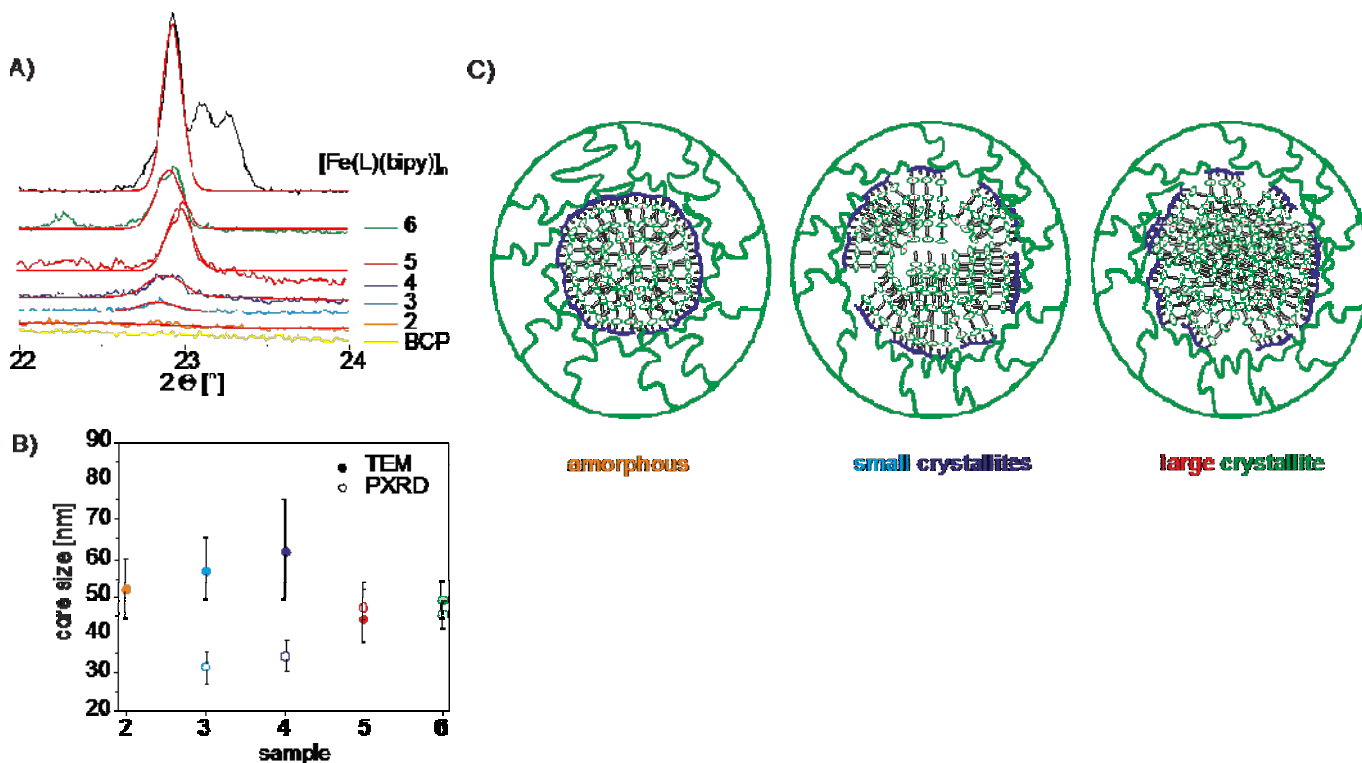


Figure 2. Particle core size and crystallinity of the CP-BCP composite micelles. A) PXRd spectra between 22° and 24° . The continuous red line resembles the fit used for the determination of the FWHM. B) Particle core size determined by TEM (dots) and calculated via Debye-Scherrer equation from the PXRd data (open circles) as function of the number of reaction cycles. C) Schematic representation of the CP-BCP composite micelle illustrating the growth of the crystalline CP parts in the core of the micelle.

Note that the size of the CP-BCP micellar core seems to be determined by the first addition of $[\text{Fe}(\text{L})(\text{bipy})]_n$. This may be explained by changes in the morphology of the $[\text{Fe}(\text{L})(\text{bipy})]_n$ in the core of the micelle. Consequently, powder X-ray diffraction (PXRd) (see Figure 2a and S5) was used to estimate the crystallinity of the CP in the BCP core. The corresponding results are summarized in Table 2 together with the results for the empty BCP micelles. In Figure 2b, the size

4. Synthesis of [Fe(L)(bipy)]_n Spin Crossover Nanoparticles using Blockcopolymer Micelles

of the core as function of the number of cycles is compared with the size of the crystalline parts determined by PXRD. Therefore, the half width of the most prominent peak in the PXRD spectra at a 2θ value of 23° , illustrated in Figure 2a, was analysed using the Debye-Scherrer equation (1)^[27]:

$$\Delta B(2\theta) = \frac{0.89\lambda}{L \cos\theta} \quad (1)$$

Where λ is the wavelength of the diffractometer (0.15418 nm), θ is the peak angle [rad], L corresponds to the mean crystal size [nm] and ΔB is the FWHM (full width at half maximum) of the peak [rad]. A continuous decrease of the line width is observed in the diffraction pattern with increasing number of cycles indicating a continuous increase of the crystalline parts. We found that sample **2** is completely amorphous. For the samples **3** and **4** the crystallite size is significantly smaller than the core size determined by TEM while for the samples **5** and **6** about the same size is obtained. We propose a change in the core crystallinity induced by the increase in [Fe(L)(bipy)] concentration, as illustrated in Figure 2c. The growth of the CP chains leads to an increase of the [Fe(L)(bipy)] density within the micelle core. This triggers the crystallization and later a rearrangement of the small crystallites to larger crystals of the size of the micelle core. A comparison of the samples **2** – **6** with the samples **16** – **20** with shorter reaction times reveal, that longer reaction times support this crystallisation process.

Table 2: Particle size (diameter) and crystallinity of the samples determined by DLS, TEM and PXRD measurements in nm

<i>cycles</i>	<i>sample</i>	<i>DLS</i> ^{a)}	<i>TEM core</i>	<i>TEM shell</i> ^{a)}	<i>PXRD (23°)</i>
0	BCP	126±22	70±8		-
1	2	147±22	52±8	101±15	-
2	3	140±13	57±8	94±15	33±3
3	4	142±12	62±13	91±12	32±3
4	5	147±15	44±6	96±12	47±3
5	6	145±13	49±5	113±15	45±3

4. Synthesis of [Fe(L)(bipy)]_n Spin Crossover Nanoparticles using Blockcopolymer Micelles

- a) The differences in the hydrodynamic diameter (DLS) and the outer diameter determined by TEM are due to drying effects.

Magnetism

The change of crystallinity of the CP core and therefore of n in [Fe(L)(bipy)] _{n} in the BCP micelle should significantly influence the SCO properties of the composite material. Due to the differences in coordination environment of the outside [Fe(L)] units of the [Fe(L)(bipy)] _{n} coordination polymer, only the inside [Fe(L)] units are expected to undergo spin crossover (SCO). Magnetic measurements of the samples **3** – **6** were done in the temperature range between 330 K and 50 K in the cooling and heating mode. The results are given as $\chi_M T$ versus T plots in Figure 3, where χ_M is the molar susceptibility and T the temperature. The ratio of high spin (HS) : low spin (LS) iron centers was confirmed by Mössbauer spectroscopy at room temperature (see Figure S6 and Table S4).

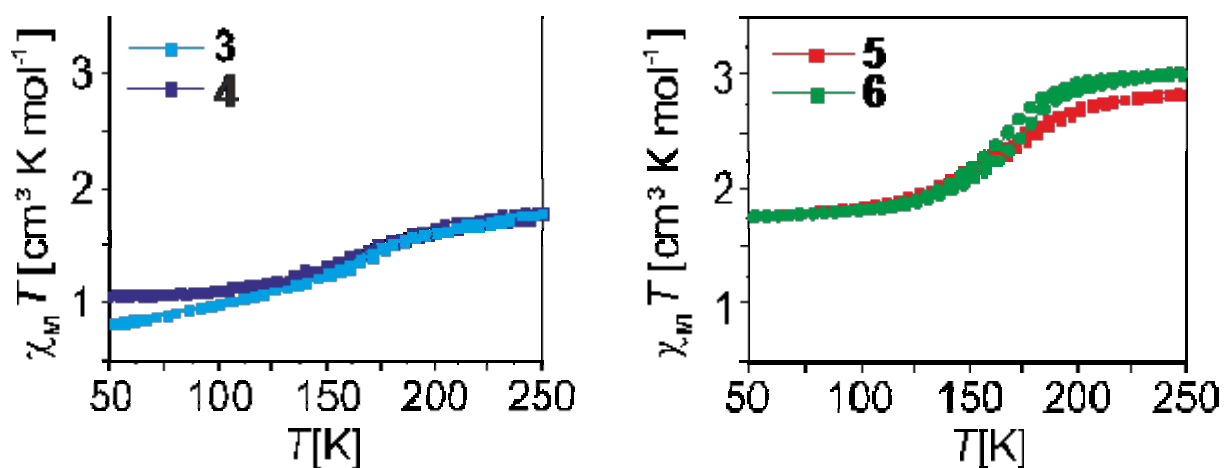


Figure 3. Plot of the $\chi_M T$ product *versus* T determined by SQUID measurements. The increase in crystallinity is reflected by an increase of the cooperative interactions (hysteresis) during the spin transition.

The room temperature $\chi_M T$ product of the samples with 2 and 3 cycles (**3** and **4**) is with $1.9 \text{ cm}^3 \text{ K mol}^{-1}$ significantly lower than the theoretical value for iron(II) in the HS state ($\chi_M T = 3.0 \text{ cm}^3 \text{ K mol}^{-1}$) due to a significant LS fraction. Upon cooling, for both samples a drop of the $\chi_M T$ product to ca. $1.0 \text{ cm}^3 \text{ K mol}^{-1}$ is observed in the temperature region between 225 K and 125 K. This can be correlated to a very gradual and incomplete spin crossover. This is in contrast to the previously described microcrystals in a P4VP matrix, where the spin transition was either quenched or a spin transition with hysteresis was observed.²³ For sample **5** the room temperature $\chi_M T$ product is with $2.9 \text{ cm}^3 \text{ K mol}^{-1}$ almost in the region expected for an iron(II) complex in the HS state. A gradual SCO is observed in the temperature region between 200 K and 125 K with about 40 % of the iron centers involved. This indicates that the number of SCO active iron centers did

increase compared to **3** and **4** (both about 30 %). This trend continues for **6** with five cycles with a room temperature $\chi_M T$ product of $3.1 \text{ cm}^3 \text{ K mol}^{-1}$, typical for Fe^{II} HS complexes. The spin transition takes place between 210 K and 125 K with 45 % of the iron center involved. From **3** to **6** a significant increase in the fraction of SCO active [Fe(L)] units is observed indicating the increase of n in [Fe(L)(bipy)] _{n} . In the case of **5** and even more pronounced in the case of **6**, different transition temperatures are observed in the heating and the cooling. The $T_{1/2}$ values (where 50% of the SCO active centers did undergo spin transition) of **6** are 162 K in the cooling and 170 K in the heating mode corresponding to a 8 K wide thermal hysteresis loop. With the increasing number of cycles an increase of the hysteresis width is observed and the SCO properties converge towards those of the bulk material (20 K hysteresis for the bulk²⁸ and 8 K for **6**, approx. 1 K hysteresis for **5**). This is directly linked to the crystal size of the CP core in the CP-BCP composite (see Figure 2).

Conclusions

In this work the synthesis of spin crossover Fe^{II} coordination polymer nanoparticles is described using blockcopolymer micelles as microreactors. An excellent control over the size of the coordination polymer is obtained via the blockcopolymer micelle size. A strong influence of the crystallinity, tunable by the number of cycles, of the coordination polymer core on the spin crossover properties of the material is observed. This is, to the best of our knowledge, a completely new approach for the synthesis of nanoparticles of coordination polymers and should be easily transferable to other coordination polymers and networks. Furthermore, the use of blockcopolymers allows a further functionalisation of the obtained nanoparticles by variation of the polymer blocks.

Experimental

Synthetic procedures

Polystyrene-*b*-Poly(4-vinylpyridine) (PS-P4VP, purum, MW \approx 150000) was synthesised as described before.^[24] 4,4'-bipyridine was obtained from Alfa Aesar and used as received. Tetrahydrofuran (THF) was purified as described in literature.²⁹ [Fe(L)(MeOH)₂] was synthesized

4. Synthesis of [Fe(L)(bipy)]_n Spin Crossover Nanoparticles using Blockcopolymer Micelles

as described before.³⁰ All syntheses were performed under inert conditions using Schlenk technique with argon (purity $\geq 99,999\%$, 5.0). The synthesis of all samples was repeated at least twice.

1: PS-P4VP (50 mg, 0.33 μmol) and [Fe(L)(MeOH)₂] (6.4 mg, 15 μmol) were added to a 50 ml flask. Subsequently THF (20 ml) was added and the mixture was heated to reflux for 2h. After cooling to room temperature, the solvent of the brown solution was removed via cold distillation to yield a brown, polymer-like powder. Elemental anal. (%) found: C 63.24, H 7.78, N 1.69

2: PS-P4VP (50 mg, 0.33 μmol) and [Fe(L)(MeOH)₂] (6.4 mg, 15 μmol) were added to a 50 ml flask. Subsequently THF (20 ml) was added and the mixture was heated to reflux for 2h. After cooling to room temperature, 4,4'-bipyridine (5.6 mg, 36 μmol) was added to the brown solution and the reaction mixture was heated for 1h to reflux. After cooling to room temperature, the solvent was removed via cold distillation to yield a brown, polymer-like powder. Elemental anal. (%) found: C 63.70, H 7.49, N 2.38.

3: The synthesis as described for sample 2 was repeated. Before solvent removal, [Fe(L)(MeOH)₂] (6.4 mg, 15 μmol) and 4,4'-bipyridine (5.6 mg, 36 μmol) were added in a second cycle and the mixture was heated for one further hour to reflux. After cooling to room temperature the solvent was removed via cold distillation to yield a brown, polymer-like powder. Elemental anal. (%) found: C 65.55, H 7.81, N 1.55.

4: The synthesis described for sample 3 was repeated, with one further cycle of addition of [Fe(L)(MeOH)₂] (6.4 mg, 15 μmol) and 4,4'-bipyridine (5.6 mg, 36 μmol) followed by further heating to reflux for 1h. After cooling to room temperature the solvent was removed via cold distillation to yield a brown, polymer-like powder. Elemental anal. (%) found: C 68.34, H 7.05, N 4.67.

5: The synthesis described for sample 4 was repeated, with one further cycle of addition of [Fe(L)(MeOH)₂] (6.4 mg, 15 μmol) and 4,4'-bipyridine (5.6 mg, 36 μmol) followed by further heating to reflux for 1h. After cooling to room temperature the solvent was removed via cold distillation to yield a brown, polymer-like powder. Elemental anal. (%) found: C 60.58, H 7.06, N 3.13.

6: The synthesis described for sample 5 was repeated, with one further cycle of addition of [Fe(L)(MeOH)₂] (6.4 mg, 15 μmol) and 4,4'-bipyridine (5.6 mg, 36 μmol) followed by further

heating to reflux for 1h. After cooling to room temperature the solvent was removed via cold distillation to yield a brown, polymer-like powder. Elemental anal. (%) found: C 63.91, H 6.94, N 4.85.

The colour turned increasingly darker from sample **2** to **6** with an increasing amount of iron. Elemental analyses reveal an increasing nitrogen contents from sample **1** to **6** in line with the increasing amount of CP. The variations in the values are due to differences in the solvent contents and contamination of the samples with grease.

Methods

Transmission electron microscopy: Transmission electron microscopy was performed with a Zeiss CEM902 electron microscope (Zeiss, Oberkochen, Germany). Samples were dispersed in toluene applying vortex several times. The dispersion was dropped on a carbon coated copper grid (Science Services, Munich). The acceleration voltage was set to 80 kV. Micrographs were taken with a MegaView III / iTEM image acquiring and processing system from Olympus Soft Imaging Systems (OSIS, Muenster, Germany) and an Orius 830 SC200W / DigitalMicrograph system from Gatan (Munich, Germany). Particles size measurements were done with “ImageJ” image processing software by Wayne Rasband (National Institutes of Health, USA).

Infrared spectroscopy: Transmission infrared spectra were collected using a PerkinElmer Spectrum 100 FT-IR (ATR). Samples were measured directly as solids.

Elemental Analysis: Carbon, nitrogen and hydrogen contents were collected at a Vario EL III. Samples were placed in tin boats. All samples were measured at least twice and the average of both measurements was used.

Energy dispersive X-ray spectroscopy: Energy dispersive X-ray spectroscopy was done at a 200 kV FEI-Titan G2 80-200 S/TEM (Eindhoven, Netherlands). Samples were dispersed in methanol applying vortex and ultrasound several times. The dispersion was dropped on a carbon filmed coated copper grid. The acceleration voltage was set to 200 kV.

Scanning electron microscopy: Scanning electron microscopy micrographs were acquired with a Zeiss LEO 1530 (Oberkochen, Germany).

Magnetic measurements: Magnetic susceptibility measurements were performed at a Quantum Design MPMS-XL-5 SQUID magnetometer in the temperature range between 50 and 300 K. The samples were prepared in gelatin capsules placed in a plastic straw. All samples were measured with a magnetic field of 3T in the settle mode with a cooling and heating rate of 5K min⁻¹ between each measurement point. The measured values were corrected for the diamagnetism of the sample holder, the polymer matrix (measured values) and the ligand (tabulated Pascal constants).

X-Ray Powder Diffraction: X-Ray Powder Diffraction data for samples **2** to **6** and the bulk [FeL(bipy)]_n were collected at a STOE StadiP X-ray powder diffractometer in transmission geometry between 5 and 45° 2 θ . Samples were placed in capillaries and Cu-K α 1 radiation was used for the measurement. Radiation was detected with a Mythen 1K detector.

Mössbauer spectroscopy: ⁵⁷Fe Mössbauer spectra were recorded in transmission geometry on a constant-acceleration using a conventional Mössbauer spectrometer with a 50 mCi ⁵⁷Co(Rh) source. The samples were sealed in the sample holder under argon atmosphere. The spectra were fitted using Recoil 1.05 Mössbauer Analysis Software.³¹ The isomer shift values are given with respect to a α -Fe reference at room temperature.

Dynamic light scattering: DLS of all samples were collected from Malvern Zetasizer Nano ZS. Samples were measured in solution in glass cuvettes from Carl Roth GmbH + Co. KG.

Acknowledgements

Financial support of the University of Bayreuth and the SFB 840 (TP A10 and B10) is gratefully acknowledged. O.K. was supported by the BayNAT program of the UBT. We thank Juliane Kary and Stella Buchmann (AC II, UBT) for their contribution to the synthesis of the CP-BCP composites.

References

- [1] E. A. Flügel, A. Ranft, F. Haase and B. V. Lotsch, *J. Mater. Chem.*, **2012**, 22, 10119–10133.
- [2] M. Sindoro, N. Yanai, A.-Y. Jee and S. Granick, *Acc. Chem. Research*, **2014**, 47, 459–469.
- [3] G. Frens, *Nat Phys Sci*, **1973**, 241, 20–22.

[4] a) H. You, S. Yang, B. Ding and H. Yang, *Chem. Soc. Rev.*, **2013**, *42*, 2880–2904; b) C. Altavilla and E. Ciliberto, eds., *Inorganic nanoparticles. Synthesis, applications, and perspectives*, CRC Press, Boca Raton, FL, **2011**.

[5] a) T.-Y. Ma, H. Li, Q.-F. Deng, L. Liu, T.-Z. Ren and Z.-Y. Yuan, *Chem. Mater.*, **2012**, *24*, 2253–2255; b) M.-H. Pham, G.-T. Vuong, F.-G. Fontaine and T.-O. Do, *Crystal Growth & Design*, **2012**, *12*, 1008–1013; c) M.-H. Pham, G.-T. Vuong, A.-T. Vu and T.-O. Do, *Langmuir*, **2011**, *27*, 15261–15267; d) Y. Yan, A. de Keizer, M. A. Cohen Stuart, M. Drechsler and N. A. Besseling, *J. Phys. Chem. B*, **2008**, *112*, 10908–10914; e) Y. Yan, Y. Lan, A. de Keizer, M. Drechsler, H. van As, M. A. Cohen Stuart, and N. A. Besseling, *Soft Matter*, 2010, **6**, 3244; f) A. Wang, W. Shi, J. Huang and Y. Yan, *Soft Matter*, **2015**, *12*, 337–357.

[6] P. N. Martinho, C. Rajnak and M. Ruben, in *Spin-Crossover Materials*, ed. M. A. Halcrow, John Wiley & Sons Ltd, Chichester, **2013**, pp. 375–404.

[7] a) M. A. Halcrow, ed., *Spin-Crossover Materials*, John Wiley & Sons Ltd, Chichester, 2013; b) O. Roubeau, *Chem. Eur. J.*, **2012**, *18*, 15230–15244; c) J. Tao, R.-J. Wei, R.-B. Huang and L.-S. Zheng, *Chem. Soc. Rev.*, **2012**, *41*, 703–737; d) A. Bousseksou, G. Molnar, L. Salmon and W. Nicolazzi, *Chem. Soc. Rev.*, **2011**, *40*, 3313–3335; e) M. C. Muñoz and J. A. Real, *Coord. Chem. Rev.*, **2011**, *255*, 2068–2093; f) J. Olguín and S. Brooker, *Coord. Chem. Rev.*, **2011**, *255*, 203–240; g) Y. Bodenthin, G. Schwarz, Z. Tomkowicz, M. Lommel, T. Geue, W. Haase, H. Möhwald, U. Pietsch and D. G. Kurth, *Coord. Chem. Rev.*, **2009**, *253*, 2414–2422.

[8] a) E. Coronado, M. Giménez-Marqués, G. Mínguez Espallargas, F. Rey and I. J. Vitórica-Yrezábal, *J. Am. Chem. Soc.*, **2013**, *135*, 15986–15989; b) E. Coronado and G. Mínguez Espallargas, *Chem. Soc. Rev.*, **2013**, *42*, 1525; c) M. Ohba, K. Yoneda, G. Agustí, M. C. Muñoz, A. B. Gaspar, J. A. Real, M. Yamasaki, H. Ando, Y. Nakao, S. Sakaki and S. Kitagawa, *Angew. Chem. Int. ed.*, **2009**, *48*, 4767–4771; d) Y. Garcia, V. Ksenofontov and P. Gütllich, *Hyperfine Interactions*, **2002**, *139-140*, 543-551-551; e) A. Galet, A. B. Gaspar, M. C. Muñoz, G. V. Bukin, G. Levchenko and J. A. Real, *Adv. Mater.*, **2005**, *17*, 2949–2953; f) J. Linares, E. Coddjovi and Y. Garcia, *Sensors*, **2012**, *12*, 4479–4492;

[9] a) J.-F. Létard, P. Guionneau and L. Goux-Capes, in *Spin Crossover in Transition Metal Compounds I-III*, ed. P. Gütllich and H. Goodwin, Springer Berlin / Heidelberg, **2004**, pp. 221–249; b) O. Kahn, *Science*, **1998**, *279*, 44–48; c) O. Kahn, C. Jay, J. Krober, R. Claude, F. Groliere, EP0666561, **1995**.

- [10] a) R. N. Muller, L. Vander Elst and S. Laurent, *J. Am. Chem. Soc.*, **2003**, *125*, 8405–8407; b) S. Venkataramani, U. Jana, M. Dommaschk, F. D. Sönnichsen, F. Tuczek and R. Herges, *Science*, **2011**, *331*, 445–448; c) M. Dommaschk, M. Peters, F. Gutzeit, C. Schütt, C. Näther, F. D. Sönnichsen, S. Tiwari, C. Riedel, S. Boretius and R. Herges, *J. Am. Chem. Soc.*, **2015**, *137*, 7552–7555; d) J. Hasserodt, J. L. Kolanowski and F. Touti, *Angew. Chem. Int. ed.*, **2014**, *53*, 60–73; e) S. J. Dorazio and J. R. Morrow, *Eur. J. Inorg. Chem.*, **2012**, 2006–2014;
- [11] S. Brooker, *Chem. Soc. Rev.*, **2015**, *44*, 2880–2892.
- [12] a) A. Tissot, *New J. Chem.*, **2014**, *38*, 1840; b) P. N. Martinho, T. Lemma, B. Gildea, G. Picardi, H. Müller-Bunz, R. J. Forster, T. E. Keyes, G. Redmond and G. G. Morgan, *Angew. Chem. Int. Ed.*, **2012**, *51*, 11995–11999; c) M. B. Duriska, S. M. Neville, B. Moubaraki, K. S. Murray, C. Balde, J.-F. Létard, C. J. Kepert and S. R. Batten, *ChemPlusChem*, **2012**, *77*, 616–623; d) A. Tokarev, L. Salmon, Y. Guari, W. Nicolazzi, G. Molnár and A. Bousseksou, *Chem. Commun.*, **2010**, *46*, 8011; e) E. Coronado, J. R. Galán-Mascarós, M. Monrabal-Capilla, J. García-Martínez and P. Pardo-Ibañez, *Adv. Mater.*, **2007**, *19*, 1359–1361; f) Y. Raza, F. Volatron, S. Moldovan, O. Ersen, V. Huc, C. Martini, F. Brisset, A. Gloter, O. Stephan, A. Bousseksou, L. Catala and T. Mallah, *Chem. Commun.*, **2011**, *47*, 11501–11503.
- [13] F. Volatron, L. Catala, E. Rivière, A. Gloter, O. Stéphan and T. Mallah, *Inorg. Chem.*, **2008**, *47*, 6584–6586.
- [14] T. Forestier, S. Mornet, N. Daro, T. Nishihara, S.-i. Mouri, K. Tanaka, O. Fouche, E. Freysz and J.-F. Letard, *Chem. Commun.*, **2008**, 4327–4329.
- [15] T. Forestier, A. Kaiba, S. Pechev, D. Denux, P. Guionneau, C. Etrillard, N. Daro, E. Freysz and J.-F. Letard, *Chem. Eur. J.*, **2009**, *15*, 6122–6130.
- [16] V. Martínez, I. Boldog, A. B. Gaspar, V. Ksenofontov, A. Bhattacharjee, P. Gülich and J. A. Real, *Chem. Mater.*, **2010**, *22*, 4271–4281.
- [17] I. Boldog, A. B. Gaspar, V. Martínez, P. Pardo-Ibañez, V. Ksenofontov, A. Bhattacharjee, P. Gülich and J. A. Real, *Angew. Chem. Int. Ed.*, **2008**, *47*, 6433–6437.
- [18] J. Larionova, L. Salmon, Y. Guari, A. Tokarev, K. Molvinger, G. Molnár and A. Bousseksou, *Angew. Chem. Int. Ed.*, **2008**, *47*, 8236–8240.

- [19] a) A. Tissot, J.-F. Bardeau, E. Rivière, F. Brisset and M.-L. Boillot, *Dalton Trans*, **2010**, 39, 7806; b) T. Zhao, L. Cuignet, M. M. Dîrtu, M. Wolff, V. Spasojevic, I. Boldog, A. Rotaru, Y. Garcia and C. Janiak, *J. Mater. Chem. C*, **2015**, 3, 7802–7812; c) J. M. Herrera, S. Titos-Padilla, Pope, Simon J. A., I. Berlanga, F. Zamora, J. J. Delgado, K. V. Kamenev, X. Wang, A. Prescimone, E. K. Brechin and E. Colacio, *J. Mater. Chem. C*, **2015**, 3, 7819–7829;
- [20] a) S. Cobo, G. Molnár, J. A. Real and A. Bousseksou, *Angew. Chem. Int. Ed*, **2006**, 45, 5786–5789; b) G. Molnár, S. Cobo, J. A. Real, F. Carcenac, E. Daran, C. Vieu and A. Bousseksou, *Adv. Mater*, **2007**, 19, 2163–2167; c) C. Bartual-Murgui, E. Natividad and O. Roubeau, *J. Mater. Chem. C*, **2015**, 3, 7916–7924; d) M. Giménez-Marqués, García-Sanz de Larrea, M. Luisa and E. Coronado, *J. Mater. Chem. C*, **2015**, 3, 7946–7953;
- [21] Y.-H. Luo, Q.-L. Liu, L.-J. Yang, Y. Sun, J.-W. Wang, C.-Q. You and B.-W. Sun, *J. Mater. Chem. C*, **2016**, 4, 8061–8069.
- [22] a) B. Weber, W. Bauer and J. Obel, *Angew. Chem. Int. Ed.*, **2008**, 47, 10098–10101; b) C. C. Lochenie, W. Bauer, A. P. Railliet, S. Schlamp, Y. Garcia and B. Weber, *Inorg. Chem.*, **2014**, 53, 11563–11572; c) R. Nowak, W. Bauer, T. Ossiander and B. Weber, *Eur. J. Inorg. Chem.*, **2013**, 975–983; d) B. Weber, W. Bauer, T. Pfaffeneder, M. M. Dîrtu, A. D. Naik, A. Rotaru and Y. Garcia, *Eur. J. Inorg. Chem.*, **2011**, 3193–3206; e) S. Schlamp, B. Weber, A. D. Naik and Y. Garcia, *Chem. Commun*, **2011**, 47, 7152–7154; f) S. Schönfeld, C. Lochenie, P. Thoma and B. Weber, *CrystEngComm*, **2015**, 17, 5389–5395; g) W. Bauer, M. M. Dîrtu, Y. Garcia and B. Weber, *CrystEngComm*, **2012**, 14, 1223; h) W. Bauer, W. Scherer, S. Altmannshofer and B. Weber, *Eur. J. Inorg. Chem.*, **2011**, 2803–2818;
- [23] C. Göbel, T. Palamarciuc, C. Lochenie and B. Weber, *Chem. Asian J.*, **2014**, 9, 2232–2238.
- [24] S. Förster and M. Antonietti, *Adv. Mater.*, **1998**, 10, 195–217.
- [25] a) S.-H. Yun, S. I. Yoo, J. C. Jung, W.-C. Zin and B.-H. Sohn, *Chem. Mater.*, **2006**, 18, 5646–5648; b) W. Lee, S. Y. Lee, X. Zhang, O. Rabin and R. M. Briber, *Nanotechnology*, **2013**, 24, 45305.
- [26] R. D. Bennett, G. Y. Xiong, Z. F. Ren and R. E. Cohen, *Chem. Mater.*, **2004**, 16, 5589–5595.
- [27] A. L. Patterson, *Phys. Rev.*, **1939**, 56, 978–982.
- [28] B. Weber, R. Tandon and D. Himsl, *Z. Anorg. Allg. Chem.*, **2007**, 633, 1159–1162.

[29] H. G. O. Becker, *Organikum. Organisch-chemisches Grundpraktikum*, Johann Ambrosius Barth, Berlin, 19th edn., **1993**.

[30] B. Weber and E.-G. Jäger, *Z. Anorg. Allg. Chem.*, **2009**, 635, 130–133.

[31] K. Lagarec and D. G. Rancourt, *Recoil, Mössbauer spectral analysis software for windows 1.0*, Department of Physics, University of Ottawa, Canada, **1998**.

Supporting Information**Optimization of the reaction conditions**

Synthesis of the CP-BCP samples 7-24:

PS-P4VP (50 mg, 0.33 μmol), [Fe(L)(MeOH)₂] (amount given in the Table) and THF (20 ml) were mixed and heated to reflux for 2h. After cooling to room temperature 4,4'-bipyridine (amount given in the Table) was added to the brown solution and the reaction mixture was heated for 1h (all samples except 16-20) or 15 min (16-20) to reflux. After cooling to room temperature the reaction was continued as given in the following overview using the same procedure as for the samples 2-6 for the different number of cycles. The results are summarized in Table S2.

Sample	cycles	Total reaction time	Reaction temperature	Amount of [Fe(L)(MeOH) ₂] and bipy per cycle
7	1	3 h	66°C	[Fe(L)(MeOH) ₂]: 6.4 mg, 15 μmol bipy: 2.3 mg, 15 μmol
8	1	3 h	66°C	[Fe(L)(MeOH) ₂]: 6.4 mg, 15 μmol bipy: 6.8 mg, 45 μmol
9	1	3 h	66°C	[Fe(L)(MeOH) ₂]: 6.4 mg, 15 μmol bipy: 9.1 mg, 60 μmol
10	1	3 h	66°C	[Fe(L)(MeOH) ₂]: 6.4 mg, 15 μmol bipy: 11.3 mg, 75 μmol
11	3	5 h	66°C	[Fe(L)(MeOH) ₂]: 6.4 mg, 15 μmol bipy: 13.8 mg, 88 μmol
12	3	5 h	66°C	[Fe(L)(MeOH) ₂]: 6.4 mg, 15 μmol bipy: 15.7 mg, 101 μmol
13	3	5 h	66°C	[Fe(L)(MeOH) ₂]: 6.4 mg, 15 μmol bipy:

4. Synthesis of [Fe(L)(bipy)]_n Spin Crossover Nanoparticles using Blockcopolymer Micelles

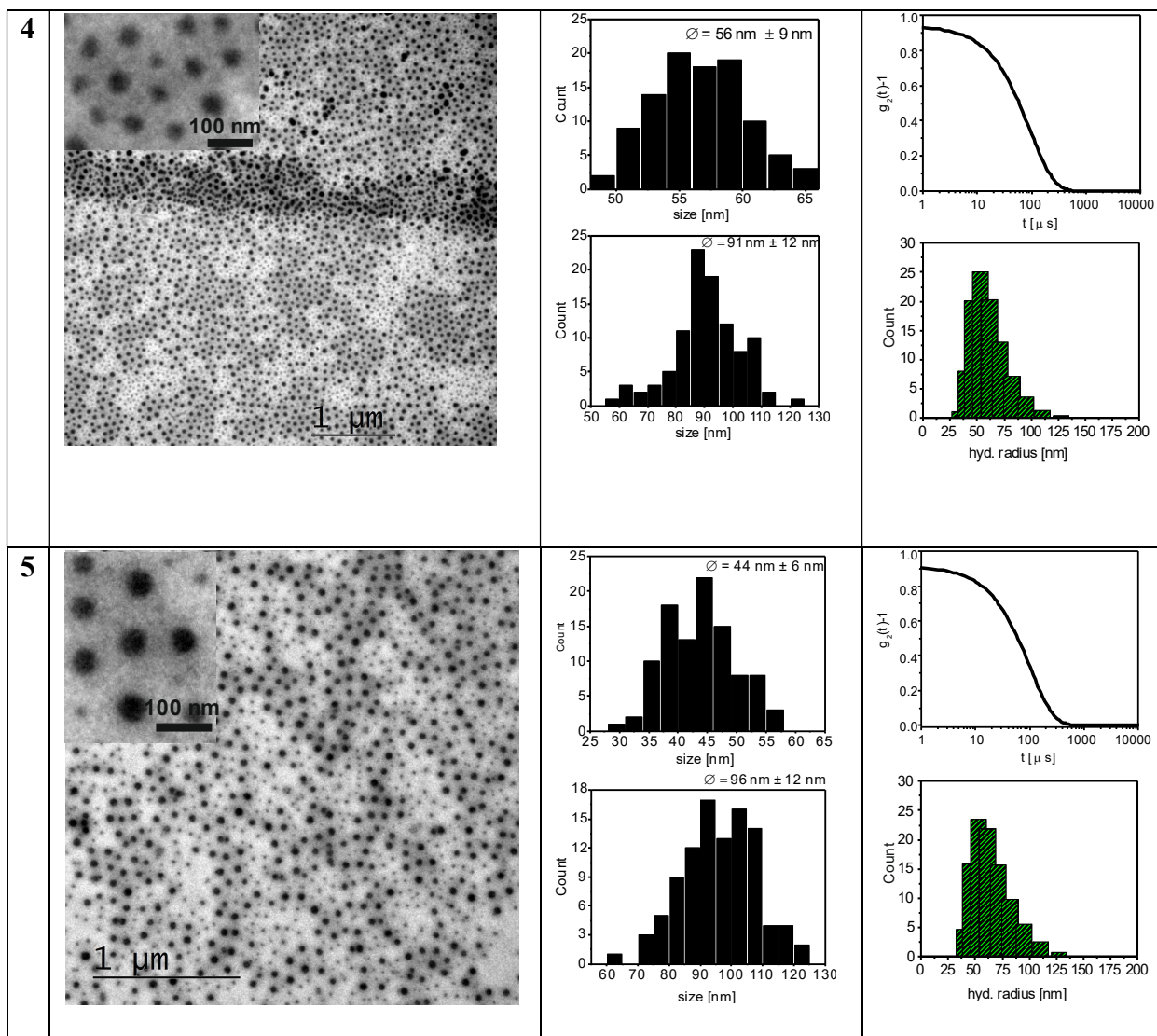
				17.9 mg, 115 μ mol
14	3	5 h	66°C	[Fe(L)(MeOH) ₂]: 6.4 mg, 15 μ mol bipy: 20.2 mg, 129 μ mol
15	3	5 h	66°C	[Fe(L)(MeOH) ₂]: 6.4 mg, 15 μ mol bipy: 22.4 mg, 144 μ mol
16	1	2.25 h	66°C	[Fe(L)(MeOH) ₂]: 6.4 mg, 15 μ mol bipy: 5.6 mg, 36 μ mol
17	2	2.5 h	66°C	[Fe(L)(MeOH) ₂]: 6.4 mg, 15 μ mol bipy: 5.6 mg, 36 μ mol
18	3	2.75 h	66°C	[Fe(L)(MeOH) ₂]: 6.4 mg, 15 μ mol bipy: 5.6 mg, 36 μ mol
19	4	3 h	66°C	[Fe(L)(MeOH) ₂]: 6.4 mg, 15 μ mol bipy: 5.6 mg, 36 μ mol
20	5	3.25 h	66°C	[Fe(L)(MeOH) ₂]: 6.4 mg, 15 μ mol bipy: 5.6 mg, 36 μ mol
21	1	3 h	RT	[Fe(L)(MeOH) ₂]: 6.4 mg, 15 μ mol bipy: 5.6 mg, 36 μ mol
22	2	4 h	RT	[Fe(L)(MeOH) ₂]: 6.4 mg, 15 μ mol bipy: 5.6 mg, 36 μ mol
23	3	5 h	RT	[Fe(L)(MeOH) ₂]: 6.4 mg, 15 μ mol bipy: 5.6 mg, 36 μ mol
24	5	7 h	RT	[Fe(L)(MeOH) ₂]: 6.4 mg, 15 μ mol bipy: 5.6 mg, 36 μ mol

4. Synthesis of [Fe(L)(bipy)]_n Spin Crossover Nanoparticles using Blockcopolymer Micelles

Table S1. Characterization of the CP-BCP composite materials (samples 2-5). The results of TEM and DLS are summarized and discussed in the main text. Each sample was prepared at least twice.

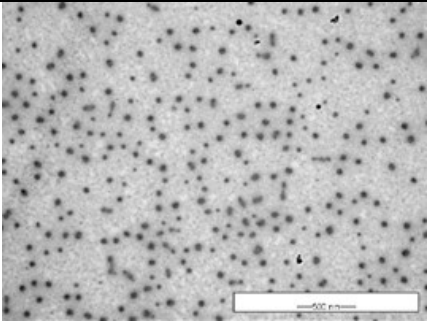
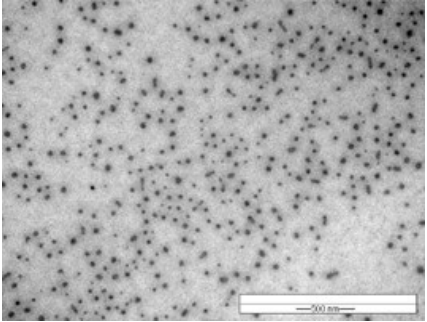
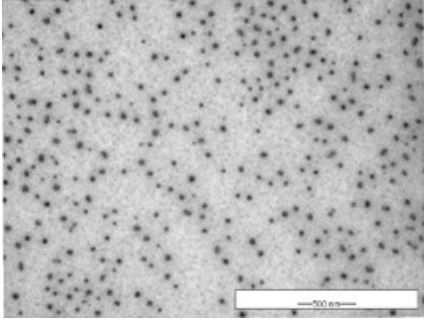
	TEM	Histogram of the TEM picture core (top) and outer diameter (bottom)	Autocorrelation function (top) and distribution of the hydrodynamic radius (bottom)
2			
3			

4. Synthesis of $[\text{Fe}(\text{L})(\text{bipy})]_n$ Spin Crossover Nanoparticles using Blockcopolymer Micelles

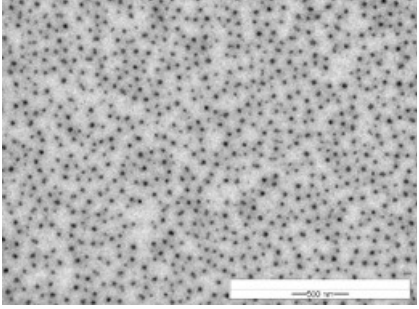
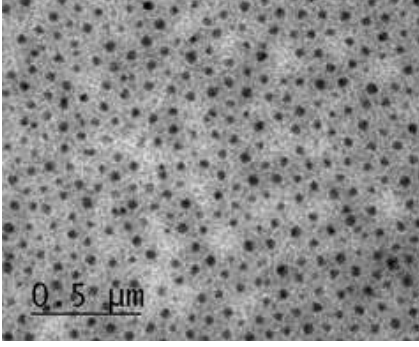
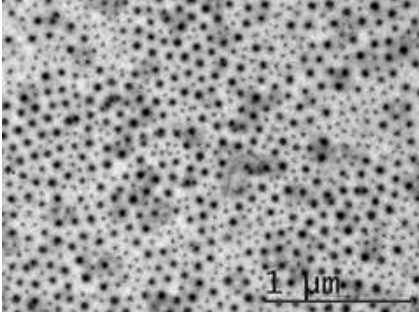
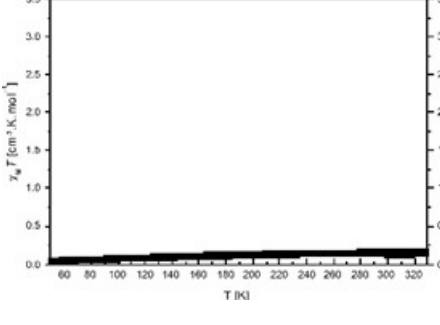
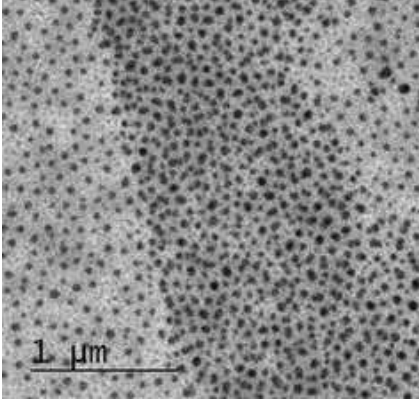
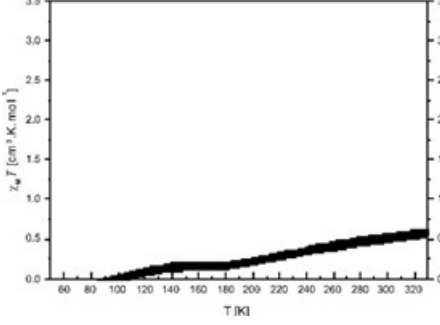


4. Synthesis of [Fe(L)(bipy)]_n Spin Crossover Nanoparticles using Blockcopolymer Micelles

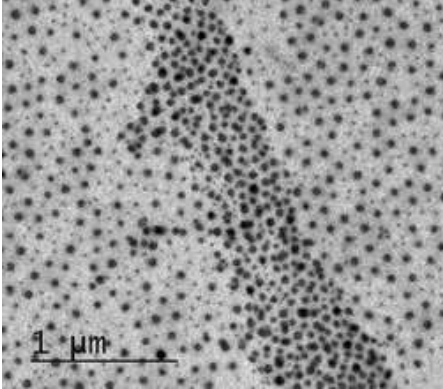
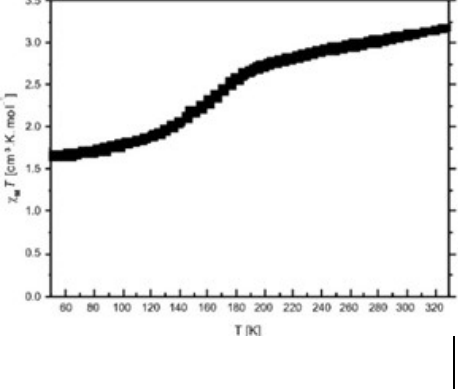
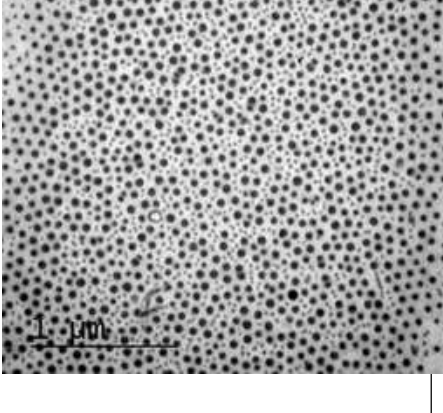
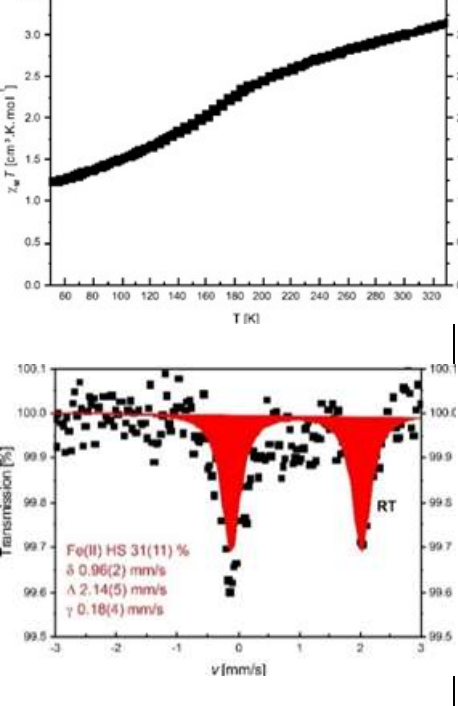
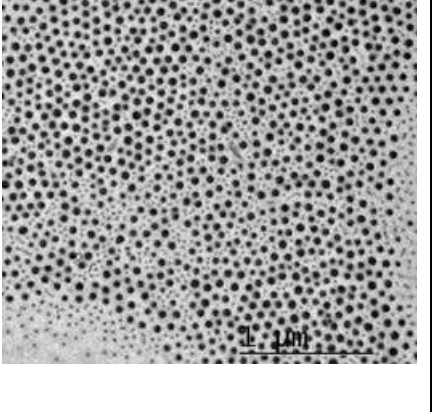
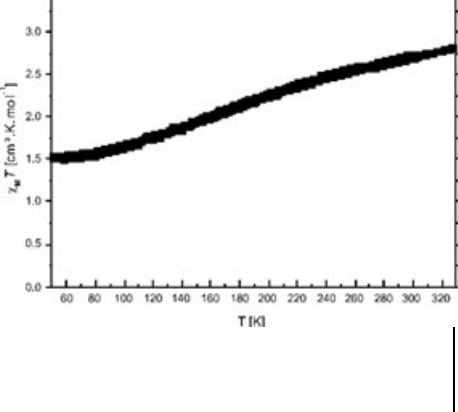
Table S2. Overview over the samples used for the determination of the optimum reaction conditions together with their TEM pictures and the results of SQUID measurements and Mössbauer Spectroscopy (if applicable). Red circles in the TEM pictures highlight significant parts.

Sample ([Fe(L)]:bipy ; cycles; temperature; time)	TEM	core Size DLS/ TEM (core)	Magnetism / Mössbauer
Variation of the Fe:bipy ratio between 1:1 to 1:10 (samples 12 – 21)			
7 (1:1; 1; 66°C; 3h)		TEM: 43±6 nm	
8 (1:3; 1; 66°C; 3h)		TEM: 40±7 nm	
9 (1:4; 1; 66°C; 3h)		TEM: 50±9 nm	

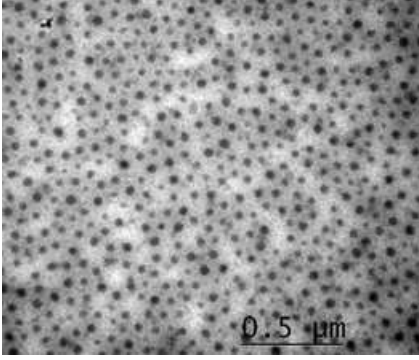
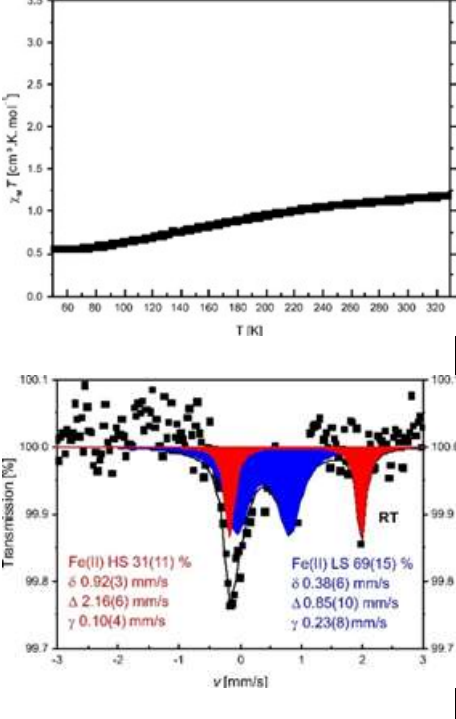
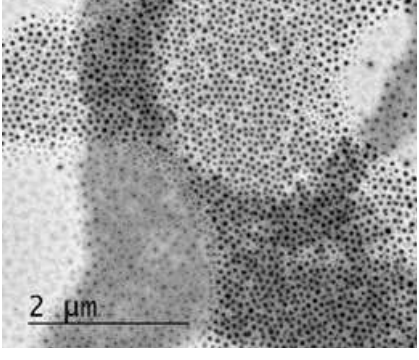
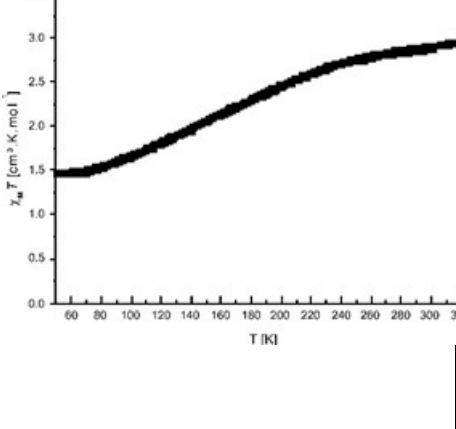
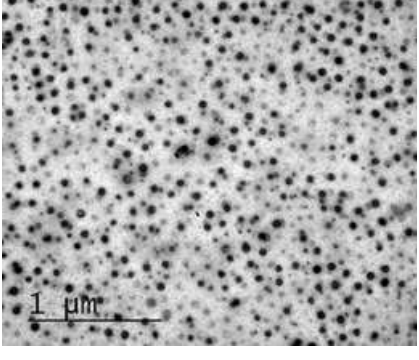
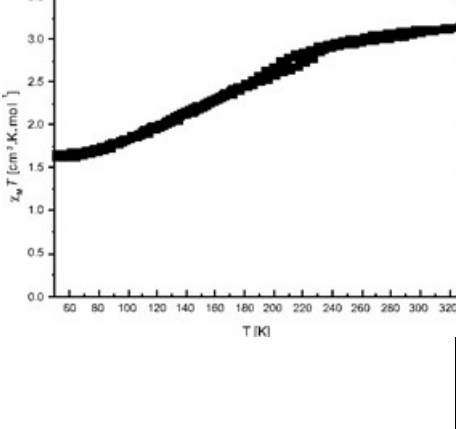
4. Synthesis of [Fe(L)(bipy)]_n Spin Crossover Nanoparticles using Blockcopolymer Micelles

<p>10 (1:5; 1; 66°C; 3h)</p>		<p>TEM: 51±8 nm</p>	
<p>15 (1:10; 3; 66°C; 5h)</p>		<p>DLS: 140 nm TEM: 36±6 nm</p>	
<p>14 (1:9; 3; 66°C; 5h)</p>		<p>DLS: 130 nm TEM: 43±7 nm</p>	
<p>13 (1:8; 3; 66°C; 5h)</p>		<p>TEM: 47±7 nm</p>	

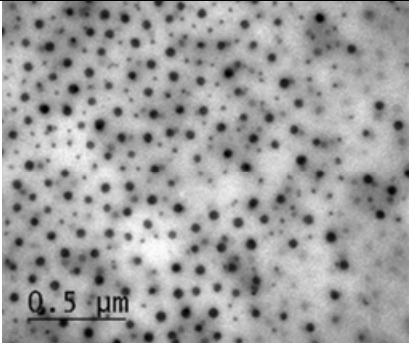
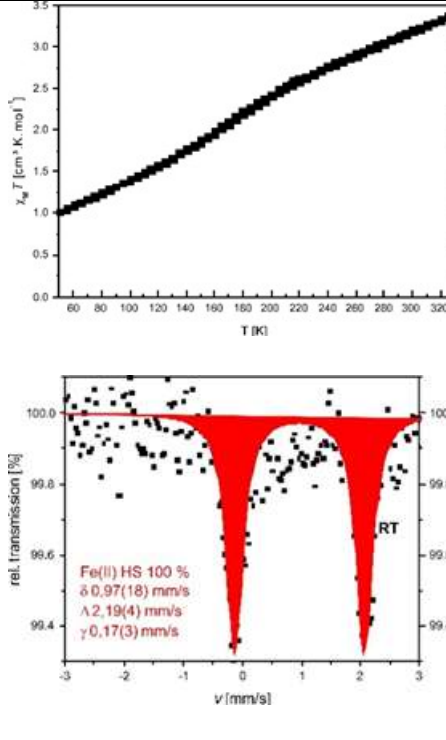
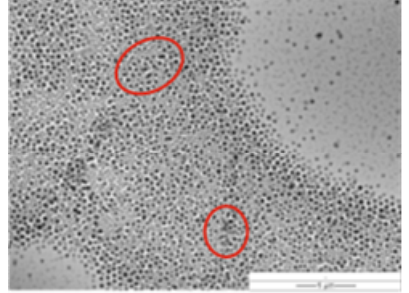
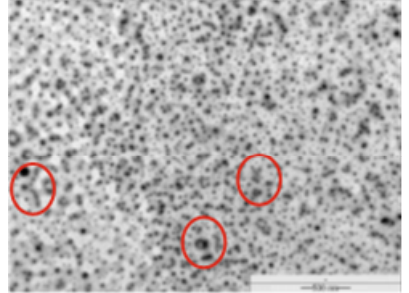
4. Synthesis of [Fe(L)(bipy)]_n Spin Crossover Nanoparticles using Blockcopolymer Micelles

<p>12 (1:7; 3; 66°C; 5h)</p>		<p>TEM: 50±8 nm</p>	
<p>11 (1:6; 3; 66°C; 5h)</p>		<p>TEM: 43±4 nm</p>	
<p>Reduction of the reaction time to 15 min (1 – 5 cycles)</p>			
<p>16 (1:2.5; 1; 66°C; 2.25h)</p>		<p>DLS: 138 nm TEM: 52±5 nm</p>	

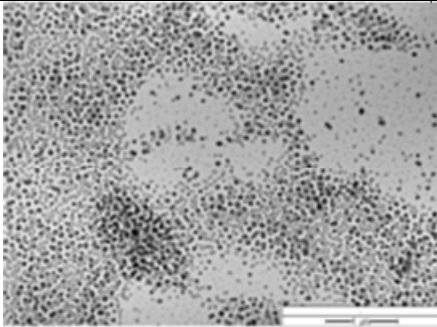
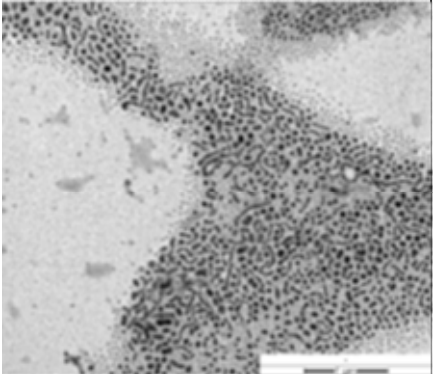
4. Synthesis of $[\text{Fe}(\text{L})(\text{bipy})]_n$ Spin Crossover Nanoparticles using Blockcopolymer Micelles

<p>17 (1:2.5; 2; 66°C; 2.5 h)</p>		<p>DLS: 146 nm</p> <p>TEM: 51±6 nm</p>	 <p> $\chi_m T$ [$\text{cm}^3 \cdot \text{K} \cdot \text{mol}^{-1}$] T (K) </p> <p> Transmission [%] ν [mm/s] </p> <p> Fe(II) HS 31(11) % δ 0.92(3) mm/s Δ 2.16(6) mm/s γ 0.10(4) mm/s </p> <p> Fe(II) LS 69(15) % δ 0.38(6) mm/s Δ 0.85(10) mm/s γ 0.23(6) mm/s </p> <p>RT</p>
<p>18 (1:2.5; 3; 66°C; 2.75 h)</p>		<p>DLS: 146 nm</p> <p>TEM: 51±10 nm</p>	 <p> $\chi_m T$ [$\text{cm}^3 \cdot \text{K} \cdot \text{mol}^{-1}$] T (K) </p> <p> Transmission [%] ν [mm/s] </p> <p> Fe(II) HS 31(11) % δ 0.92(3) mm/s Δ 2.16(6) mm/s γ 0.10(4) mm/s </p> <p> Fe(II) LS 69(15) % δ 0.38(6) mm/s Δ 0.85(10) mm/s γ 0.23(6) mm/s </p> <p>RT</p>
<p>19 (1:2,5; 4; 66°C; 3 h)</p>		<p>DLS: 147 nm</p> <p>TEM: 53±5 nm</p>	 <p> $\chi_m T$ [$\text{cm}^3 \cdot \text{K} \cdot \text{mol}^{-1}$] T (K) </p> <p> Transmission [%] ν [mm/s] </p> <p> Fe(II) HS 31(11) % δ 0.92(3) mm/s Δ 2.16(6) mm/s γ 0.10(4) mm/s </p> <p> Fe(II) LS 69(15) % δ 0.38(6) mm/s Δ 0.85(10) mm/s γ 0.23(6) mm/s </p> <p>RT</p>

4. Synthesis of $[\text{Fe}(\text{L})(\text{bipy})]_n$ Spin Crossover Nanoparticles using Blockcopolymer Micelles

<p>20 (2:2.5; 5; 66°C; 3.25 h)</p>		<p>TEM: 42±5 nm</p>	
<p>Stirring at room temperature (1 – 5 cycles)</p>			
<p>21 (1:2.5; 1; RT; 3h)</p>		<p>TEM: 56±7 nm</p>	
<p>22 (1:2.5; 2; RT; 4h)</p>		<p>TEM: 35±6 nm</p>	

4. Synthesis of [Fe(L)(bipy)]_n Spin Crossover Nanoparticles using Blockcopolymer Micelles

23 (1:2.5; 3; RT; 5h)		TEM: 58±9 nm	
24 (1:2.5; 5; RT; 7h)		TEM: 63±13 nm	

4. Synthesis of [Fe(L)(bipy)]_n Spin Crossover Nanoparticles using Blockcopolymer Micelles

Table S3. Mössbauer parameters of the samples **1** and **3 – 6** at room temperature. Given are the isomer shift δ [mms^{-1}], the quadrupole splitting ΔE_Q [mms^{-1}], the half width of the lines Γ [mms^{-1}], and the fraction of HS sites [%].

compound	Site	δ [$\text{mm}\cdot\text{s}^{-1}$]	ΔE_Q [$\text{mm}\cdot\text{s}^{-1}$]	Γ [$\text{mm}\cdot\text{s}^{-1}$]	A/A_{tot} [%]
1	Fe ^{II} LS	0.38(4)	0.69(3)	0.22(3)	81(6)
	Fe ^{II} HS	0.96(3)	2.23(3)	0.32(2)	19(7)
3	Fe ^{II} LS	0.38(4)	1.01(8)	0.38(4)	47(4)
	Fe ^{II} HS	0.96(3)	2.21(6)	0.32(3)	53(4)
4	Fe ^{II} LS	0.45(9)	0.84(16)	0.49(12)	45(15)
	Fe ^{II} HS	0.93(2)	2.20(4)	0.24(6)	55(12)
5	Fe ^{II} LS	0.28(4)	1.02(8)	0.22(12)	16(6)
	Fe ^{II} HS	0.97(13)	2.15(3)	0.32(4)	84(8)
6	Fe ^{II} LS	-	-	-	-
	Fe ^{II} HS	0.95(5)	2.17(1)	0.28(2)	100

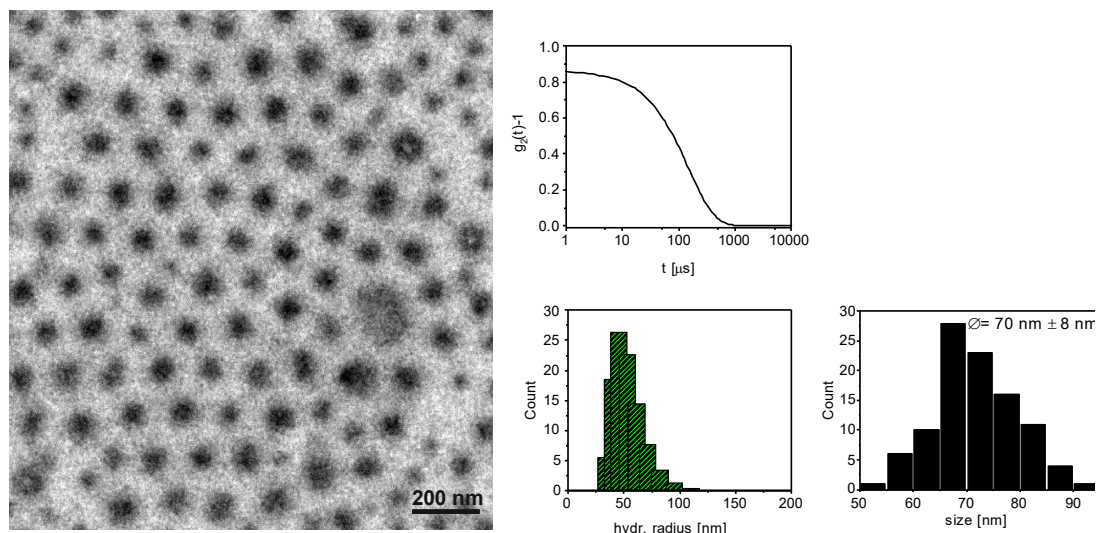


Figure S1. Left: TEM picture of the empty PS-P4VP BCP. Middle: Results of dynamic light scattering of the PS-P4VP-BCP in THF showing a hydrodynamic diameter of 126 nm. Right: size histogram from the TEM picture given on the left with an average diameter of 70 nm.

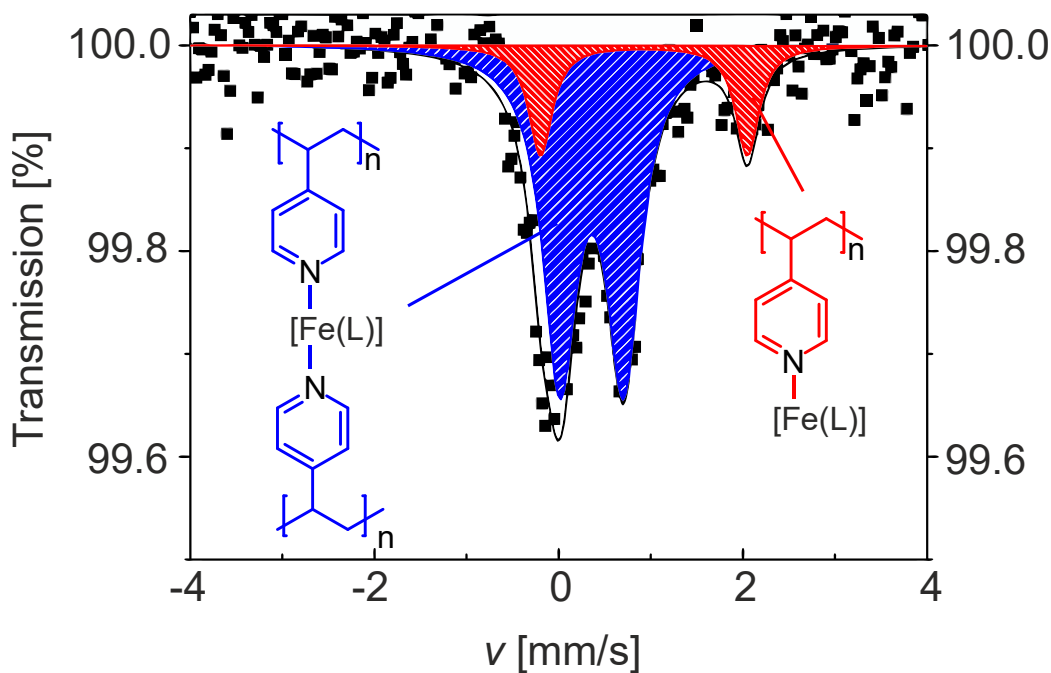


Figure S2. Mössbauer spectrum of **1** at room temperature. Two doublets are observed corresponding to two different species $[\text{Fe}(\text{L})(\text{vp})]$ and $[\text{Fe}(\text{L})(\text{vp})_2]$. The majority species (blue doublet, 80 %) with an isomer shift δ of 0.38(4) mm/s and a quadrupole splitting ΔE_Q of 0.69(3) mm/s corresponds to an octahedral LS complex $[\text{Fe}(\text{L})(\text{vp})_2]$, while the parameters of the minority species (red doublet, 20 %, $\delta = 0.96(3)$ mm/s and $\Delta E_Q = 2.25(9)$ mm/s) is characteristic for an HS complex $[\text{Fe}(\text{L})(\text{vp})]$.

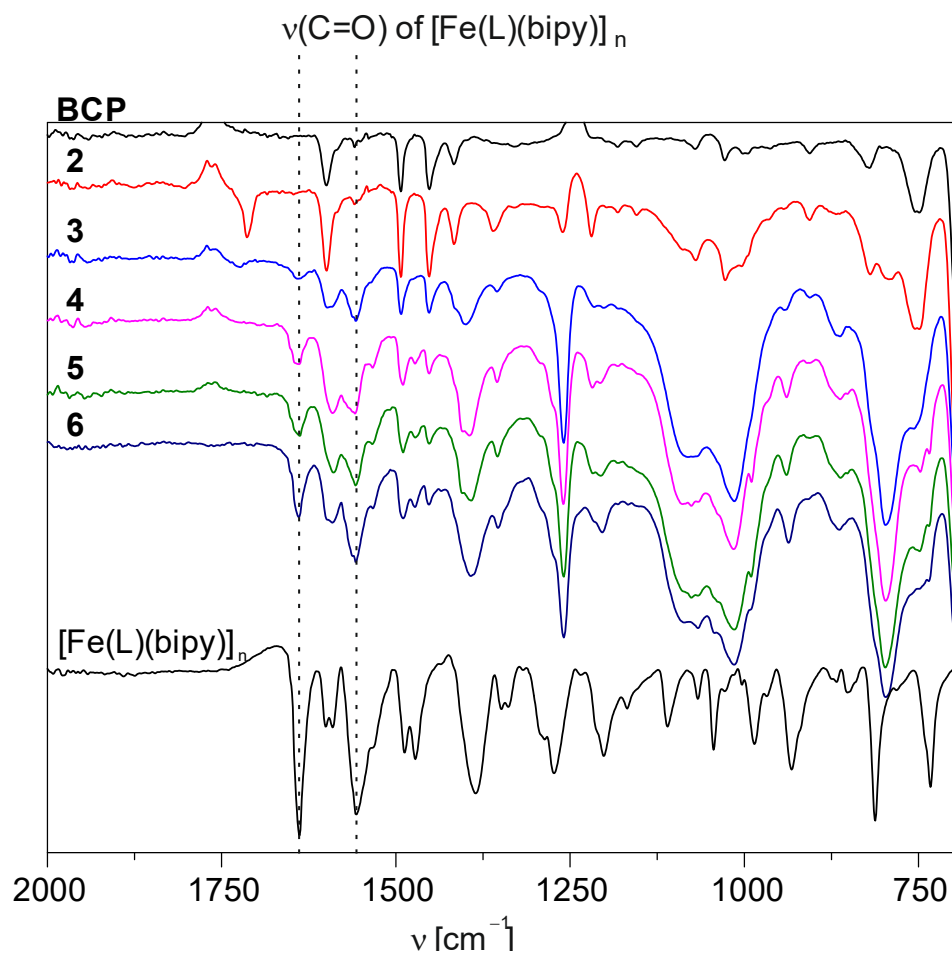


Figure S3. IR spectra of the BCP, $[\text{Fe}(\text{L})(\text{bipy})]_n$ and the composite samples 2 – 6.

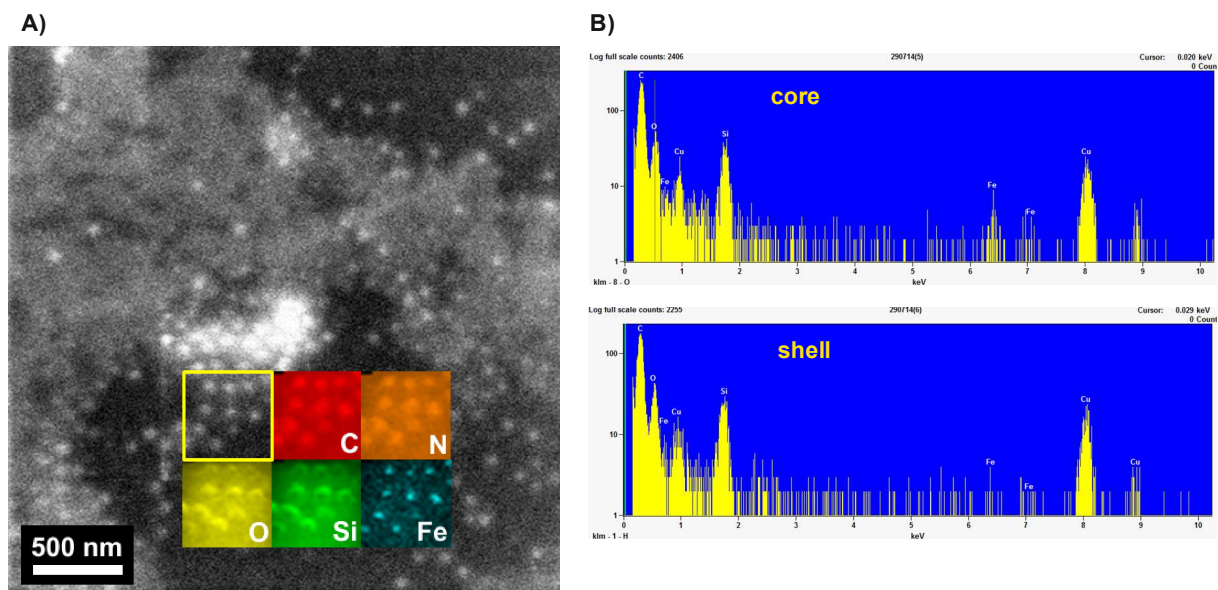


Figure S4. A) 2D-EDX screening of CP-BCP micelles of sample **6** to show the distribution of iron (blue), carbon (red), nitrogen (orange), oxygen (yellow) and silicon (green) in the sample. A significant difference is observed for the iron distribution in the core (bright, high amount of iron) and the shell (dark, low amount of iron). B) EDX analysis of the core and the shell of the CP-BCP micelle showing a significant difference in the iron distribution.

As shown in Figure S4A the spherical core of the NPs (bright spot) shows mainly the elements carbon, iron and nitrogen. In contrast to this, there is almost no iron in the outer shell, while carbon and nitrogen are evenly distributed over the whole particle. The EDX analysis (Fig. S4B) is given for the core (top) and the outer shell (bottom) of the NPs. It also confirms that the core of the NP has a significant amount of iron while the shell is nearly iron-free. The copper signal in both measurements arises from the TEM grids and the silicon most likely from the synthesis of the CP-BCP composite materials (small amount of grease).

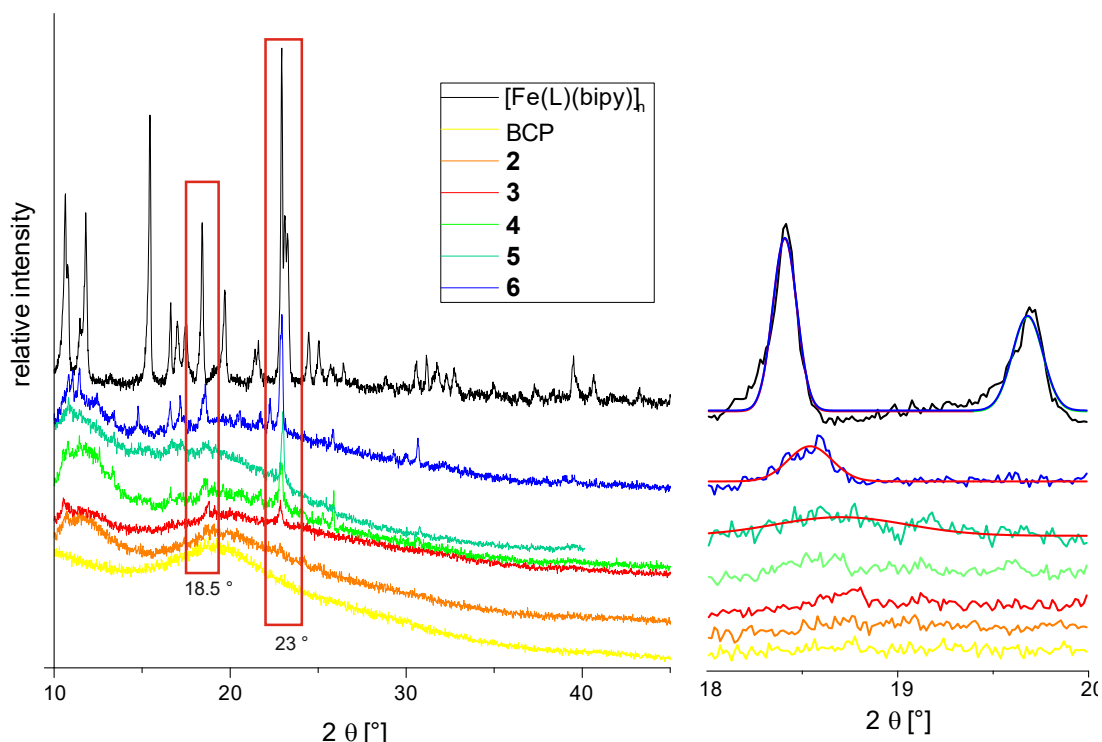


Figure S5. PXRD spectra in the 10 – 45 2θ range of the samples **2** – **6**, the bulk complex [Fe(L)(bipy)]_n and the BCP. The peaks used for the calculation of the particle size are indicated with red squares. For the complex [Fe(L)(bipy)]_n a good agreement between the particle size calculated from the two different peaks is observed (in both cases around 60 nm). For the composite material the particle sizes determined from the 18.5° peak are smaller (10 nm for **5** and 30 nm for **6**) compared to the values obtained for the 23° peak discussed in the manuscript. The continuous line resembles the fit used for the determination of the half width.

To analyze the crystallinity of the obtained particles, powder X-ray diffraction data were collected for the different samples. After one cycle (sample **2**), no reflexes are observed indicating a completely amorphous material. With increasing number of cycles, some broad reflexes appear in a similar region as for the bulk [Fe(L)(bipy)]_n. Those reflexes are significantly broader and less well defined than those reported for microcrystals of [Fe(L)(bipy)]_n in a P4VP matrix.¹ Even after 5 cycles (sample **6**), the typical PXRD pattern of the bulk material is not observed – some reflexes are missing. This indicates that the crystalline parts of the particles are much smaller than those obtained in the P4VP matrix.

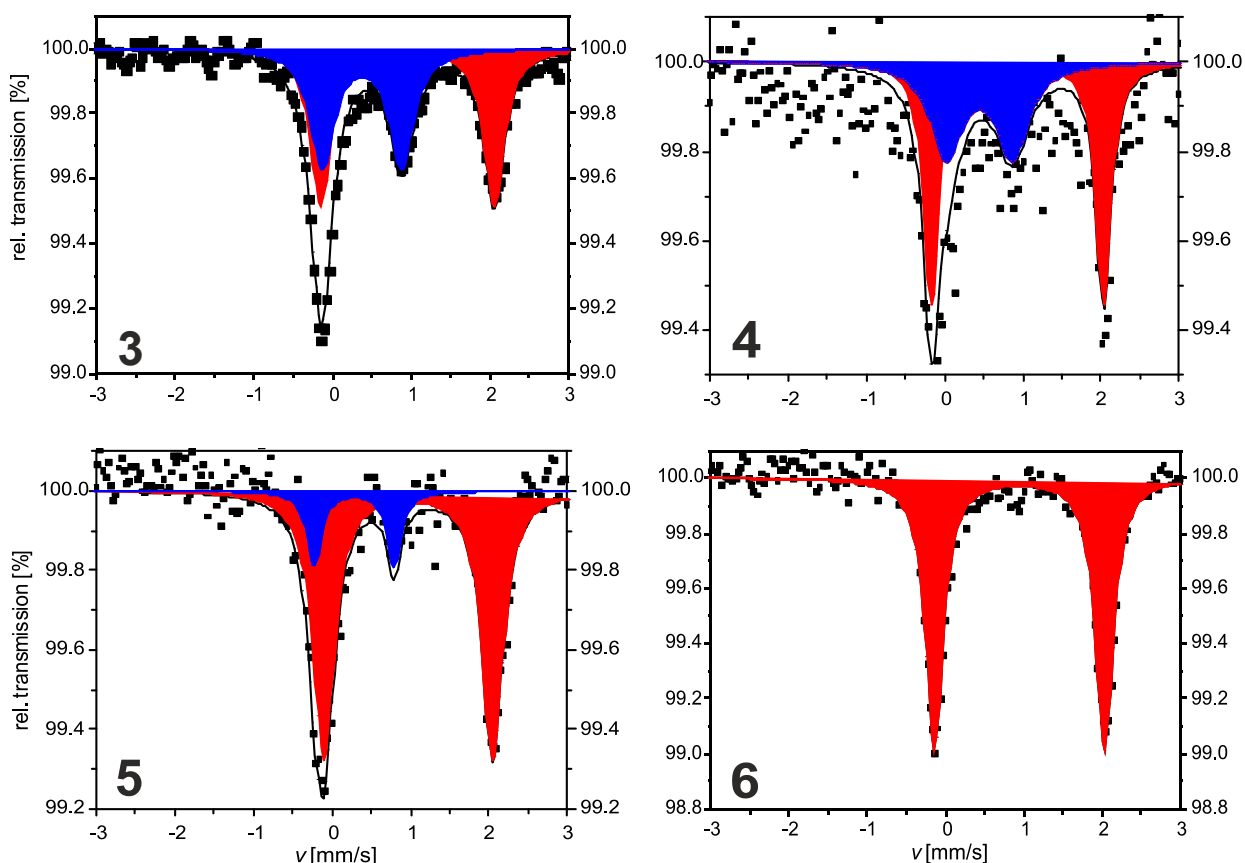


Figure S6. Room temperature Mössbauer spectra of the samples **3** – **6**. The black squares are the results from the measurements and the solid lines correspond to the fit with the low-spin doublet given in blue and the high-spin doublet given in red for each sample. The corresponding Mössbauer parameters are summarized in Table S4.

For all spectra, the signal intensity is comparatively low (around 1 % absorption) and the half width of the lines (Γ) is between 0.2 and 0.5 mm/s. This is significantly broader than the values observed for the sub-microcrystals of $[\text{Fe}(\text{L})(\text{bipy})]$ in the P4VP matrix.¹ Both observations are typical for nanoparticles. For the iron complex $[\text{FeL}]$ in the polymer matrix before addition of the bridging ligand bipy (sample **1**, in Figure S2) two doublets are observed. The main species with an area of 81(6) % shows Mössbauer parameters ($\delta = 0.38(4)$ mm/s, $\Delta E_Q = 0.69(3)$ mm/s) typical for octahedral iron(II) LS sites of this ligand type.^{2,3} This corresponds to a complex with two vinylpyridine units coordinating at the iron center. The second doublet ($\delta = 0.96(3)$ mm/s, $\Delta E_Q = 2.23(3)$ mm/s) shows typical parameter for iron(II) HS complexes of this ligand type.^{2,3} This HS site with an area of 19(7) % corresponds to an iron(II) species with one vinylpyridine coordinated

4. Synthesis of [Fe(L)(bipy)]_n Spin Crossover Nanoparticles using Blockcopolymer Micelles

to the iron center leaving the sixth coordination site free or occupied by one solvent molecule. Iron(II) complexes of this ligand type with an N₃O₂ or an N₃O₃ coordination sphere are usually in the HS state.⁴⁻⁶ Upon addition of bipy, the desired coordination polymer is formed. Magnetic measurements on the bulk material revealed an abrupt and complete spin transition with hysteresis (18K, $T_{1/2\downarrow} = 219\text{K}$ and $T_{1/2\uparrow} = 237\text{K}$) below room temperature,⁷⁻⁹ thus at room temperature the complex is in the HS state. In agreement with this, upon addition of bipy the area of the LS doublet decreases and the area of the HS doublet increases. The Mössbauer parameters of the HS state do not change significantly upon coordination of the pyridine and are in the same range as observed for the bulk material and sub-microcrystals of [Fe(L)(bipy)] in P4VP.¹ When going from **3** to **6**, with an increasing number of reaction cycles, the area fraction of the LS species continuously decreases until for sample **6** only one HS doublet is observed (see Table 3).

References

1. Göbel, C.; Palamarciuc, T.; Lochenie, C.; Weber, B. *Chem. Asian J.* **2014**, *9* (8), 2232–2238.
2. Bauer, W.; Lochenie, C.; Weber, B. *Dalton Trans.* **2014**, *43* (5), 1990–1999.
3. C. Lochenie, C.; Bauer, W.; Railliet, A. P.; Schlamp, S.; Garcia, Y.; Weber, B. *Inorg. Chem.* **2014**, *53* (21), 11563–11572.
4. Weber, B.; Kaps, E.; Obel, J.; Bauer, W. *Z. Anorg. Allg. Chem.* **2008**, *634* (8), 1421–1426.
5. Bauer, W.; Weber, B. *Acta Cryst. C* **2008**, *64* (6), m237.
6. Weber, B.; Jäger, E.-G. *Eur. J. Inorg. Chem.* **2009**, (4), 465–477.
7. Weber, B.; Tandon, R.; Himsl, D. *Z. Anorg. Allg. Chem.* **2007**, *633* (8), 1159–1162.
8. Weber, B.; Kaps, E. S.; Desplanches, C.; Létard, J. *Eur. J. Inorg. Chem.* **2008**, *2008* (19), 2963–2966.
9. Baldé, C.; Bauer, W.; Kaps, E.; Neville, S.; Desplanches, C.; Chastanet, G.; Weber, B.; Létard, J. F. *Eur. J. Inorg. Chem.* **2013**, (15), 2744–2750.

5. Synthesis of [Fe(L_{eq})(L_{ax})]_n Coordination Polymer Nanoparticles using Blockcopolymer Micelles

Christoph Göbel¹, Ottokar Klimm¹, Florian Puchtler², Sabine Rosenfeldt³, Stephan Förster³ and Birgit Weber^{*1}

Address: ¹Inorganic Chemistry II, University of Bayreuth, Universitätsstr. 30, 95440 Bayreuth, Germany ²Inorganic Chemistry I, University of Bayreuth, Universitätsstr. 30, 95440 Bayreuth, Germany and ³Physical Chemistry I and Bavarian Polymer Institute, University of Bayreuth, Universitätsstr. 30, 95440 Bayreuth, Germany

Email: weber@uni-bayreuth.de, <http://www.ac2-weber.uni-bayreuth.de>

* Corresponding author

Published in *Beilstein J. Nanotech.*, **2017**, *8*, 1318–1327.

Reproduced by permission of the Beilstein Journal of Nanotechnology

Abstract

Spin crossover compounds are a class of materials that can change their spin state from high spin (HS) to low spin (LS) by external stimuli such as light, pressure or temperature. Applications demand compounds with defined properties concerning the size and switchability that are maintained when the compound is integrated into composite materials. Here, we report the synthesis of $[\text{Fe}(\text{L}_{\text{eq}})(\text{L}_{\text{ax}})]_n$ coordination polymer (CP) nanoparticles using self-assembled polystyrene-*block*-poly(4-vinylpyridine) (PS-*b*-P4VP) block copolymer (BCP) micelles as template. Variation of the solvent (THF and toluene) and L_{ax} ($\text{L}_{\text{ax}} = 1,2\text{-di}(\text{pyridine-4-yl})\text{ethane}$ (bpea), *trans*-1,2-di(pyridine-4-yl)ethene (bpee), and 1,2-di(pyridine-4-yl)ethyne (bpey); $\text{L}_{\text{eq}} = 1,2\text{-phenylenebis}(\text{iminomethylidene})\text{-bis}(2,4\text{-pentanedionato})(2\text{-})$) allowed the determination of the preconditions for the selective formation of nanoparticles. A low solubility of the CP in the used solvent and a high stability of the Fe-L bond with regard to ligand exchange are necessary for the formation of composite nanoparticles where the BCP micelle is filled with the CP, as in the case of the $[\text{FeL}_{\text{eq}}(\text{bpey})]_n@BCP$. Otherwise the formation of microcrystals next to the CP-BCP nanoparticles is observed above a certain $[\text{Fe}(\text{L}_{\text{eq}})(\text{L}_{\text{ax}})]_n$ concentration. The core of the nanoparticles is about 45 nm in diameter due to the templating effect of the BCP micelle, independent of the used iron complex and $[\text{Fe}(\text{L}_{\text{eq}})(\text{L}_{\text{ax}})]_n$ concentration. The spin crossover properties of the composite material are similar to the bulk for $[\text{FeL}_{\text{eq}}(\text{bpea})]_n@BCP$ while pronounced differences are observed in the case of $[\text{FeL}_{\text{eq}}(\text{bpey})]_n@BCP$ nanoparticles.

Introduction

Nanomaterials and especially nanocomposites of coordination polymers (CPs) and (porous) coordination networks are of great interest in today's research due to their various applications as sensors, data storage devices, catalysts or contrast agents.^[1-5] For these applications the formation of stable, uniform and monodisperse particles with defined properties is necessary. Synthetic procedures for nanoparticles with size control (gold,^[6, 7] metal oxide^[8, 9]) and/or shape control (gold and silver^[10]) are already well-known. The reduction of metal salts is very common for noble metals,^[11] while (fast) precipitation or inverse micelle technique are often used for metal oxide (mostly magnetite).^[12] For coordination polymers (CP) or networks a limited amount of methods are applicable due to the very demanding reaction conditions and/or incompatible reactants.

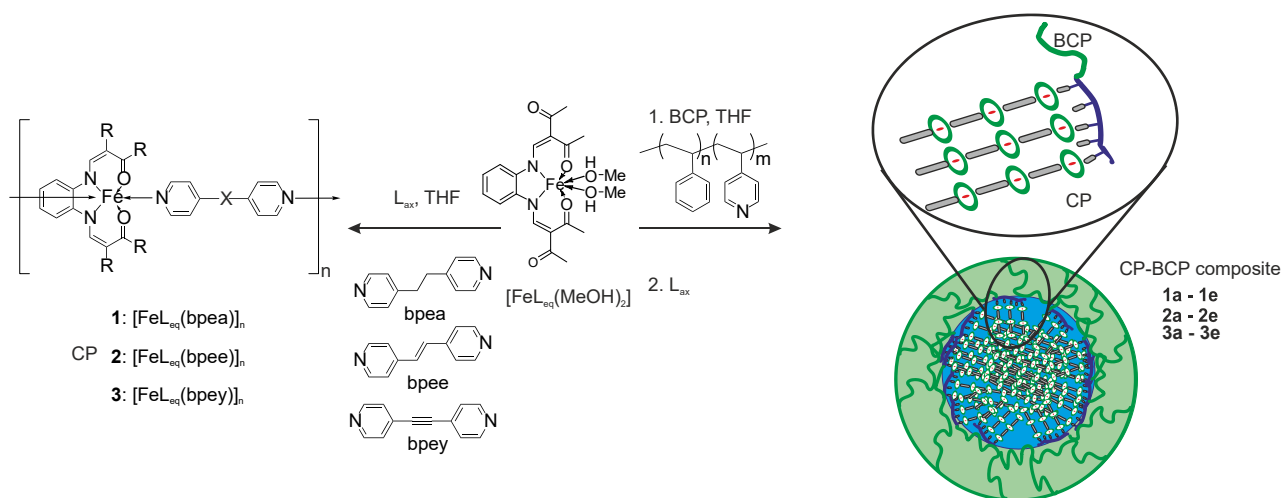
Recently we demonstrated that the use of block copolymers (BCPs) is a highly promising and easy approach for the size control of CPs.^[13] The BCPs form micellar structures through self-assembly in specific solvents and can therefore be used as nanoreactors.^[14–16] Using this approach, a very controlled miniaturisation of coordination polymers or networks can be envisioned, provided it is easily transferable to other systems. In this work we will analyse, which preconditions need to be fulfilled for a successful synthesis of uniform CP-BCP nanoparticles.

Coordination polymers with spin crossover (SCO) properties are well known in the literature,^[4, 5, 17, 18] but their miniaturisation into precisely defined nanomaterials with SCO properties comparable to those of the bulk material is still in its infancy.^[19–23] SCO materials can be switched by external stimuli like temperature, pressure or light between a high-spin (HS) and a low-spin (LS) state.^[5, 18] Switching between these two states alters physical properties like magnetism, structure or colour which make these materials interesting for sensors,^[2, 24–26] display devices^[27–29] or as functional contrast agents.^[30–34] The SCO properties deeply depend on the precise control of size and crystallinity of the nanocomposite. Mostly the inverse micelle technique is used for the preparation of nanoparticles,^[35–39] however, the spin crossover properties of the bulk are often lost upon miniaturisation and only few examples preserving the hysteresis (bistability) in a nanostructured system are known.^[40–43, 21] This is most likely due to a loss of the crystallinity of the particles. Especially SCO complexes are highly sensitive to small changes in the crystal packing and thus excellently suited to investigate the impact of nanostructuring of the material. In our recent work^[13] we used the block copolymer polystyrene-*b*-poly(4-vinylpyridine) (PS-*b*-P4VP) to prepare spherical nanoparticles of the 1D spin crossover coordination polymer [FeL_{eq}(bipy)]_n. We were able control the crystallinities of the [FeL_{eq}(bipy)]_n core through successive addition of starting material and by variation of the reaction time and temperature. Having a high crystallinity of the core, the SCO properties were closer to those of the bulk material (thermal hysteresis loop).

We herein report the synthesis of three further coordination polymer block copolymer nanocomposites (CP-BCP) using the same synthesis strategy. This allows us to investigate the influence of the coordination polymer on the formation and SCO activity of the final nanocompound. The CPs differ in the axial ligands (L_{ax}), namely 1,2-di(pyridine-4-yl)ethane (bpea), *trans*-1,2-di(pyridine-4-yl)ethene (bpee) and 1,2-di(pyridine-4-yl)ethyne (bpey) (Scheme 1). The ligands were chosen due to their different flexibility. From the synthesis of the bulk

5. Synthesis of $[\text{Fe}(\text{Leq})(\text{Lax})]_n$ Coordination Polymer Nanoparticles using Blockcopolymer Micelles

complexes it is known, that an increasing flexibility of the ligand leads to an increase in solubility of the obtained CP.^[44, 45] This way we can investigate the impact of the solubility of the CP on the selective formation of nanoparticles in the BCP micelle cores. In Scheme 1, the general approach and the abbreviations used for the different samples are given.



Scheme 1: Synthesis of the three different coordination polymers $[\text{FeLeq}(\text{bpea})]_n$ (**1**), $[\text{FeLeq}(\text{bpee})]_n$ (**2**) and $[\text{FeLeq}(\text{bpey})]_n$ (**3**) and the respective coordination polymer block copolymer composites (CP-BCP) $[\text{FeLeq}(\text{bpea})]_n@ \text{BCP}$ (**1a - 1e**), $[\text{FeLeq}(\text{bpee})]_n@ \text{BCP}$ (**2a - 2e**) and $[\text{FeLeq}(\text{bpey})]_n@ \text{BCP}$ (**3a - 3e**).

Results and Discussion

Bulk complexes

The magnetic properties of SCO coordination polymers often depend on solvent molecules included in the crystal packing.^[46-49] To allow comparison between bulk material and nanoparticles and to study the influence of nanostructuring on magnetism, the bulk complexes were synthesised in THF and their magnetic properties were investigated. $[\text{FeLeq}(\text{bpea})]_n$ and $[\text{FeLeq}(\text{bpee})]_n$ were already synthesised in methanol,^[44, 50] the coordination polymer $[\text{FeLeq}(\text{bpey})]_n$ is described here the first time. The coordination polymers **1**, **2** and **3** were synthesised by dissolving the Fe^{II} complex $[\text{FeLeq}(\text{MeOH})_2]$ and the respective axial ligand in THF. The solution was refluxed for 1h. After cooling down overnight, the fine crystalline precipitate was filtered off and dried *in vacuo* to yield brown or dark violet powders respectively.

In Figure 1, the magnetic properties of **1** ([FeL_{eq}(bpea)]_n) and **3** ([FeL_{eq}(bpey)]_n) as plot of the $\chi_M T$ product (χ_M = magnetic susceptibility, T = temperature) versus temperature is given. Sample **1** is paramagnetic at RT with a $\chi_M T$ value of 3.25 cm³Kmol⁻¹, typical for Fe^(II) in the HS state.^[51] Upon cooling the $\chi_M T$ value is constant down to 140 K where an abrupt, incomplete spin crossover occurs. In the first step, the $\chi_M T$ value descends to 1.78 cm³Kmol⁻¹ at 120 K corresponding to about 50% of the iron centres in the HS state. Further cooling reveals a second, gradual and incomplete step with a $\chi_M T$ value of 0.93 cm³Kmol⁻¹ at 50 K; about one third of the iron centres remains in the HS state. Upon heating, a 3 K wide hysteresis is observed in the region of the first step with $T_{1/2\uparrow}$ =127 K and $T_{1/2\downarrow}$ =130 K. In the temperature range between 75 K and 100 K first a decrease and then an increase of the $\chi_M T$ product upon heating is observed. This is due to a kinetic trapping effect, often observed in this temperature region when the thermal spin transition temperature ($T_{1/2}$) and the transition temperature for the thermally trapped excited spin state (T_{TIESST}) are in close proximity.^[52, 44, 53, 54] The two-step behaviour is similar to the one observed for {[FeL_{eq} bpea]}·0.25 MeOH)_n, where the temperatures differ slightly and the second step is complete.^[44] The differences due to the impact of the different solvents are also reflected in the powder diffraction patterns (SI, Figure S1) where some of the reflexes are shifted compared to the sample prepared in methanol. Sample **2** ([FeL_{eq}(bpee)]_n) is paramagnetic at RT with a $\chi_M T$ value of 3.20 cm³Kmol⁻¹ (SI, Figure S2). Upon cooling the sample remains in the HS state over the whole temperature range, as already reported for the complex synthesised from methanol.^[50] Sample **3** ([FeL_{eq}(bpey)]) is paramagnetic at RT with a $\chi_M T$ value of 3.23 cm³Kmol⁻¹, typical for iron(II) complexes in the HS state (bottom of Figure 1). Upon cooling the $\chi_M T$ value is almost constant down to 190 K ($\chi_M T$ value: 3.14 cm³Kmol⁻¹), where an abrupt and incomplete spin transition occurs with about 50% of the iron centres involved. The $\chi_M T$ value drops to 1.73 cm³Kmol⁻¹ at 165 K and no further changes are observed down to 50 K ($\chi_M T$ value: 1.63 cm³Kmol⁻¹). Upon heating up to 300 K an abrupt spin transition takes place revealing a hysteresis with a width of 10 K and $T_{1/2\downarrow}$ = 177 K and $T_{1/2\uparrow}$ = 187 K. Mössbauer spectra were collected for all three samples to verify the HS state at room temperature. The spectra (SI, Figure S3) reveal one quadrupole split doublet in each case with parameters for the quadrupole splitting ΔE_Q and an isomer shift δ (SI, Table S1) in the range expected for iron(II) HS complexes of this ligand type.^[55] The steps and the incomplete spin crossover observed in the magnetic measurements could be due to inequivalent iron centers.^[56, 57] The Mössbauer spectra do not support this as no line broadening (FWHM Γ in the SI, Table 1) is observed and the doublet is very symmetric in each case. Thus the steps

observed in the transition curve are due to the packing of the CP in the crystal and will strongly depend on the crystallinity of the material.

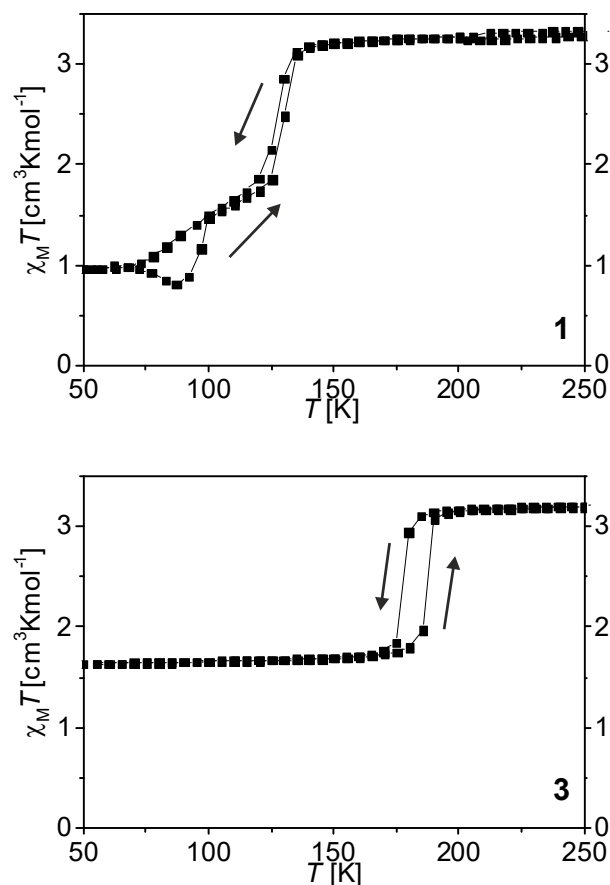


Figure 1: Magnetic susceptibility data for the coordination polymers $[\text{FeL}_{\text{eq}}(\text{bpea})]_n$ (**1**) and $[\text{FeL}_{\text{eq}}(\text{bpey})]_n$ (**3**) which undergo spin crossover.

Synthesis of the nanocomposite

For the CP-BCP composites $[\text{FeL}_{\text{eq}}(\text{bpea})]_n@BCP$ (**1a - 1e**), $[\text{FeL}_{\text{eq}}(\text{bpee})]_n@BCP$ (**2a - 2e**) and $[\text{FeL}_{\text{eq}}(\text{bpey})]_n@BCP$ (**3a - 3e**), the starting iron(II) complex $[\text{FeL}_{\text{eq}}(\text{MeOH})_2]$ and the block copolymer were dissolved in THF and refluxed for 2h. After cooling down to room temperature, the respective bridging ligand was added and the mixture was refluxed again for 1h. Depending on the number of additions of starting material, either the solvent is removed by cold distillation (1 cycle, samples **1a**, **2a**, **3a**) or a further cycle of addition of $[\text{FeL}_{\text{eq}}(\text{MeOH})_2]$ and axial ligand (simultaneously for all further cycles) followed by reflux for 1 hour was performed prior to solvent

removal (samples **1-3 b-e** for 2 to 5 cycles). The resulting solids were dried *in vacuo*. IR spectroscopy was used to follow the formation of the coordination polymer in the BCP matrix. The corresponding spectra are given in the Supporting Information, Figure S4. The increasing relative intensity of the C=O stretching vibration of [FeL_{eq}] clearly indicates the formation of the coordination polymer in the matrix.

Room temperature Mössbauer spectra were collected for the samples [FeL_{eq}(bpea)]_n@BCP after 4 and 5 cycles (**1d** and **1e**) and [FeL_{eq}(bpey)]_n@BCP after 4 and 5 cycles (**3d** and **3e**) to get a deeper insight into the sample composition. The corresponding spectra are given in the SI, Figure S5 and the Mössbauer parameters are summarised in the SI, Table S2. For the composite materials, different iron species are possible due to the coordination of the starting complex [Fe(L_{eq})] to the vinylpyridine parts of the equatorial ligand that can be distinguished using Mössbauer spectroscopy. Sample **1d** shows two different doublets which correspond to an Fe^(II) HS and Fe^(II) LS species (75% and 25%). The LS species derives from two P4VP units coordinated to the iron centre as already shown.^[13, 58] For sample **1e** again two doublets are observed with a similar HS:LS ratio (Table S2). The sample **3d** also shows two different iron species from which one corresponds to an iron(II) in the HS state and the other one to an iron(II) in the LS state, however, the HS:LS ratio changes to 83% : 17%. For sample **3e** only one doublet is observed that can be assigned to an iron(II) HS species. It concludes that in the case of [FeL_{eq}(bpey)]_n@BCP the HS fraction increases with higher cycles since more or longer coordination polymer is formed in the BCP micelle, in agreement with previous observations for [FeL_{eq}(bipy)]_n@BCP.^[13, 58] In the case of [FeL_{eq}(bpea)]_n@BCP a different behavior is observed that is indicative for differences in the sample composition.

Characterisation of the nanocomposite

Particle sizes of the nanocomposites were determined by dynamic light scattering (DLS) in solution, transmission electron microscopy (TEM) and powder X-ray diffraction (PXRD) in the solid. The hydrodynamic diameter of the polymeric micelles loaded with the CP measured by DLS is constant within the error of the measurement throughout all measured samples with sizes around 150 nm (SI, Figure S6). This is in agreement with the results reported previously for similar composite nanoparticles with 4,4'-bipyridine as bridging axial ligand.^[13] In Figure 2, a TEM picture, the size distribution obtained from TEM and DLS, and the SQUID measurement of **3e**

5. Synthesis of $[\text{Fe}(\text{Leq})(\text{Lax})]_n$ Coordination Polymer Nanoparticles using Blockcopolymer Micelles

$([\text{FeL}_{\text{eq}}(\text{bpey})]_n)@BCP$, 5 cycles) is given as typical representative of all samples. A detailed characterisation of all samples with TEM is given in the Supporting Information, Table S3. The TEM picture of **3e** in Figure 2a clearly reveals the formation of spherical nanoparticles with a core-shell nature. The differences in contrast of the iron containing CP and the BCP prove that the CP nanoparticles are solely formed in the core of the nanocomposite.

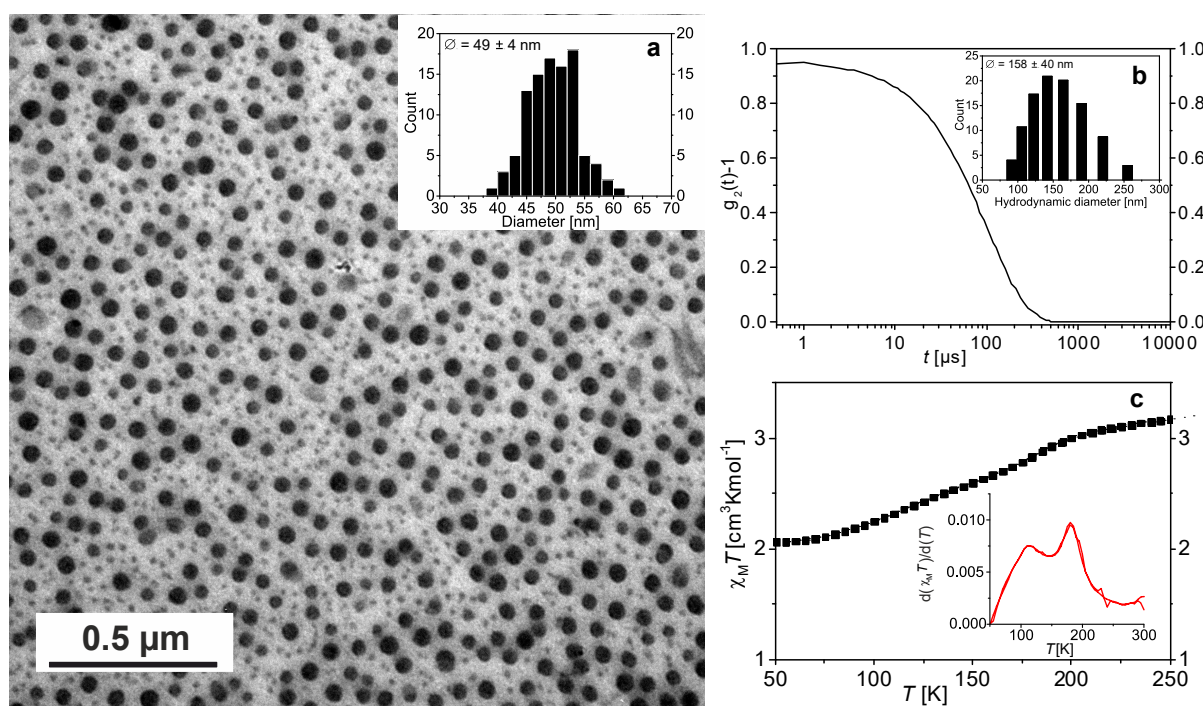


Figure 2: Characterisation of CP-BCP composite micelles. a) TEM picture of **3e** ($([\text{FeL}_{\text{eq}}(\text{bpey})]_n)@BCP$, 5 cycles) illustrating the core shell nature of the particles with size histogram of the core. b) Autocorrelation function from dynamic light scattering of **3e** in THF (43 wt%) with size histogram. c) Magnetic susceptibility data displayed as $\chi_M T$ vs. T for **3e**. In the inset the first derivative of the $\chi_M T$ vs. T plot is given to illustrate the steps in the transition curve more clearly.

The particle core diameter is significantly smaller in comparison to the hydrodynamic radius due to the polymeric nature of the BCP (solvent swollen). Within the error of the measurement, the NP core size is in the same order of magnitude for all samples with an average size of 45 nm,

5. Synthesis of [Fe(L_{eq})(L_{ax})_n] Coordination Polymer Nanoparticles using Blockcopolymer Micelles

demonstrating the excellent size control by the micelles itself. The NP core size is independent of the number of cycles and independent of the used coordination polymer clearly demonstrating the high potential of the templating effect of BCP micelles (cage effect).

In order to investigate, if the flexibility of the used bridging ligand has an impact on regioselectivity of the nanoparticle core formation, the samples were carefully analysed for the observation of microcrystals as function of the increasing CP concentration (number of cycles, e.g. [FeL_{eq}(bpea)]_n@BCP = **1a-e** for 1 to 5 cycles of addition of starting material) in the composite material. The results are summarised in Table 1.

Table 1: Investigation of the core size [nm] and crystallinity of the CP-BCP composite obtained from TEM. MC denotes the observation of microcrystals.

L _{ax} \cycles	1 (a)	2 (b)	3 (c)	4 (d)	5 (e)
bpea (1a-e)	42±5	46±4	49±4	46±4	49±4 /MC
bpee (2a-e)	40±4	46±5	42±4	48±4 /MC	47±4 /MC
bpey (3a-e)	48±5	46±4	49±6	49±4	49±4
bipy ^[13]	52±8	57±8	62±13	44±6	49±5

The first microcrystals (3-6 μm) were observed for bpee as bridging ligand after 4 cycles of addition of starting material (**2d**), while for the more flexible bpea the first microcrystals are observed only after five cycles (**1e**, 1.5-2 μm). In the case of the more rigid bpey, no microcrystals are observed for up to five cycles of addition of the complex. This cannot solely be explained with the rigid nature of the ligand, that increases in the order bpea < bpee < bpey. The results can be explained, if the stability of the complexes with regard to M-L ligand exchange with excess axial ligands and/or solvent molecules is considered. For octahedral complexes, a weak ligand field splitting leads to the occupation of antibonding orbitals (HS complexes) and by this supports ligand exchange. A fast ligand exchange will increase the probability of the formation of microcrystals outside the BCP micelle. In this case the templating effect of the BCP micelles does not work. In agreement with this consideration, the pure HS complex [FeL_{eq}(bpee)]_n with the

weakest ligand field splitting is the first one where microcrystals are observed, while for the spin crossover complexes [FeL_{eq}(bpea)]_n, [FeL_{eq}(bpey)]_n and the previously investigated [FeL_{eq}(bipy)]_n the expected order with regard to the rigid nature of the ligand is observed. With increasing solubility of the complex (increasing flexibility of the ligand) in the solvent used for the synthesis of the nanomaterial, the probability for the formation of microcrystals outside the BCP micelle increases. In agreement with this, it was not possible to synthesise nanoparticles of the coordination polymer [FeL_{eq}(bppa)]_n,^[44] where bppa = 1,3-di(pyridine-4-yl)propane, a very flexible ligand (high solubility) is used. Syntheses were also performed in toluene to investigate the solvent influence on the nanoparticle synthesis. It should be pointed out that previous investigations showed that the complexes have a higher solubility in toluene compared to tetrahydrofuran. In agreement with this, first microcrystals were observed already after 2 cycles for all ligands. In the SI, Figure S7, a TEM picture of [FeL_{eq}(bpea)]_n@BCP after two cycles synthesised in toluene is given as typical representative. Thus the higher solubility of the coordination polymers in toluene favours the formation microcrystals outside of the block copolymer micelle and reduces the regio-selectivity.

The influence of the CP concentration on the crystallinity of the CP-BCP nanocomposite core was investigated using PXRD. In the SI, Figure S8, the PXRD patterns of the composite materials are compared with those of the bulk materials **1-3**. In all cases, the crystallinity of the particles increases with higher CP concentration which is indicated by sharper reflexes. It should be pointed out, that in the case of the samples **3a-e**, even after 5 cycles some of the prominent reflexes observed for the bulk material are missing. Either the crystallinity of the obtained NPs is still very low or a different packing compared to the bulk material is obtained.

In Figure 2c (**3e**) and the SI, Figure S9 (**1d,e**; **2d,e** and **3d,e**) the χ_{MT} versus T plots of the composite materials after 4 and 5 cycles are given. Previous investigations showed, that the amorphous nanoparticles showed gradual spin crossover very different to that of the bulk material. An increasing crystallinity of the nanoparticles did change the spin crossover behaviour towards those of the bulk complexes. Consequently, magnetic measurements were done for the samples after 4 and 5 cycles of addition of complex in the temperature range between 300 K and 50 K in the cooling and heating mode. In the case of **1d**, a gradual spin transition is observed with about 30% of the iron centres involved and $T_{1/2} = 122$ K, close to the first step of the bulk material. In contrast, sample **1e** (contains microcrystals) shows a less gradual but still incomplete spin

crossover with a small hysteresis of 5 K. The $\chi_{\text{M}}T$ value is $3.25 \text{ cm}^3\text{Kmol}^{-1}$ at RT and decreases to $1.03 \text{ cm}^3\text{Kmol}^{-1}$ at 50 K with $T_{1/2\downarrow}$ of 109 K and $T_{1/2\uparrow}$ of 114 K. Interestingly, the step in the transition curve which is present in the bulk material is not observed for sample **1e**. **3d** shows a very gradual spin crossover in the temperature range between 225 K and 100 K with about 30% of the iron centres involved. This is very different to the abrupt spin transition with hysteresis of the bulk material. For sample **3e**, also a very gradual spin crossover is observed upon cooling. Two steps can be distinguished around 175 K and 110 K (see first derivative in Figure 2c). While the first step is in a similar range as the one observed for the bulk material, the second step has no relation to the spin crossover properties of the bulk material. This is in good agreement with the results from the PXRD, where pronounced differences between the diffraction pattern of the bulk CP and the nanocomposite are observed. Apparently, a different crystalline polymorph is obtained. The $\chi_{\text{M}}T$ value is $2.07 \text{ cm}^3\text{Kmol}^{-1}$ at 50 K indicating that 65 % of the iron centres are still in the HS state.

Conclusion

This work focused on the transfer of the concept for the formation of nanoparticles of coordination polymers in a block copolymer matrix. The central goal was to demonstrate that this concept of block copolymers as microreactors is not restricted to one specific coordination polymer and can easily be applied to other systems. Therefore, three coordination polymers have been chosen to be incorporated inside the block copolymer as nanoparticles. As expected, it can be found that the coordination polymer does not have an influence on the size of the CP-BCP composite and that the final size arises mainly from the BCP. However, the formation of stable nanoparticles critically depends on the coordination polymer and the solvent used for the synthesis. The investigations reveal an interplay between two different effects: (1) The rigidity and stacking features of the bridging ligand influences the solubility of the CP and a low solubility is favourable for the selective formation of crystalline nanoparticles in the BCP micelle. (2) Weak field ligands lead to HS complexes where anti-bonding orbitals are occupied. This supports ligand exchange and prevents the templating effect of the BCP micelle. We found that the CP-BCP composites with the most rigid ligand ([FeL_{eq}(bpey)]_n@BCP, **3a-3e**) form the most stable crystalline nanoparticles that are spin crossover active. For the HS complexes [FeL_{eq}(bpee)]_n@BCP, (**2a-2e**), first microcrystals

5. Synthesis of $[\text{Fe}(\text{Leq})(\text{Lax})]_n$ Coordination Polymer Nanoparticles using Blockcopolymer Micelles

are observed after 4 cycles and for $[\text{FeL}_{\text{eq}}(\text{bpea})]_n@BCP$, (**1a-1e**) with the most flexible ligand microcrystals are observed after 5 cycles in THF.

Experimental

All syntheses were performed under inert conditions using argon 5.0 (purity $\geq 99,999\%$) and Schlenk technique. The synthesis of all samples was repeated at least twice. Polystyrene-*b*-poly(4-vinylpyridine) (PS-P4VP, purum, MW ≈ 150000) was synthesised as described before.^[15] 1,2-di(pyridine-4-yl)ethane (bpea) and trans-1,2-di(pyridine-4-yl)ethene (bpee) were obtained from Sigma Aldrich and used as received. Tetrahydrofurane (THF) p.a. and toluene were obtained from Sigma Aldrich and degassed with argon for at least 30 min. [FeL_{eq}(MeOH)₂] was synthesized as described before.^[59] The ligand bpey was synthesised according to the literature.^[60]

Synthesis

The same synthesis procedures were used for all samples independent of the used L_{ax}. Therefore, the general procedures are given for [FeL_{eq}(bpea)]_n (**1**) and the composite materials [FeL_{eq}(bpea)]_n@BCP (**1a-1e**) and the specific values for [FeL_{eq}(bpee)]_n (**2**) / [FeL_{eq}(bpey)]_n (**3**) and the composite materials [FeL_{eq}(bpee)]_n@BCP (**2a-2e**) / [FeL_{eq}(bpey)]_n@BCP (**3a-3e**) are given in brackets. The synthesis of the composite materials in toluene was done using the same procedures and amounts as described for THF. Due to the observation of microcrystals at a very early stage, the products were not characterized further.

1 (2/3): 200 mg (0.45 mmol) [FeL_{eq}(MeOH)₂] and 206 mg (204 mg/202 mg) (1.125 mmol, 2.5 eq) bpea (bpee/bpey) were dissolved in 20 mL THF in a 50 mL flask. The solution was refluxed for 1 h. After cool-down to RT, the solution was let for crystallisation overnight. The solid was filtered, washed with THF once and dried *in vacuo* to yield a brown (dark violet) powder. Elemental anal. (%): calc. C 63.61, H 5.34, N 9.89, found C 62.91, H 5.19, N 9.22 (calc. C 63.84, H 5.00, N 9.93, found C 63.15, H 6.05, N 9.18, / calc. C 64.07, H 4.66, N 9.96, found C 63.63, H 4.77, N 9.25).

1a, 1 cycle (**2a/3a**): 50 mg (0.33 μ mol) PS-*b*-P4VP and 6.7 mg (15 μ mol) [FeL_{eq}(MeOH)₂] were dissolved in 20 mL THF in a 50 ml flask. The solution was refluxed for 2h. After, 6.9 mg (6.8 mg/6.8 mg) (37.5 μ mol, 2.5 eq) bpea (bpee/bpey) was added and refluxed again for 1h. The solution was cooled down to room temperature and the solvent was removed via cold distillation to

yield a brown, polymer-like solid. Elemental anal. (%) found: C 64.96, H 7.44, N 2.82 (C 71.23, H 7.24, N 3.10 / C 59.99, H 7.46, N 2.48).

1b, 2 cycles (**2b/3b**): The synthesis for 1 cycle was repeated. Prior to solvent removal, 6.7 mg (15 μ mol) [FeL_{eq}(MeOH)₂] and 6.9 mg (6.8 mg/6.8 mg g) (37.5 μ mol, 2.5 eq) bpea (bpee/bpey) were added for a new cycle and refluxed for another hour. The solvent was removed via cold distillation to yield a dark brown, polymer-like solid. Elemental anal. (%) found: C 61.98, H 7.35, N 3.38 (C 59.75, H 7.43, N 3.37 / C 57.18, H 7.42, N 3.05).

1c, 3 cycles (**2c/3c**): The synthesis for 2 cycles was repeated and one more cycle was realised. 6.7 mg (15 μ mol) [FeL_{eq}(MeOH)₂] and 6.9 mg (6.8 mg/6.8 mg) (37.5 μ mol, 2.5 eq) bpea (bpee/bpey) were added and refluxed for another hour before the solvent was removed via cold distillation to yield a dark brown, polymer-like solid. Elemental anal. (%) found: C 69.43, H 7.30, N 5.00 (C 63.08, H 7.21, N 3.71 / C 70.94, H 6.67, N 4.88).

1d, 4 cycles (**2d/3d**): The synthesis for 3 cycles was repeated and one more cycle was realised. 6.7 mg (15 μ mol) [FeL_{eq}(MeOH)₂] and 6.9 mg (6.8 mg/6.8 mg) (37.5 μ mol, 2.5 eq) bpea (bpee/bpey) were added and refluxed for another hour before the solvent was removed via cold distillation to yield a dark brown, polymer-like solid. Elemental anal. (%) found: C 68.18, H 6.55, N 5.64 (C 71.09, H 6.79, N 5.90 / C 68.04, H 6.18, N 5.48).

1e, 5 cycles (**2e/3e**): The synthesis for 4 cycles was repeated and one more cycle was realised. 6.7 mg (15 μ mol) [FeL_{eq}(MeOH)₂] and 6.9 mg (6.8 mg/6.8 mg) (37.5 μ mol, 2.5 eq) bpea (bpee/bpey) were added and refluxed for another hour before the solvent was removed via cold distillation to yield a dark brown, polymer-like solid. Elemental anal. (%) found: C 68.09, H 6.97, N 5.86 (C 68.12, H 6.63, N 6.09 / C 65.92, H 6.04, N 5.70).

The colour of the samples became darker with increasing cycles due to the higher amount of iron inside the samples.

Characterisation methods

Transmission electron microscopy. Transmission electron microscopy was made at a Zeiss CEM902 electron microscope (Zeiss, Oberkochen, Germany). Samples were dispersed in toluene applying vortex. The solution was dropped on a copper grid (mesh 200, Science Services,

Munich). Electron acceleration voltage was set to 80 kV. Micrographs were taken with a MegaView III / iTEM image acquiring and processing system from Olympus Soft Imaging Systems (OSIS, Münster, Germany) and an Orius 830 SC200W / DigitalMicrograph system from Gatan (Munich, Germany). Particles size measurements were done with “ImageJ” image processing software by Wayne Rasband (National Institutes of Health, USA).

Elemental Analysis. Carbon, nitrogen and hydrogen content was collected at a Vario EL III with acetanilide as standard. The samples were placed in tin boats and measured at least twice. The average of the measurements was used.

Infrared measurements. Transmission infrared spectra were collected from a Perkin Elmer Spectrum 100 FT-IR (ATR). The samples were measured directly as solids.

Magnetic measurements. Magnetic susceptibility measurements were performed at a Quantum Design MPMS-XL-5 SQUID magnetometer. Field strength of 3 T was applied and a temperature range of 50–300 K was used to determine the temperature dependency of the magnetism and the spin crossover behaviour. Settle mode was used in all measurements with a cooling and heating rate of 5 K/min. The samples were prepared in gelatine capsules placed in a plastic straw. The measured values were corrected for the diamagnetism of the sample holder, the polymer matrix (measured values) and the ligand (tabulated Pascal constants).

Dynamic light scattering. The samples were measured at a Malvern Instruments Zetasizer Nano ZS90 in glass cuvettes from Carl Roth GmbH + Co. KG at 25 °C. One measurement consists of three consecutive runs.

Mössbauer spectroscopy. ⁵⁷Fe Mössbauer spectra were recorded in transmission geometry on a constant-acceleration using a conventional Mössbauer spectrometer with a 50 mCi ⁵⁷Co(Rh) source. The samples were sealed in the sample holder in an argon atmosphere. The spectra were fitted using Recoil 1.05 Mössbauer Analysis Software.^[61] The isomer shift values are given with respect to a α -Fe reference at room temperature.

Powder X-Ray diffraction. Powder X-Ray diffraction data for all samples were collected at a STOE StadiP X-Ray diffractometer in transmission geometry between 5° and 30° 2 θ . Samples **1**, **2** and **3** were placed in a flat carrier and composite samples **1a** – **3e** were placed on flat surfaces. Cu-K α 1 radiation was used for the measurement and the radiation was detected with a Mythen 1K detector.

Supporting Information

In the Supporting Information the characterization of the bulk complexes (PXRD, magnetism, Mössbauer spectra and Mössbauer parameter), the full characterization of the composite materials **1-3 a-e** (IR spectra, DLS, PXRD, Mössbauer spectra and Mössbauer parameters of **1d**, **1e**, **3d** and **3e**, TEM pictures and magnetic measurements of **1d**, **1e**, **2d**, **2e**, **3d** and **3e**) and a TEM picture of the composite material synthesised from toluene is given.

Supporting Information File 1: SI_BJNANO

File Name: SI_BJNANO

File Format: pdf

Title: Supporting Information file

Acknowledgements

Financial support of the University of Bayreuth and the SFB 840 (TP A10 and B10) is gratefully acknowledged. O.K. was supported by the BayNAT program of the UBT. We thank Juliane Kary for her contribution to the synthesis of the CP and CP-BCP composites.

References

- [1] Sindoro, M.; Yanai, N.; Jee, A.-Y.; Granick, S. *Acc. Chem. Res.* **2014**, *47* (2), 459–469. doi:10.1021/ar400151n
- [2] Coronado, E.; Giménez-Marqués, M.; Mínguez Espallargas, G.; Rey, F.; Vitorica-Yrezábal, I. *J. J. Am. Chem. Soc.* **2013**, *135* (43), 15986–15989. doi:10.1021/ja407135k
- [3] Zhao-Yang Li, O. S.; Yao, Z.-S.; Kang, S.; Kanegawa, S. Multifunctional Materials Combining Spin-Crossover with Conductivity and Magnetic Ordering. In *Spin-Crossover Materials*; Halcrow, M. A., Ed.; John Wiley & Sons Ltd: Chichester, **2013**; pp 303–319.

- [4] Gaspar, A. B.; Weber, B. Spin Crossover Phenomenon in Coordination Compounds. In *Molecular Magnetic Materials*; Sieklucka, B., Pinkowicz, D., Eds.; Wiley-VCH Verlag GmbH & Co. KGaA: Weinheim, Germany, **2017**; pp 231–252.
- [5] Halcrow, M. A., Ed. *Spin-Crossover Materials*; John Wiley & Sons Ltd: Chichester, 2013.
- [6] Turkevich, J.; Stevenson, P. C.; Hillier, J. *Discuss. Faraday Soc.* **1951**, *11*, 55. doi:10.1039/DF95111100055
- [7] Frens, G. *Nat Phys Sci* **1973**, *241* (105), 20–22. doi:10.1038/physci241020a0
- [8] Sun, S.; Zeng, H. *J. Am. Chem. Soc.* **2002**, *124* (28), 8204–8205. doi:10.1021/ja026501x
- [9] Lu, A.-H.; Salabas, E. L.; Schuth, F. *Angew. Chem. Int. Ed.* **2007**, *46* (8), 1222–1244. doi:10.1002/anie.200602866
- [10] Sun, Y.; Xia, Y. *Science* **2002**, *298* (5601), 2176–2179. doi:10.1126/science.1077229
- [11] Brust, M.; Fink, J.; Bethell, D.; Schiffrin, D. J.; Kiely, C. *J. Chem. Soc., Chem. Commun.* **1995** (16), 1655. doi:10.1039/C39950001655
- [12] Gupta, A. K.; Gupta, M. *Biomaterials* **2005**, *26* (18), 3995–4021. doi:10.1016/j.biomaterials.2004.10.012
- [13] Klimm, O.; Göbel, C.; Rosenfeldt, S.; Puchtler, F.; Miyajima, N.; Marquardt, K.; Drechsler, M.; Breu, J.; Förster, S.; Weber, B. *Nanoscale* **2016**, *8* (45), 19058–19065.
- [14] Förster, S.; Zisenis, M.; Wenz, E.; Antonietti, M. *J. Chem. Phys.* **1996**, *104* (24), 9956.
- [15] Förster, S.; Antonietti, M. *Adv. Mater.* **1998**, *10* (3), 195–217.
- [16] Fan, Z.; Chen, X.; Kohn Serrano, M.; Schmalz, H.; Rosenfeldt, S.; Förster, S.; Agarwal, S.; Greiner, A. *Angew. Chem. Int. Ed.* **2015**, *54* (48), 14539–14544.
- [17] Carmen Muñoz, M.; Antonio Real, J. Polymeric Spin-Crossover Materials. In *Spin-Crossover Materials*; Halcrow, M. A., Ed.; John Wiley & Sons Ltd: Chichester, 2013; pp 121–146.
- [18] Gütlich, P.; Gaspar, A. B.; Garcia, Y. *Beilstein J. Org. Chem.* **2013**, *9*, 342–391.

- [19] Martinho, P. N.; Rajnak, C.; Ruben, M. Nanoparticles, Thin Films and Surface Patterns from Spin-Crossover Materials and Electrical Spin State Control. In *Spin-Crossover Materials*; Halcrow, M. A., Ed.; John Wiley & Sons Ltd: Chichester, 2013; pp 375–404.
- [20] Herrera, J. M.; Titos-Padilla, S.; Pope, Simon J. A.; Berlanga, I.; Zamora, F.; Delgado, J. J.; Kamenev, K. V.; Wang, X.; Prescimone, A.; Brechin, E. K.; Colacio, E. *J. Mater. Chem. C* **2015**, *3* (30), 7819–7829. doi:10.1039/c5tc00685f
- [21] Giménez-Marqués, M.; García-Sanz de Larrea, M. Luisa; Coronado, E. *J. Mater. Chem. C* **2015**, *3* (30), 7946–7953. doi:10.1039/c5tc01093d
- [22] Roubeau, O. *Chem. Eur. J.* **2012**, *18* (48), 15230–15244. doi:10.1002/chem.201201647
- [23] Luo, Y.-H.; Liu, Q.-L.; Yang, L.-J.; Sun, Y.; Wang, J.-W.; You, C.-Q.; Sun, B.-W. *J. Mater. Chem. C* **2016**, *4* (34), 8061–8069. doi:10.1039/c6tc02796b
- [24] Coronado, E.; Mínguez Espallargas, G. *Chem. Soc. Rev.* **2013**, *42* (4), 1525.
- [25] Ohba, M.; Yoneda, K.; Agustí, G.; Muñoz, M. C.; Gaspar, A. B.; Real, J. A.; Yamasaki, M.; Ando, H.; Nakao, Y.; Sakaki, S.; Kitagawa, S. *Angew. Chem. Int. Ed.* **2009**, *48* (26), 4767–4771.
- [26] Linares, J.; Codjovi, E.; Garcia, Y. *Sensors* **2012**, *12* (4), 4479–4492.
- [27] Létard, J.-F.; Guionneau, P.; Goux-Capes, L. Towards Spin Crossover Applications. In *Spin Crossover in Transition Metal Compounds I-III*; Gütllich, P., Goodwin, H., Eds.; Topics in Current Chemistry 233-235; Springer Berlin / Heidelberg, 2004; pp 221–249.
- [28] Kahn, O. *Science* **1998**, *279* (5347), 44–48. doi:10.1126/science.279.5347.44
- [29] Kahn, O.; Jay, C.; Krober, J.; Claude, R.; Groliere, F. Spin-transition chemical compounds, and devices comprising read-, memory-, and erase-units, active medium which contains at least one of those compounds, EP0666561, **1995**.
- [30] Muller, R. N.; Vander Elst, L.; Laurent, S. *J. Am. Chem. Soc.* **2003**, *125* (27), 8405–8407.
- [31] Venkataramani, S.; Jana, U.; Dommaschk, M.; Sonnichsen, F. D.; Tuczek, F.; Herges, R. *Science* **2011**, *331* (6016), 445–448.
- [32] Dommaschk, M.; Peters, M.; Gutzeit, F.; Schütt, C.; Näther, C.; Sonnichsen, F. D.; Tiwari, S.; Riedel, C.; Boretius, S.; Herges, R. *J. Am. Chem. Soc.* **2015**, *137* (24), 7552–7555.

- [33] Hasserodt, J.; Kolanowski, J. L.; Touti, F. *Angew. Chem. Int. Ed.* **2014**, *53* (1), 60–73.
- [34] Nowak, R.; Prasetyanto, E. A.; Cola, L. de; Bojer, B.; Siegel, R.; Senker, J.; Rössler, E.; Weber, B. *Chem. Commun.* **2017**, *53* (5), 971–974.
- [35] Volatron, F.; Catala, L.; Rivière, E.; Gloter, A.; Stéphan, O.; Mallah, T. *Inorg. Chem* **2008**, *47* (15), 6584–6586. doi:10.1021/ic800803w
- [36] Forestier, T.; Mornet, S.; Daro, N.; Nishihara, T.; Mouri, S.-i.; Tanaka, K.; Fouche, O.; Freysz, E.; Letard, J.-F. *Chem. Commun.* **2008** (36), 4327–4329. doi:10.1039/B806347H
- [37] Boldog, I.; Gaspar, A. B.; Martínez, V.; Pardo-Ibañez, P.; Ksenofontov, V.; Bhattacharjee, A.; Gütlich, P.; Real, J. A. *Angew. Chem. Int. Ed.* **2008**, *47* (34), 6433–6437. doi:10.1002/anie.200801673
- [38] Forestier, T.; Kaiba, A.; Pechev, S.; Denux, D.; Guionneau, P.; Etrillard, C.; Daro, N.; Freysz, E.; Letard, J.-F. *Chem. Eur. J.* **2009**, *15* (25), 6122–6130. doi:10.1002/chem.200900297
- [39] Martínez, V.; Boldog, I.; Gaspar, A. B.; Ksenofontov, V.; Bhattacharjee, A.; Gütlich, P.; Real, J. A. *Chem. Mater* **2010**, *22* (14), 4271–4281. doi:10.1021/cm101022u
- [40] Larionova, J.; Salmon, L.; Guari, Y.; Tokarev, A.; Molvinger, K.; Molnár, G.; Bousseksou, A. *Angew. Chem. Int. Ed.* **2008**, *47* (43), 8236–8240.
- [41] Cobo, S.; Molnár, G.; Real, J. A.; Bousseksou, A. *Angew. Chem. Int. Ed.* **2006**, *45* (35), 5786–5789.
- [42] Molnár, G.; Cobo, S.; Real, J. A.; Carcenac, F.; Daran, E.; Vieu, C.; Bousseksou, A. *Adv. Mater* **2007**, *19* (16), 2163–2167.
- [43] Bartual-Murgui, C.; Natividad, E.; Roubeau, O. *J. Mater. Chem. C* **2015**, *3* (30), 7916–7924.
- [44] Bauer, W.; Scherer, W.; Altmannshofer, S.; Weber, B. *Eur. J. Inorg. Chem.* **2011** 2803–2818. doi:10.1002/ejic.201001363
- [45] Baldé, C.; Bauer, W.; Kaps, E.; Neville, S.; Desplanches, C.; Chastanet, G.; Weber, B.; Létard, J. F. *Eur. J. Inorg. Chem.* **2013**, 2744–2750. doi:10.1002/ejic.201201422
- [46] Šalitroš, I.; Fuhr, O.; Ruben, M. *Materials* **2016**, *9* (7), 585. doi:10.3390/ma9070585

- [47] Dankhoff, K.; Lochenie, C.; Puchtler, F.; Weber, B. *Eur. J. Inorg. Chem.* **2016**, 2016 (13-14), 2136–2143. doi:10.1002/ejic.201501175
- [48] C. Lochenie, C.; Bauer, W.; Railliet, A. P.; Schlamp, S.; Garcia, Y.; Weber, B. *Inorg. Chem.* **2014**, 53 (21), 11563–11572. doi:10.1021/ic501624b
- [49] Nowak, R.; Bauer, W.; Ossiander, T.; Weber, B. *Eur. J. Inorg. Chem.* **2013**, (5-6), 975–983. doi:10.1002/ejic.201201051
- [50] Weber, B. *Coord. Chem. Rev.* **2009**, 253 (19-20), 2432–2449. doi:10.1016/j.ccr.2008.10.002
- [51] Weber, B. *Koordinationschemie. Grundlagen und aktuelle Trends*; Springer Spektrum: Berlin [u.a.], 2014.
- [52] Brooker, S. *Chem. Soc. Rev.* **2015**, 44 (10), 2880–2892. doi:10.1039/c4cs00376d
- [53] Schönfeld, S.; Lochenie, C.; Thoma, P.; Weber, B. *CrystEngComm* **2015**, 17 (29), 5389–5395. doi:10.1039/C5CE00800J
- [54] Money, V. A.; Carbonera, C.; Elhaïk, J.; Halcrow, M. A.; Howard, J. A. K.; Létard, J.-F. *Chem. Eur. J* **2007**, 13 (19), 5503–5514. doi:10.1002/chem.200601312
- [55] Bauer, W.; Pfaffeneder, T.; Achterhold, K.; Weber, B. *Eur. J. Inorg. Chem.* **2011** (21), 3183–3192. doi:10.1002/ejic.201100224
- [56] Weber, B.; Kaps, E. *Heteroatom Chem.* **2005**, 16 (5), 391–397. doi:10.1002/hc.20108
- [57] Weber, B.; Carbonera, C.; Desplances, C.; Létard, J.-F. *Eur. J. Inorg. Chem.* **2008**, 2008 (10), 1589–1598. doi:10.1002/ejic.200701216
- [58] Göbel, C.; Palamarciuc, T.; Lochenie, C.; Weber, B. *Chem. Asian J.* **2014**, 9 (8), 2232–2238. doi:10.1002/asia.201402144
- [59] Weber, B.; Jäger, E.-G. *Eur. J. Inorg. Chem.* **2009**, 2009 (4), 465–477. doi:10.1002/ejic.200800891
- [60] Tanner, M.; Ludi, A. *Chimica* **1980**, 34, 23–24.
- [61] K. Lagarec; D. G. Rancourt. *Recoil, mössbauer spectral analysis software for windows 1.0*: Department of Physics, University of Ottawa, Canada, 1998.

5. Synthesis of $[\text{Fe}(\text{Leq})(\text{Lax})]_n$ Coordination Polymer Nanoparticles using Blockcopolymer Micelles

Supporting Information

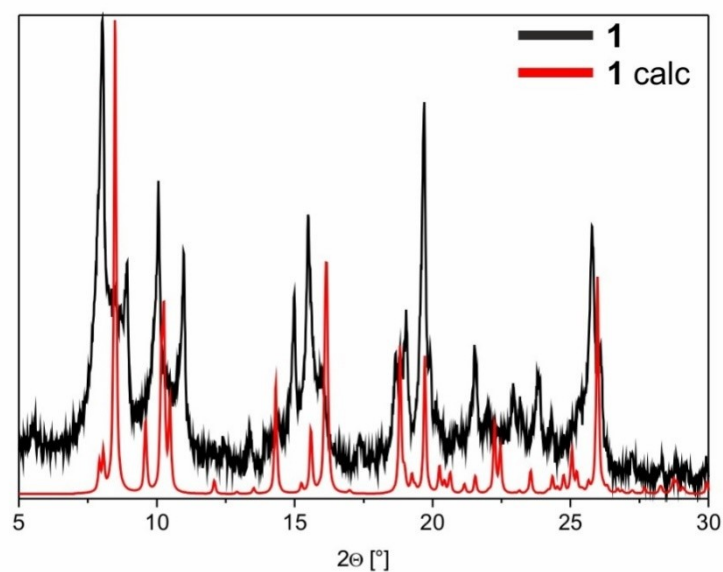


Figure S1: Comparison of the powder X-Ray diffraction pattern of $[\text{Fe}(\text{L}_{\text{eq}})(\text{bpea})]$ (**1**) and $[\text{Fe}(\text{L}_{\text{eq}})(\text{bpea})]\cdot 0.25 \text{ MeOH}$ (synthesised in methanol, calculated from single crystal data).^[1]

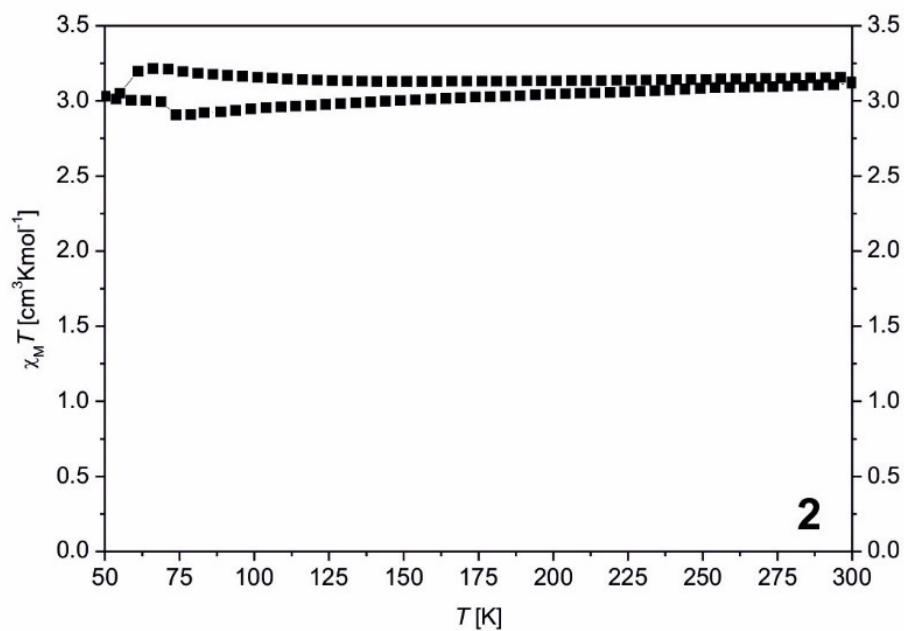
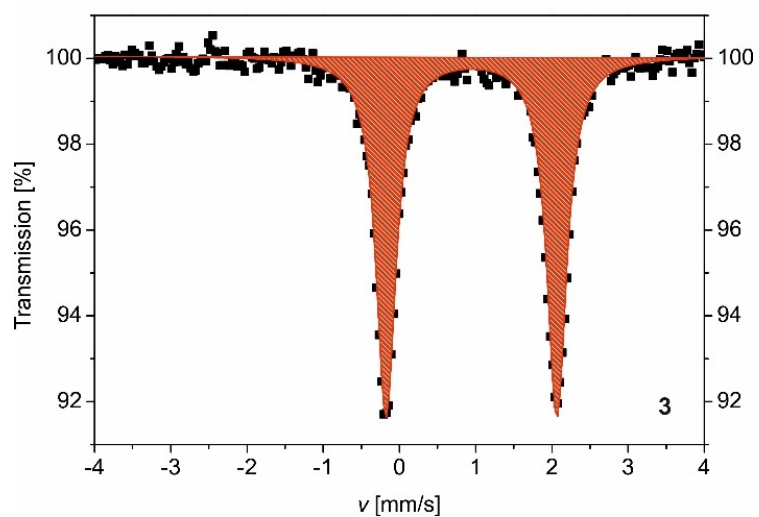
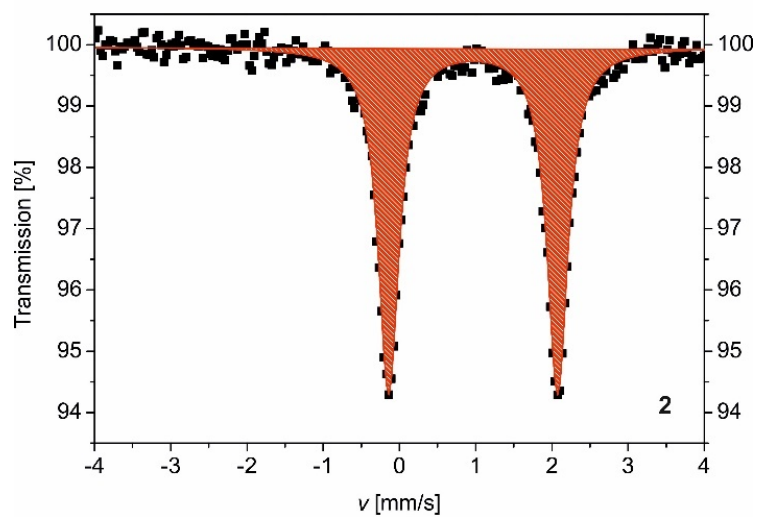
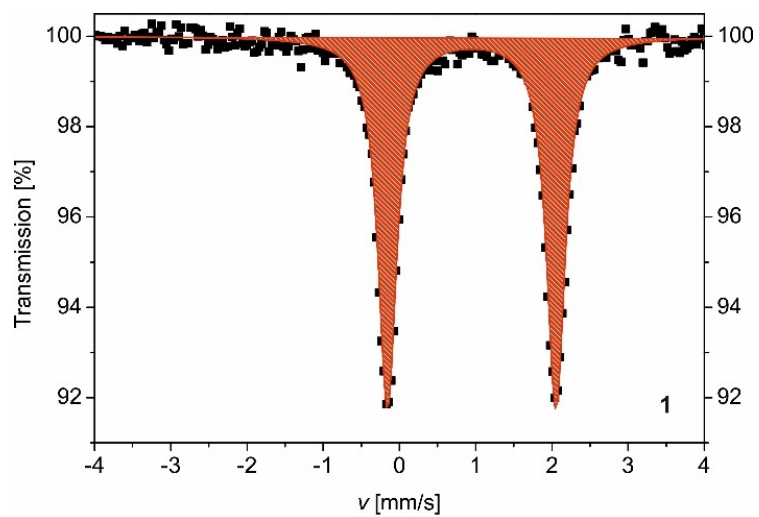


Figure S2: Plot of the $\chi_M T$ product versus temperature for (**2**).

5. Synthesis of $[\text{Fe}(\text{Leq})(\text{Lax})]_n$ Coordination Polymer Nanoparticles using Blockcopolymer Micelles



5. Synthesis of [Fe(L_{eq})(L_{ax})]_n Coordination Polymer Nanoparticles using Blockcopolymer Micelles

Figure S3: Mössbauer spectra of **1** (top), **2** (centre) and **3** (bottom). In each case one single doublet is observed with Mössbauer parameters (Table S1) characteristic for an iron(II) HS complex.

Table S1: Mössbauer parameters of the samples (**1**, **2** and **3**).

sample	site	δ [mm/s]	ΔE_Q [mm/s]	Γ [mm/s]	Area [%]
1	Fe(II) HS	0.947(3)	2.210(6)	0.147(5)	100
2	Fe(II) HS	0.966(4)	2.216(7)	0.164(6)	100
3	Fe(II) HS	0.944(3)	2.240(6)	0.156(5)	100

5. Synthesis of $[\text{Fe}(\text{Leq})(\text{Lax})]_n$ Coordination Polymer Nanoparticles using Blockcopolymer Micelles

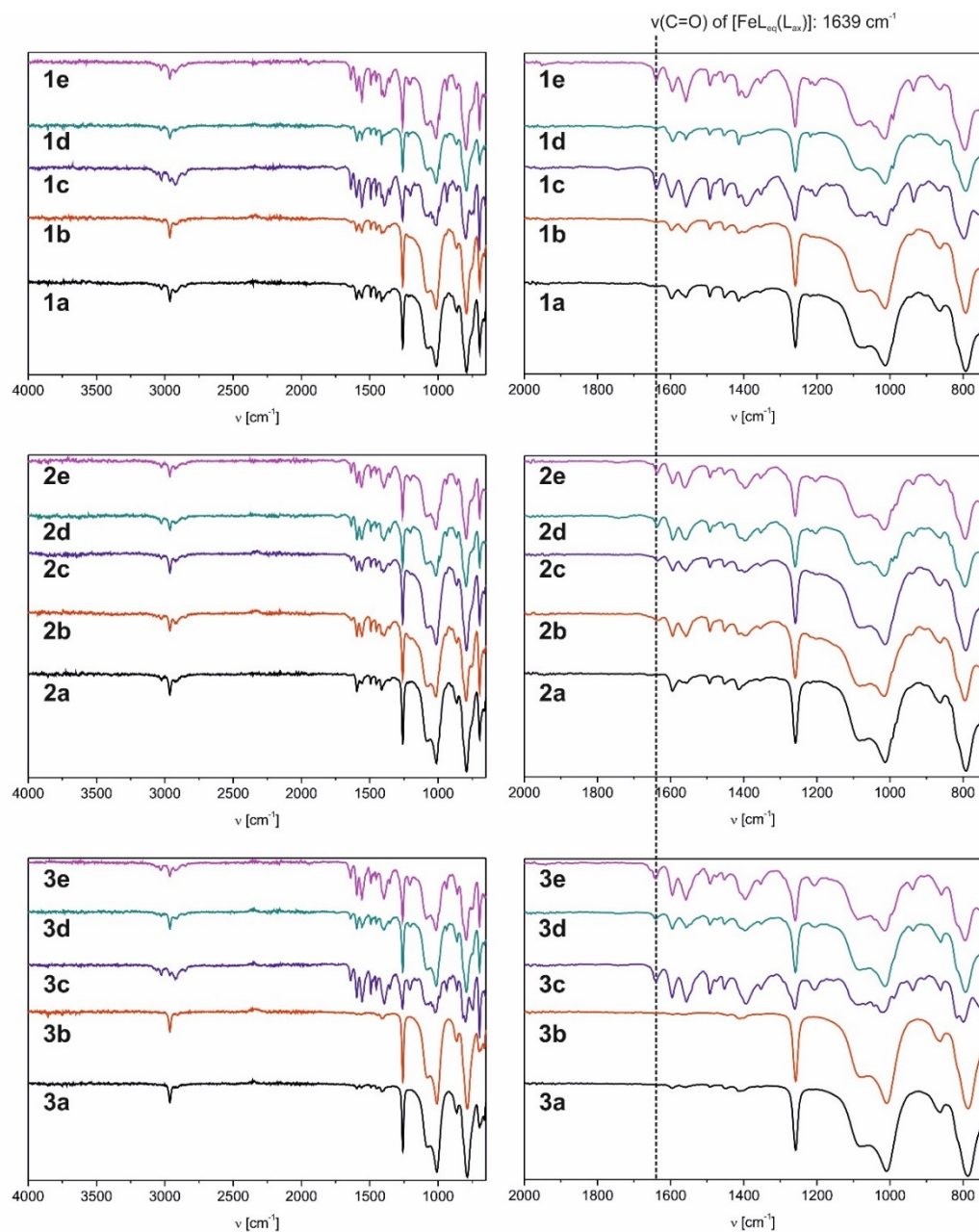


Figure S4: IR spectra of **1a-1e** (top left), **2a-2e** (centre left) and **3a-3e** (bottom left) and the relevant area between 2000 cm^{-1} and 750 cm^{-1} to show the C=O vibration band the samples **1a-1e** (top right), **2a-2e** (centre right) and **3a-3e** (bottom right).

5. Synthesis of [Fe(Leq)(Lax)]_n Coordination Polymer Nanoparticles using Blockcopolymer Micelles

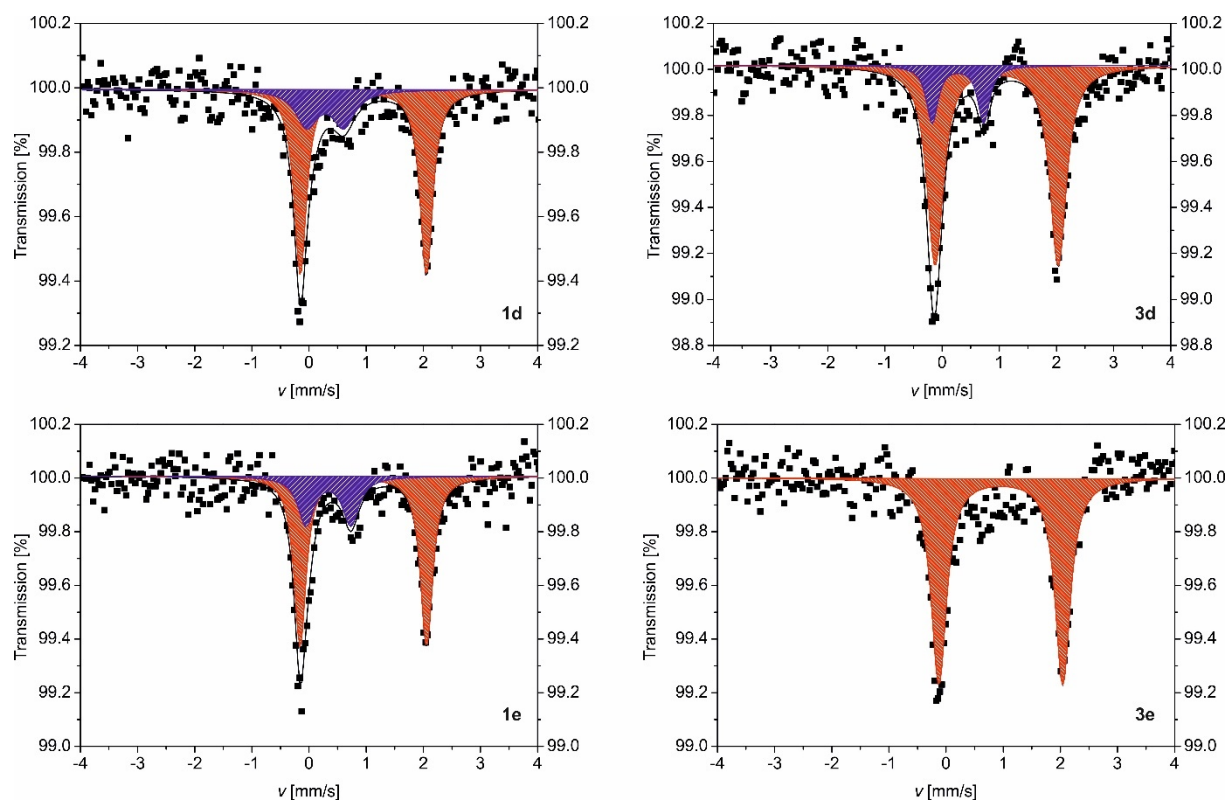


Figure S5: Mössbauer spectra of **1d** (top left), **1e** (bottom left), **3d** (top right) and **3e** (bottom right). The red doublet corresponds to an iron(II) HS species and the blue doublet corresponds to an iron(II) LS species. The Mössbauer parameters are given in Table S2.

Table S2: Mössbauer parameters of the samples **1d**, **1e**, **3d** and **3e**.

sample	site	δ [mm/s]	ΔE_Q [mm/s]	Γ [mm/s]	Area [%]
1d	Fe(II) LS	0.28(11)	0.65(18)	0.24(14)	26(9)
	Fe(II) HS	0.951(14)	2.21(3)	0.132(19)	74(9)
1e	Fe(II) LS	0.34(6)	0.79(12)	0.17(8)	28(9)
	Fe(II) HS	0.951(14)	2.21(3)	0.12(2)	72(9)
3d	Fe(II) LS	0.28(6)	0.90(12)	0.12(6)	17(6)
	Fe(II) HS	0.95(2)	2.15(4)	0.17(2)	83(9)
3e	Fe(II) HS	0.958(12)	2.17(2)	0.161(18)	100

5. Synthesis of [Fe(Leq)(Lax)]_n Coordination Polymer Nanoparticles using Blockcopolymer Micelles

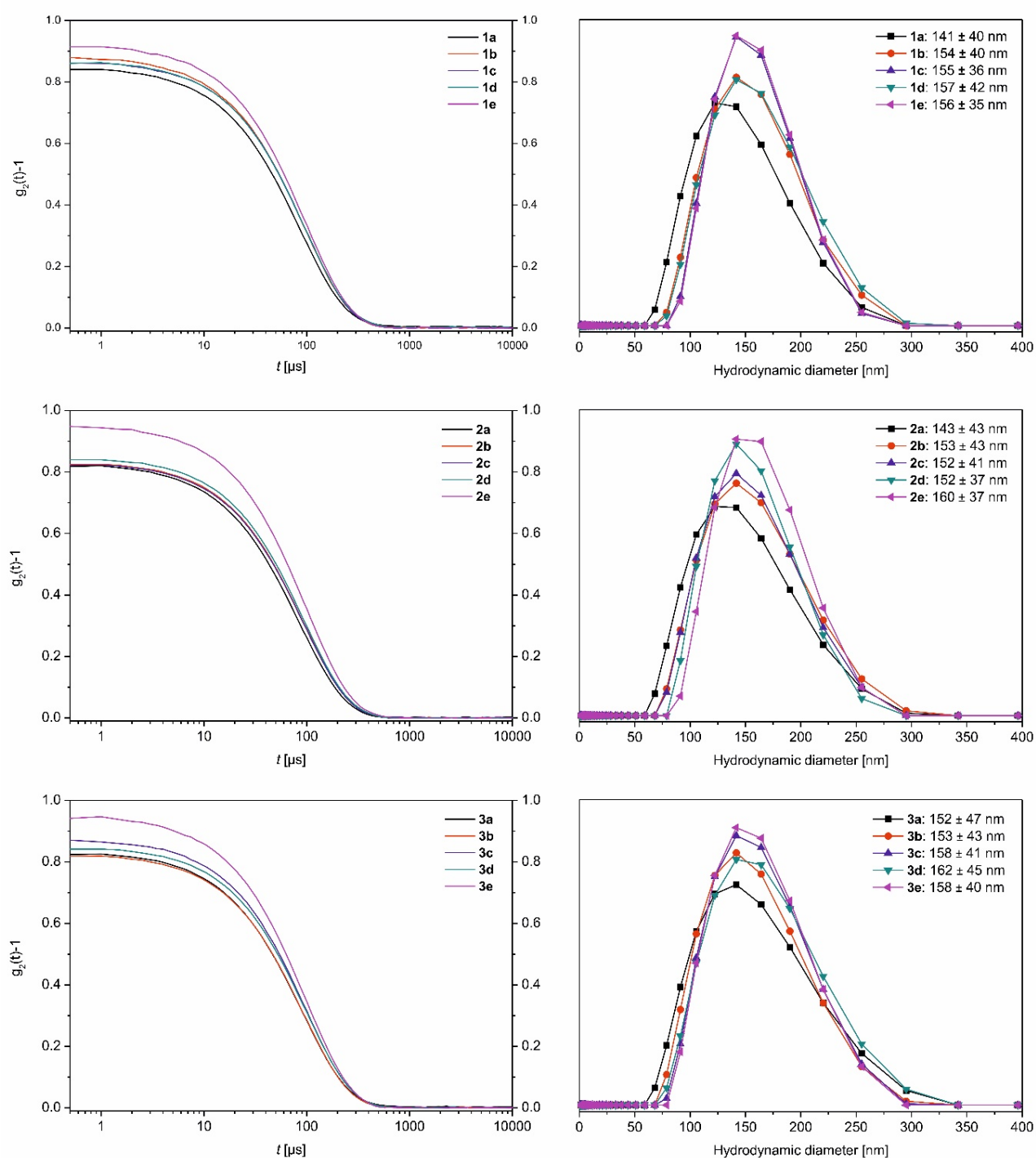
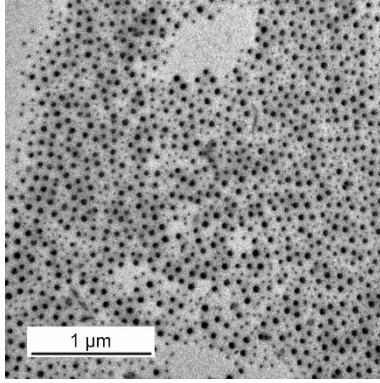
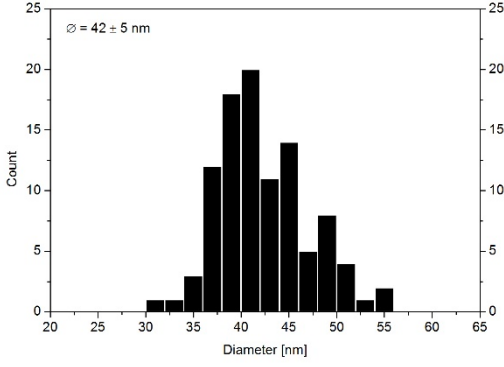
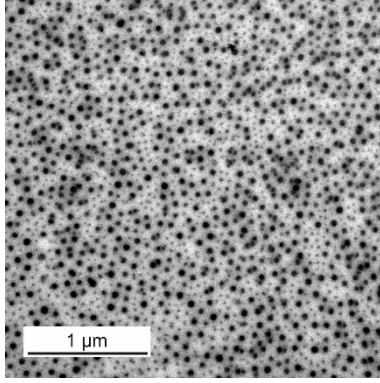
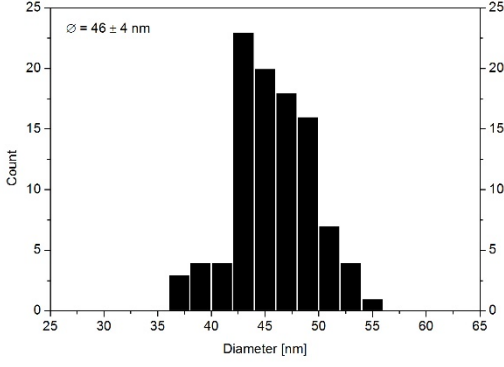
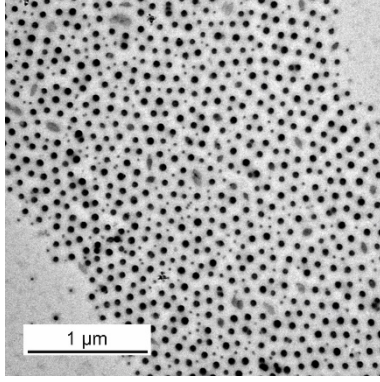
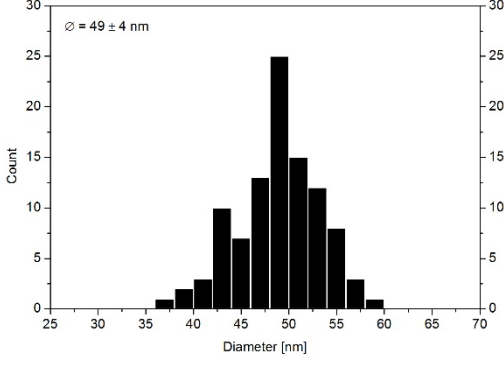


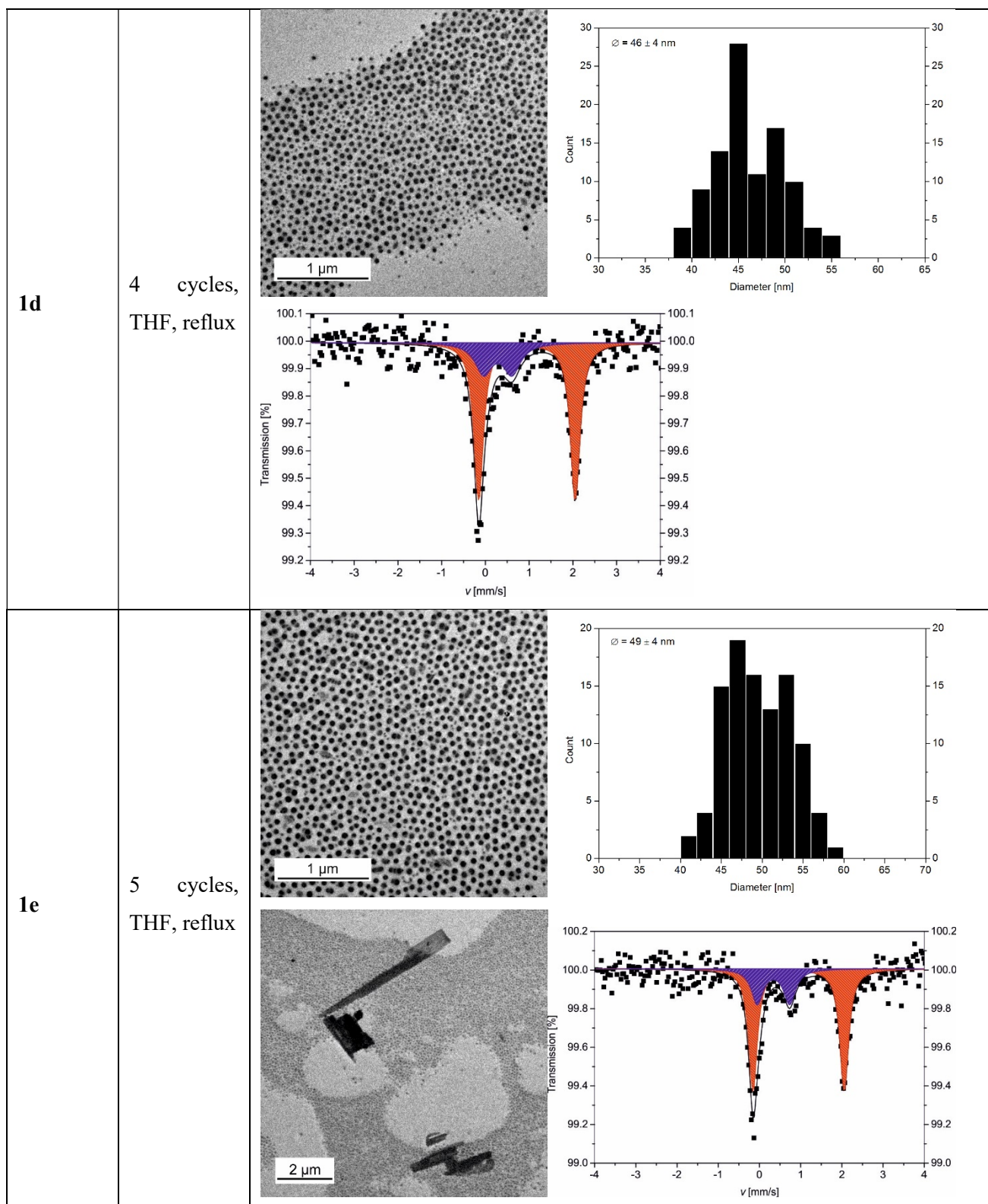
Figure S6: DLS measurement of the nanocomposites in THF, 43w%. Correlation functions of **1a-1e** (top left), **2a-2e** (centre left) and **3a-3e** (bottom left) and the resulting hydrodynamic diameter of the polymeric micelles in THF of **1a-1e** (top right), **2a-2e** (centre right) and **3a-3e** (bottom right).

5. Synthesis of [Fe(Leq)(Lax)]_n Coordination Polymer Nanoparticles using Blockcopolymer Micelles

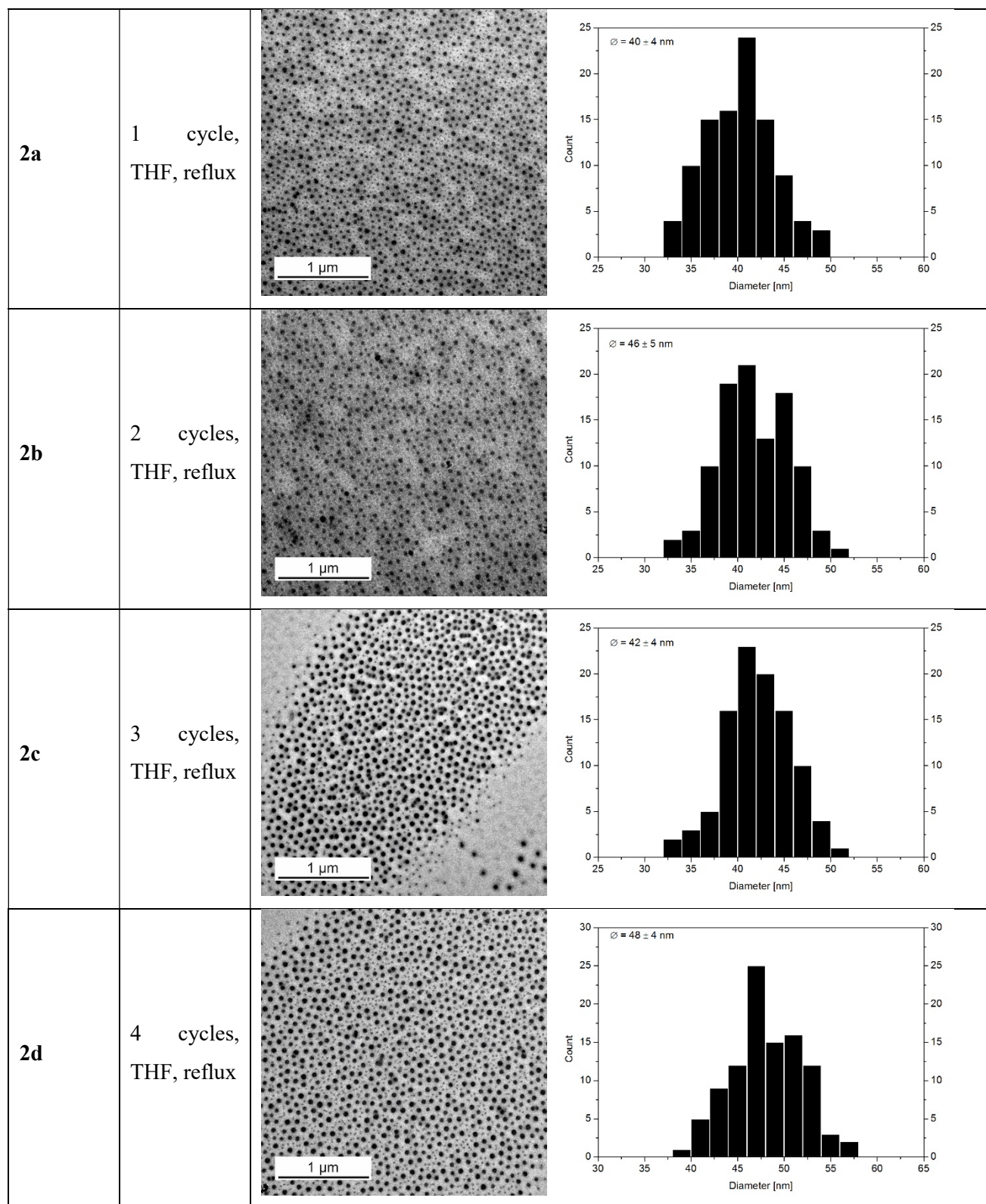
Table S3: Summarised characterisation for the different composite samples (**1a-3e**). An exemplary TEM picture and the size distribution are given for TEM measurements. The particle sizes are given in the pictures.

sample	Reaction conditions	TEM nanoparticles, TEM size distribution, TEM microcrystals (if any) and Mössbauer spectra (if any).
1a	1 cycle, THF, reflux	 
1b	2 cycles, THF, reflux	 
1c	3 cycles, THF, reflux	 

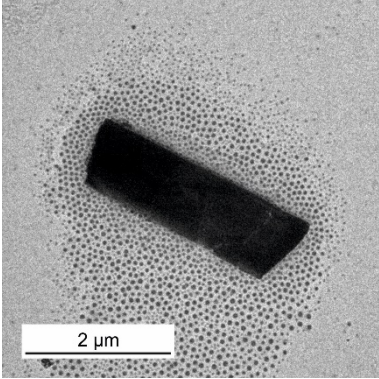
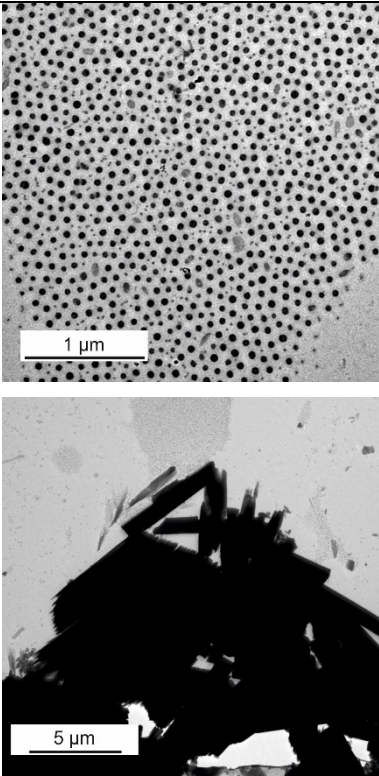
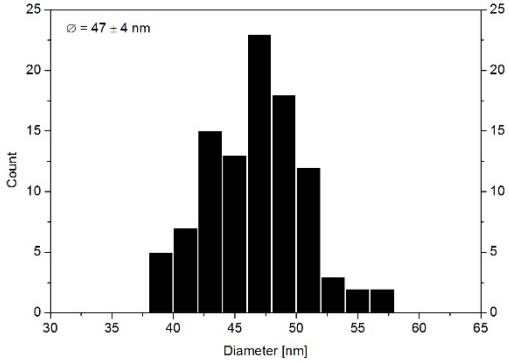
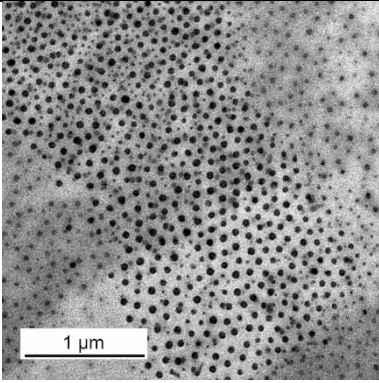
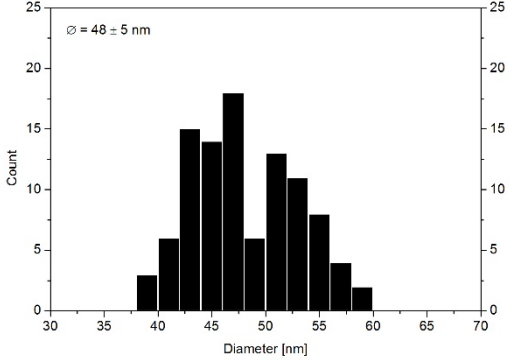
5. Synthesis of [Fe(Leq)(Lax)]_n Coordination Polymer Nanoparticles using Blockcopolymer Micelles



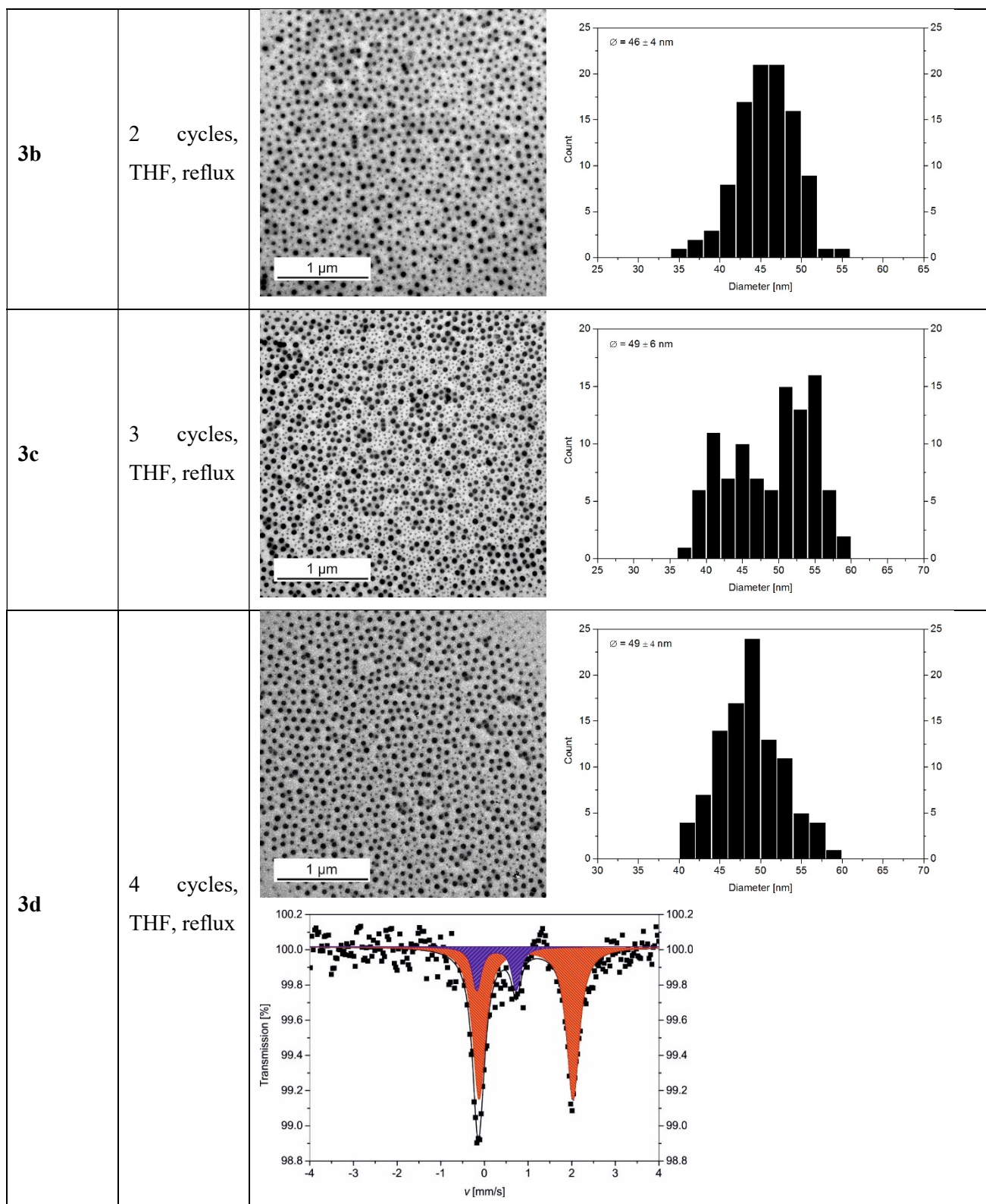
5. Synthesis of [Fe(Leq)(Lax)]_n Coordination Polymer Nanoparticles using Blockcopolymer Micelles



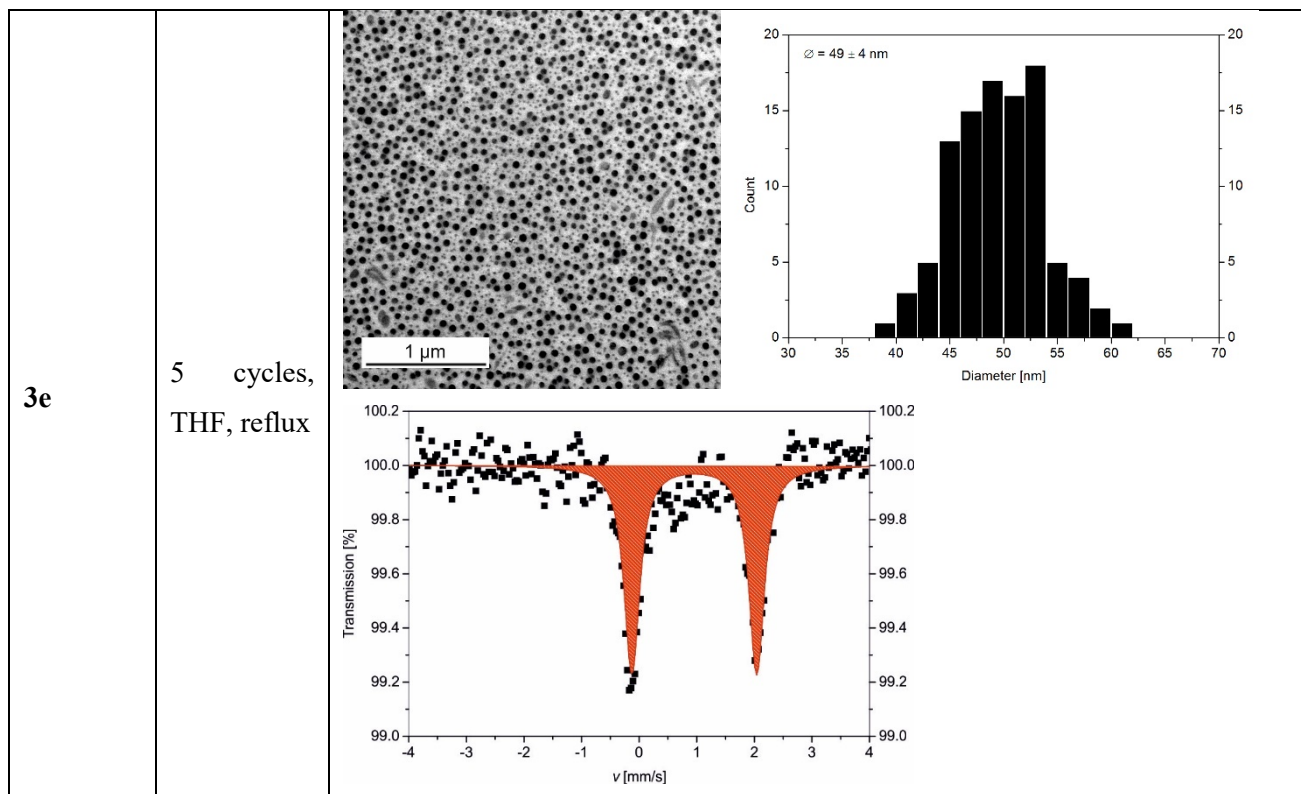
5. Synthesis of [Fe(Leq)(Lax)]_n Coordination Polymer Nanoparticles using Blockcopolymer Micelles

			
<p>2e</p>	<p>5 cycles, THF, reflux</p>		 <p>∅ = 47 ± 4 nm</p>
<p>3a</p>	<p>1 cycle, THF, reflux</p>		 <p>∅ = 48 ± 5 nm</p>

5. Synthesis of [Fe(Leq)(Lax)]_n Coordination Polymer Nanoparticles using Blockcopolymer Micelles



5. Synthesis of [Fe(Leq)(Lax)]_n Coordination Polymer Nanoparticles using Blockcopolymer Micelles



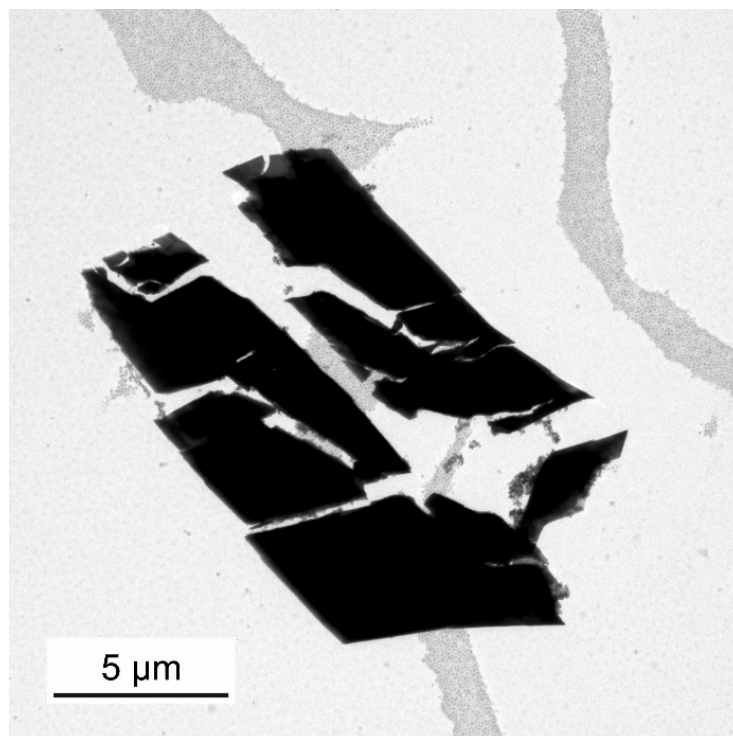


Figure S7: Exemplary TEM picture of $[\text{FeL}_{\text{eq}}(\text{bpea})]_n@BCP$ after two cycles synthesised in toluene to show microcrystals of the coordination polymer.

5. Synthesis of $[\text{Fe}(\text{Leq})(\text{Lax})]_n$ Coordination Polymer Nanoparticles using Blockcopolymer Micelles

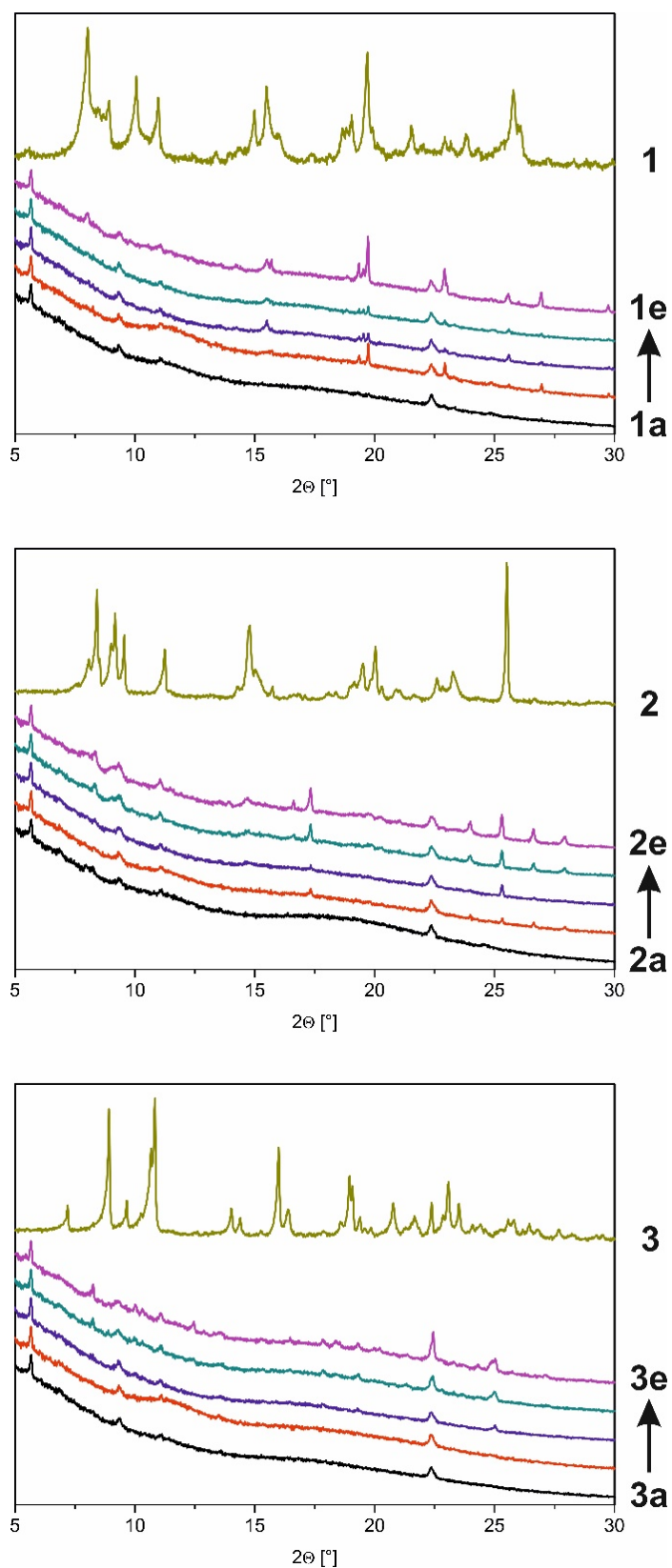


Figure S8: Powder X-Ray diffraction pattern of **1** and **1a-1e** (top), **2** and **2a-2e** (centre) and **3** and **3a-3e** (bottom).

5. Synthesis of [Fe(Leq)(Lax)]_n Coordination Polymer Nanoparticles using Blockcopolymer Micelles

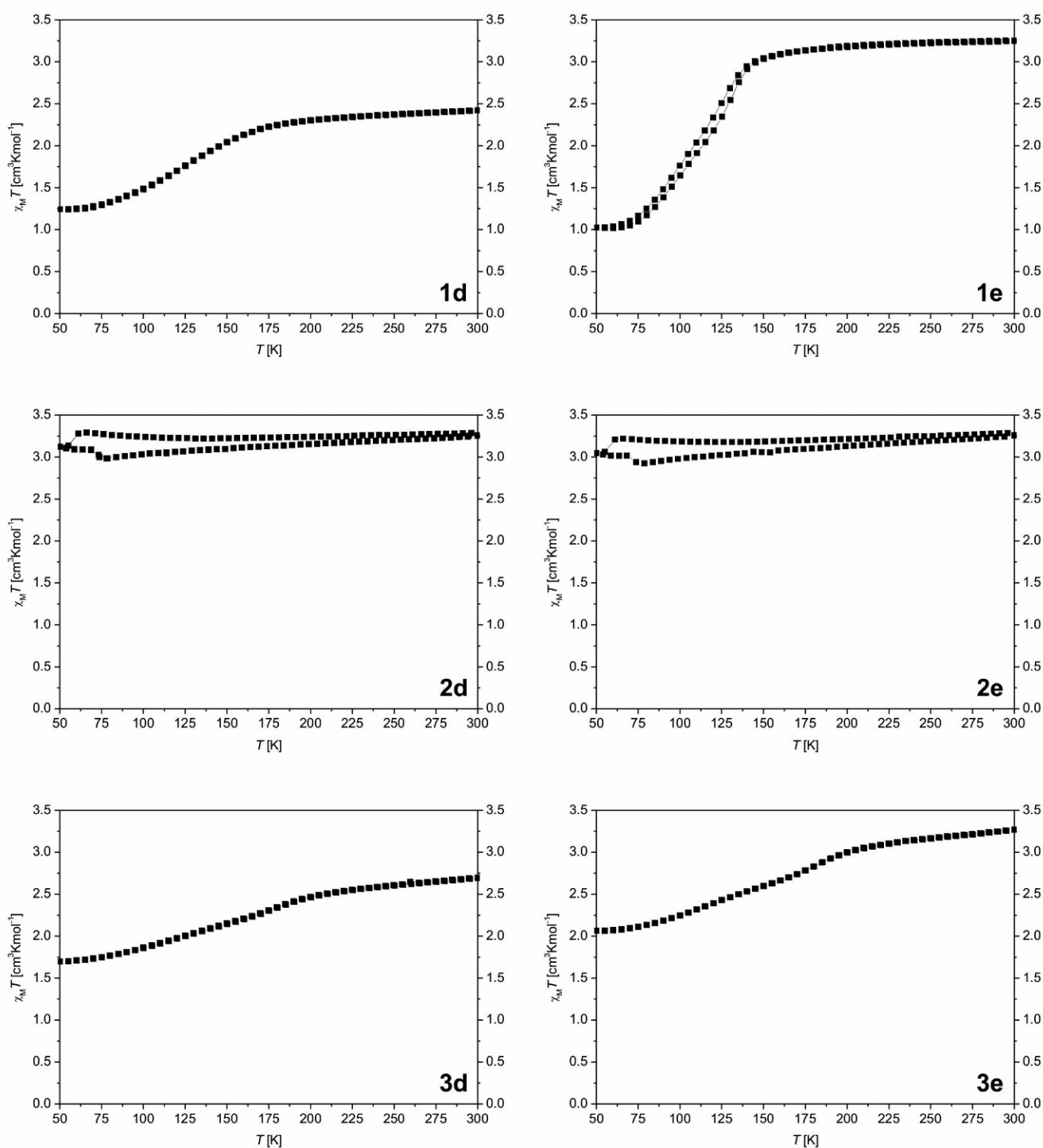


Figure S9: $\chi_M T$ vs. T plots of the samples **1d** (top left), **1e** (bottom left), **3d** (top right) and **3e** (bottom right). The results for the samples **2d** to **2e** are identical to the bulk material [FeL_{eq}(bpee)]_n; the $\chi_M T$ product is constant in the temperature region investigated and no

indication for spin crossover is observed. This is not surprising, as relatively large microcrystals are observed.

References

1. Bauer, W.; Scherer, W.; Altmannshofer, S.; Weber, B. *Eur. J. Inorg. Chem.* **2011** 2803–2818. doi:10.1002/ejic.201001363

6. The influence of the block copolymer composition on particle size and shape of Fe(II) SCO nanoparticles in block copolymer micelles

Ottokar Klimm¹, Christoph Göbel¹, Florian Puchtler², Sabine Rosenfeldt³, Stephan Förster³ and Birgit Weber^{*1}

Address: ¹Inorganic Chemistry VI, University of Bayreuth, Universitätsstr. 30, 95440 Bayreuth, Germany ²Inorganic Chemistry I, University of Bayreuth, Universitätsstr. 30, 95440 Bayreuth, Germany and ³Physical Chemistry I and Bavarian Polymer Institute, University of Bayreuth, Universitätsstr. 30, 95440 Bayreuth, Germany

Email: weber@uni-bayreuth.de, <http://www.ac4.uni-bayreuth.de>

* Corresponding author

To be submitted

Abstract

In this work a synthesis of the Fe(II) spin crossover (SCO) coordination polymer $[\text{Fe}(\text{Lb})(\text{bipy})]_n$ (with $\text{Lb} = 1,2\text{-phenylenebis(iminomethylidene)bis(2,4-pentanedionato)(2-)}$ and $\text{bipy} = 4,4'\text{-bipyridine}$) nanoparticles is described using polystyrene-*b*-poly-(4-vinylpyridine) (PS-*b*-P4VP) block copolymer micelles as nanoreactors. A control of the spin crossover properties can be achieved by precise tuning of the crystallinity of the coordination polymer via successive addition of the starting material $[\text{Fe}(\text{L})(\text{MeOH})_2]$ and bipy in different reaction cycles. With different molecular masses and amounts of P4VP of the BCPs a size and shape control is aimed. Such a size and shape control is, to the best of our knowledge, a completely new approach for the synthesis of nanoparticles of coordination polymers and should be easily transferable to other coordination polymers and networks.

Introduction

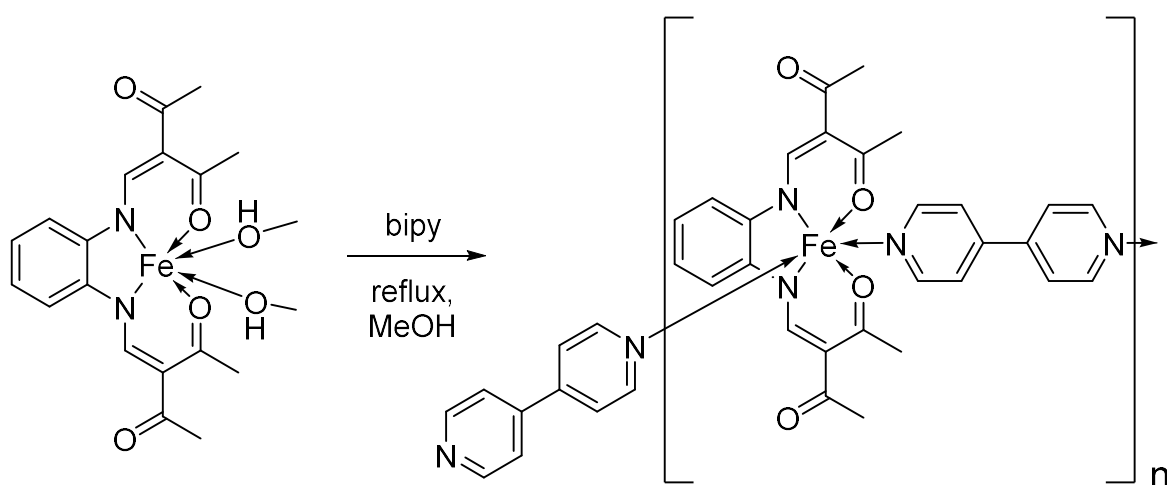
Nowadays nanocomposites of functional materials are essential for applications as sensors^[1-3], switches or data storage (electronic), catalysts or smart contrast agents in medicine.^[4-8,9-13] Spin crossover compounds are a class of complexes of high interest due to the possibility to be switched or triggered by an external stimuli as temperature, pressure or light. Nanoparticles of known bulk materials often show completely new applications.^[14-16] SCO compounds often react very sensitive to changes in crystal structure or packing, even adding or removing solvent molecules can lead to completely different behaviour. The precise tune of nanomaterials is a complex task. The goal is to synthesise size and shape controlled and monodisperse nanocomposites.^[17-20] Various methods are well-known to produce such nanocomposites (i.e. micelle techniques or other methods) by top-down or bottom-up approaches. In former works, we presented a new approach to synthesise nanoscaled CPs in a block copolymer (BCP) matrix of polystyrene-*b*-poly-(4-vinylpyridine) (PS-*b*-P4VP).^[21] Due to selfassembly, BCPs form nanoreactors similar to inverse micelles and a very controlled miniaturisation can be gained.^[22-24] Those approaches should be transferable to many other SCO systems to form nanosized CPs. 1D CPs of $[\text{Fe}(\text{Lb})(\text{bipy})]_n@BCP$ ^[21,25] and $[\text{Fe}(\text{Lb})(\text{bpey})]_n@BCP$ were synthesised already.^[26] The crystallinity of the nanoparticles can be controlled by sequentially adding starting material in different reaction cycles to gain a slow CP growth into the BCP matrix.^[21] By varying temperature and reaction time, the shape and distribution of the particles can also be varied. In this work, the influence of the molecular mass

6. The influence of the block copolymer composition on particle size and shape of Fe(II) SCO nanoparticles in block copolymer micelles

and the amount of P4VP of the used BCPs is examined, to control size and shape of the received nanoparticles. By increasing or reducing the molecular mass of the used BCP it can be possible to vary the size of the nanocomposites towards larger or smaller particles.^[22] Changes in the PS : P4VP ratio can lead to a change of shape of the nanocomposites. A critical concentration of P4VP can lead to a transformation from spherical nanoparticles towards nanorods, vesicles or a mixture of spherical and non spherical nanoparticles.^[22,23] SCO nanocomposites are well-known in literature, but the miniaturisation towards specific sizes and shapes is not remarkable shown yet. Thus it is difficult to synthesise nanocomposites with the same or at least similar properties than the bulk material.

Results and Discussion

$[\text{Fe}(\text{Lb})(\text{bipy})]_n$ was used in this work (Scheme 1). For the synthesis of the coordination polymer (CP) three different blockcopolymer (BCP) composite materials were used. An overview of the polymers used in this work and all sample numbers is given in Table 1 and Table 2. The empty BCP was stirred in THF for BCP-1 and toluene for BCP-2 and -3 to gain self assembly. The precursor complex $[\text{Fe}(\text{Lb})(\text{MeOH})_2]$ was added and stirred for two hours. The bridging ligand 4,4'-bipyridine (**bipy**) was added and refluxed for one hour to gain a slow particle growth in the BCP composite matrix. Thus one reaction cycle (RC) was done. To obtain different crystallinities of the nanoparticles, 1-5 RC were done (Table 2).



Scheme 1: Fe(II) CP used in this work to synthesise SCO nanoparticles in different BCP matrices.

6. The influence of the block copolymer composition on particle size and shape of Fe(II) SCO nanoparticles in block copolymer micelles

Table 1: Overview of the used block copolymers, their molecular weights and units of PS and P4VP.

Polymer	molecular weight [g·mol ⁻¹]	units P4VP	units PS	ratio P4VP : PS
BCP-1	150000	204	1234	≈ 1:6
BCP-2	100000	240	720	≈ 1:3
BCP-3	250000	785	1608	≈ 1:2

Table 2: Overview of all samples, RC and solvents used in this work.

sample	BCP	RC	solvent
1	1	1	THF
2	1	2	THF
3	1	3	THF
4	1	4	THF
5	1	5	THF
6	2	1	toluene
7	2	2	toluene
8	2	3	toluene
9	2	4	toluene
10	2	5	toluene
11	3	1	toluene
12	3	2	toluene
13	3	3	toluene
14	3	4	toluene
15	3	5	toluene

A Fe(II) SCO CP was incorporated into three different BCPs. In Figure 1 transmission electron microscopy (TEM) images of sample **5** (5 RC), sample **10** (5 RC) and sample **15** (5 RC) are given to show the various morphologies of the used BCPs.

6. The influence of the block copolymer composition on particle size and shape of Fe(II) SCO nanoparticles in block copolymer micelles

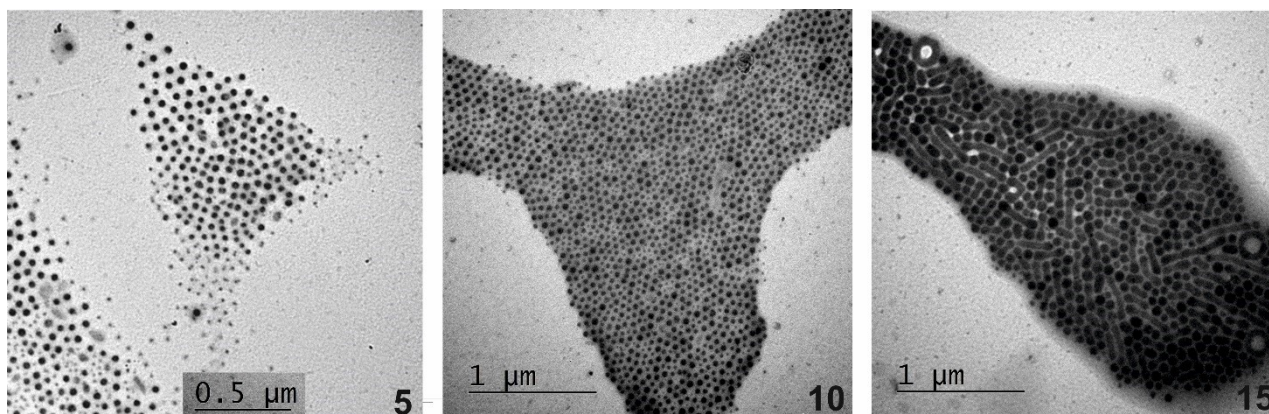


Figure 1: Different shapes of nanoparticles in BCP-1 (left), BCP-2 (middle) and BCP-3 (right) at five RC. BCP-3 leads to a mixture of spherical nanoparticles, nanorods and vesicles.

For BCP-1 and BCP-2, pure spherical nanoparticles are obtained, BCP-3 shows a mixture of spherical nanoparticles, nanorods and vesicles. Based on the differences in contrast, the iron complexes in the P4VP part forms the core while the PS part gives the shell of the nanoparticle. BCP-3 shows the most contrast and the largest particles. A hexagonal 1D packing effect for the nanoparticles in BCP-1, -2 and -3 is observed. Due to the loss of the core-shell character from BCP-1 towards BCP-3, the hexagonal packing effect is much stronger towards BCP-3 showed in Figure S5 in the SI. An overview about the particle sizes of the empty BCPs, two and five RC measured via TEM and dynamic light scattering (DLS) (Figure S4) in each BCP is given in Table 3. Scanning electron microscopy (SEM) was used for samples 4 and 5, to clear up there a no crystals build (Figure S10).

6. The influence of the block copolymer composition on particle size and shape of Fe(II) SCO nanoparticles in block copolymer micelles

Table 3: Overview of particle sizes of empty BCPs and synthesised nanoparticles at two and five reaction cycles in BCP-1, BCP-2 and BCP-3 measured by TEM, DLS and PXRD

<i>cycles</i>	<i>sample</i>	<i>DLS</i> [nm]	<i>TEM core</i> [nm]	<i>TEM shell</i> [nm]	<i>PXRD (23°)</i> [nm]
0	BCP-1	126±22	70±8		-
2	2	140±13	57±8	94±15	33±3
5	5	145±13	49±5	113±15	45±3
0	BCP-2	104±19	23±3		-
2	7	116±10	42±4	72±7	-
5	10	109±20	46±4	67±6	72±4
0	BCP-3	147±19	52±4		-
2	12	136±13	74±6	93±8	-
5	15	154±18	75±6	92±9	68±4

Control of the crystallinity of the nanoparticles

To show the growth of the CP in the BCP matrix and the rising crystallinity of the nanoparticles, powder-XRD (PXRD) and IR measurements were done (Figure 2). The characteristic C=O bond at about 1600 cm⁻¹ increases with higher amount of [Fe(Lb)(bipy)]_n with higher number of RCs. The rising crystallinity of the nanoparticles is shown in the PXRD measurements. With higher number of RCs the characteristic signals for [Fe(Lb)(bipy)]_n compared to the bulk material appear. IR and PXRD measurements of samples **6-10** and **11-15** are given in Figure 2.

6. The influence of the block copolymer composition on particle size and shape of Fe(II) SCO nanoparticles in block copolymer micelles

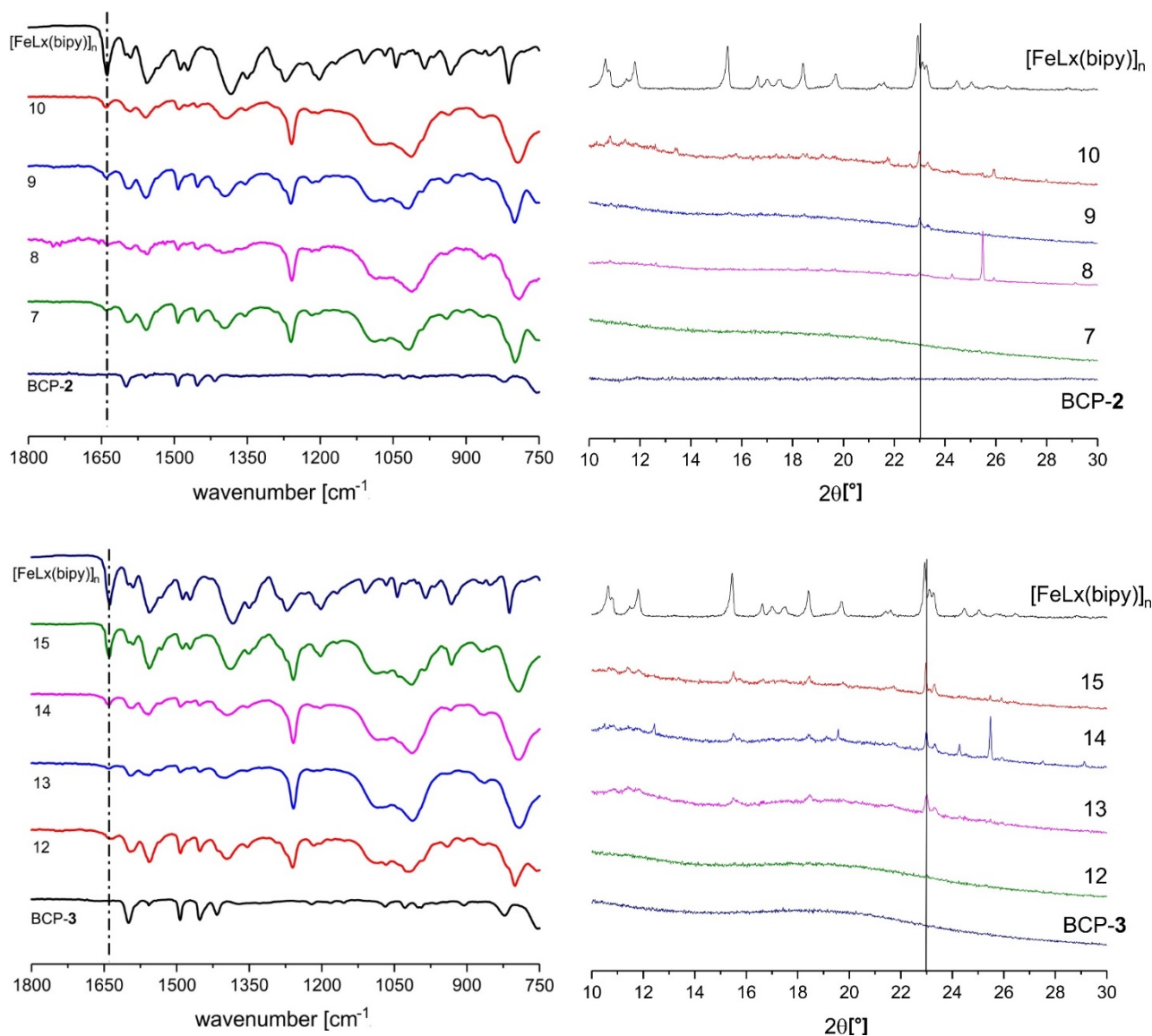


Figure 2: Powder X-Ray diffraction pattern of 7-10 in BCP-2 (top, right) and 12-15 in BCP-3 (bottom, right) and IR spectra of 7-10 in BCP-2 (top, left) and 12-15 in BCP-3 (bottom, left) with the relevant area between 2000 cm^{-1} and 750 cm^{-1} to show a rise of the C=O vibration band about 1600 cm^{-1} with higher number of RCs.

Magnetism

The change of crystallinity of the CP core and therefore of n in $[\text{Fe}(\text{Lb})(\text{bipy})]_n$ in the BCP micelle should significantly influence the SCO properties of the composite material. Due to the differences in coordination environment of the outside $[\text{Fe}(\text{Lb})]$ units of the $[\text{Fe}(\text{Lb})(\text{bipy})]_n$ coordination polymer, only the inside $[\text{Fe}(\text{Lb})]$ units are expected to undergo spin crossover (SCO).^[21] Magnetic

6. The influence of the block copolymer composition on particle size and shape of Fe(II) SCO nanoparticles in block copolymer micelles

measurements of the samples **7-10** and **12-15** were done in the temperature range between 300 K and 50 K in the cooling and heating mode. The results are given as $\chi_M T$ versus T plots in Figure 2 and Figure S7-S8 in the SI where χ_M is the molar susceptibility and T the temperature. To show a characteristic tendency for the change of SCO properties with different reaction cycles, 2 and 5 cycles are shown for each CP-BCP. Sample **7** shows a room temperature $\chi_M T$ about $3.3 \text{ cm}^3 \text{Kmol}^{-1}$ which is in the expected value of $3.0\text{-}3.3 \text{ cm}^3 \text{Kmol}^{-1}$ for Fe(II) HS. The $\chi_M T$ value at 50 K is about $1.8 \text{ cm}^3 \text{Kmol}^{-1}$ after an incomplete gradual SCO. Room temperature $\chi_M T$ of **10** is about $3.4 \text{ cm}^3 \text{Kmol}^{-1}$, which is expected for Fe(II) HS. An abrupt SCO with a 25 K hysteresis takes place. The $T_{1/2}$ values (where 50% of the SCO active centres did undergo spin transition) of **10** are 205 K in the cooling and 230 K in the heating mode corresponding to a 25 K wide thermal hysteresis loop. The $\chi_M T$ value at 50 K is about $2.1 \text{ cm}^3 \text{Kmol}^{-1}$, which is significantly higher than the expected value for an Fe(II) LS characteristic for an incomplete ST. The magnetic properties of **10** are close to the bulk material (20 K hysteresis for the bulk and 25 K for **10**). The use of BCP micelles leads to a larger and more gradual, but incomplete hysteresis after five RC compared to the bulk material. **12** shows a room temperature $\chi_M T$ value about $3.2 \text{ cm}^3 \text{Kmol}^{-1}$ which is in the range of Fe(II) HS. The $\chi_M T$ value at 50 K is about $1.9 \text{ cm}^3 \text{Kmol}^{-1}$ after an incomplete gradual SCO. Room temperature $\chi_M T$ of **15** is about $3.2 \text{ cm}^3 \text{Kmol}^{-1}$ which is expected for Fe(II) HS. An abrupt SCO with a 25 K hysteresis takes place. The $T_{1/2}$ values (where 50% of the SCO active centres did undergo spin transition) of **15** are 210 K in the cooling and 235 K in the heating mode corresponding to a 25 K wide thermal hysteresis loop. The $\chi_M T$ value at 50 K is about $1.6 \text{ cm}^3 \text{Kmol}^{-1}$, which is significantly higher than the expected value for an Fe(II) LS characteristic for an incomplete ST. The magnetic properties of **15** are close to those of the bulk material similar to **10**.

6. The influence of the block copolymer composition on particle size and shape of Fe(II) SCO nanoparticles in block copolymer micelles

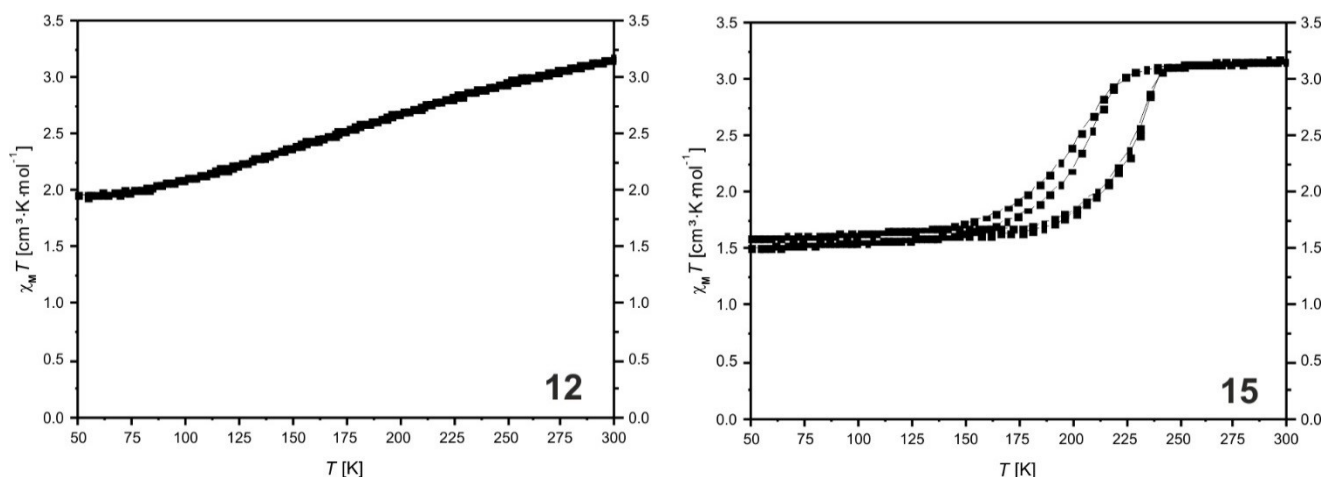


Figure 3: SQUID measurements of [Fe(Lb)(bipy)]_n@BCP-3 with two (left) and five RC (right). With rising crystallinity of the SCO nanoparticles, the ST changes from an incomplete gradual (left) to an incomplete SCO with a 25 K wide hysteresis (right).

Conclusion

In this work, we showed the possibility to tune the BCPs to get a size control for synthesised nanoparticles. The size control of the given nanoparticles via changing the molecular mass and the amounts of P4VP in the block copolymers was shown. With higher molecular weight the particle size of the nanoparticles is increased. Thus, it is possible to synthesise BCPs with special molecular masses to get targeted nanoparticles and have a size control. To gain other shapes of nanoparticles varying the amount of P4VP toward higher percentages was done. Up to 25% of P4VP, pure spherical nanoparticles appear. Between 25% and 33%, a conversion towards a mixture of spherical nanoparticles, nanorods and vesicles appears. SCO compounds in BCP-2 and BCP-3 matrix (33% of P4VP) showed SCO properties similar to the bulk material of [Fe(Lb)(bipy)]_n. It was possible to change the shape of the nanoparticles towards a mixture of spherical nanoparticles, nanorods and vesicles. In a future work it has to be investigated, if more than 33% of P4VP lead to pure nanorods or vesicles. Furthermore, varying the second, non-coordinating block of the BCPs, other abilities appear i.e. P4VP-*b*-H3TP (conductivity) or P4VP-*b*-PEO (water soluble).

Experimental

Synthetic procedure

Polystyrene-*b*-poly(4-vinylpyridine) (BCP-1, purum, MW \approx 150000, 15% P4VP), polystyrene-*b*-poly(4-vinylpyridine) (BCP-2, purum, MW \approx 100000, 25% P4VP) and polystyrene-*b*-poly(4-vinylpyridine) (BCP-3, purum, MW \approx 250000, 33% P4VP) were synthesized as described before.^[21] 4,4'-bipyridine was obtained from Alfa Aesar and used as received. Toluene (Tol) was purified as described in literature. [Fe(L)(MeOH)₂] was synthesised as described before. All syntheses were performed under inert conditions using Schlenk technique with argon (purity \geq 99,999%, 5.0). The syntheses of all samples were repeated at least twice.

6: BCP-2 (50 mg, 0.5 μ mol) and [Fe(L)(MeOH)₂] (5.7 mg, 13 μ mol) were added to a 50 ml flask. Subsequently toluene (20 ml) was added and the mixture was heated to reflux for 2h. After cooling to room temperature, 4,4'-bipyridine (5.0 mg, 32 μ mol) was added to the brown solution and the reaction mixture was heated to reflux for 1h. After cooling to room temperature the solvent was removed via cold distillation to yield a brown, polymer-like powder.

7: The synthesis as described for sample **6** was repeated. Before solvent removal, [Fe(L)(MeOH)₂] (5.7 mg, 13 μ mol) and 4,4'-bipyridine (5.0 mg, 32 μ mol) were added in a second cycle and the mixture was heated to reflux for one further hour. After cooling to room temperature the solvent was removed via cold distillation to yield a brown, polymer-like powder. Elemental anal. (%) found: C 71.71, H 7.10, N 4.99.

8: The synthesis described for sample **7** was repeated, with one further cycle of addition of [Fe(L)(MeOH)₂] (5.7 mg, 13 μ mol) and 4,4'-bipyridine (5.0 mg, 32 μ mol) followed by further heating to reflux for 1h. After cooling to room temperature the solvent was removed via cold distillation to yield a brown, polymer-like powder. Elemental anal. (%) found: C 67.92, H 6.82, N 5.23.

9: The synthesis described for sample **8** was repeated, with one further cycle of addition of [Fe(L)(MeOH)₂] (5.7 mg, 13 μ mol) and 4,4'-bipyridine (5.0 mg, 32 μ mol) followed by further heating to reflux for 1h. After cooling to room temperature the solvent was removed via cold distillation to yield a brown, polymer-like powder. Elemental anal. (%) found: C 64.85, H 6.59, N 6.15.

6. The influence of the block copolymer composition on particle size and shape of Fe(II) SCO nanoparticles in block copolymer micelles

10: The synthesis described for sample **9** was repeated, with one further cycle of addition of [Fe(L)(MeOH)₂] (5.7 mg, 13 μmol) and 4,4'-bipyridine (5.0 mg, 32 μmol) followed by further heating to reflux for 1h. After cooling to room temperature the solvent was removed via cold distillation to yield a brown, polymer-like powder. Elemental anal. (%) found: C 64.84, H 6.57, N 6.46.

The colour turned increasingly darker from sample **6** to **10** with an increasing amount of iron.

11: BCP-3 (50 mg, 0.2 μmol) and [Fe(L)(MeOH)₂] (6.4 mg, 15 μmol) were added to a 50 ml flask. Subsequently toluene (20 ml) was added and the mixture was heated to reflux for 2h. After cooling to room temperature, 4,4'-bipyridine (5.6 mg, 36 μmol) was added to the brown solution and the reaction mixture was heated for 1h to reflux. After cooling to room temperature the solvent was removed via cold distillation to yield a brown, polymer-like powder.

12: The synthesis as described for sample **11** was repeated. Before solvent removal, [Fe(L)(MeOH)₂] (6.4 mg, 15 μmol) and 4,4'-bipyridine (5.6 mg, 36 μmol) were added in a second cycle and the mixture was heated to reflux for one further hour. After cooling to room temperature the solvent was removed via cold distillation to yield a brown, polymer-like powder. Elemental anal. (%) found: C 74.40, H 7.01, N 5.08.

13: The synthesis described for sample **12** was repeated, with one further cycle of addition of [Fe(L)(MeOH)₂] (6.4 mg, 15 μmol) and 4,4'-bipyridine (5.6 mg, 36 μmol) followed by further heating to reflux for 1h. After cooling to room temperature the solvent was removed via cold distillation to yield a brown, polymer-like powder. Elemental anal. (%) found: C 72.10, H 6.93, N 4.87.

14: The synthesis described for sample **13** was repeated, with one further cycle of addition of [Fe(L)(MeOH)₂] (6.4 mg, 15 μmol) and 4,4'-bipyridine (5.6 mg, 36 μmol) followed by further heating to reflux for 1h. After cooling to room temperature the solvent was removed via cold distillation to yield a brown, polymer-like powder. Elemental anal. (%) found: C 73.28, H 6.87, N 5.61.

15: The synthesis described for sample **14** was repeated, with one further cycle of addition of [Fe(L)(MeOH)₂] (6.4 mg, 15 μmol) and 4,4'-bipyridine (5.6 mg, 36 μmol) followed by further heating to reflux for 1h. After cooling to room temperature the solvent was removed via cold

6. The influence of the block copolymer composition on particle size and shape of Fe(II) SCO nanoparticles in block copolymer micelles

distillation to yield a brown, polymer-like powder. Elemental anal. (%) found: C 61.34, H 6.92, N 4.76.

The colour turned increasingly darker from sample **11** to **15** with an increasing amount of iron.

Methods

Transmission electron microscopy: Transmission electron microscopy was performed with a Zeiss CEM902 electron microscope (Zeiss, Oberkochen, Germany). Samples were dispersed in toluene applying vortex several times. The dispersion was dropped on a carbon coated copper grid (Science Services, Munich). The acceleration voltage was set to 80 kV. Micrographs were taken with a MegaView III / iTEM image acquiring and processing system from Olympus Soft Imaging Systems (OSIS, Muenster, Germany) and an Orius 830 SC200W / DigitalMicrograph system from Gatan (Munich, Germany). Particles size measurements were done with “ImageJ” image processing software by Wayne Rasband (National Institutes of Health, USA).

Infrared spectroscopy: Transmission infrared spectra were collected using a PerkinElmer Spectrum 100 FT-IR (ATR). Samples were measured directly as solids.

Elemental Analysis: Carbon, nitrogen and hydrogen contents were collected at a Vario EL III. Samples were placed in tin boats. All samples were measured at least twice and the average of both measurements was used.

Energy dispersive X-ray spectroscopy: Energy dispersive X-ray spectroscopy was done at a 200 kV FEI-Titan G2 80-200 S/TEM (Eindhoven, Netherlands). Samples were dispersed in methanol applying vortex and ultrasound several times. The dispersion was dropped on a carbon filmed coated copper grid. The acceleration voltage was set to 200 kV.

Scanning electron microscopy: Scanning electron microscopy micrographs were acquired with a Zeiss LEO 1530 (Oberkochen, Germany).

Magnetic measurements: Magnetic susceptibility measurements were performed at a Quantum Design MPMS-XL-5 SQUID magnetometer in the temperature range between 50 and 300 K. The samples were prepared in gelatin capsules placed in a plastic straw. All samples were measured with a magnetic field of 3T in the settle mode with a cooling and heating rate of 5K min⁻¹ between

6. The influence of the block copolymer composition on particle size and shape of Fe(II) SCO nanoparticles in block copolymer micelles

each measurement point. The measured values were corrected for the diamagnetism of the sample holder, the polymer matrix (measured values) and the ligand (tabulated Pascal constants).

X-Ray Powder Diffraction: X-Ray Powder Diffraction data for samples 2 to 6 and the bulk [FeL(bipy)]_n were collected at a STOE StadiP X-ray powder diffractometer in transmission geometry between 5 and 45° 2 θ . Samples were placed in a flat carrier and Cu-K α 1 radiation was used for the measurement. Radiation was detected with a Mythen 1K detector.

Mössbauer spectroscopy: ⁵⁷Fe Mössbauer spectra were recorded in transmission geometry on a constant-acceleration using a conventional Mössbauer spectrometer with a 50 mCi ⁵⁷Co(Rh) source. The samples were sealed in the sample holder in an argon atmosphere. The spectra were fitted using Recoil 1.05 Mössbauer Analysis Software.³⁰ The isomer shift values are given with respect to a α -Fe reference at room temperature.

Dynamic light scattering: DLS of all samples were collected from Malvern Zetasizer Nano ZS. Samples were measured in solution in glass cuvettes from Carl Roth GmbH + Co. KG.

References

- [1] Coronado, E.; Mínguez Espallargas, G. *Chem. Soc. Rev.* **2013**, *42* (4), 1525.
- [2] Ohba, M.; Yoneda, K.; Agustí, G.; Muñoz, M. C.; Gaspar, A. B.; Real, J. A.; Yamasaki, M.; Ando, H.; Nakao, Y.; Sakaki, S.; Kitagawa, S. *Angew. Chem. Int. Ed.* **2009**, *48* (26), 4767–4771.
- [3] Linares, J.; Coddjovi, E.; Garcia, Y. *Sensors* **2012**, *12* (4), 4479–4492.
- [4] Sindoro, M.; Yanai, N.; Jee, A.-Y.; Granick, S. *Acc. Chem. Res.* **2014**, *47* (2), 459–469.
- [5] Coronado, E.; Giménez-Marqués, M.; Mínguez Espallargas, G.; Rey, F.; Vitorica-Yrezabal, I. *J. Am. Chem. Soc.* **2013**, *135* (43), 15986–15989. doi:10.1021/ja407135k
- [6] Zhao-Yang Li, O. S.; Yao, Z.-S.; Kang, S.; Kanegawa, S. Multifunctional Materials Combining Spin-Crossover with Conductivity and Magnetic Ordering. In *Spin-Crossover Materials*; Halcrow, M. A., Ed.; John Wiley & Sons Ltd: Chichester, 2013; pp 303–319.

6. The influence of the block copolymer composition on particle size and shape of Fe(II) SCO nanoparticles in block copolymer micelles

- [7] Gaspar, A. B.; Weber, B. Spin Crossover Phenomenon in Coordination Compounds. In *Molecular Magnetic Materials*; Sieklucka, B., Pinkowicz, D., Eds.; Wiley-VCH Verlag GmbH & Co. KGaA: Weinheim, Germany, 2017; pp 231–252.
- [8] Halcrow, M. A., Ed. *Spin-Crossover Materials*; John Wiley & Sons Ltd: Chichester, **2013**.
- [9] R. N. Muller, L. Vander Elst, S. Laurent, *J. Am. Chem. Soc.* **2003**, *125* (27), 8405–8407.
- [10] S. Venkataramani, U. Jana, M. Dommaschk, F. D. Sönnichsen, F. Tuczek, R. Herges, *Science* **2011**, *331* (6016), 445–448.
- [11] M. Dommaschk, M. Peters, F. Gutzeit, C. Schütt, C. Näther, F. D. Sönnichsen, S. Tiwari, C. Riedel, S. Boretius, R. Herges, *J. Am. Chem. Soc.* **2015**, *137* (24), 7552–7555.
- [12] J. Hasserodt, J. L. Kolanowski, F. Touti, *Angew. Chem. Int. Ed.* **2014**, *53* (1), 60–73.
- [13] R. Nowak, E. A. Prasetyanto, L. de Cola, B. Bojer, R. Siegel, J. Senker, E. Rössler, B. Weber, *Chem. Commun.* **2017**, *53* (5), 971–974.
- [14] Gaspar, A. B.; Weber, B. Spin Crossover Phenomenon in Coordination Compounds. In *Molecular Magnetic Materials*; Sieklucka, B., Pinkowicz, D., Eds.; Wiley-VCH Verlag GmbH & Co. KGaA: Weinheim, Germany, **2017**; pp 231–252.
- [15] Carmen Muñoz, M.; Antonio Real, J. Polymeric Spin-Crossover Materials. In *Spin-Crossover Materials*; Halcrow, M. A., Ed.; John Wiley & Sons Ltd: Chichester, **2013**; pp 121–146.
- [16] Gütlich, P.; Gaspar, A. B.; Garcia, Y. *Beilstein J. Org. Chem.* **2013**, *9*, 342–391.
- [17] Larionova, J.; Salmon, L.; Guari, Y.; Tokarev, A.; Molvinger, K.; Molnár, G.; Bousseksou, A. *Angew. Chem. Int. Ed.* **2008**, *47* (43), 8236–8240.
- [18] Cobo, S.; Molnár, G.; Real, J. A.; Bousseksou, A. *Angew. Chem. Int. Ed.* **2006**, *45* (35), 5786–5789.
- [19] Molnár, G.; Cobo, S.; Real, J. A.; Carcenac, F.; Daran, E.; Vieu, C.; Bousseksou, A. *Adv. Mater* **2007**, *19* (16), 2163–2167.
- [20] Bartual-Murgui, C.; Natividad, E.; Roubeau, O. *J. Mater. Chem. C* **2015**, *3* (30), 7916–7924.
- [21] O. Klimm, C. Göbel, S. Rosenfeldt, F. Puchtler, N. Miyajima, K. Marquardt, M. Drechsler, J. Breu, S. Förster, B. Weber, *Nanoscale* **2016**, *8* (45), 19058–19065.
-

6. The influence of the block copolymer composition on particle size and shape of Fe(II) SCO nanoparticles in block copolymer micelles

- [22] Förster, S.; Zisenis, M.; Wenz, E.; Antonietti, M. *J. Chem. Phys.* **1996**, *104* (24), 9956.
- [23] Förster, S.; Antonietti, M. *Adv. Mater.* **1998**, *10* (3), 195–217.
- [24] Fan, Z.; Chen, X.; Kohn Serrano, M.; Schmalz, H.; Rosenfeldt, S.; Förster, S.; Agarwal, S.; Greiner, A. *Angew. Chem. Int. Ed.* **2015**, *54* (48), 14539–14544.
- [25] W. Bauer, W. Scherer, S. Altmannshofer, and B. Weber, *Eur. J. Inorg. Chem.* **2011**, 2803–2818.
- [26] C. Göbel, O. Klimm, F. Puchtler, S. Rosenfeldt, S. Förster and B. Weber, *Beilstein J. Nanotech.*, **2017**, submitted.

6. The influence of the block copolymer composition on particle size and shape of Fe(II) SCO nanoparticles in block copolymer micelles

Supporting Information

Figure S1: Mössbauer spectra of **8** (top left), **9** (top right) in BCP-2, **12** (bottom left) and **14** (bottom right) in BCP-3. The red doublet corresponds to an Fe(II) HS species and the blue doublet corresponds to an Fe(II) LS species. The Mössbauer parameters are given in Table S2.

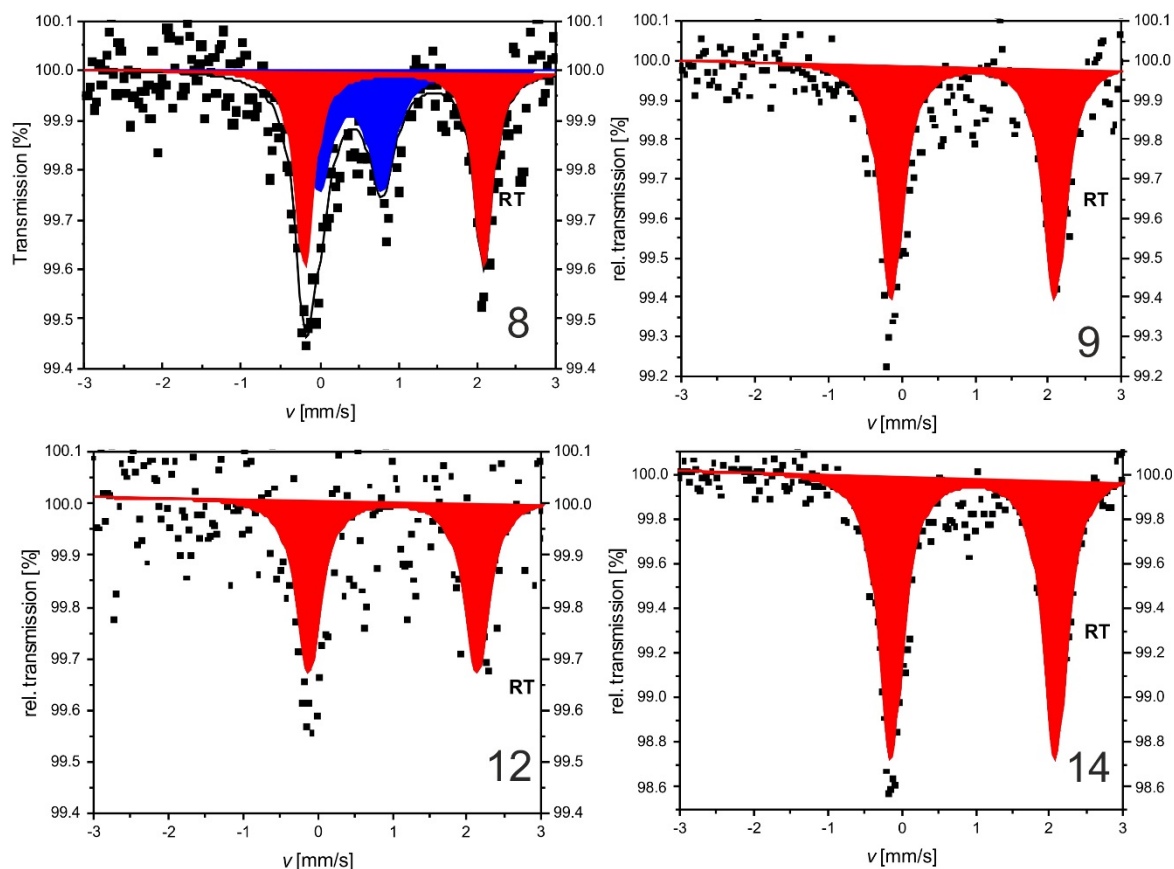
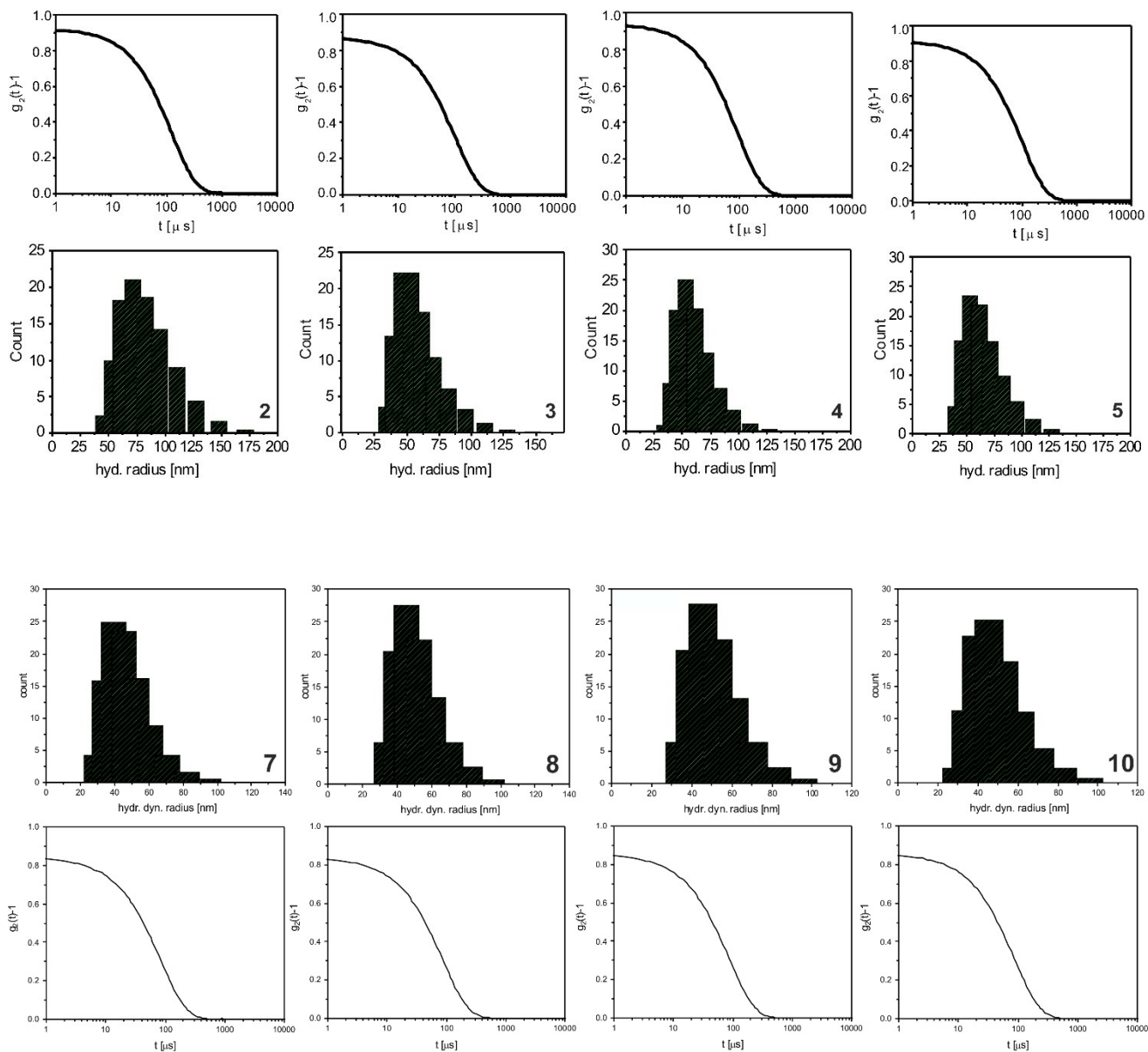


Table S1: Mössbauer parameters of the samples **8** and **9** in BCP-2 and **12** and **14** in BCP-3.

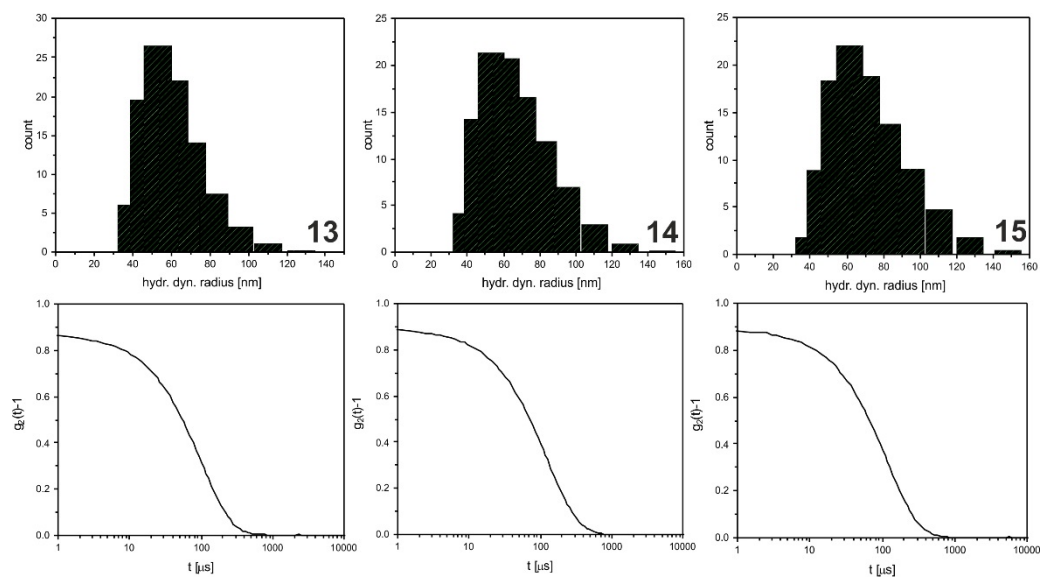
sample	site	δ [mm/s]	ΔE_Q [mm/s]	Γ [mm/s]	Area [%]
8	Fe(II) LS	0.39(6)	0.81(10)	0.21(8)	45(11)
	Fe(II) HS	0.95(3)	2.28(5)	0.15(4)	55(12)
9	Fe(II) HS	0.98(17)	2.23(4)	0.19(3)	100
12	Fe(II) HS	1.00(6)	2.25(17)	0.20(9)	100
14	Fe(II) HS	0.97(9)	2.22(19)	0.20(15)	100

6. The influence of the block copolymer composition on particle size and shape of Fe(II) SCO nanoparticles in block copolymer micelles

Figure S2: DLS measurement of the nanocomposites in THF and toluene, 43w%. Correlation functions of **2-5** (top, from left to right) (THF), **7-10** (centre, from left to right) and **13-15** (bottom, from left to right) (toluene).

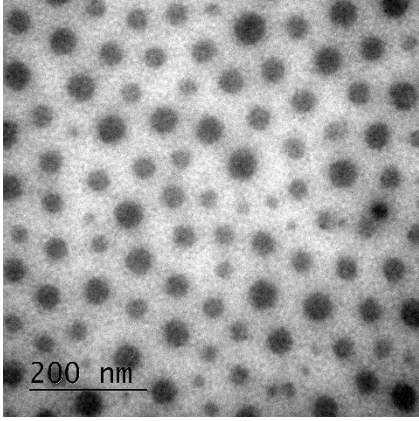
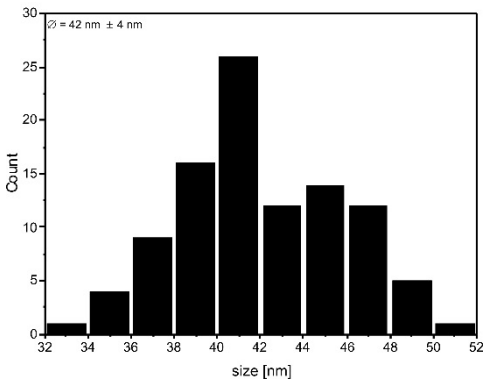
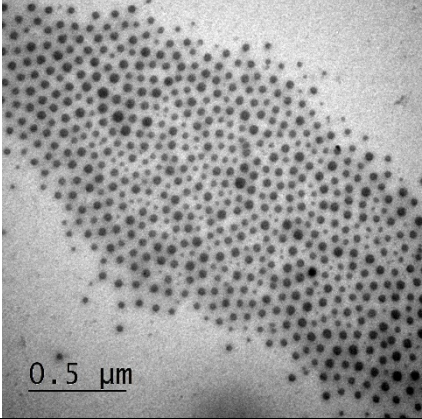
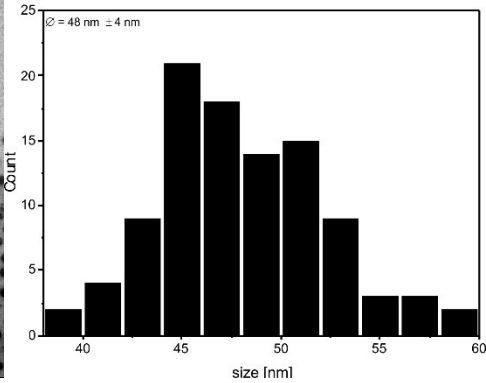
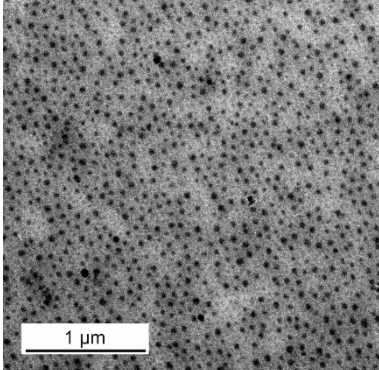
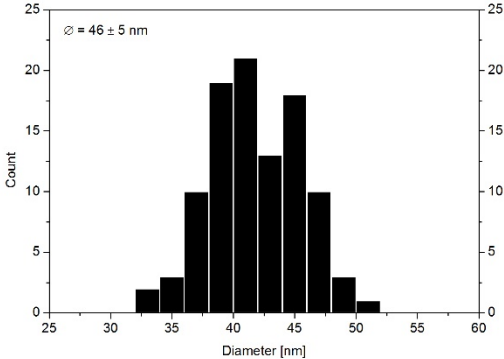


6. The influence of the block copolymer composition on particle size and shape of Fe(II) SCO nanoparticles in block copolymer micelles

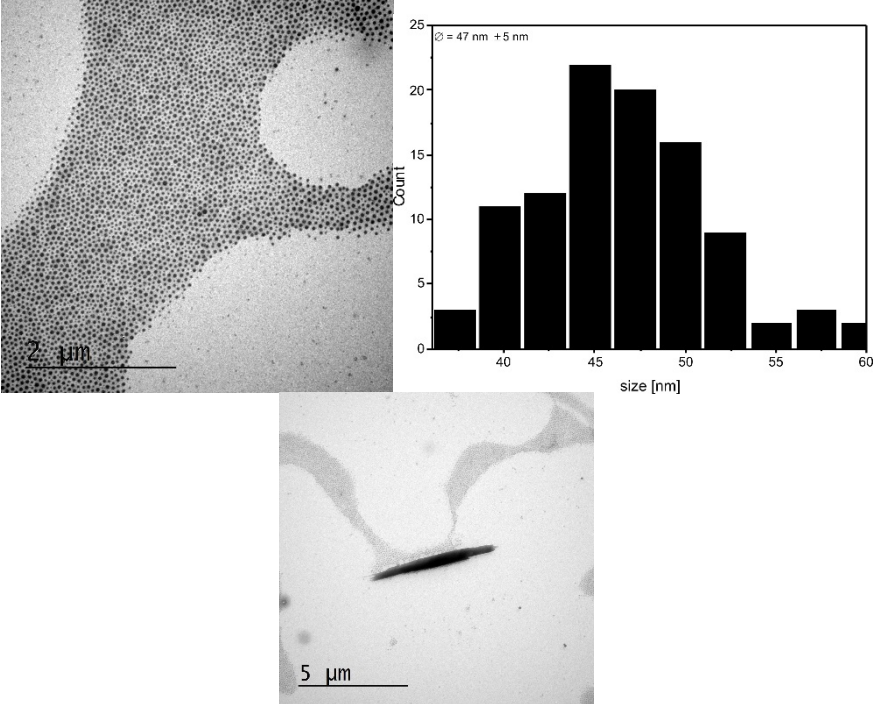
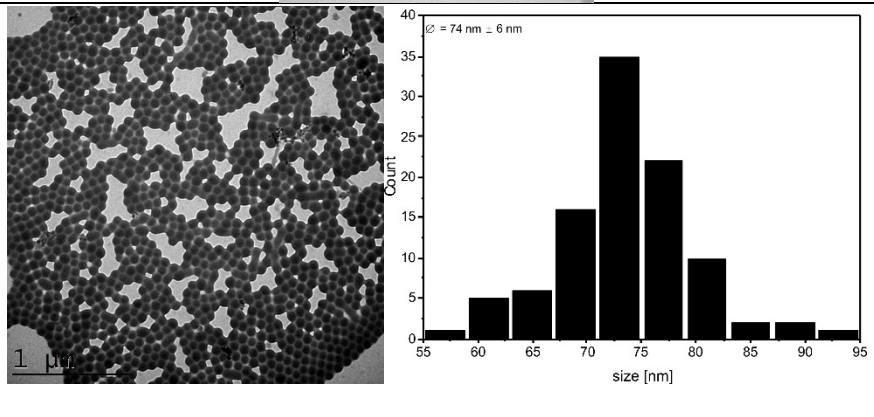
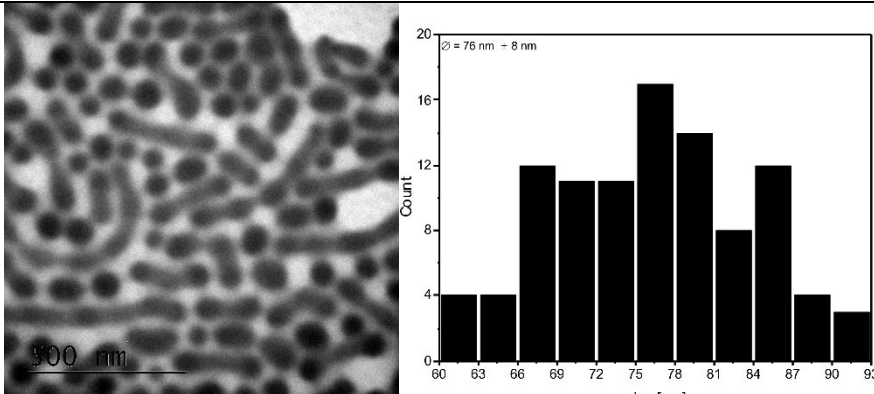


6. The influence of the block copolymer composition on particle size and shape of Fe(II) SCO nanoparticles in block copolymer micelles

Table S2: Summarised characterisation for the different composite samples (6-9 and 12-14). An exemplary TEM picture and the size distribution are given for TEM measurements. The particle sizes are given in the pictures.

sample	Reaction conditions	TEM nanoparticles, TEM size distribution and TEM microcrystals (if any)
6	1 cycles, toluene, reflux, BCP-2	 
7	2 cycle, toluene, reflux, BCP-2	 
8	3 cycles, toluene, reflux, BCP-2	 

6. The influence of the block copolymer composition on particle size and shape of Fe(II) SCO nanoparticles in block copolymer micelles

<p>9</p>	<p>4 cycles, toluene, reflux, BCP-2</p>	 <p>TEM image showing spherical nanoparticles. Scale bar: 2 μm.</p> <p>Histogram showing particle size distribution. Mean diameter: $\bar{\phi} = 47 \text{ nm} \pm 5 \text{ nm}$.</p> <table border="1"> <caption>Estimated Histogram Data for Sample 9</caption> <thead> <tr> <th>Size [nm]</th> <th>Count</th> </tr> </thead> <tbody> <tr><td>35</td><td>3</td></tr> <tr><td>40</td><td>11</td></tr> <tr><td>45</td><td>12</td></tr> <tr><td>50</td><td>22</td></tr> <tr><td>55</td><td>20</td></tr> <tr><td>60</td><td>16</td></tr> <tr><td>65</td><td>9</td></tr> <tr><td>70</td><td>2</td></tr> <tr><td>75</td><td>3</td></tr> <tr><td>80</td><td>2</td></tr> </tbody> </table>	Size [nm]	Count	35	3	40	11	45	12	50	22	55	20	60	16	65	9	70	2	75	3	80	2				
Size [nm]	Count																											
35	3																											
40	11																											
45	12																											
50	22																											
55	20																											
60	16																											
65	9																											
70	2																											
75	3																											
80	2																											
<p>12</p>	<p>2 cycles, toluene, reflux, BCP-3</p>	 <p>TEM image showing spherical nanoparticles. Scale bar: 1 μm.</p> <p>Histogram showing particle size distribution. Mean diameter: $\bar{\phi} = 74 \text{ nm} \pm 6 \text{ nm}$.</p> <table border="1"> <caption>Estimated Histogram Data for Sample 12</caption> <thead> <tr> <th>Size [nm]</th> <th>Count</th> </tr> </thead> <tbody> <tr><td>55</td><td>1</td></tr> <tr><td>60</td><td>5</td></tr> <tr><td>65</td><td>6</td></tr> <tr><td>70</td><td>16</td></tr> <tr><td>75</td><td>35</td></tr> <tr><td>80</td><td>22</td></tr> <tr><td>85</td><td>10</td></tr> <tr><td>90</td><td>2</td></tr> <tr><td>95</td><td>1</td></tr> </tbody> </table>	Size [nm]	Count	55	1	60	5	65	6	70	16	75	35	80	22	85	10	90	2	95	1						
Size [nm]	Count																											
55	1																											
60	5																											
65	6																											
70	16																											
75	35																											
80	22																											
85	10																											
90	2																											
95	1																											
<p>13</p>	<p>3 cycle, toluene, reflux, BCP-3</p>	 <p>TEM image showing rod-like nanoparticles. Scale bar: 500 nm.</p> <p>Histogram showing particle size distribution. Mean diameter: $\bar{\phi} = 76 \text{ nm} \pm 8 \text{ nm}$.</p> <table border="1"> <caption>Estimated Histogram Data for Sample 13</caption> <thead> <tr> <th>Size [nm]</th> <th>Count</th> </tr> </thead> <tbody> <tr><td>60</td><td>4</td></tr> <tr><td>63</td><td>4</td></tr> <tr><td>66</td><td>12</td></tr> <tr><td>69</td><td>11</td></tr> <tr><td>72</td><td>11</td></tr> <tr><td>75</td><td>17</td></tr> <tr><td>78</td><td>14</td></tr> <tr><td>81</td><td>8</td></tr> <tr><td>84</td><td>12</td></tr> <tr><td>87</td><td>4</td></tr> <tr><td>90</td><td>2</td></tr> <tr><td>93</td><td>1</td></tr> </tbody> </table>	Size [nm]	Count	60	4	63	4	66	12	69	11	72	11	75	17	78	14	81	8	84	12	87	4	90	2	93	1
Size [nm]	Count																											
60	4																											
63	4																											
66	12																											
69	11																											
72	11																											
75	17																											
78	14																											
81	8																											
84	12																											
87	4																											
90	2																											
93	1																											

6. The influence of the block copolymer composition on particle size and shape of Fe(II) SCO nanoparticles in block copolymer micelles

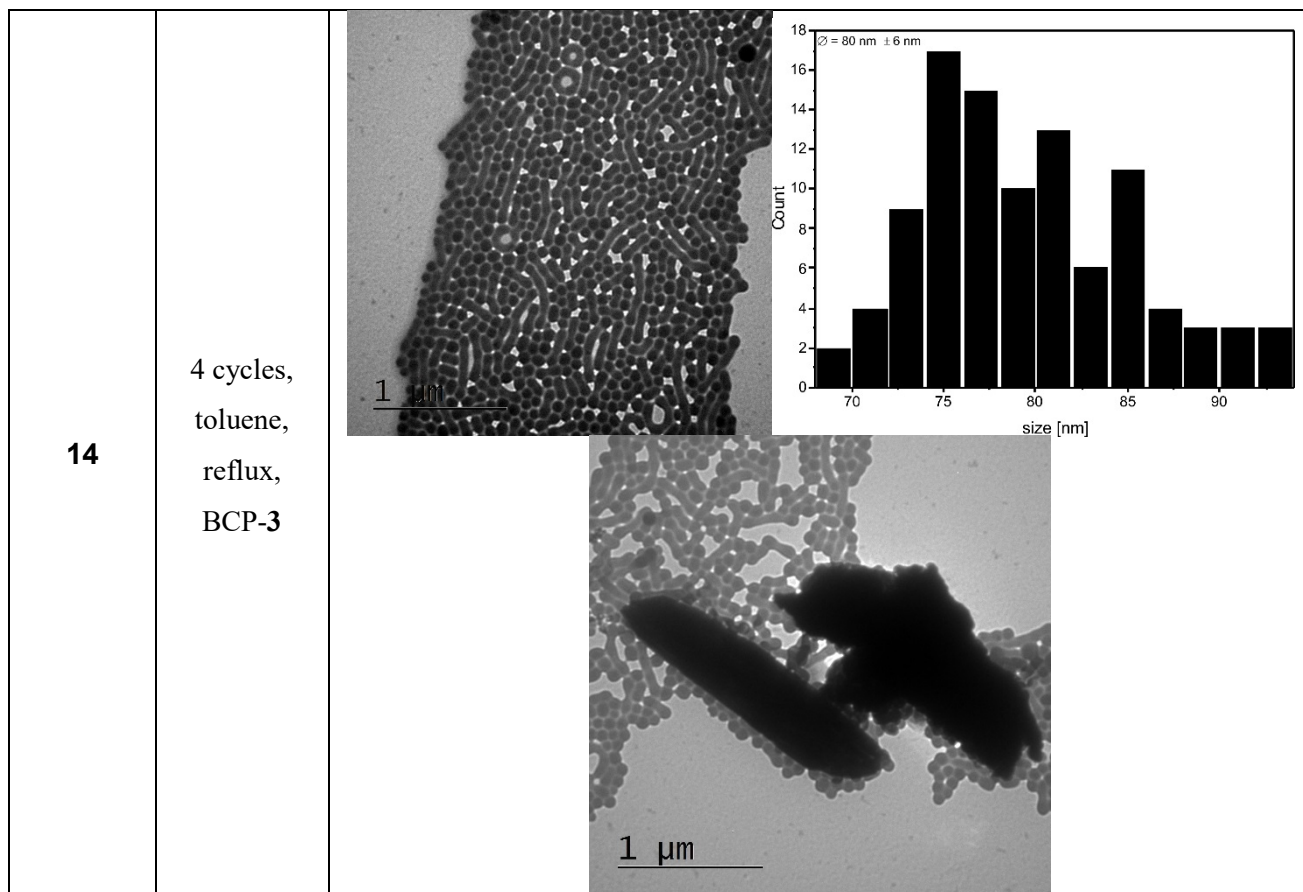
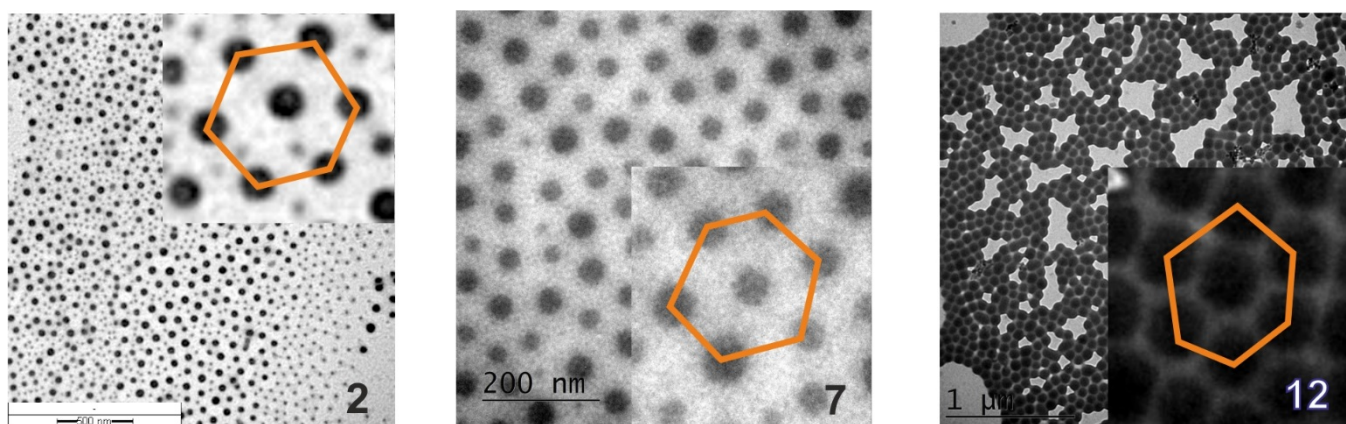


Figure S3: TEM images of **2** in BCP-1 (left), **7** in BCP-2 (middle) and **12** in BCP-3 (right) to show a 1D hexagonal particle distribution.



7. Synthesis of different Fe(II) SCO nanoparticles with SCO over and below room temperature using BCP micelles

Figure S4: $\chi_M T$ vs. T plots of the samples 7 (top left), 8 (top right), 9 (bottom left) and 10 (bottom right) in BCP-2.

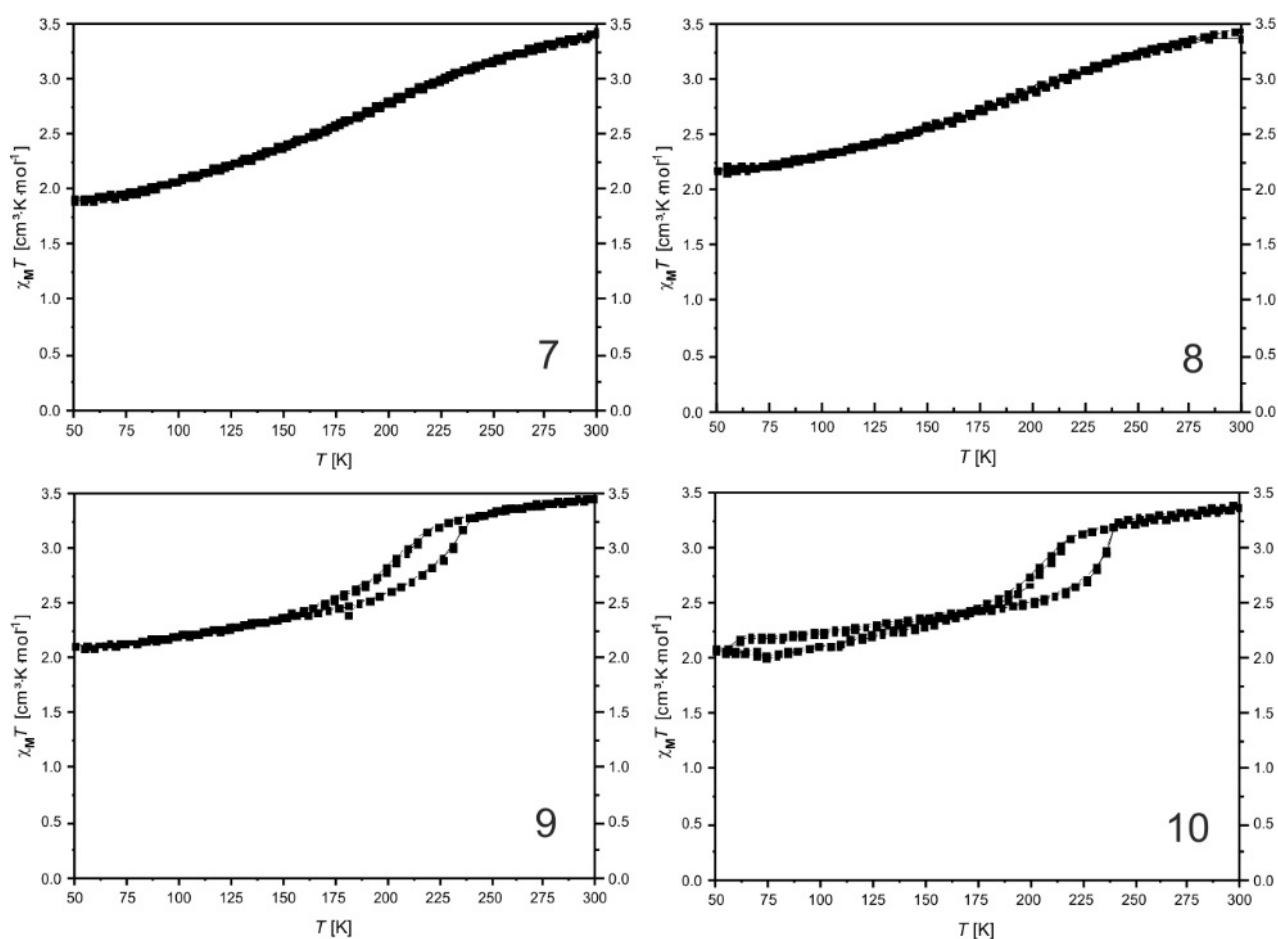
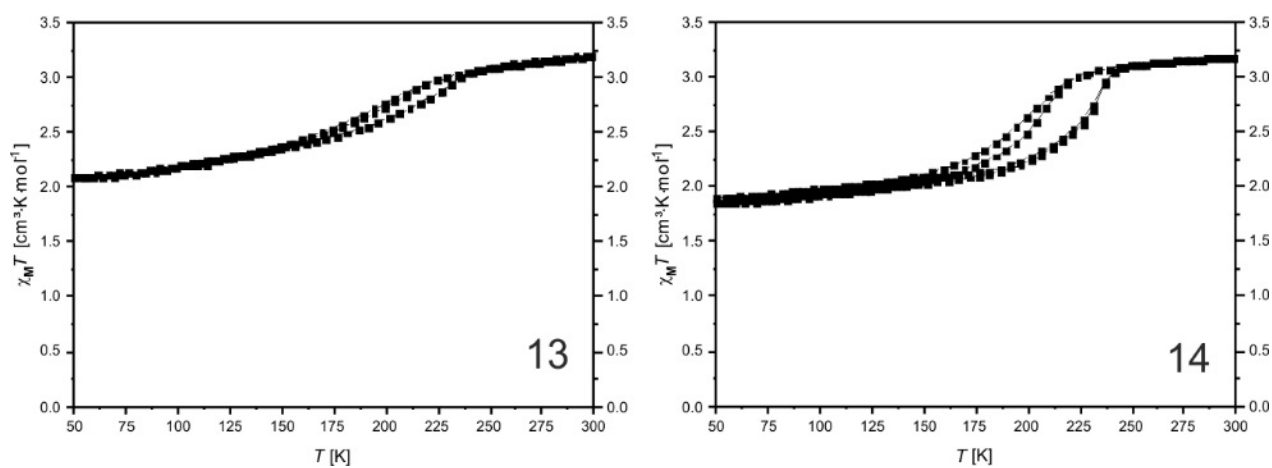


Figure S5: $\chi_M T$ vs. T plots of the samples 13 (left) and 14 (right) in BCP-3.



7. Synthesis of different Fe(II) SCO nanoparticles with SCO over and below room temperature using BCP micelles

Ottokar Klimm¹, Christoph Göbel¹, Florian Puchtler², Sabine Rosenfeldt³, Stephan Förster³ and Birgit Weber^{*1}

Address: ¹Inorganic Chemistry VI, University of Bayreuth, Universitätsstr. 30, 95440 Bayreuth, Germany ²Inorganic Chemistry I, University of Bayreuth, Universitätsstr. 30, 95440 Bayreuth, Germany and ³Physical Chemistry I and Bavarian Polymer Institute, University of Bayreuth, Universitätsstr. 30, 95440 Bayreuth, Germany

Email: weber@uni-bayreuth.de, <http://www.ac4.uni-bayreuth.de>

* Corresponding author

To be submitted

Abstract

This work deals with the synthesis of nanoparticles of the Fe(II) spin crossover coordination polymer $[\text{Fe}(\text{Lc})(\text{bipy})]_n$ (with $\text{Lc} = (E,E)\text{-}\{\text{dimethyl-2,2'}\text{-}[1,2\text{-phenylenebis(imino-methyldyne)]bis(3-oxobutanato)(2-)-N,N',O^3,O^3'}\}$ and $\text{bipy} = 4,4'\text{-bipyridine}$) using polystyrene-*b*-poly(4-vinylpyridine) (PS-*b*-P4VP) block copolymer micelles as nanoreactors. Due to two different polymorphs, $[\text{Fe}(\text{Lc})(\text{bipy})]_n$ can lead to different SCO types with different magnetic properties. Slow diffusion without reflux leads to a SCO with a 6 K wide hysteresis above RT and fast diffusion with reflux leads to a gradual SCO below RT. A precised tuning of the SCO properties and the visual identity of the nanoparticles was possible through different reaction cycles (RC) and the variety of different block copolymers (ratio P4VP:PS and molecular mass).

Introduction

Spin crossover compounds are a class of complexes from great interest due to the possibility to be switched or triggered by an external stimuli as temperature, pressure or light.^[1] Nanocomposites of functional materials as SCO complexes are necessary for applications as sensors^[2-4], switches or data storage (electronic), catalysts or smart contrast agents in medicine^[5-14]. SCO compounds often react very sensitive to changes in crystal structure or crystal packing, even adding or removing solvent molecules can lead to completely different behaviour. Nanoparticles of known bulk complexes often show completely new applications and the precise tune of nanomaterials is a difficult duty.^[15-18] Various methods are well-known to produce such nanocomposites (i.e. micelle techniques or other methods) by top-down or bottom-up approaches.^[19,20] The goal of this work is to synthesise size and shape controlled and monodisperse nanocomposites. In former works, we presented a new approach to synthesise nanoscaled CPs in a block copolymer (BCP) matrix of polystyrene-*b*-poly(4-vinylpyridine) (PS-*b*-P4VP). Due to self-assembly, the BCPs form nanoreactors similar to inverse micelles.^[21-23] Those techniques should be transferable to many other SCO systems to form nanosized CPs. 1D CPs of $[\text{Fe}(\text{Lb})(\text{bipy})]_n@BCP$ ^[24], $[\text{Fe}(\text{Lb})(\text{bpea})]_n@BCP$ and $[\text{Fe}(\text{Lb})(\text{bpey})]_n@BCP$ were synthesised already.^[25] The crystallinity of the nanoparticles can be controlled by sequentially adding starting material in different reaction cycles to gain a slow CP growth into the BCP matrix.^[24] By varying temperature and reaction time, the shape and distribution of the particles can also be varied. In a former work, the influence of the molecular mass and the amount of P4VP from the used BCPs was examined, to control size and shape of

7. Synthesis of different Fe(II) SCO nanoparticles with SCO over and below room temperature using BCP micelles

received nanoparticles.^[26] In this work, a Fe(II) complex with two different SCO properties was used to synthesise nanoparticles. Without reflux a slow diffusion approach leads to a SCO with a 6 K wide hysteresis above room temperature (RT) and with reflux, the synthesis leads to a gradual SCO below RT. By varying the reaction conditions both SCO species should appear. Two different BCPs were used to get nanoparticles in different sizes and shapes.

Results and Discussion

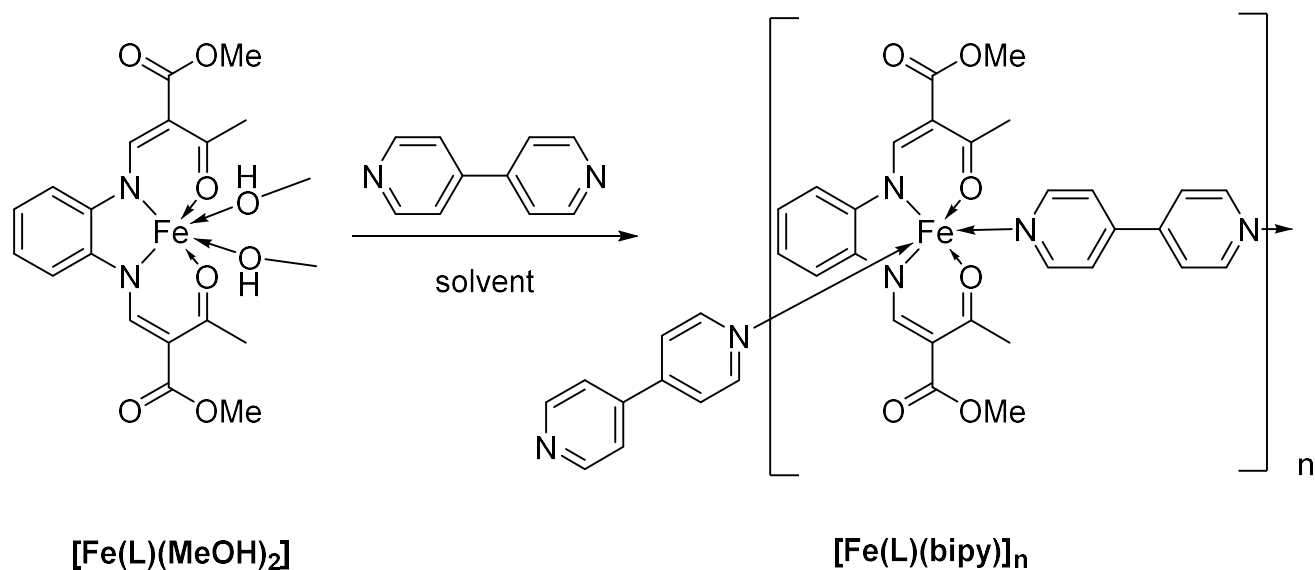
[Fe(Lc)(bipy)]_n was used in this work (Scheme 1). For the synthesis of the coordination polymer (CP) in a BCP nanoreactor two different BCPs are used. An overview of the polymers and all sample numbers is given in Table 1 and Table 2. The empty BCPs were stirred in toluene to gain self assembly. To gain fast diffusion the precursor complex [Fe(Lc)(MeOH)₂] was added and stirred for two hours under reflux. The bridging ligand 4,4'-bipyridine (**bipy**) was added and refluxed for one hours to gain a slow particle growth in the BCP composite matrix. Thus one reaction cycle (RC) was done. To obtain different crystallinities of the nanoparticles, 1-5 RC were done (Table 2). To gain slow diffusion the precursor complex [Fe(Lc)(MeOH)₂] was added to the empty BCPs and stirred for three hours without reflux. The bridging ligand 4,4'-bipyridine (**bipy**) was added and stirred for two hours to gain a slow particle growth in the BCP composite matrix. To obtain different crystallinities of the nanoparticles, 1-5 RC were done (Table 2).

Table 1: Overview of used block copolymers, molecular weights and units of PS and P4VP

Polymer	molecular weight	units P4VP	units PS	ratio P4VP : PS
BCP-1	150000	204	1234	≈ 1:6
BCP-2	250000	785	1608	≈ 1:2

The investigated CP-BCP composite material consists of a BCP micelle with an incorporated CP. The used CP was synthesised from [Fe(L)(MeOH)₂] with a bridging ligand 4,4'-bipyridine (**bipy**) showed in Scheme 1.

7. Synthesis of different Fe(II) SCO nanoparticles with SCO over and below room temperature using BCP micelles



Scheme 1: Representation of the used Fe(II) CP to gain SCO nanoparticles in BCP matrix.

For BCP-1 and BCP-2, pure spherical nanoparticles are obtained, with only a few reaction cycles. With an increasing number of RC for BCP-2 refluxed and BCP-1 and BCP-2 without reflux, a mixture of spherical nanoparticles and nanorods and vesicles appeared. Table 2 gives an overview of all sample numbers, RCs and used BCPs in this work. Based on the differences in contrast, the Fe(II) complexes in the P4VP part form the core while the PS part gives the shell. From BCP-1 to BCP-2 the particles move together much closer and a loss of the characteristic core-shell behaviour is observed (Figure 1).

7. Synthesis of different Fe(II) SCO nanoparticles with SCO over and below room temperature using BCP micelles

Table 2: Overview of sample numbers, RCs and used BCPs.

sample	BCP	RC	solvent
1	1	2	toluene
2	1	3	toluene
3	1	4	toluene
4	1	5	toluene
5	1	2	toluene
6	1	3	toluene
7	1	4	toluene
8	1	5	toluene
9	2	2	toluene
10	2	3	toluene
11	2	4	toluene
12	2	5	toluene
13	2	2	toluene
14	2	3	toluene

7. Synthesis of different Fe(II) SCO nanoparticles with SCO over and below room temperature using BCP micelles

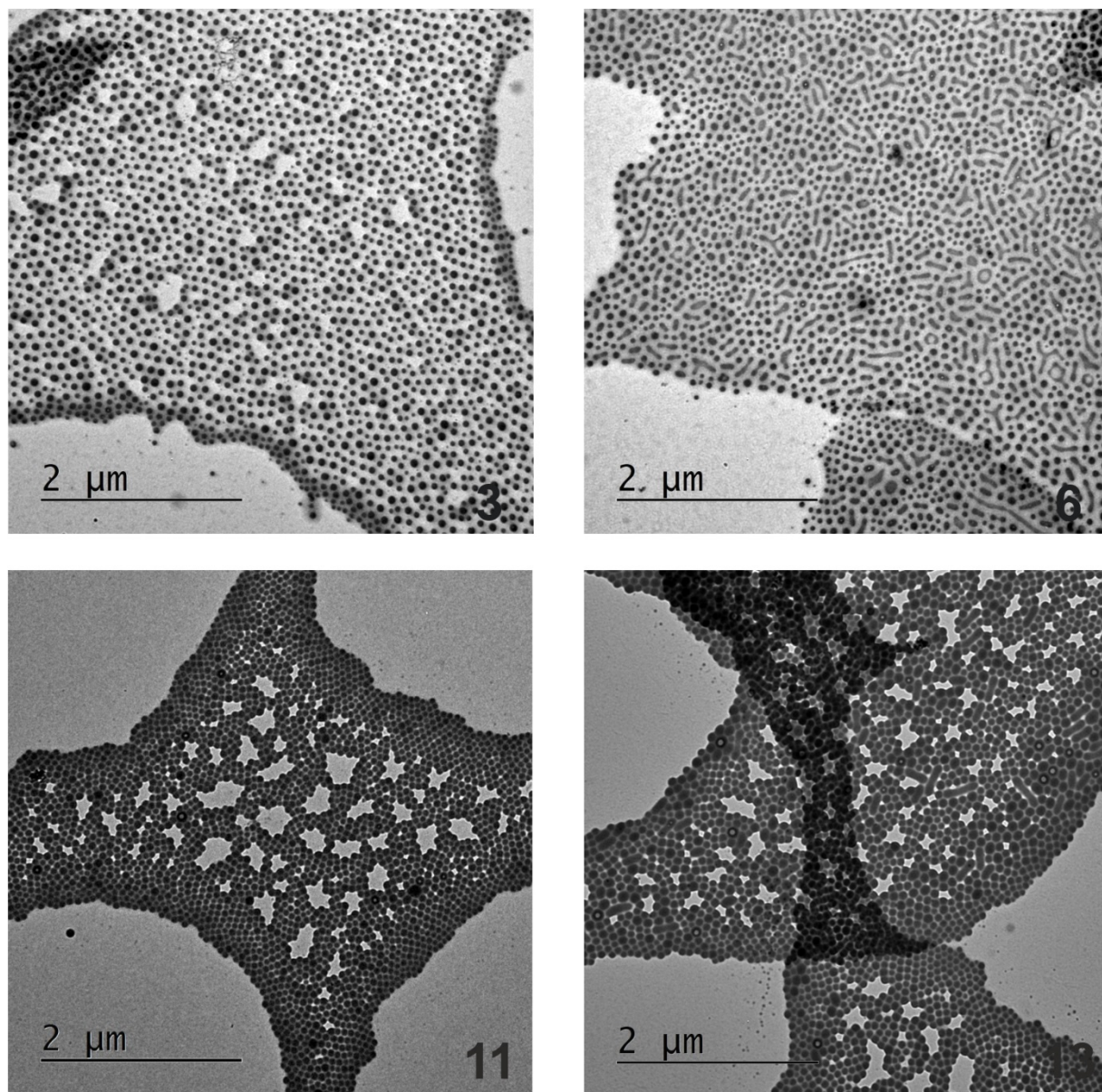


Figure 1: TEM images to show the particle shape with different reaction conditions. Fe(II) SCO nanoparticles in BCP-1 with reflux after four RC (top left), in BCP-1 without reflux after three RC (top right), in BCP-2 with reflux after four RC (bottom left) and in BCP-2 without reflux after two RC (bottom right).

Apparently the complex $[\text{Fe}(\text{Lc})(\text{bipy})]_n$ precipitates faster than $[\text{Fe}(\text{Lb})(\text{bipy})]_n$. Products synthesised in BCP-1 with a lower molecular mass of $150000 \text{ g}\cdot\text{mol}^{-1}$ lead to sub-micro crystals at five RC (4). Products synthesised in BCP-1 without reflux lead to sub-micro crystals at five RC (7). A change toward BCP-2 showed no sub-micro crystals for five RC with reflux and sub-micro crystals at three RC (14) without reflux. BCP-2 shows the most contrast and the largest particles

7. Synthesis of different Fe(II) SCO nanoparticles with SCO over and below room temperature using BCP micelles

(Figure 2). Also, there is a hexagonal 1D packing effect for the nanoparticles showed in the SI (Figure S4).

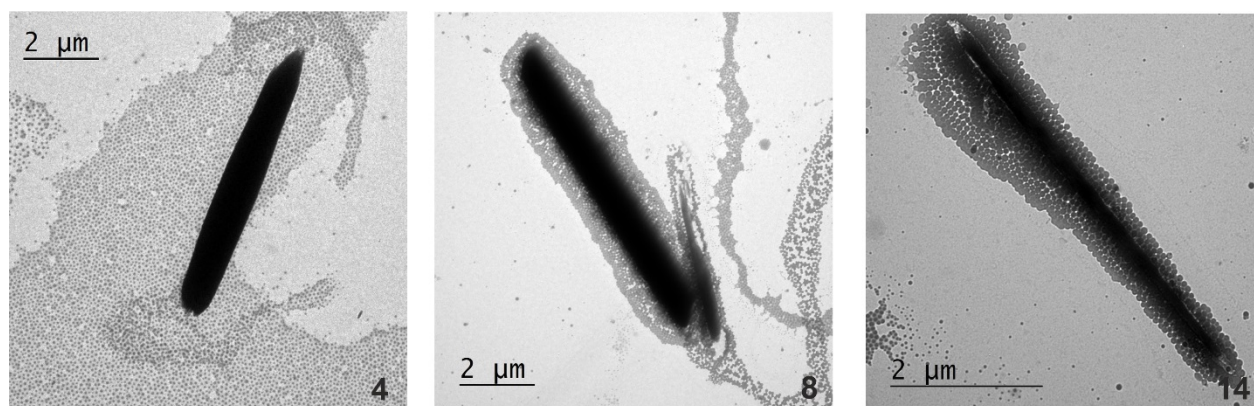


Figure 2: TEM images of Fe(II) SCO sub-micro crystals in BCP-1 with reflux after five RC (left), in BCP-1 without reflux after four RC (middle) and BCP-2 without reflux after 3 RC (right).

In Table 3, an overview is given about the particle sizes and the growth of sub-micro crystals by TEM images and DLS measurements. For samples with sub-micro crystals, the particle sizes are not listed in Table 3. There is a slight increase in the hydrodynamic radius upon loading the BCP micelle with the CP. For the loaded CP–BCP micelles the same core and total diameter were obtained in the range of the error. This indicates that the BCP micelle is an ideal template for the synthesis of spherical particles. BCP-1 leads to sub-micro crystals at five RCs with reflux and four RCs without reflux. BCP-2 leads to no sub-micro crystals with reflux and sub-micro crystals at three RCs without reflux.

7. Synthesis of different Fe(II) SCO nanoparticles with SCO over and below room temperature using BCP micelles

Table 3: Overview of particle sizes of empty BCPs and synthesised nanoparticles at two, three and five reaction cycles in BCP-1 and BCP-2 with and without reflux measured by TEM and DLS.

BCP	sample	RC	DLS [nm]	TEM [nm]
1	BCP-1	0	126±22	70±8
1	1	2	168±13	59±9
1	2	3	--	64±7
1	4	5	sub-micro crystals	sub-micro crystals
1	5	2	193±12	42±9
1	6	3	--	52±13
1	8	5	sub-micro crystals	sub-micro crystals
2	BCP-2	0	147±19	52±4
2	9	2	127±13	75±7
2	10	3	--	74±6
2	12	5	no pure spherical particles	75±6
2	13	2	135±12	76±9
2	14	3	sub-micro crystals	sub-micro crystals

Control of the crystallite size of the coordination polymer

An amount of P4VP between 25% and 30% leads to first formations of rods and vesicle-like structures next to the characteristic spherical nanoparticles. Also, the synthesis without refluxing leads to a mixture of typical spherical nanoparticles and nanorods and vesicles as well BCP-1 as BCP-2. A change from BCP-1 to BCP-2 leads to a loss in the characteristic core-shell behaviour. TEM imaging was used to determine the diameter of the nanoparticles in the dried state. Samples

7. Synthesis of different Fe(II) SCO nanoparticles with SCO over and below room temperature using BCP micelles

with BCP-1 led to sub-micro crystals at five RCs with reflux and four RCs without reflux. For BCP-2 no sub-micro crystals appeared with reflux. Without refluxing, sub-micro crystals occurred after three RCs (**14**). Powder XRD was measured from $[\text{Fe}(\text{Lc})(\text{bipy})]_n$ in BCP-1 and -2. Two, three and five RCs were shown to illustrate the growth in crystallinity of the gained nanoparticles (Figure 3).

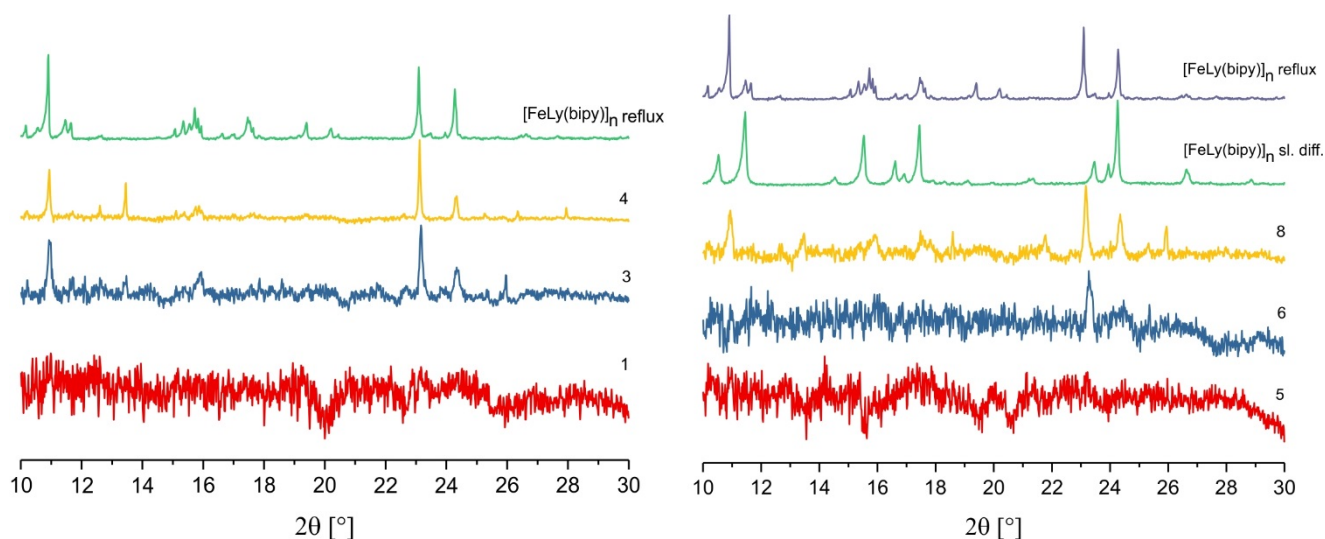


Figure 3: PXRD measurements of $[\text{Fe}(\text{Lc})(\text{bipy})]_n@BCP-1$ with fast diffusion with reflux (left) and with slow diffusion without reflux (right). Two, three and five RCs are shown to illustrate the increase of crystallinity up to sub-micro crystals for five RCs (**4**, **8**).

PXRD measurements of **14** show a 2θ peak at about 26° , which is characteristic for the μ -oxido complex (Figure S5). Thus the sub-micro crystals shown with TEM imaging can be the partial oxidised product of $[\text{Fe}(\text{Lc})(\text{bipy})]_n$.

Magnetism

The change of crystallinity of the CP core and therefore of n in $[\text{Fe}(\text{Lc})(\text{bipy})]_n$ in the BCP micelle should significantly influence the SCO properties of the composite material. Also, samples with sub-micro crystals should show significant influence on the SCO properties. Due to the differences in coordination environment of the outside $[\text{Fe}(\text{Lc})]$ units of the $[\text{Fe}(\text{Lc})(\text{bipy})]_n$ coordination polymer, only the inside $[\text{Fe}(\text{Lc})]$ units are expected to undergo spin crossover (SCO). Magnetic measurements of the samples **1–4** and **10–12** were done in the temperature range between 300 K and 50 K in the cooling and heating mode. Samples **6–8** were measured in the temperature range

7. Synthesis of different Fe(II) SCO nanoparticles with SCO over and below room temperature using BCP micelles

between 350 K and 100 K in the cooling and heating mode. The results are given as $\chi_M T$ versus T plots in Figure 2 and Figure S6 and S7 in the SI where χ_M is the molar susceptibility and T the temperature. To show a characteristic tendency for the change of SCO properties with different RC, 3 and 5 cycles are shown for each CP-BCP. Samples **2** and **4** belong to BCP-1 with reflux. Sample **2** shows a room temperature $\chi_M T$ about $3.1 \text{ cm}^3 \text{Kmol}^{-1}$ which is in the expected value of about $3.1 \text{ cm}^3 \text{Kmol}^{-1}$ for Fe(II) HS. The $\chi_M T$ at 50K is about $1.2 \text{ cm}^3 \text{Kmol}^{-1}$ which is due to an incomplete gradual SCO between 260 K and 90 K. Room temperature $\chi_M T$ of **4** is about $3.2 \text{ cm}^3 \text{Kmol}^{-1}$, which is expected for Fe(II) HS. From **2** to **4** an significant increase of SCO active [Fe(Lc)] units is observed indicating the increase of n in $[\text{Fe}(\text{Lc})(\text{bipy})]_n$ and a small hysteresis of about 8 K is observed between 200 K and 208 K (Figure 3). This hysteresis is due to the formation of sub-micro crystals outside the BCP matrix as showed in Figure 2 and also in the SI by PXRD measurements.

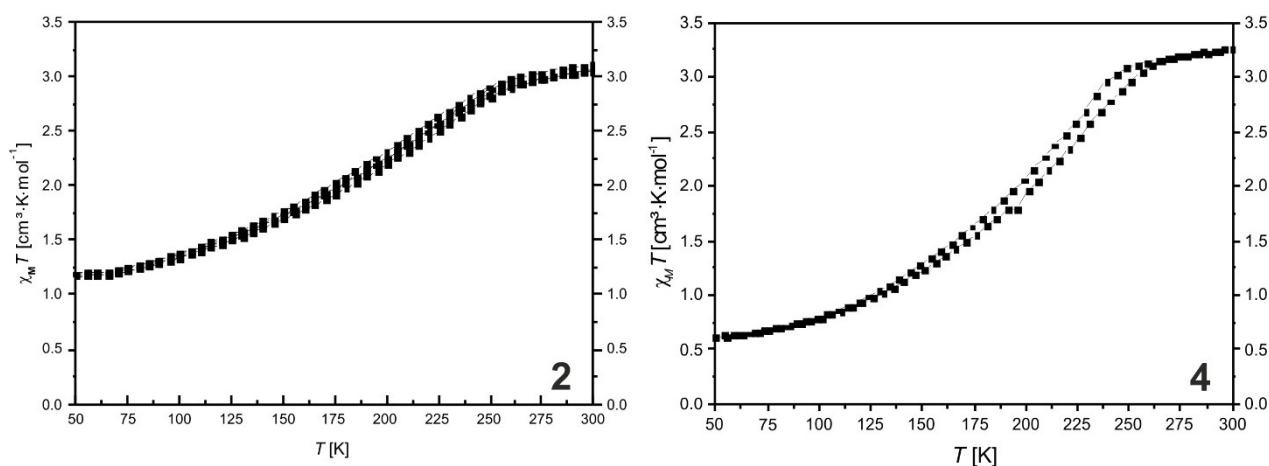


Figure 4: SQUID measurements of $[\text{Fe}(\text{Lc})(\text{bipy})]_n@BCP-1$ with reflux after three RCs (left) **2** and five RCs (right) **4**.

Samples **6** and **8** belong to BCP-1 without reflux. Due to different crystal packing the CP of $[\text{Fe}(\text{Lc})(\text{bipy})]_n$ the synthesis without reflux leads to different SCO behaviours. A SCO with hysteresis above RT appears. Sample **6** shows a HS $\chi_M T$ at 350 K of about $3.2 \text{ cm}^3 \text{Kmol}^{-1}$ which is in the expected value of $3.0 \text{ cm}^3 \text{Kmol}^{-1}$ for Fe(II) HS. The $\chi_M T$ at 100 K is about $1.0 \text{ cm}^3 \text{Kmol}^{-1}$. An incomplete SCO with a 28 K wide hysteresis with $T_{1/2} \uparrow$ of 338 K and $T_{1/2} \downarrow$ of 310 K was observed, followed by an incomplete gradual SCO between 300 K and 100 K. Both types of SCO for $[\text{Fe}(\text{Lc})(\text{bipy})]_n$ are observed, due to two different crystal packings. HS $\chi_M T$ of **8** at 350 K is about $3.4 \text{ cm}^3 \text{Kmol}^{-1}$, which is expected for Fe(II) HS. An incomplete SCO with a 35 K wide

7. Synthesis of different Fe(II) SCO nanoparticles with SCO over and below room temperature using BCP micelles

hysteresis with $T_{1/2}$ values of 338 K in the cooling mode and 303 K in the heating mode was observed, followed by an incomplete gradual SCO between 300 K and 100 K. For **8** sub-micro crystals are observed shown in Figure 2 with TEM images and Figure-3 by PXRD measurements. Compared to the bulk material (8 K hysteresis), the hysteresis of **6** and **8** is much larger, but incomplete. The bulk material showed either SCO above or below RT. Sample **6** as well sample **8** show a mixture of both SCO species.

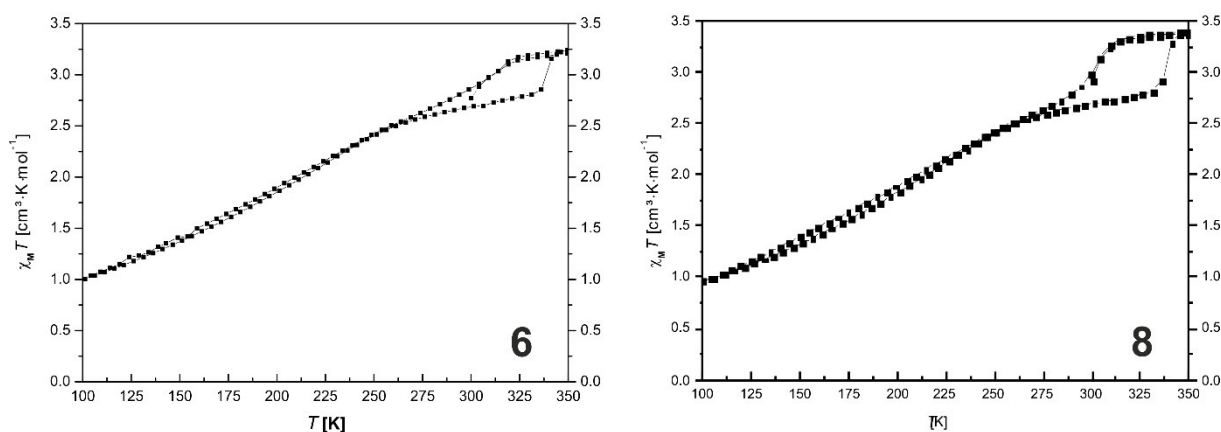


Figure 5: SQUID measurements of $[\text{Fe}(\text{Lc})(\text{bipy})]_n@BCP-1$ without reflux for three RC (left) **6** and five RC (right) **8**.

Samples **10** and **12** belong to BCP-2 with reflux. **10** shows a room temperature $\chi_M T$ of about $3.3 \text{ cm}^3 \text{Kmol}^{-1}$ which is in the range of Fe(II) HS. The $\chi_M T$ at 50 K is about $2.3 \text{ cm}^3 \text{Kmol}^{-1}$ after an incomplete gradual SCO between 270 K and 80 K. Room temperature $\chi_M T$ of **12** is about $3.3 \text{ cm}^3 \text{Kmol}^{-1}$ which is expected for Fe(II) HS. A SCO with a 9 K wide hysteresis with $T_{1/2}$ values of 198 K in the cooling and 189 K in the heating mode is observed. The magnetic properties of **12** are close to the bulk material with a gradual SCO between 270 K and 110 K with a small incomplete hysteresis between 250 K and 235 K. Samples **10** and **12** do not show sub-micro crystal. The increasing SCO properties are due to the formation of higher crystalline nanoparticles. A change in shape towards a mixture of spherical nanoparticles, nanorods and vesicles also leads to better SCO behaviour, because of the alignment and self-assembly of larger particles in the range of more than 100 nm.

7. Synthesis of different Fe(II) SCO nanoparticles with SCO over and below room temperature using BCP micelles

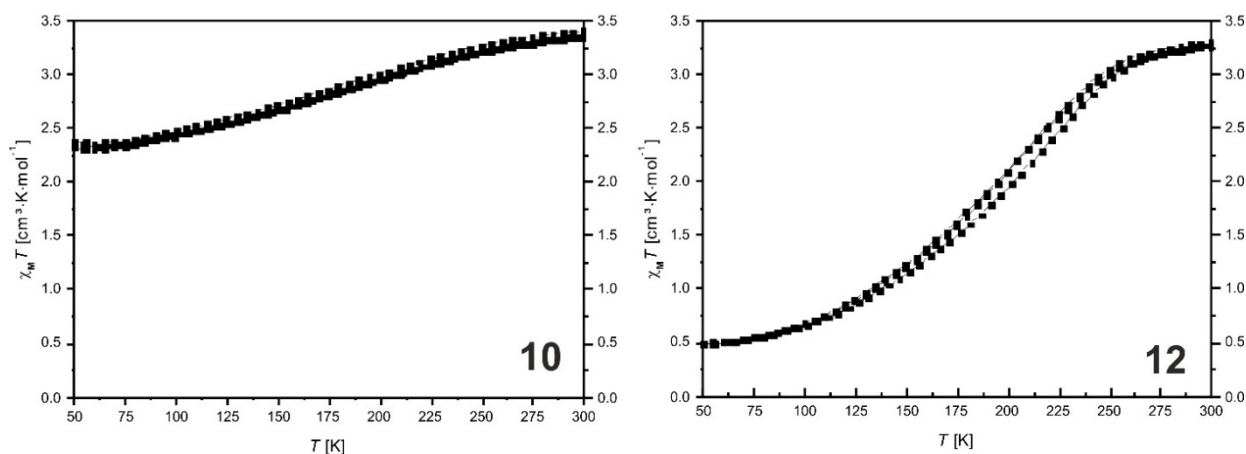


Figure 6: SQUID measurements of $[\text{Fe}(\text{Lc})(\text{bipy})]_n@BCP-2$ with reflux for three RC (left) **10** and five RC (right) **12**.

Conclusion

In this work, we showed the possibility to synthesise CP@BCP with different SCO properties. The synthesis with and without reflux led to SCO above and below RT. By using different BCPs with various molecular masses and amounts of P4VP it was possible to control shape and size of the observed nanoparticles. Thus the first step towards SCO devices is done. A functional SCO material with a SCO in the range of RT was produced. The critical concentrations for the appearance of sub-micro crystals was given in this work too. The BCP micelles synthesised without reflux lead to nanorods or vesicles similar the synthesis with reflux in BCP-2 led to nanorods and vesicles with higher amount of RC. Furthermore varying the second, non-coordinating block of the BCPs, other abilities appear i.e. P4VP-*b*-H3TP (conductivity) or P4VP-*b*-PEO (water soluble).

Experimental

Synthetic procedure

Polystyrene-*b*-Poly(4-vinylpyridine) (BCP-1, purum, MW \approx 150000, 15% P4VP) and Polystyrene-*b*-Poly(4-vinylpyridine) (BCP-2, purum, MW \approx 250000, 33% P4VP) were synthesised as described before. 4,4'-bipyridine was obtained from Alfa Aesar and used as received. Toluene (Tol) was purified as described in literature.^[24] [Fe(L)(MeOH)₂] was synthesised as described before. All syntheses were performed under inert conditions using Schlenk technique with argon (purity \geq 99,999%, 5.0). The synthesis of all samples was repeated at least twice.

1: BCP-1 (50 mg, 0.33 μ mol) and [Fe(L)(MeOH)₂] (6.4 mg, 15 μ mol) were added to a 50 ml flask. Subsequently toluene (20 ml) was added and the mixture was heated to reflux for 2h. After cooling to room temperature, 4,4'-bipyridine (5.6 mg, 36 μ mol) was added to the brown solution and the reaction mixture was heated for 1h to reflux. Before solvent removal, [Fe(L)(MeOH)₂] (6.4 mg, 15 μ mol) and 4,4'-bipyridine (5.6 mg, 36 μ mol) were added in a second cycle and the mixture was heated for one further hour to reflux. After cooling to room temperature the solvent was removed via cold distillation to yield a brown, polymer-like powder. Elemental anal. (%) found: C 59.85, H 7.20, N 3.02

2: The synthesis as described for sample **1** was repeated. Before solvent removal, [Fe(L)(MeOH)₂] (6.4 mg, 15 μ mol) and 4,4'-bipyridine (5.6 mg, 36 μ mol) were added in a third cycle and the mixture was heated for one further hour to reflux. After cooling to room temperature the solvent was removed via cold distillation to yield a brown, polymer-like powder. Elemental anal. (%) found: C 62.31, H 6.84, N 4.48.

3: The synthesis described for sample **2** was repeated, with one further cycle of addition of [Fe(L)(MeOH)₂] (6.4 mg, 15 μ mol) and 4,4'-bipyridine (5.6 mg, 36 μ mol) followed by further heating to reflux for 1h. After cooling to room temperature the solvent was removed via cold distillation to yield a brown, polymer-like powder. Elemental anal. (%) found: C 58.53, H 7.01, N 4.09.

4: The synthesis described for sample **3** was repeated, with one further cycle of addition of [Fe(L)(MeOH)₂] (6.4 mg, 15 μ mol) and 4,4'-bipyridine (5.6 mg, 36 μ mol) followed by further heating to reflux for 1h. After cooling to room temperature the solvent was removed via cold

7. Synthesis of different Fe(II) SCO nanoparticles with SCO over and below room temperature using BCP micelles

distillation to yield a brown, polymer-like powder. Elemental anal. (%) found: C 60.00, H 6.67, N 5.24.

The color turned increasingly darker from sample **1** to **4** with an increasing amount of iron.

5: BCP-1 (50 mg, 0.2 μmol) and $[\text{Fe}(\text{L})(\text{MeOH})_2]$ (6.4 mg, 15 μmol) were added to a 50 ml flask. Subsequently toluene (20 ml) was added and the mixture was stirred at room temperature (RT) for 3h. Afterwards, 4,4'-bipyridine (5.6 mg, 36 μmol) was added to the brown solution and the reaction mixture stirred at RT for 2h. Before solvent removal, $[\text{Fe}(\text{L})(\text{MeOH})_2]$ (6.4 mg, 15 μmol) and 4,4'-bipyridine (5.6 mg, 36 μmol) were added in a second cycle and the mixture was stirred at RT for two further hours. Afterwards the solvent was removed via cold distillation to yield a brown, polymer-like powder. Elemental anal. (%) found: C 78.78, H 6.77, N 4.57.

6: The synthesis as described for sample **5** was repeated. Before solvent removal, $[\text{Fe}(\text{L})(\text{MeOH})_2]$ (6.4 mg, 15 μmol) and 4,4'-bipyridine (5.6 mg, 36 μmol) were added in a third cycle and the mixture was stirred at RT for two further hours. Afterwards the solvent was removed via cold distillation to yield a brown, polymer-like powder. Elemental anal. (%) found: C 70.99, H 7.67, N 5.05.

7: The synthesis described for sample **6** was repeated, with one further cycle of addition of $[\text{Fe}(\text{L})(\text{MeOH})_2]$ (6.4 mg, 15 μmol) and 4,4'-bipyridine (5.6 mg, 36 μmol) followed by further stirring at RT for 2h. Afterwards the solvent was removed via cold distillation to yield a brown, polymer-like powder. Elemental anal. (%) found: C 69.40, H 6.18, N 6.00.

8: The synthesis described for sample **7** was repeated, with one further cycle of addition of $[\text{Fe}(\text{L})(\text{MeOH})_2]$ (6.4 mg, 15 μmol) and 4,4'-bipyridine (5.6 mg, 36 μmol) followed by further stirring at RT for 2h. Afterwards the solvent was removed via cold distillation to yield a brown, polymer-like powder. Elemental anal. (%) found: C 72.63, H 5.69, N 6.87.

The color turned increasingly darker from sample **5** to **8** with an increasing amount of iron.

9: BCP-2 (50 mg, 0.2 μmol) and $[\text{Fe}(\text{L})(\text{MeOH})_2]$ (6.4 mg, 15 μmol) were added to a 50 ml flask. Subsequently toluene (20 ml) was added and the mixture was heated to reflux for 2h. After cooling to room temperature, 4,4'-bipyridine (5.6 mg, 36 μmol) was added to the brown solution and the reaction mixture was heated for 1h to reflux. Before solvent removal, $[\text{Fe}(\text{L})(\text{MeOH})_2]$ (6.4 mg, 15 μmol) and 4,4'-bipyridine (5.6 mg, 36 μmol) were added in a second cycle and the mixture was

7. Synthesis of different Fe(II) SCO nanoparticles with SCO over and below room temperature using BCP micelles

heated for one further hour to reflux. After cooling to room temperature the solvent was removed via cold distillation to yield a brown, polymer-like powder. Elemental anal. (%) found: C 69.40, H 7.49, N 2.38.

10: The synthesis as described for sample **9** was repeated. Before solvent removal, $[\text{Fe}(\text{L})(\text{MeOH})_2]$ (6.4 mg, 15 μmol) and 4,4'-bipyridine (5.6 mg, 36 μmol) were added in a third cycle and the mixture was heated for one further hour to reflux. After cooling to room temperature the solvent was removed via cold distillation to yield a brown, polymer-like powder. Elemental anal. (%) found: C 65.55, H 7.05, N 4.70.

11: The synthesis described for sample **10** was repeated, with one further cycle of addition of $[\text{Fe}(\text{L})(\text{MeOH})_2]$ (6.4 mg, 15 μmol) and 4,4'-bipyridine (5.6 mg, 36 μmol) followed by further heating to reflux for 1h. After cooling to room temperature the solvent was removed via cold distillation to yield a brown, polymer-like powder.

12: The synthesis described for sample **11** was repeated, with one further cycle of addition of $[\text{Fe}(\text{L})(\text{MeOH})_2]$ (6.4 mg, 15 μmol) and 4,4'-bipyridine (5.6 mg, 36 μmol) followed by further heating to reflux for 1h. After cooling to room temperature the solvent was removed via cold distillation to yield a brown, polymer-like powder.

The color turned increasingly darker from sample **9** to **12** with an increasing amount of iron.

13: BCP-1 (50 mg, 0.2 μmol) and $[\text{Fe}(\text{L})(\text{MeOH})_2]$ (6.4 mg, 15 μmol) were added to a 50 ml flask. Subsequently toluene (20 ml) was added and the mixture was stirred at room temperature (RT) for 3h. Afterwards, 4,4'-bipyridine (5.6 mg, 36 μmol) was added to the brown solution and the reaction mixture stirred at RT for 2h. Before solvent removal, $[\text{Fe}(\text{L})(\text{MeOH})_2]$ (6.4 mg, 15 μmol) and 4,4'-bipyridine (5.6 mg, 36 μmol) were added in a second cycle and the mixture was stirred at RT for two further hours. Afterwards the solvent was removed via cold distillation to yield a brown, polymer-like powder. Elemental anal. (%) found: C 70.66, H 6.94, N 3.76.

14: The synthesis as described for sample **5** was repeated. Before solvent removal, $[\text{Fe}(\text{L})(\text{MeOH})_2]$ (6.4 mg, 15 μmol) and 4,4'-bipyridine (5.6 mg, 36 μmol) were added in a third cycle and the mixture was stirred at RT for two further hours. Afterwards the solvent was removed via cold distillation to yield a brown, polymer-like powder. Elemental anal. (%) found: C 71.14, H 6.70, N 5.82.

7. Synthesis of different Fe(II) SCO nanoparticles with SCO over and below room temperature using BCP micelles

The color turned increasingly darker from sample **13** to **14** with an increasing amount of iron.

Methods

Transmission electron microscopy: Transmission electron microscopy was performed with a Zeiss CEM902 electron microscope (Zeiss, Oberkochen, Germany). Samples were dispersed in toluene applying vortex several times. The dispersion was dropped on a carbon coated copper grid (Science Services, Munich). The acceleration voltage was set to 80 kV. Micrographs were taken with a MegaView III / iTEM image acquiring and processing system from Olympus Soft Imaging Systems (OSIS, Muenster, Germany) and an Orius 830 SC200W / DigitalMicrograph system from Gatan (Munich, Germany). Particles size measurements were done with “ImageJ” image processing software by Wayne Rasband (National Institutes of Health, USA).

Elemental Analysis: Carbon, nitrogen and hydrogen contents were collected at a Vario EL III. Samples were placed in tin boats. All samples were measured at least twice and the average of both measurements was used.

Magnetic measurements: Magnetic susceptibility measurements were performed at a Quantum Design MPMS-XL-5 SQUID magnetometer in the temperature range between 50 and 300 K. The samples were prepared in gelatin capsules placed in a plastic straw. All samples were measured with a magnetic field of 3T in the settle mode with a cooling and heating rate of 5K min⁻¹ between each measurement point. The measured values were corrected for the diamagnetism of the sample holder, the polymer matrix (measured values) and the ligand (tabulated Pascal constants).

X-Ray Powder Diffraction: X-Ray Powder Diffraction data for samples 1 to 14 and the bulk [Fe(Lc)(bipy)]_n were collected at a STOE StadiP X-ray powder diffractometer in transmission geometry between 5 and 45° 2 θ . Samples were placed in a flat carrier and Cu-K α 1 radiation was used for the measurement. Radiation was detected with a Mythen 1K detector.

Mössbauer spectroscopy: ⁵⁷Fe Mössbauer spectra were recorded in transmission geometry on a constant-acceleration using a conventional Mössbauer spectrometer with a 50 mCi ⁵⁷Co(Rh) source. The samples were sealed in the sample holder in an argon atmosphere. The spectra were fitted using Recoil 1.05 Mössbauer Analysis Software.³⁰ The isomer shift values are given with respect to a α -Fe reference at room temperature.

Dynamic light scattering: DLS of all samples were collected from Malvern Zetasizer Nano ZS. Samples were measured in solution in glass cuvettes from Carl Roth GmbH + Co. KG.

References

- [1] a) M. A. Halcrow, ed., *Spin-Crossover Materials*, John Wiley & Sons Ltd, Chichester, 2013; b) O. Roubeau, *Chem. Eur. J.*, **2012**, *18*, 15230–15244; c) J. Tao, R.-J. Wei, R.-B. Huang and L.-S. Zheng, *Chem. Soc. Rev.*, **2012**, *41*, 703–737; d) A. Bousseksou, G. Molnar, L. Salmon and W. Nicolazzi, *Chem. Soc. Rev.*, **2011**, *40*, 3313–3335; e) M. C. Muñoz and J. A. Real, *Coord. Chem. Rev.*, **2011**, *255*, 2068–2093; f) J. Olguín and S. Brooker, *Coord. Chem. Rev.*, **2011**, *255*, 203–240; g) Y. Bodenthin, G. Schwarz, Z. Tomkowicz, M. Lommel, T. Geue, W. Haase, H. Möhwald, U. Pietsch and D. G. Kurth, *Coord. Chem. Rev.*, **2009**, *253*, 2414–2422.
- [2] Coronado, E.; Mínguez Espallargas, G. *Chem. Soc. Rev.* **2013**, *42* (4), 1525.
- [3] Ohba, M.; Yoneda, K.; Agustí, G.; Muñoz, M. C.; Gaspar, A. B.; Real, J. A.; Yamasaki, M.; Ando, H.; Nakao, Y.; Sakaki, S.; Kitagawa, S. *Angew. Chem. Int. Ed.* **2009**, *48* (26), 4767–4771.
- [4] Linares, J.; Codjovi, E.; Garcia, Y. *Sensors* **2012**, *12* (4), 4479–4492.
- [5] Sindoro, M.; Yanai, N.; Jee, A.-Y.; Granick, S. *Acc. Chem. Res.* **2014**, *47* (2), 459–469.
- [6] Coronado, E.; Giménez-Marqués, M.; Mínguez Espallargas, G.; Rey, F.; Vitorica-Yrezábal, I. *J. Am. Chem. Soc.* **2013**, *135* (43), 15986–15989. doi:10.1021/ja407135k
- [7] Zhao-Yang Li, O. S.; Yao, Z.-S.; Kang, S.; Kanegawa, S. Multifunctional Materials Combining Spin-Crossover with Conductivity and Magnetic Ordering. In *Spin-Crossover Materials*; Halcrow, M. A., Ed.; John Wiley & Sons Ltd: Chichester, 2013; pp 303–319.
- [8] Gaspar, A. B.; Weber, B. Spin Crossover Phenomenon in Coordination Compounds. In *Molecular Magnetic Materials*; Sieklucka, B., Pinkowicz, D., Eds.; Wiley-VCH Verlag GmbH & Co. KGaA: Weinheim, Germany, 2017; pp 231–252.
- [9] Halcrow, M. A., Ed. *Spin-Crossover Materials*; John Wiley & Sons Ltd: Chichester, **2013**.
- [10] R. N. Muller, L. Vander Elst, S. Laurent, *J. Am. Chem. Soc.* **2003**, *125* (27), 8405–8407.

7. Synthesis of different Fe(II) SCO nanoparticles with SCO over and below room temperature using BCP micelles

- [11] S. Venkataramani, U. Jana, M. Dommaschk, F. D. Sönnichsen, F. Tucek, R. Herges, *Science* **2011**, *331* (6016), 445–448.
- [12] M. Dommaschk, M. Peters, F. Gutzeit, C. Schütt, C. Näther, F. D. Sönnichsen, S. Tiwari, C. Riedel, S. Boretius, R. Herges, *J. Am. Chem. Soc.* **2015**, *137* (24), 7552–7555.
- [13] J. Hasserodt, J. L. Kolanowski, F. Touti, *Angew. Chem. Int. Ed.* **2014**, *53* (1), 60–73.
- [14] R. Nowak, E.A. Prasetyanto, L. de Cola, B. Bojer, R. Siegel, J. Senker, E. Rössler, B. Weber, *Chem. Commun.* **2017**, *53* (5), 971–974.
- [15] Larionova, J.; Salmon, L.; Guari, Y.; Tokarev, A.; Molvinger, K.; Molnár, G.; Bousseksou, A. *Angew. Chem. Int. Ed.* **2008**, *47* (43), 8236–8240.
- [16] Cobo, S.; Molnár, G.; Real, J. A.; Bousseksou, A. *Angew. Chem. Int. Ed.* **2006**, *45* (35), 5786–5789.
- [17] Molnár, G.; Cobo, S.; Real, J. A.; Carcenac, F.; Daran, E.; Vieu, C.; Bousseksou, A. *Adv. Mater* **2007**, *19* (16), 2163–2167.
- [18] Bartual-Murgui, C.; Natividad, E.; Roubeau, O. *J. Mater. Chem. C* **2015**, *3* (30), 7916–7924.
- [19] J. Eastoe, M. J. Hollamby, L. Hudson, *Adv. Colloid Interface Sci.*, **2006**, *128-130*, 5–15.
- [20] I. Boldog, A. B. Gaspar, V. Martinez, P. Pardo-Ibañez, V. Ksenofontov, A. Bhattacharjee, P. Gütlich, J. A. Real, *Angew. Chem., Int. Ed.*, **2008**, *47*, 6433–6437.
- [21] Förster, S.; Zisenis, M.; Wenz, E.; Antonietti, M. *J. Chem. Phys.* **1996**, *104* (24), 9956.
- [22] Förster, S.; Antonietti, M. *Adv. Mater.* **1998**, *10* (3), 195–217.
- [23] Fan, Z.; Chen, X.; Kohn Serrano, M.; Schmalz, H.; Rosenfeldt, S.; Förster, S.; Agarwal, S.; Greiner, A. *Angew. Chem. Int. Ed.* **2015**, *54* (48), 14539–14544.
- [24] O. Klimm, C. Göbel, S. Rosenfeldt, F. Puchtler, N. Miyajima, K. Marquardt, M. Drechsler, J. Breu, S. Förster, B. Weber, *Nanoscale* **2016**, *8* (45), 19058–19065.
- [25] C. Göbel, O. Klimm, F. Puchtler, S. Rosenfeldt, S. Förster and B. Weber, *Beilstein J. Nanotech.*, **2017**, submitted.

7. Synthesis of different Fe(II) SCO nanoparticles with SCO over and below room temperature using BCP micelles

[26] O. Klimm, C. Göbel, F. Puchtler, S. Rosenfeldt, S Förster, B. Weber, (2017), *The influence of block copolymer tuning to particle size and shape of Fe(II) SCO nanoparticles in block copolymer micelles*, to be submitted.

Supporting Information

Figure S1: Mössbauer spectra of **6** (left) and **8** (right) in BCP-1 without reflux. The red doublet corresponds to an Fe(II) HS species and the blue doublet corresponds to an Fe(II) LS species. The Mössbauer parameters are given in Table S1.

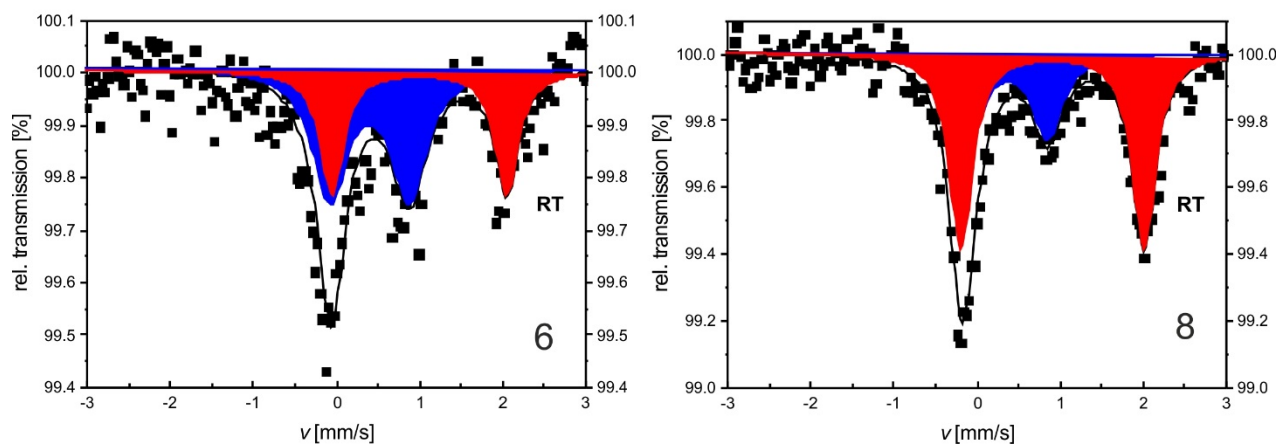


Table S1: Mössbauer parameters of the samples **6** and **8** in BCP-1.

sample	site	δ [mm/s]	ΔE_Q [mm/s]	Γ [mm/s]	Area [%]
6	Fe(II) LS	0.40(7)	0.95(13)	0.26(7)	61(12)
	Fe(II) HS	1.00(6)	2.11(12)	0.17(7)	39(12)
8	Fe(II) LS	0.38(5)	0.95(10)	0.22(6)	35(7)
	Fe(II) HS	0.91(19)	2.21(4)	0.17(7)	65(7)

7. Synthesis of different Fe(II) SCO nanoparticles with SCO over and below room temperature using BCP micelles

Figure S2: Mössbauer spectra of **14** in BCP-2 without reflux. The red doublet corresponds to and Fe(II) HS. The Mössbauer parameters are given in Table S2.

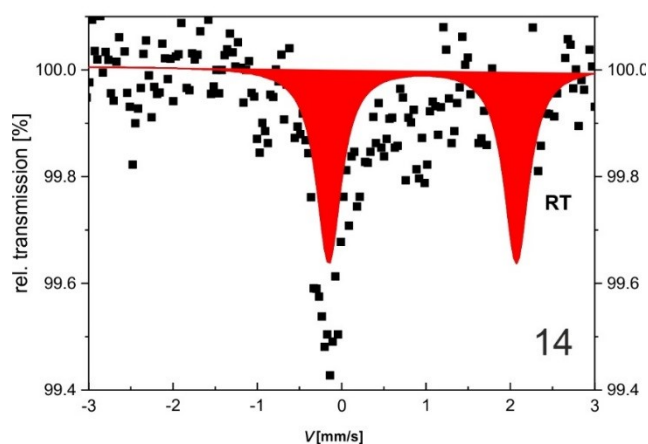
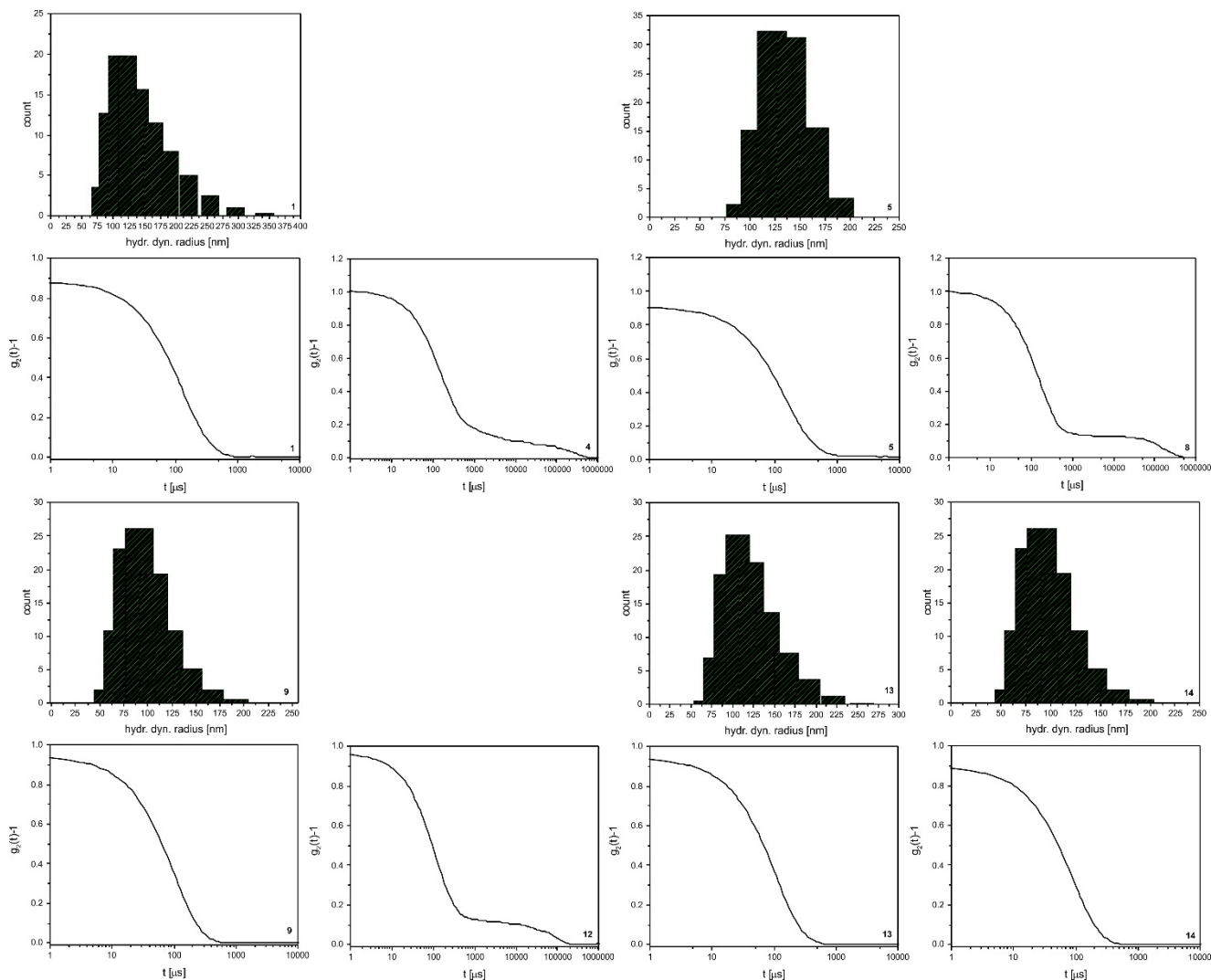


Table S2: Mössbauer parameters of sample **14** in BCP-3.

sample	site	δ [mm/s]	ΔE_Q [mm/s]	Γ [mm/s]	Area [%]
14	Fe(II) HS	0.96(3)	2.23(6)	0.18(5)	100

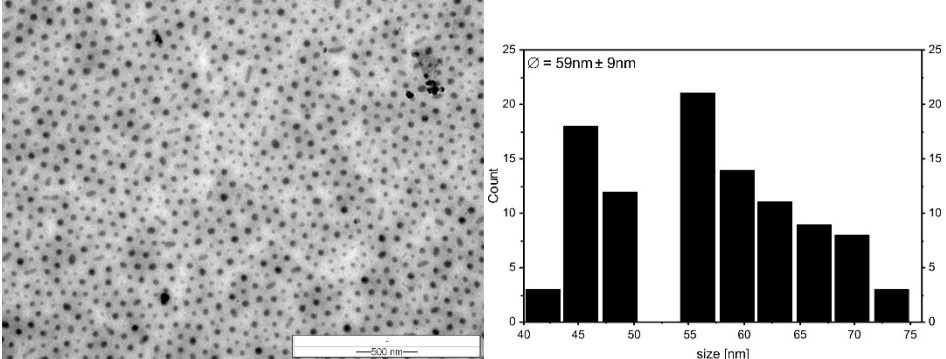
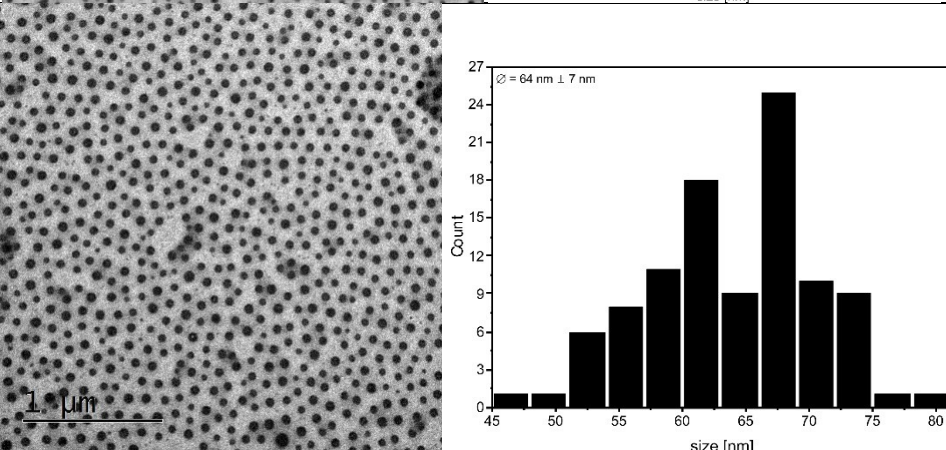
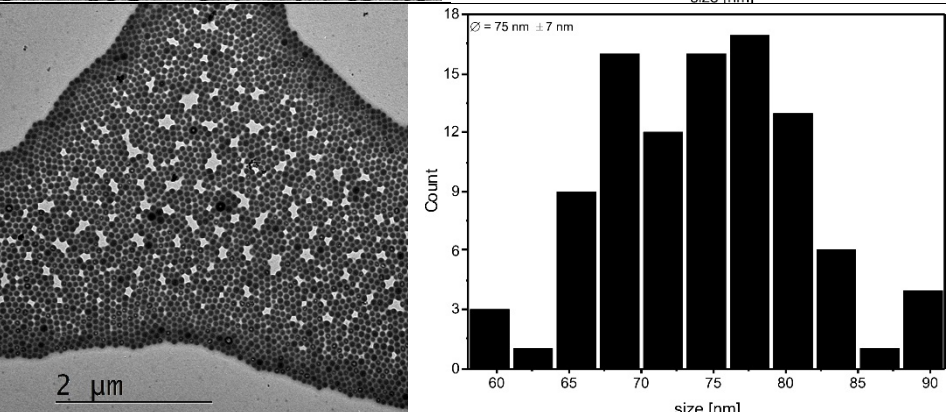
7. Synthesis of different Fe(II) SCO nanoparticles with SCO over and below room temperature using BCP micelles

Figure S3: DLS measurement of the nanocomposites in toluene, 43w%. Correlation functions of **1**, **4** (top left and left middle), **5**, **8** in BCP-1 (top right middle and right), **9**, **12** (bottom left and left middle) and **13**, **14** in BCP-2 (bottom right middle and right).

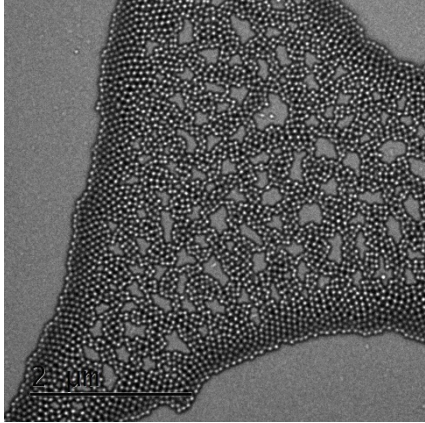
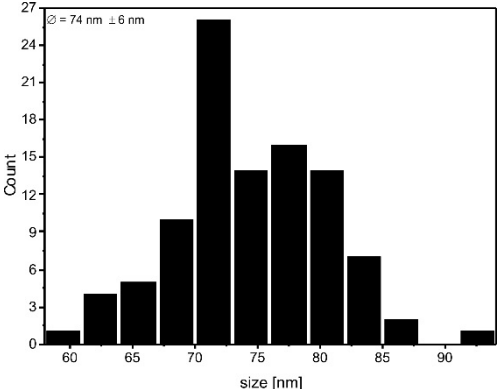
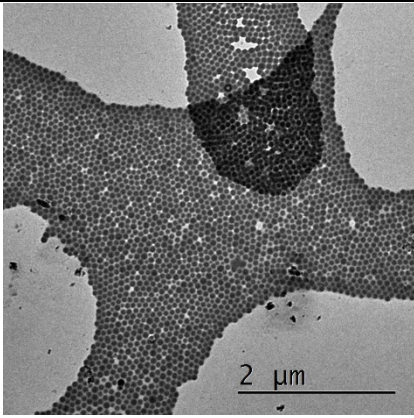
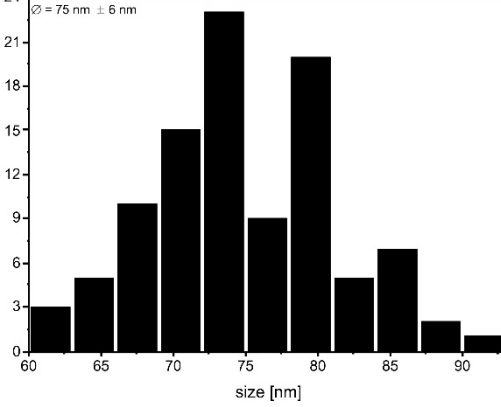


7. Synthesis of different Fe(II) SCO nanoparticles with SCO over and below room temperature using BCP micelles

Table S3: Summarised characterisation for the different composite samples (1 and 2 and 9,10 and 12). An exemplary TEM picture and the size distribution are given for TEM measurements. The particle sizes are given in the pictures.

sample	Reaction conditions	TEM nanoparticles, TEM size distribution and TEM microcrystals (if any)
1	2 cycle, toluene, reflux, BCP-1	
2	3 cycles, toluene, reflux, BCP-1	
9	2 cycles, toluene, reflux, BCP-2	

7. Synthesis of different Fe(II) SCO nanoparticles with SCO over and below room temperature using BCP micelles

<p>10</p>	<p>3 cycles, toluene, reflux, BCP-2</p>		 <table border="1"> <caption>Size Distribution Data for 3 Cycles</caption> <thead> <tr> <th>Size [nm]</th> <th>Count</th> </tr> </thead> <tbody> <tr><td>60</td><td>1</td></tr> <tr><td>62</td><td>4</td></tr> <tr><td>64</td><td>5</td></tr> <tr><td>66</td><td>10</td></tr> <tr><td>68</td><td>26</td></tr> <tr><td>70</td><td>14</td></tr> <tr><td>72</td><td>16</td></tr> <tr><td>74</td><td>14</td></tr> <tr><td>76</td><td>7</td></tr> <tr><td>78</td><td>2</td></tr> <tr><td>80</td><td>1</td></tr> </tbody> </table>	Size [nm]	Count	60	1	62	4	64	5	66	10	68	26	70	14	72	16	74	14	76	7	78	2	80	1
Size [nm]	Count																										
60	1																										
62	4																										
64	5																										
66	10																										
68	26																										
70	14																										
72	16																										
74	14																										
76	7																										
78	2																										
80	1																										
<p>12</p>	<p>5 cycles, toluene, reflux, BCP-2</p>		 <table border="1"> <caption>Size Distribution Data for 5 Cycles</caption> <thead> <tr> <th>Size [nm]</th> <th>Count</th> </tr> </thead> <tbody> <tr><td>60</td><td>3</td></tr> <tr><td>62</td><td>5</td></tr> <tr><td>64</td><td>10</td></tr> <tr><td>66</td><td>15</td></tr> <tr><td>68</td><td>23</td></tr> <tr><td>70</td><td>9</td></tr> <tr><td>72</td><td>20</td></tr> <tr><td>74</td><td>5</td></tr> <tr><td>76</td><td>7</td></tr> <tr><td>78</td><td>2</td></tr> <tr><td>80</td><td>1</td></tr> </tbody> </table>	Size [nm]	Count	60	3	62	5	64	10	66	15	68	23	70	9	72	20	74	5	76	7	78	2	80	1
Size [nm]	Count																										
60	3																										
62	5																										
64	10																										
66	15																										
68	23																										
70	9																										
72	20																										
74	5																										
76	7																										
78	2																										
80	1																										

7. Synthesis of different Fe(II) SCO nanoparticles with SCO over and below room temperature using BCP micelles

Figure S4: TEM images of **9** and **13** to show 1D hexagonal packing effect of the $[\text{Fe}(\text{Lc})(\text{bipy})]_n$ nanoparticles in BCP-2.

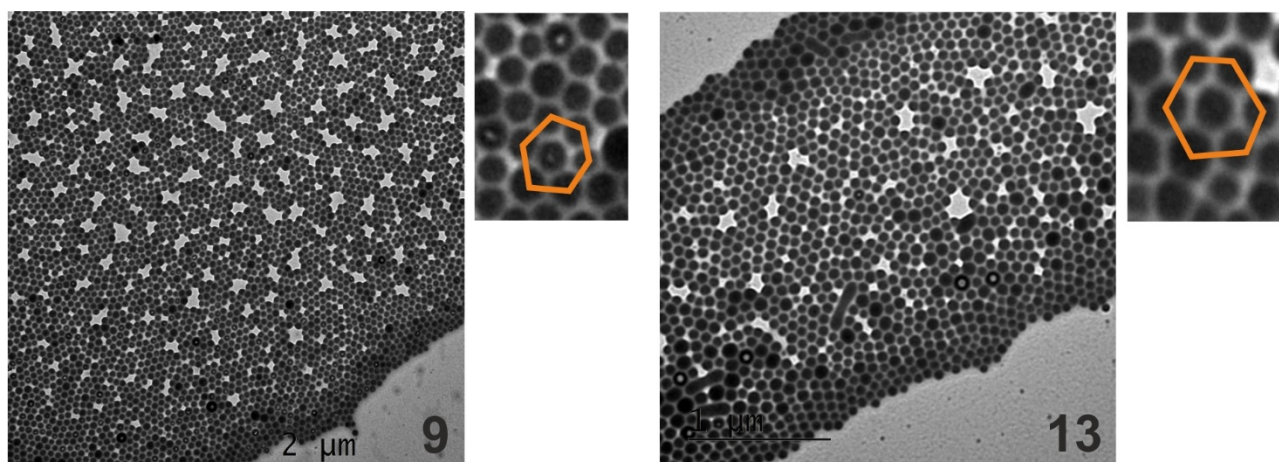
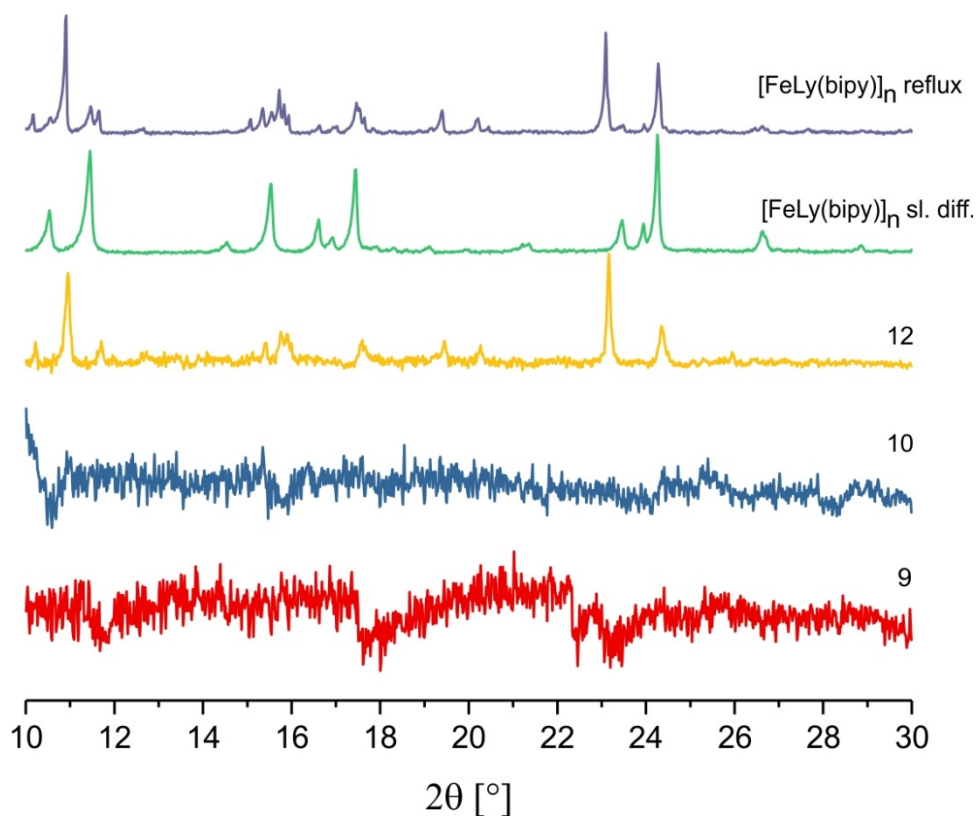


Figure S5: Powder X-Ray diffraction pattern of **9**, **10** and **12** in BCP-2 with reflux. All Samples show characteristic signals from the bulk material with reflux in fast diffusion.



7. Synthesis of different Fe(II) SCO nanoparticles with SCO over and below room temperature using BCP micelles

Figure S6: Powder X-Ray diffraction pattern of **13** and **14** in BCP-2 without reflux. No characteristic peak was given for sample **13**. For sample **14** a 2θ peaks at about 13.2° , 18.5° and 26° appeared, which are characteristic for the oxidised μ -oxido complex.

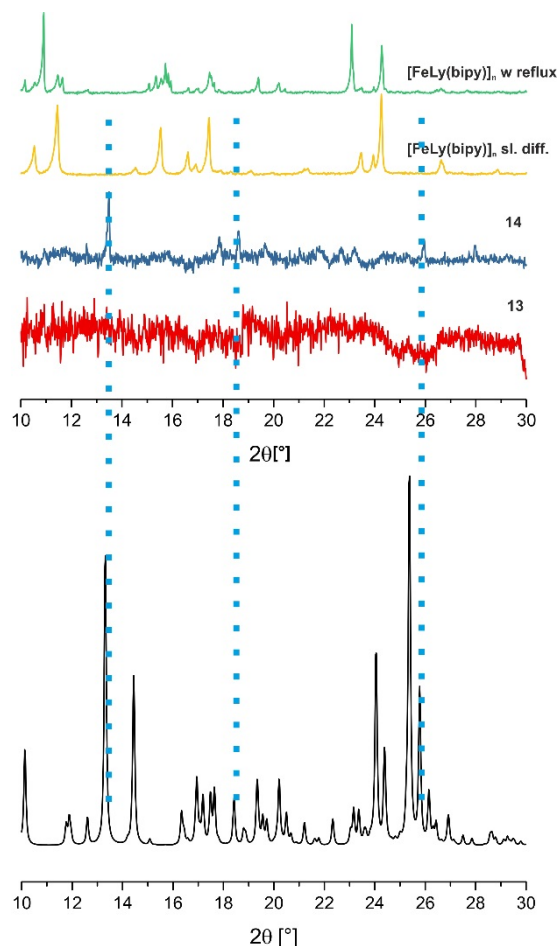
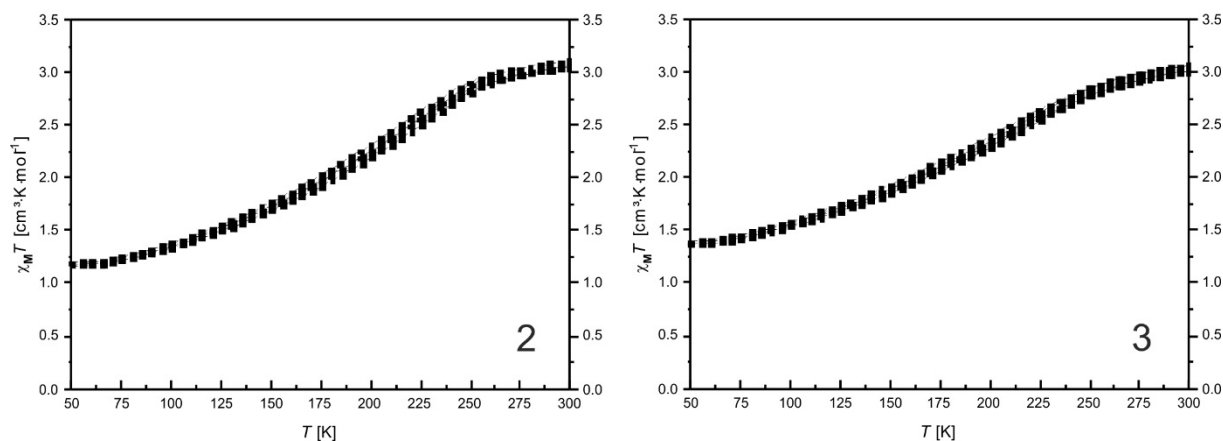


Figure S7: $\chi_M T$ vs. T plots of the samples **2** (left) and **3** (right) in BCP-1 with reflux.



7. Synthesis of different Fe(II) SCO nanoparticles with SCO over and below room temperature using BCP micelles

Figure S8: $\chi_M T$ vs. T plots of sample 7 in BCP-1 without reflux.

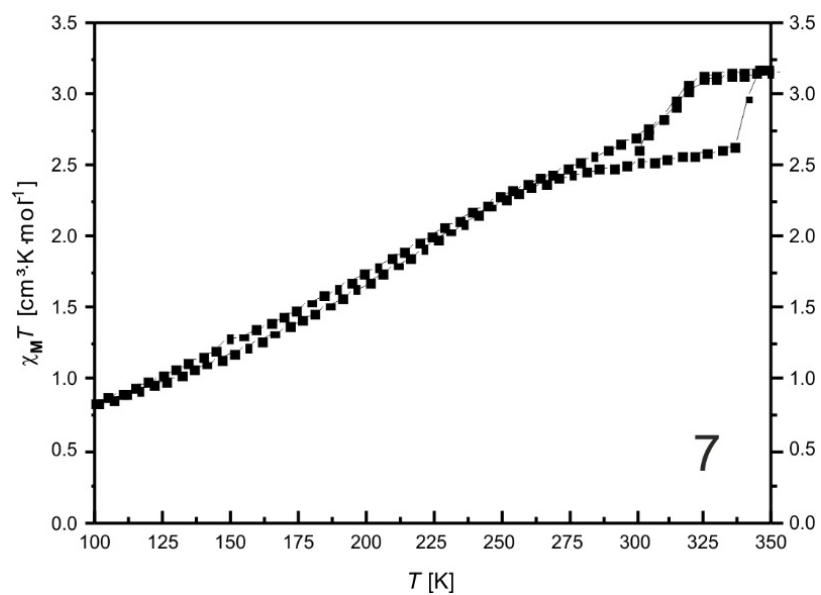
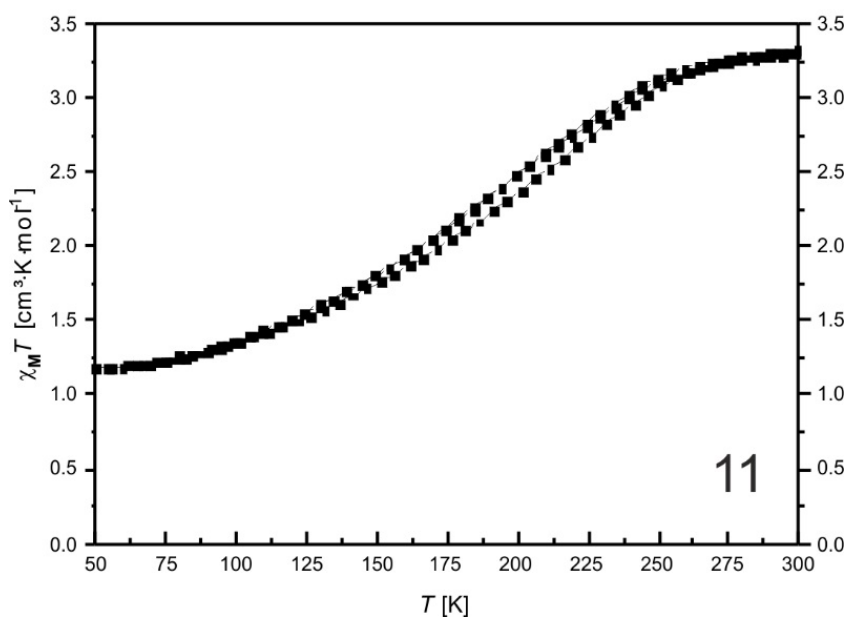


Figure S9: $\chi_M T$ vs. T plots of sample 11) in BCP-3 with reflux.



8 List of Publications

C. Lochenie, A. Gebauer, O. Klimm, F. Puchtler, B. Weber, *New J. Chem.*, **2016**, *40*, 4687–4695.

„Iron(II) spin crossover complexes with diamidonaphthalene-based Schiff base-like ligands: 1D coordination polymers “

Ottokar Klimm,^a Christoph Göbel,^a Sabine Rosenfeldt,^b Florian Puchtler,^c Nobuyoshi Miyajima,^d Katharina Marquardt,^d Markus Drechsler,^e Josef Breu,^c Stephan Förster,^b and Birgit Weber*^a, *Nanoscale*, **2016**, *8*, 19058–19065.

“Synthesis of [Fe(L)(bipy)]_n spin crossover nanoparticles using blockcopolymer micelles”

Christoph Göbel^a, Ottokar Klimm^a, Florian Puchtler^b, Sabine Rosenfeldt^c, Stephan Förster^c and Birgit Weber^{a*}, *Beilstein J. Nanotech.*, **2017**, *8*, 1318–1327.

“Synthesis of [Fe(L_{eq})(L_{ax})]_n Coordination Polymer Nanoparticles using Blockcopolymer Micelles”

Wittmann, Thomas; Mondal, Arobendo; Tschense, Carsten; Wittmann, Johannes ; Klimm, Ottokar; Siegel, Renee; Corzilius, Björn; Weber, Birgit; Kaupp, Martin; Senker, Jürgen, *J. Am. Chem. Soc.*, **2018**, *140* (6), 2135–2144.

“Probing Interactions of N-Donor Molecules with Open Metal Sites within Paramagnetic Cr-MIL-101: A Solid-State NMR Spectroscopic and Density Functional Theory Study”

Contributions to national and international conferences

1. O. Klimm, Christoph Göbel, Tatiana Palamarciuc, Birgit Weber: **Poster** "Nanostrukturierung von Fe(II) Spin-Crossover-Komplexen", 10th Koordinationschemietagung, Kaiserslautern, Germany,

02.-04.02.14.

2. O. Klimm, Birgit Weber: **Oral Presentation** “Nanostrukturierung von Fe(II) Spin-Crossover-Komplexen“, 1st Doktorandensymposium SFB 840, Windischeschenbach, Germany, 26.03.-28.03.14.

3. O. Klimm, B. Weber: **Oral Presentation** " Fe(II) SCO nanoparticles in Polymer matrix ", 11th Koordinationschemietagung, Paderborn, Germany, 22.-24.03.15.

4. O. Klimm, Birgit Weber: **Oral Presentation** „Fe^(II) SCO nanoparticles in Polymer matrix“, 2nd Doktoranden-symposium SFB 840, Windischeschenbach, Germany, 29.-30.04.2015

5. O. Klimm, Birgit Weber: **Oral Presentation** "Schaltbare Koordinationsnetzwerke-Nanostrukturierung und funktionale Linker ", COORNETs, Günzburg, Germany, 02.-03.07.15.

9 Acknowledgment

First I thank Prof. Dr. Weber for giving me the opportunity to make my Ph.D. in her workgroup, as well as for the support, help, advices, ideas, scientific discussions, and the freedom of research I was given.

I thank my (ex)colleagues Katja Dankhoff, Christoph Göbel, Hannah Kurz, Dr. Charles Lochenie, Dr. René Nowak, Dr. Stephan Schlamp, Johannes Weihermüller and Lisa Zappe for the good working atmosphere, for the help they provided when I needed it.

I thank the AK Prof. Dr. Kempe for the technical, scientific, and administrative support and the research cooperations we had. This thesis could not have been written without the access to the CHN analysis. I thank my cooperation partners Prof. Dr. Förster, Prof. Dr. Breu, Dr. Markus Drechsler, Dr. Daniela Pirner, Florian Puchtler, Dr. Sabine Rosenfeldt.

I thank Thomas Beppler (LOT) for the technical support with the SQUID. I also thank the team of the glass blowing workshop, they made an awesome work to repair or built glass apertures when I needed them.

A special thank goes to my personally good friends Paul Reichstein and Niklas Weihermüller who helped me in all complicated situations of my Ph.D., to not go crazy from time to time.

Also, a special thank goes to my girlfriend Yvonne from Neustadt bei Coburg, for being my personal supporter and for giving me her affection in all life situations. I love you!

This work would not have been possible without the students who worked with me as intern or HiWi: Linda Barnau, Stella Buchmann, Simon Gemeinhardt, Hannah Gottschling, Vitali Gotwich, Franka Gruschwitz, Juliane Kary, Luisa Mai, Nicolas Mödl, Dominic Rosenbach and Bernd Steiger. Their work made my research go forward, or backward, in both cases I learned a lot.

Zuletzt bedanke ich mich aus tiefstem Herzen bei meiner Familie und meinen Freunden in meiner alten Heimat Thüringen, für ihre stete liebevolle Unterstützung und Ablenkung, wenn ich es am nötigsten gebraucht habe.

10 Declaration

(Eidesstattliche) Versicherungen und Erklärungen

(§ 9 Satz 2 Nr. 3 PromO BayNAT)

Hiermit versichere ich eidesstattlich, dass ich die Arbeit selbstständig verfasst und keine anderen als die von mir angegebenen Quellen und Hilfsmittel benutzt habe (vgl. Art. 64 Abs. 1 Satz 6 BayHSchG).

(§ 9 Satz 2 Nr. 3 PromO BayNAT)

Hiermit erkläre ich, dass ich die Dissertation nicht bereits zur Erlangung eines akademischen Grades eingereicht habe und dass ich nicht bereits diese oder eine gleichartige Doktorprüfung endgültig nicht bestanden habe.

(§ 9 Satz 2 Nr. 4 PromO BayNAT)

Hiermit erkläre ich, dass ich Hilfe von gewerblichen Promotionsberatern bzw. -vermittlern oder ähnlichen Dienstleistern weder bisher in Anspruch genommen habe noch künftig in Anspruch nehmen werde.

(§ 9 Satz 2 Nr. 7 PromO BayNAT)

Hiermit erkläre ich mein Einverständnis, dass die elektronische Fassung meiner Dissertation unter Wahrung meiner Urheberrechte und des Datenschutzes einer gesonderten Überprüfung unterzogen werden kann.

(§ 9 Satz 2 Nr. 8 PromO BayNAT)

Hiermit erkläre ich mein Einverständnis, dass bei Verdacht wissenschaftlichen Fehlverhaltens Ermittlungen durch universitätsinterne Organe der wissenschaftlichen Selbstkontrolle stattfinden können.

.....
Ort, Datum, Unterschrift